



Universiteit
Leiden
The Netherlands

Allosteric modulation and ligand binding kinetics at the Kv11.1 channel

Yu, Z.

Citation

Yu, Z. (2015, October 20). *Allosteric modulation and ligand binding kinetics at the Kv11.1 channel*. Retrieved from <https://hdl.handle.net/1887/35951>

Version: Corrected Publisher's Version

License: [Licence agreement concerning inclusion of doctoral thesis in the Institutional Repository of the University of Leiden](#)

Downloaded from: <https://hdl.handle.net/1887/35951>

Note: To cite this publication please use the final published version (if applicable).

Cover Page



Universiteit Leiden



The handle <http://hdl.handle.net/1887/35951> holds various files of this Leiden University dissertation.

Author: Yu, Zhiyi

Title: Allosteric modulation and ligand binding kinetics at the Kv11.1 channel

Issue Date: 2015-10-20

Allosteric modulation and ligand binding kinetics
at the K_v11.1 channel

Zhiyi Yu

The research described in this thesis was performed in Division of Medicinal Chemistry at the Leiden Academic Centre for Drug Research, Leiden University (Leiden, The Netherlands).

Cover design: Shuo Mi and Zhiyi Yu

Thesis layout: Zhiyi Yu

Printed in the Netherlands

©Copyright, Zhiyi Yu, 2015. All right reserved.

No part of this book may be reproduced in any form or by any means without permission of the author.

Allosteric modulation and ligand binding kinetics at the K_v11.1 channel

Proefschrift

ter verkrijging van
de graad van Doctor aan de Universiteit Leiden,
op gezag van Rector Magnificus prof. mr. C.J.J.M. Stolker,
volgens besluit van het College voor Promoties
te verdedigen op dinsdag 20 oktober 2015
klokke 13:45 uur

door

Zhiyi Yu
geboren te Hubei, China
in 1986

Promotiecommissie

Promotor: Prof. Dr. A.P. IJzerman

Co-promotor: Dr. L.H. Heitman

Overige Leden: Prof. Dr. M. Danhof
Mevr. Prof. Dr. C. Mummery
Dr. M. van der Heyden
Prof. Dr. P.H. van der Graaf

Contents

Chapter 1	General introduction	7
Chapter 2	Kinetic studies of the $K_v11.1$ (hERG) channel	23
Chapter 3	Allosteric modulators of the $K_v11.1$ (hERG) channel: radioligand binding assays reveal allosteric characteristics of dofetilide analogues	63
Chapter 4	Allosteric modulation of $K_v11.1$ (hERG) channels protects against drug-induced ventricular arrhythmias	89
Chapter 5	Synthesis and biological evaluation of negative allosteric modulators of the $K_v11.1$ (hERG) channel	121
Chapter 6	$K_v11.1$ (hERG)-induced cardiotoxicity: a molecular insight from a binding kinetics study of prototypic $K_v11.1$ inhibitors	157
Chapter 7	Structure-affinity relationships (SARs) and structure-kinetics relationships (SKRs) of $K_v11.1$ (hERG) blockers	185
Chapter 8	Conclusions and perspectives	223
Summary		237
Samenvatting		241
Curriculum Vitae		245
List of publications		247
Acknowledgements		249



Chapter 1

General introduction



Ion channels are transmembrane proteins that create a gated and water-filled pore to allow the flow of ions down their electrochemical gradient between the intracellular and extracellular environment.^{1, 2} They are selective for a wide range of cations and anions, such as Na^+ , K^+ , Ca^{2+} , and Cl^- ions. The distribution of ion channels has been found in cell membranes as well as the membranes of intracellular mitochondria, endoplasmic reticulum, and nucleus, which suggests their crucial physiological functions in a plethora of excitable and non-excitable tissues. Accordingly, ion channels are important targets for many drugs in current use. Indeed, application of ion channel modulators as medications was operative long before their existence had been demonstrated.³ For instance, in the 19th century cocaine extraction from coca leaves gave rise to a pharmaceutical class of local anesthetics, which are selective sodium channel blockers.⁴ In addition to the widespread therapeutic properties, ion channels are also crucially related to human toxicology due to their involvement in human physiology. $\text{K}_v11.1$ (hERG) channel induced cardiotoxicity has become a thorny issue for the pharmaceutical industry in the past years. Blockade of the $\text{K}_v11.1$ channel leads to the prolongation of cardiac action potential duration (APD) and long QT syndrome, which in some individuals can degenerate into ventricular arrhythmias and sudden cardiac death.⁵ It has been pointed out that 50% of drugs recalled by the FDA from 1995 to 2000 were also $\text{K}_v11.1$ blockers.⁶ In this thesis, I, therefore, focus on parameters that might determine the $\text{K}_v11.1$ toxicity of compounds at the molecular level, as well as possible strategies for relieving the $\text{K}_v11.1$ -related cardiac side effects of drugs. In order to provide some background for the research and concepts that are discussed in this thesis, a brief overview of ion channels has been outlined. Subsequently, the target receptor, the $\text{K}_v11.1$ channel, is introduced, followed by a summary of objectives and contents of this thesis.

Ion channels

Several hundred genes in the human genome encode the pore-forming ion channels across plasma membranes.¹ According to the precise control of channel gating, ion channels are classified as ligand- and voltage-gated channels, of which the opening and closure are mediated by a specific ligand and membrane voltage, respectively.⁷

Ligand-gated ion channels

Ligand-gated ion channels (LGICs) are oligomeric protein assemblies that span the cell membrane and form both the binding site for an endogenous ligand and an ion-conducting pore, which converts a chemical signal into an ion flux through

the membrane.^{8,9} Based on homology in their amino acid sequence and topology of their component subunits, LGICs are divided into three superfamilies, including P2X, ionotropic glutamate, and Cys-loop receptors.¹⁰ They play an important role in fast synaptic transmission and in the modulation of cellular activity, in particular for basic brain functions like learning, memory and attention.

P2X receptors

P2X receptors are non-selective cationic channels gated by extracellular ATP, which are permeable to Na⁺, K⁺, Ca²⁺, and in some cases also to Cl⁻ ions.¹¹ A P2X channel contains three subunits, and each subunit is composed of two transmembrane domains connected by a large, glycosylated extracellular loop, and intracellular C- and N-terminus (**Figure 1A**).⁹ At present, there are seven P2X receptor subtypes found in mammals, which are termed P2X₁ to P2X₇.¹² These channels play paramount roles in various physiological processes such as nerve transmission, pain sensation, the response to inflammation, multiple facets of diabetes, and tumor cell growth, making them attractive drug targets in recent years.¹²⁻¹⁴

Ionotropic glutamate receptors

Ionotropic glutamate receptors are cation-selective ion channels that open their ion-conducting pores in response to the binding of glutamate.¹⁵ This channel is made up of four homologous subunits with each subunit containing three transmembrane segments, an intracellular C-terminus and extracellular N-terminus (**Figure 1B**).⁹ The ionotropic glutamate receptors are grouped into three subtypes according to their distinct responses to certain small molecule agonists: N-methyl-D-aspartate (NMDA), α -amino-3-hydroxy-5-methyl-4-isoxazolepropionic-acid (AMPA) and kainate (KA) receptors.^{10, 15, 16} These distinct ion channels are implicated in almost all aspects of nervous system development and function, and their dysfunctions can be linked to epilepsy or chronic neurodegenerative conditions like schizophrenia, Alzheimer's and Parkinson's diseases, as well as stroke.^{15, 16}

Cys-loop receptors

The Cys-loop receptors, named from the conserved cysteine loop in their extracellular domain, constitute the largest subfamily amongst all LGICs.^{9, 17} The best characterized members of the Cys-loop receptor superfamily are nicotinic acetylcholine receptors (nAChRs), serotonin type 3 receptors (5-HT₃Rs), GABA receptors type A (GABA_ARs), glycine receptors (GlyRs) and zinc activated chan-

nels (ZACs).¹⁸ Although these ion channels exhibit diverse kinetic and pharmacological profiles, they share a common structure of five identical subunits that are pseudo-symmetrically arranged to form a rosette with a central ion-conducting pore for either anion (GABA_ARs and GlyRs) or cation (nAChRs, 5-HT₃Rs, and ZACs) flux.^{17, 19} As shown in **Figure 1C**, each subunit of the channel is made up of an extensive N-terminus and a short C-terminus on the extracellular side, and four transmembrane segments.⁸ All these receptors are very important targets for a wide variety of drugs, and their dysfunctions are associated with different kinds of diseases. For example, nAChRs have been demonstrated to play many critical roles in brain and body functions, indicating their therapeutic modulation of Alzheimer's disease, epileptic disorders and chronic pain.²⁰⁻²² Likewise, GABA_ARs have been unraveled to regulate the controlling neuronal activity in distinct brain regions, and dysfunction of this ion channel involves a range of central nervous system diseases such as anxiety, insomnia, muscle spasms, Alzheimer's disease and schizophrenia.^{23, 24}

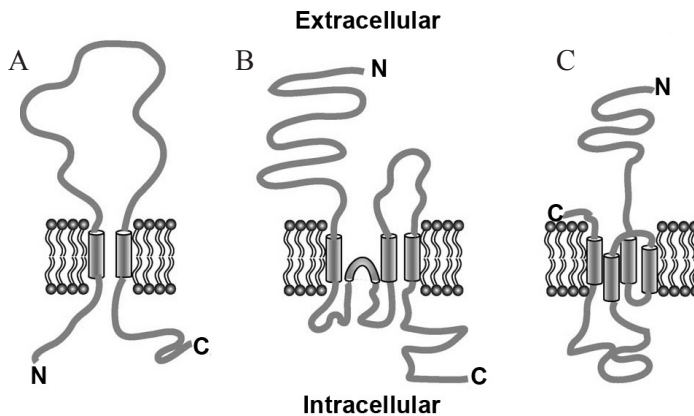


Figure 1. Schematic representation of a single subunit from the three superfamilies of ligand-gated ion channels across the membrane: (A) P2X receptors, (B) Ionotropic glutamate receptors, and (C) Cys-loop receptors.⁹

Voltage-gated ion channels

Voltage-gated ion channels (VGICs) are integral transmembrane proteins that conduct selected inorganic ions at high rates across the membrane in response to changes in transmembrane voltage.²⁵ The VGIC superfamily, with 143 members in the human genome, forms the third largest family of signal-transduction proteins, following the G protein-coupled receptors and protein kinases.^{26, 27} As shown in **Figure 2**, ten families are included in this VGIC superfamily: voltage-gated sodium/calcium/potassium channels (Na_v/Ca_v/K_v), calcium-activated

potassium channels (K_{Ca}), cyclic nucleotide-modulated (CNG) ion channels, hyperpolarization-activated cyclic nucleotide-modulated (HCN) channels, transient receptor potential (TRP) channels, two-pore channels (TPCs), inwardly rectifying potassium channels (K_{ir}) and two-pore potassium channels (K_{2p}).^{10, 28} All these channels are composed of a common cation-selective pore-forming module containing two transmembrane segments and an intervening pore loop.¹⁰ Except for K_{ir} and K_{2p} channels, all other ion channels consist of four subunits symmetrically arranged around the central ion-conducting pore, and each subunit encompasses six transmembrane segments (S1-S6).^{10, 26, 27} Amongst these segments, S1-S4 segments form the voltage-sensor domain with four to eight positively charged residues in the S4 segment conferring voltage dependence, whereas S5 and S6 make up the pore domain including the ionic pore with the selectivity filter.¹ Movement of the voltage sensors and pore domains constitutes three main conformational states of the VGICs: closed, open and inactivated states. On the other hand, K_{ir} and K_{2p} , which are composed of four and three subunits respectively, are structurally the simplest VGICs with only pore-forming segments for each subunit. These two potassium channels are regulated by membrane lipids and intracellular 'ligands', as diverse as G proteins, Mg^{2+} ions, polyamines and ATP.¹⁰ Apart from the main subunits, VGICs also possess some smaller, auxiliary subunits to modify their functions, increasing the diversity and complexity of this superfamily. VGICs play a fundamental role in most aspects of cell physiology and underlie complex integrative processes like learning and memory in the brain and coordinated movements of the muscles, which makes them the molecular target for a number of therapeutic agents and also toxins.²⁷

Potassium-selective channels with 78 members are the most diverse and widespread group of ion channels, whereas K_v channels, in humans encoded by 40 genes and divided into 12 subfamilies (K_v1 -12), form the largest family among these potassium channels.^{29, 30} All K_v channels have a high level of structural similarity, and play a pivotal role in a variety of cellular processes, such as functioning of excitable cells, cell apoptosis, growth and differentiation, the release of neurotransmitters and hormones, and maintenance of cardiac activity.³¹ Therefore, K_v channels constitute potential drug targets and provide tremendous opportunities for treating cancer, autoimmune diseases, metabolic, neurological and cardiovascular disorders. However, K_v channels also present a challenge to the development of K_v -targeted medications, of which the $K_v11.1$ channel is an explicit example with its promiscuity to drug binding, resulting in drug-induced ventricular arrhythmias.²

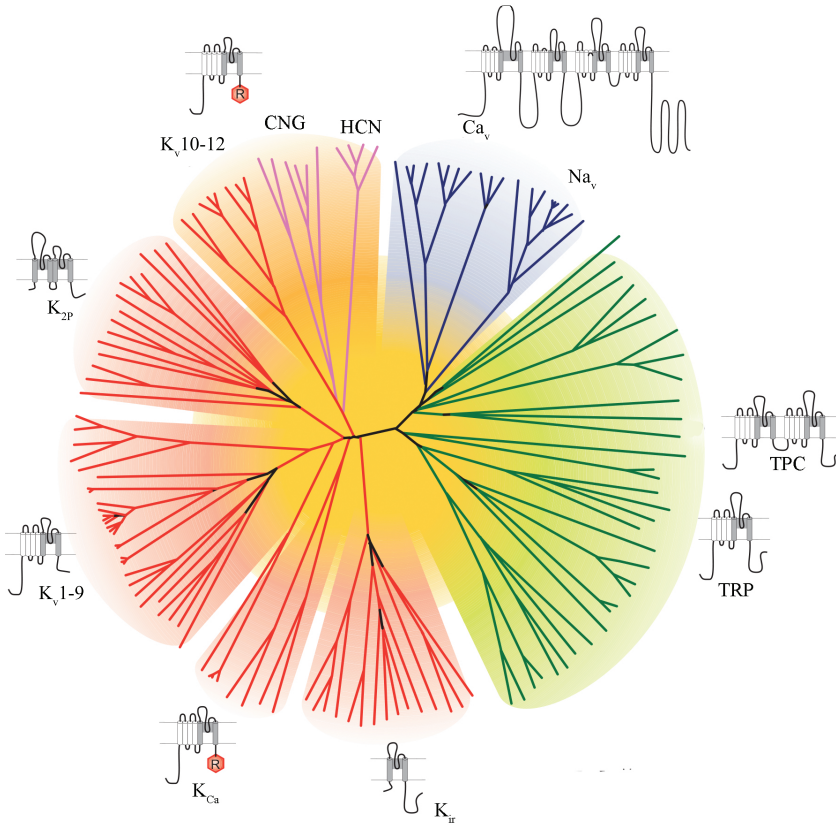


Figure 2. A phylogenetic tree of voltage-gated ion channels, and a schematic representation of the structure of each voltage-gated ion channel within this superfamily.²⁸

The K_v 11.1 channel

Overview of the K_v 11.1 channel

The K_v 11.1 channel, of which the pore-forming α -subunits are encoded by the human ether-à-go-go-related gene (hERG), carries a rapidly activating delayed rectifier potassium current (I_{Kr}) underlying its essential role in cardiac action potential repolarization.³² In addition, the K_v 11.1 channel has been found to be expressed in various brain regions, smooth muscle cells, endocrine cells, and a wide range of tumor cell lines, which implicates the channel's therapeutic opportunities beyond the cardiac system.^{32, 33} However, due to its involvement in life-threatening cardiac arrhythmias, the terminology “hERG” or “ K_v 11.1” has become notorious in the drug discovery community. Hence, much attention has been paid to K_v 11.1-induced cardiotoxicity over the past decades, which makes

its role in the heart best characterized.

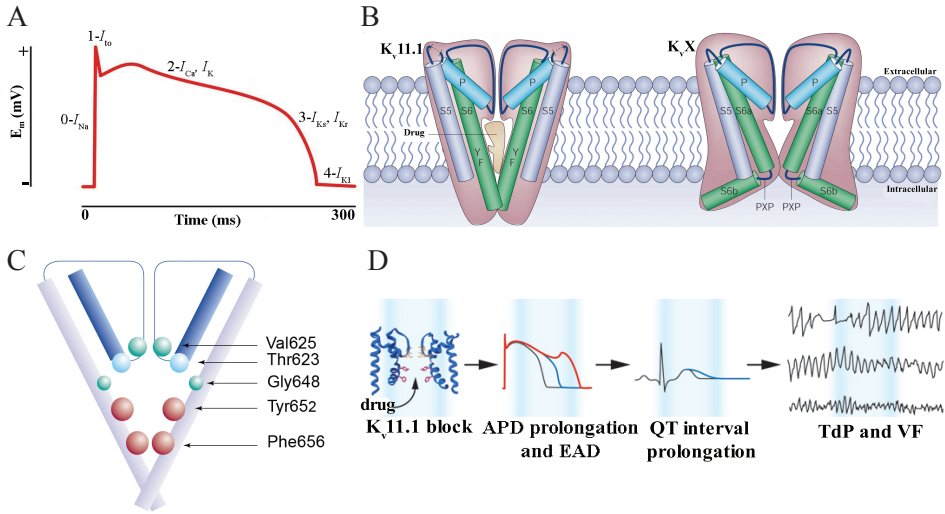


Figure 3. (A) The ventricular action potential waveform indicating the major ionic currents that contribute to its morphology and duration ($I_{Na^{+}}$: inward sodium current, I_{to} : transient outward potassium current; $I_{Ca^{2+}}$: L-type inward calcium current; I_K : outward repolarizing potassium current; $I_{K^{slow}}$: slowly activating delayed rectifier potassium current; $I_{K^{fast}}$: rapidly activating delayed rectifier potassium current; I_{K1} : inward rectifier potassium current).^{34, 35} (B) Structure of the pores of the $K_v11.1$ channel and other K_v channels: the presence of a Pro-X-Pro (PXP) motif in the S6 helix of other K_v channels causes a kink and thereby reduces the size of the channel pore cavity.³⁶ (C) Amino acids that are crucial for high-affinity binding of prototypical $K_v11.1$ blockers.³⁷ (D) Mechanism of cardiac arrhythmias induced by $K_v11.1$ blockade.³⁸

The $K_v11.1$ channel displays unusual gating properties that impact cardiac electrical function. Upon membrane depolarization the $K_v11.1$ channel opens slowly but inactivates rapidly, while it recovers rapidly from inactivation but deactivates slowly during repolarization.^{5, 34} Therefore, the $K_v11.1$ channel conducts robust outward currents ($I_{K^{fast}}$) relatively late in the ventricular action potential, accelerating the phase 3 repolarization without significantly disturbing the preceding plateau phase 2 (**Figure 3A**). Nevertheless, the $K_v11.1$ channel lacks a Pro-X-Pro (PXP) motif existing in other K_v channels (**Figure 3B**), resulting in a larger cavity that can accommodate a wide range of drugs.³⁶ Furthermore, the $K_v11.1$ channel has multiple aromatic rings lining the pore (**Figure 3C**), which facilitates the binding of drugs containing aromatic rings at the channel.³⁷ Collectively, a number of drugs including cardiac and non-cardiac medications can bind to the $K_v11.1$ channel. As depicted in **Figure 3D**, drug block of the $K_v11.1$ channel at the molecular level induces APD prolongation, early afterdepolariza-

tions (EADs) and heterogeneity of repolarization.³⁸ This generates a lengthening of the QT interval in the electrocardiogram at the tissue level, which can further lead to life-threatening arrhythmias like Torsade de Pointes (TdP) and ventricular fibrillation (VF). Therefore, it has become obligatory routine practice for all pharmaceutical and biotechnology companies to screen for $K_v11.1$ liability of drug candidates in the early stage of drug development. More details on the structural features and physiological functions of $K_v11.1$ channel will be stated in the chapter 2.

Ligands for the $K_v11.1$ channel

Blockers and modulatory activators

A large number of structurally diverse compounds have been shown to bind to the $K_v11.1$ channel. In most cases these drugs reduce the I_{Kr} by directly blocking the conduction pore or less frequently by interfering with channel trafficking to the surface membrane, and these drugs are referred to as $K_v11.1$ blockers.^{32, 39, 40} In addition, some blockers like APETx1 exert their inhibitory effects on the $K_v11.1$ current by modulating the gating properties of the channel.^{41, 42} On the other hand, a small amount of compounds have also been characterized as $K_v11.1$ activators, which have the opposite activity of blockers and thus enhance the I_{Kr} current.^{39, 43}

Most $K_v11.1$ blockers share a common binding region within the aqueous inner cavity at the pore of the channel, where residues Tyr652 and Phe656 are found to be crucial for drug binding via hydrophobic and electrostatic interplays, including π - π and π -cation interactions.^{37, 39} Apart from the intracellular binding pocket, various scorpion, spider and sea anemone toxins inhibit the $K_v11.1$ channel from the extracellular side or by binding to the voltage-sensor domain.⁴² With regard to the $K_v11.1$ activators, different binding locations at the channel have been identified, depending on the mechanisms by which they potentiate the I_{Kr} . According to the primary action model, these $K_v11.1$ activators are separated into types 1 and 2 classes.^{32, 39} Type 1 $K_v11.1$ channel activators attenuate the inactivation and deactivation rates of the channel, whereas type 2 activators primarily impair the channel's inactivation rate. Distinct from each other as well as blockers, type 1 and type 2 $K_v11.1$ activators bind to a site between the pore and voltage sensor and a region that is closer to the selectivity filter, respectively. Additionally, several type 2 $K_v11.1$ activators like NS1643 and PD307243 have been proposed to interact with the channel at the extracellular face.^{43, 44} Taken together, multiple binding sites exist at the $K_v11.1$ channel, which illustrates the potential for different ligands to display either competitive or allosteric interactions depending on their binding sites relative to one another (**Figure 4A**).⁴⁵

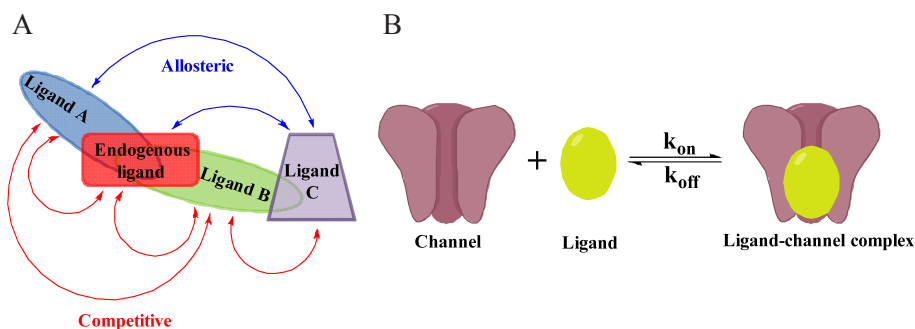


Figure 4. Simple schematic representations of the ligand-channel interaction: (A) Arrows demonstrate a competitive (endogenous ligand with ligands A and B, ligand B with ligands A and C) or allosteric interaction (ligand C with ligand A and endogenous ligand) of different ligands based on their binding sites relative to one another,⁴⁵ and (B) Single-step binding of a ligand to the $K_v11.1$ channel.

Binding kinetics of ligands

The specific ligand-receptor interaction is the chemical basis of virtually all biological activities of compounds.⁴⁶ As shown in **Figure 4B**, binding of a $K_v11.1$ ligand to the channel can be considered as a single-step reaction in the simplest scenario. At first, the ligand binds to the $K_v11.1$ channel with a second-order association rate (k_{on}), and then detaches from the channel with a first-order dissociation rate (k_{off}). In a closed system, the extent of ligand-channel binding is commonly quantified in terms of the equilibrium dissociation constant (K_D) defined as the value of k_{off}/k_{on} or its (often inhibitory) affinity (IC_{50} or K_i). To date, more and more evidence from a wide range of receptors has addressed the concept that *in vivo* efficacy of a ligand is not only described by the *in vitro* measured equilibrium dissociation constant, but also depends on its association and, more critically, dissociation rates.⁴⁷⁻⁴⁹ A ligand's residence time (RT), i.e. the reciprocal of its dissociation rate, may be at the basis of the ligand's duration of action and target selectivity.⁴⁸ As for the $K_v11.1$ channel, a 30-fold safety margin, quantified as the ratio of IC_{50} and maximum plasma concentration (C_{max}), has been proposed to define the cardiac safety of $K_v11.1$ blockers.⁵⁰ However, the binding of a $K_v11.1$ ligand to the channel remains a dynamic process in which binding (association) and unbinding (dissociation) events develop over time.⁵¹ Moreover, the approach in which only the IC_{50} value is considered, is rather arbitrary and may not satisfactorily account for the degree of ion channel inhibition reached in various conditions, leading to unsatisfactory quantitative predictions.^{51,52} Importantly, $K_v11.1$ blockers with similar IC_{50} values but different binding kinetics at the channel

have been reported to pose distinct proarrhythmic risks.^{52, 53} Therefore, binding kinetics of ligand- $K_v11.1$ interactions constitute a critical component in understanding the mechanism of action, and thus should be incorporated within the present screening strategy to improve the risk profiles of drug candidates.^{51, 52, 54}

Objectives and outline of this thesis

Drug-induced arrhythmia due to blockade of the $K_v11.1$ channel has emerged as an unanticipated side effect of many pharmacological agents and is a major obstacle for drug development. Although much attention has been paid to screening $K_v11.1$ liability of drug candidates over the past decades, the current testing paradigm has important limitations and may have led to withdrawal of blockbusters on the present market or stopping the development of potentially valuable therapeutics. Therefore, investigating the mechanism of action of ligands at the $K_v11.1$ channel, where in particular the ligand binding kinetics may yield comprehensive understanding of $K_v11.1$ -related cardiotoxicity, may further provide new strategies for circumventing this side effect in drug development. In addition, compounds that can relieve the unintended $K_v11.1$ blockade of drugs, e.g., allosteric modulators, are of considerable interest because of their potential to prevent drug-induced arrhythmia via combination therapy.

In **Chapter 2**, the gating kinetics and ligand binding characteristics at the $K_v11.1$ channel are extensively discussed, following the basic introduction of the channel biosynthesis, structure and function, and pharmacological target and anti-target applications in drug development.

At the start of this project, high-throughput assays had not been reported to characterize allosteric modulators of the $K_v11.1$ channel, nor had ligand binding kinetics been determined at the channel. Thus, [3H]astemizole and [3H]dofetilide binding assays were developed and utilized to identify positive and negative allosteric modulators of the $K_v11.1$ channel in **Chapter 3**.

Based on the work in chapter 3, a novel negative allosteric modulator (LUF7244) was identified in several different [3H]dofetilide binding assays in **Chapter 4**. LUF7244 was found to reduce the $K_v11.1$ affinity of dofetilide, astemizole, sertindole and cisapride in a [3H]dofetilide competitive displacement assay, and more importantly, to prevent the proarrhythmic effects induced by astemizole, sertindole and cisapride in a newly validated neonatal rat ventricular myocyte model. This research raises the possibility to resume the clinical use of unintended $K_v11.1$ blockers via pharmacological combination therapy. Following this, in **Chapter 5** the synthesis of a series of possible allosteric modulators and the evaluation of their allosteric effects on [3H]dofetilide binding at the chan-

nel are reported. Compared to LUF7244, several more potent negative allosteric modulators were obtained via small chemical modifications.

In **Chapter 6**, a novel [^3H]dofetilide competition association assay was developed and validated to evaluate the kinetic parameters of fifteen prototypical $K_v11.1$ blockers at the channel. Next to that, an immobilized artificial membrane column was applied to measure the membrane affinity of these blockers to elucidate the effect of membrane affinity of ligands on their affinity and kinetic parameters. In addition to varied affinity values and association rates of $K_v11.1$ ligands at the channel, **Chapter 7** focuses on the discovery of blockers with diversified dissociation rates or RTs. Compounds with very short (< 1 min) and much longer RTs (> 100 min) were disclosed in this chapter, which enabled the construction of a “ $k_{\text{on}}-k_{\text{off}}-K_D$ ” kinetic map for all these compounds. Additionally, results from patch clamp studies implicated the importance of RTs in regulating the functional IC_{50} values of $K_v11.1$ blockers.

Overall, allosteric modulation and binding kinetics of ligands at the $K_v11.1$ channel have been thoroughly studied in this thesis. The general conclusions and future perspectives for this field of research have been summarized in **Chapter 8**. Hopefully, the findings in this thesis will add to the current understanding in ligand- $K_v11.1$ interactions, and also provide effective opportunities for abrogating $K_v11.1$ -induced cardiotoxicity.

References

1. Bagal, S. K.; Brown, A. D.; Cox, P. J.; Omoto, K.; Owen, R. M.; Pryde, D. C.; Siders, B.; Skerratt, S. E.; Stevens, E. B.; Storer, R. I.; Swain, N. A. Ion channels as therapeutic targets: A drug discovery perspective. *J. Med. Chem.* **2012**, *56*, 593-624.
2. Restrepo-Angulo, I.; Vizcaya-Ruiz, D.; Camacho, J. Ion channels in toxicology. *J. Appl. Toxicol.* **2010**, *30*, 497-512.
3. Camerino, D. C.; Tricarico, D.; Desaphy, J.-F. Ion channel pharmacology. *Neurotherapeutics* **2007**, *4*, 184-198.
4. Ruetsch, Y. A.; Boni, T.; Borgeat, A. From cocaine to ropivacaine: The history of local anesthetic drugs. *Curr. Top. Med. Chem.* **2001**, *1*, 175-182.
5. Sanguinetti, M. C.; Tristani-Firouzi, M. hERG potassium channels and cardiac arrhythmia. *Nature* **2006**, *440*, 463-469.
6. Mathes, C. Ion channels in drug discovery and development. *Drug Discov. Today* **2003**, *8*, 1022-1024.
7. Lerche, H.; Jurkat-Rott, K.; Lehmann-Horn, F. Ion channels and epilepsy. *Am. J. Med. Genet.* **2001**, *106*, 146-159.
8. Li, S.; Wong, A. H.; Liu, F. Ligand-gated ion channel interacting proteins and their

role in neuroprotection. *Front Cell. Neurosci.* **2014**, *8*, 1-5.

9. Hogg, R. C.; Buisson, B.; Bertrand, D. Allosteric modulation of ligand-gated ion channels. *Biochem. Pharmacol.* **2005**, *70*, 1267-1276.

10. Harmar, A. J.; Hills, R. A.; Rosser, E. M.; Jones, M.; Buneman, O. P.; Dunbar, D. R.; Greenhill, S. D.; Hale, V. A.; Sharman, J. L.; Bonner, T. I.; Catterall, W. A.; Davenport, A. P.; Delagrangé, P.; Dollery, C. T.; Foord, S. M.; Gutman, G. A.; Laudet, V.; Neubig, R. R.; Ohlstein, E. H.; Olsen, R. W.; Peters, J.; Pin, J.; Ruffolo, R. R.; Searls, D. B.; Wright, M. W.; Spedding, M. IUPHAR-DB: The IUPHAR database of G protein-coupled receptors and ion channels. *Nucleic Acids Res.* **2009**, *37*, D680-D685.

11. Petrushenko, Y. A. P2X Receptors: Peculiarities of the structure and modulation of the functions. *Neurophysiology* **2012**, *44*, 163-173.

12. Young, M. T. P2X receptors: Dawn of the post-structure era. *Trends Biochem. Sci.* **2010**, *35*, 83-90.

13. Adinolfi, E.; Capece, M.; Amoroso, F.; Marchi, E.; Franceschini, A. Emerging Roles of P2X receptors in cancer. *Curr. Med. Chem.* **2014**, *22*, 878-890.

14. Fotino, C.; Vergani, A.; Fiorina, P.; Pileggi, A. P2X receptors and diabetes. *Curr. Med. Chem.* **2014**, *22*, 891-901.

15. Sobolevsky, A. I. Structure and gating of tetrameric glutamate receptors. *J. Physiol.* **2015**, *593*, 29-38.

16. Stawski, P.; Janovjak, H.; Trauner, D. Pharmacology of ionotropic glutamate receptors: A structural perspective. *Bioorg. Med. Chem.* **2010**, *18*, 7759-7772.

17. Thompson, A. J.; Lester, H. A.; Lummis, S. C. The structural basis of function in Cys-loop receptors. *Q. Rev. Biophys.* **2010**, *43*, 449-499.

18. Jensen, M. L.; Schousboe, A.; Ahring, P. K. Charge selectivity of the Cys-loop family of ligand-gated ion channels. *J. Neurochem.* **2005**, *92*, 217-225.

19. Nys, M.; Kesters, D.; Ulens, C. Structural insights into Cys-loop receptor function and ligand recognition. *Biochem. Pharmacol.* **2013**, *86*, 1042-1053.

20. Sadigh-Eteghad, S.; Majdi, A.; Talebi, M.; Mahmoudi, J.; Babri, S. Regulation of nicotinic acetylcholine receptors in Alzheimer's disease: A possible role of chaperones. *Eur. J. Pharmacol.* **2015**, *755*, 34-41.

21. Ghasemi, M.; Hadipour-Niktarash, A. Pathologic role of neuronal nicotinic acetylcholine receptors in epileptic disorders: Implication for pharmacological interventions. *Rev. Neurosci.* **2015**, *26*, 199-223.

22. Del Bufalo, A.; Cesario, A.; Salinaro, G.; Fini, M.; Russo, P. Alpha9Alpha10 nicotinic acetylcholine receptors as target for the treatment of chronic pain. *Curr. Pharm. Des.* **2014**, *20*, 6042-6047.

23. Rudolph, U.; Möhler, H. GABA_A receptor subtypes: Therapeutic potential in down syndrome, affective disorders, schizophrenia, and autism. *Annu. Rev. Pharmacol. Toxicol.* **2013**, *54*, 483-507.

24. Michels, G.; Moss, S. J. GABA_A receptors: Properties and trafficking. *Crit. Rev. Biochem. Mol. Biol.* **2007**, *42*, 3-14.
25. Sands, Z.; Grottesi, A.; Sansom, M. S. Voltage-gated ion channels. *Curr. Biol.* **2005**, *15*, R44-R47.
26. Börjesson, S. I.; Elinder, F. Structure, function, and modification of the voltage sensor in voltage-gated ion channels. *Cell Biochem. Biophys.* **2008**, *52*, 149-174.
27. Frank, H. Y.; Yarov-Yarovoy, V.; Gutman, G. A.; Catterall, W. A. Overview of molecular relationships in the voltage-gated ion channel superfamily. *Pharmacol. Rev.* **2005**, *57*, 387-395.
28. Yu, F. H.; Catterall, W. A. The VGL-chanome: A protein superfamily specialized for electrical signaling and ionic homeostasis. *Sci. Signal.* **2004**, *2004*, 1-17.
29. Gutman, G. A.; Chandy, K. G.; Grissmer, S.; Lazdunski, M.; Mckinnon, D.; Pardo, L. A.; Robertson, G. A.; Rudy, B.; Sanguinetti, M. C.; Stühmer, W.; Wang, X. International union of pharmacology. LIII. nomenclature and molecular relationships of voltage-gated potassium channels. *Pharmacol. Rev.* **2005**, *57*, 473-508.
30. Wulff, H.; Castle, N. A.; Pardo, L. A. Voltage-gated potassium channels as therapeutic targets. *Nat. Rev. Drug Discov.* **2009**, *8*, 982-1001.
31. Grizel, A.; Glukhov, G.; Sokolova, O. Mechanisms of activation of voltage-gated potassium channels. *Acta Naturae* **2014**, *6*, 10-26.
32. Vandenberg, J. I.; Perry, M. D.; Perrin, M. J.; Mann, S. A.; Ke, Y.; Hill, A. P. hERG K⁺ channels: Structure, function, and clinical significance. *Physiol. Rev.* **2012**, *92*, 1393-1478.
33. Babcock, J. J.; Li, M. hERG channel function: Beyond long QT. *Acta Pharmacol. Sin.* **2013**, *34*, 329-335.
34. Crump, S. M.; Abbott, G. W. Arrhythmogenic KCNE gene variants: Current knowledge and future challenges. *Front. Genet.* **2014**, *5*, 1-7.
35. Nachimuthu, S.; Assar, M. D.; Schussler, J. M. Drug-induced QT interval prolongation: Mechanisms and clinical management. *Ther. Adv. Drug Saf.* **2012**, *3*, 241-253.
36. Benos, D.; Bezánilla, F.; Chien, K.; Choe, S.; Clapham, D.; Dougherty, D.; Lazdunski, M.; Levitan, I.; Lewis, R. The state of ion channel research in 2004. *Nat. Rev. Drug Discov.* **2004**, *3*, 239-278.
37. Vandenberg, J. I.; Walker, B. D.; Campbell, T. J. hERG K⁺ channels: Friend and foe. *Trends Pharmacol. Sci.* **2001**, *22*, 240-246.
38. Roden, D. M.; Viswanathan, P. C. Genetics of acquired long QT syndrome. *J. Clin. Invest.* **2005**, *115*, 2025-2032.
39. Perry, M.; Sanguinetti, M.; Mitcheson, J. Symposium review: Revealing the structural basis of action of hERG potassium channel activators and blockers. *J. Physiol.* **2010**, *588*, 3157-3167.
40. Rampe, D.; Brown, A. M. A history of the role of the hERG channel in cardiac risk

assessment. *J. Pharmacol. Toxicol. Methods* **2013**, *68*, 13-22.

41. Zhang, M.; Liu, X.; Diochot, S.; Lazdunski, M.; Tseng, G.-N. APETx1 from sea anemone *Anthopleura elegantissima* is a gating modifier peptide toxin of the human ether-à-go-go-related potassium channel. *Mol. Pharmacol.* **2007**, *72*, 259-268.

42. Jiménez-Vargas, J.; Restano-Cassulini, R.; Possani, L. Toxin modulators and blockers of hERG K⁺ channels. *Toxicon* **2012**, *60*, 492-501.

43. Zhou, P.; Babcock, J.; Liu, L.; Li, M.; Gao, Z. Activation of human ether-à-go-go related gene (hERG) potassium channels by small molecules. *Acta Pharmacol. Sin.* **2011**, *32*, 781-788.

44. Xu, X.; Recanatini, M.; Roberti, M.; Tseng, G.-N. Probing the binding sites and mechanisms of action of two human ether-à-go-go-related gene channel activators, 1,3-bis-(2-hydroxy-5-trifluoromethyl-phenyl)-urea (NS1643) and 2-[2-(3,4-dichloro-phenyl)-2,3-dihydro-1H-isoinol-5-ylamino]-nicotinic acid (PD307243). *Mol. Pharmacol.* **2008**, *73*, 1709-1721.

45. Christopoulos, A.; Changeux, J.-P.; Catterall, W. A.; Fabbro, D.; Burris, T. P.; Cidlowski, J. A.; Olsen, R. W.; Peters, J. A.; Neubig, R. R.; Pin, J.; Sexton, P. M.; Kenakin, T. P.; Ehlert, F. J.; Spedding, M.; Langmead, C. J. International union of basic and clinical pharmacology. XC. multisite pharmacology: Recommendations for the nomenclature of receptor allosterism and allosteric ligands. *Pharmacol. Rev.* **2014**, *66*, 918-947.

46. Vogt, A. D.; Di Cera, E. Conformational selection or induced fit? A critical appraisal of the kinetic mechanism. *Biochemistry* **2012**, *51*, 5894-5902.

47. Pan, A. C.; Borhani, D. W.; Dror, R. O.; Shaw, D. E. Molecular determinants of drug-receptor binding kinetics. *Drug Discov. Today* **2013**, *18*, 667-673.

48. Copeland, R. A.; Pompliano, D. L.; Meek, T. D. Drug-target residence time and its implications for lead optimization. *Nat. Rev. Drug Discov.* **2006**, *5*, 730-739.

49. Lu, H.; Tonge, P. J. Drug-target residence time: Critical information for lead optimization. *Curr. Opin. Chem. Biol.* **2010**, *14*, 467-474.

50. Redfern, W. S.; Carlsson, L.; Davis, A. S.; Lynch, W. G.; MacKenzie, I.; Palethorpe, S.; Siegl, P. K. S.; Strang, I.; Sullivan, A. T.; Wallis, R.; Camm, A. J.; Hammond, T. G. Relationships between preclinical cardiac electrophysiology, clinical QT interval prolongation and torsade de pointes for a broad range of drugs: Evidence for a provisional safety margin in drug development. *Cardiovasc. Res.* **2003**, *58*, 32-45.

51. Di Veroli, G. Y.; Davies, M. R.; Zhang, H.; Abi-Gerges, N.; Boyett, M. R. High-throughput screening of drug-binding dynamics to hERG improves early drug safety assessment. *Am. J. Physiol. Heart Circ. Physiol.* **2013**, *304*, H104-H117.

52. Di Veroli, G. Y.; Davies, M. R.; Zhang, H.; Abi-Gerges, N.; Boyett, M. R. hERG inhibitors with similar potency but different binding kinetics do not pose the same proarrhythmic risk: Implications for drug safety assessment. *J. Cardiovasc. Electrophysiol.* **2014**, *25*, 197-207.

53. Townsend, C. Is there a need to add another dimension (time) to the evaluation of the arrhythmogenic potential of new drug candidates in vitro? *Circulation* **2014**, *130*, 219-220.
54. Hill, A. P.; Perrin, M. J.; Heide, J.; Campbell, T. J.; Mann, S. A.; Vandenberg, J. I. Kinetics of drug interaction with the K_v11.1 potassium channel. *Mol. Pharmacol.* **2014**, *85*, 769-776.



Chapter 2

Kinetic studies of the $K_v11.1$ (hERG) channel

Zhiyi Yu
Sinziana Cristea
Martin B. Rook
Laura H. Heitman
Adriaan P. IJzerman



Abstract

The $K_v11.1$ channel, encoded by the human ether-à-go-go-related gene (hERG), mediates a rapid delayed rectifying potassium current (I_{kr}) underlying repolarization of the cardiac action potential. This channel has been proven to be involved in a diversity of physiologic and pathological processes. “Loss-of-function” mutations in the gene or blockade of the channel by a wide range of prescription medications can prolong the cardiac action potential duration (APD), producing the long QT syndrome (LQTS) that is associated with a markedly increased risk of ventricular arrhythmias and sudden cardiac arrest. On the other hand, “gain-of-function” mutations in the gene shorten the ventricular APD and cause the short QT syndrome (SQTs). Accordingly, the $K_v11.1$ channel has elicited intense scientific interest in the past several decades. The counter-intuitive gating kinetics of the channel have been suggested to play a specific role in suppressing arrhythmias, and recent studies have pointed out the requirement of incorporating ligand binding kinetics with channel block affinity to refine the $K_v11.1$ liability of drug candidates. In this review, the biogenesis, structure, function, and pharmacological applications of the $K_v11.1$ channel are briefly outlined first. Afterwards, the unusual gating kinetics of the channel together with the influences on its gating are summarized. Finally, binding and corresponding kinetics of ligands at the channel as well as assay conditions and techniques for measuring these parameters are discussed.

Introduction

Ion channels are membrane-spanning proteins that conduct ions across the cell and internal organelle membranes. They are involved in a tremendously diverse range of fundamental physiological processes, from rapid responses driven by the neuronal system or fast contractile forces produced by skeletal and smooth muscles to more protracted procedures such as cell growth, differentiation and migration.¹ After G protein-coupled receptors (GPCRs), ion channels constitute the second largest target class for known drugs.² Potassium-selective channels, represented by some 70 known loci in the mammalian genome, are the largest and most diverse group of ion channels.³ This superfamily of potassium channels is mainly divided into three groups: voltage-gated potassium channels (K_v), inward rectifying potassium channels (K_{ir}) and calcium-activated potassium channels (K_{Ca}). Of these, K_v channels are the largest group, and they are encoded by 40 genes and further divided into 12 subfamilies (K_v1-12).⁴

The K_v11 family name, “ether-à-go-go” (EAG) coined by Kaplan and Trout in 1969, was a humorous reference to the similarity between the go-go dancers of the 1960s and the way the legs of a mutant fly shake under ether anesthesia.⁵ In this family, the $K_v11.1$ channel, of which the pore-forming subunit is encoded by the human ether-à-go-go related gene (hERG), has received the greatest scientific scrutiny due to its association with potentially life-threatening cardiac arrhythmias. The $K_v11.1$ channel is often referred to by several partial synonyms: KCNH2 and hERG to the gene, I_{Kr} to the native current, and $K_v11.1$ to the fully assembled channel. Missense mutations on human chromosome 7 where KCNH2 is located or pharmacological blockade of the $K_v11.1$ channel lead to a prolongation of the action potential (AP) duration (APD) that could translate into long QT syndrome (LQTS), Torsades de Pointes (TdP) and sudden death.^{5,6} Electrophysiological studies on these mutants and $K_v11.1$ blockers have revealed that gating kinetics of the channel play an important role in I_{Kr} suppression.⁷⁻⁹ Moreover, the assessment of $K_v11.1$ liability for drug candidates only with IC_{50} values is considered to be unrefined. Therefore, more attention should be paid to the binding kinetics of ligands at the channel in order to achieve a better understanding of the underlying mechanisms of drug actions and subsequently to evaluate more comprehensively their proarrhythmic profiles.¹⁰ In this context, this review will focus on gating kinetics and ligand binding kinetics investigated on the $K_v11.1$ channel as well as a general introduction of the channel production cycle, its structure, physiological functions, and pharmacological applications during the drug development process.

Production and degradation of the $K_v11.1$ channel

The production of the $K_v11.1$ channel begins in the nucleus with transcribing *KCNH2* to mRNA, which then acts with the ribosome to synthesize polypeptides. The resulting polypeptide chains are assisted by cytosolic chaperones (heat shock protein 70 [Hsp70] and 90 [Hsp90]) to prevent misfolding or protein degradation, and are further used in the formation of channel subunits in the endoplasmic reticulum.¹¹ The produced subunits assemble into a tetramer (immature channel) that is exported to the Golgi apparatus, where the channel undergoes a complex glycosylation to obtain a mature and stable conformation before being trafficked to the plasma membrane. The $K_v11.1$ trafficking is an essential process that contributes to the maturation of the channel ensuring its proper physiological functions.¹¹ In some cases, the defective trafficking of mutant channels results in a QT interval prolongation, which can be rescued by pharmacological chaperones that stabilize the $K_v11.1$ channel by binding to specific sites of the channel inner pore.⁵ On the other side, degradation of mature channels occurs in lysosomes after being internalized in endocytic vesicles and tagged with ubiquitin. In addition, when the $K_v11.1$ maturation process is defective, its subunits are also tagged by ubiquitination for degradation and further transferred to the proteasomes or recycled via recycling endosomes. The $K_v11.1$ channel density at the cell surface is determined by the balance between the transport of mature channels to the cell membrane and their corresponding degradation.

Structural features and physiological functions of the $K_v11.1$ channel

Structure

Consistent with other K_v channels, the $K_v11.1$ channel has a tetrameric structure formed by four α -subunits (**Figure 1A**) and auxiliary subunits. As shown in **Figure 1B**, each α -subunit is composed of six transmembrane segments that constitute two major domains with helices S1-S4 contributing to the voltage-sensing domain (VSD) and helices S5-S6 together with the pore loop outlining the pore domain. The VSD undergoes conformational changes upon perturbation of the transmembrane potential through an array of positively charged residues located within S4 helices, whereby the lengthy S5-Pore linker, also known as the “turret”, is a peculiar feature of the $K_v11.1$ channel. The α -subunits co-assemble along the pore axis to form the cavity and selectivity filter (SF) of the channel to allow the central ion conduction. The stability of the SF (**Figure 1C**) is dominated by the

interaction of surrounding pore helices with filter residues.⁶ With regard to the auxiliary subunits, a β -subunit, MinK-related peptide 1 (MiRP1), has an important role in accelerating I_{Kr} deactivation and modulating the response of the $K_v11.1$ channel to drugs.¹² Missense mutations in the KCNE2 gene encoding the MiRP1 have been identified to associate with LQTS and ventricular fibrillations.¹³ Notably, the expression levels of MiRP1 in atria and ventricular muscle appear to be low, and thus, exert minor effects on biophysical and pharmacological properties of the channel.¹⁴ However, it is highly expressed in Purkinje fibers of the ventricular conduction system and atrial pacemaker cells.

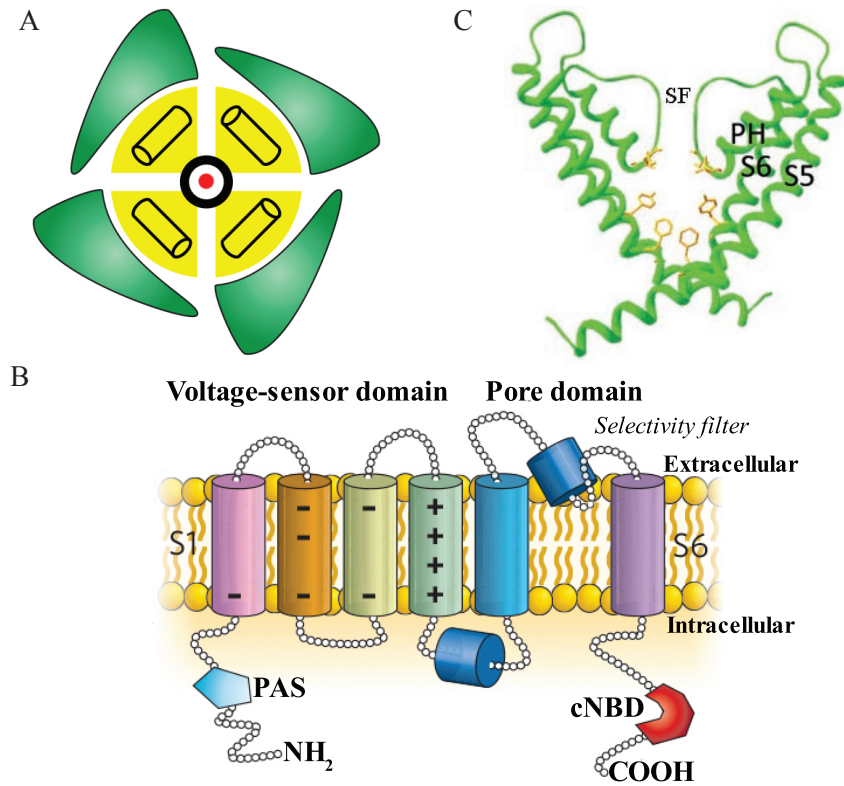


Figure 1. (A) The tetrameric structure of the $K_v11.1$ channel with the voltage-sensing domain (VSD) colored in green and pore region in yellow, and the red dot representing the potassium ions flow.⁵ (B) Schematic diagram of a single $K_v11.1$ subunit containing 6 α -helical transmembrane domains (S1-S6).⁶ (C) Homology model of the selectivity filter (SF) of the $K_v11.1$ channel based on the crystal structure of the $K_v1.2$ channel.¹⁵

Like all other potassium channels, the structure of the $K_v11.1$ channel is mainly divided into transmembrane and cytoplasmic regions. The four α -subunits and auxiliary subunits are located in the transmembrane segment, while the NH₂- and COOH-terminals are arranged at the cytoplasmic side. The extracellular loop

between S5 and the pore region contains a glycosylation site that is important for maturation and trafficking of the channel protein.⁸ The NH₂-terminal contains a Per-Arnt-Sim (PAS) domain and a stretch of 240 amino acids that are responsible for protein trafficking and definition of the K_v11 family, respectively.^{5, 16} On the other hand, the COOH-terminal linked to the S6 helice consists of a cyclic nucleotide binding site (cNBD), contributing to the opening and closure of the permeation pathway for ions. A major difference between the K_v11.1 channel and other 6-transmembrane domain potassium channels is derived from the vestibule site. The K_v11.1 channel has a larger central cavity due to the absence of a Pro-X-Pro (XPX) motif from the S6 domain that causes the inner helices to bend in other potassium channels.¹⁷ This structural openness is also supported by drug-trapping experiments which indicate that the K_v11.1 channel can accommodate a wide variety of structurally diverse drugs and large molecules.¹⁸ These K_v11.1 blockers are able to access the binding sites inside the pore, within S6 domains and the end of pore helices, where the important residues for high-affinity blockade of compounds are located.³

Physiological functions

The K_v11.1 channel is expressed in multiple organs including heart, central nervous system (CNS), gastrointestinal tract (GIT) and endocrine system, and its physiological functions differ according to their distributions in these specific tissues.^{6, 19} In the CNS of mammals this channel maintains the membrane potential and development of neurons of the spinal cord and carotid glomus cells, whereas it regulates the gut motility in the GIT. In the endocrine system the K_v11.1 channel has been found to be involved in insulin secretion and epinephrine release in chromaffin cells. Apart from these functions, the K_v11.1 channel has a dominant presence in normal human cardiomyocytes where its physiological function is best characterized.

As shown in **Figure 2**, the generation of the myocardial AP reflects the sequential activation and inactivation of a series of ion channels, and the AP can be divided into five different phases.^{6, 20, 21} In Phase 0, a rapid depolarization occurs when the openings of potassium channels decrease and fast sodium channels open. During Phase 1, there is an early and fast repolarization mainly due to the inactivation of sodium channels and activation of the transient outward potassium channels (I_{to}). Thereafter, the activation of the long opening calcium channels (L-type Ca²⁺, I_{Ca}) produces a small steady influx of Ca²⁺, which counteracts the outward K⁺ currents induced by an ultra-rapid potassium delayed rectifier. This leads to the formation of a prolonged plateau called Phase 2. The repolarization

in Phase 3 is rapid and robust, and it is initiated by deactivation of sodium and calcium channels and activation of $K_v11.1$ (I_{Kr}) and $K_v7.1$ (I_{Ks}) channels. The $K_v11.1$ channel plays a very important role in Phase 3 repolarization because of its unique gating kinetics: slow activation and fast inactivation coupled to fast recovery from inactivation and slow deactivation. This rapid and delayed rectifier potassium currents (I_{Kr}) terminate the cardiac AP and return the membrane potential to baseline (Phase 4). Since the $K_v11.1$ channel closes (de-activates) slowly towards the end of the repolarization, there is a constant efflux of potassium ions through the channel. Thus, the resting cell membrane potential is close to the Nernst equilibrium potential for potassium. This also contributes to the refractoriness of cardiac cells in the early diastolic period immediately after repolarization.⁵ When a premature beat occurs during the early diastolic period, a large outward current antagonizes the depolarization of the cell and thus propagation of the beat. In this case, functional reduction of I_{Kr} by “loss-of-function” mutations or pharmacological blockade on the $K_v11.1$ channel translates into a clinical setting in patients prone to arrhythmias determined by premature beats. As shown in **Figure 2**, different waveforms in the electrocardiogram (ECG) reflect distinct phases of the APD in a cardiomyocyte.

Target and antitarget of the $K_v11.1$ channel in drug development

Roles in cancer

Changes in the expression of the $K_v11.1$ channel have been associated with dysregulations of cell proliferation in a plethora of tumor types from different cell lineages. The $K_v11.1$ channel in tumor cells has been postulated to facilitate cell migration in diverse hematopoietic neoplasm through an integrin-related signaling pathway and to enhance the proliferation, invasiveness and lymph node dissemination of cells as well as to reduce cell differentiation.^{23, 24} By contrast, the $K_v11.1$ channel has not been expressed at a significantly high levels in the corresponding non-cancerous cells. Therefore, the $K_v11.1$ channel, in different tissues, may be used as a biomarker for abnormal cell behaviors and proliferation. Nevertheless, the $K_v11.1$ channel has also been unraveled to induce cell apoptosis in various cell types by different mechanisms, independent of their capacity to inhibit cell proliferation via cell cycle arrest.²⁴ Further exploration of this apoptotic pathway together with the channel up-regulation in different tumor types may lead to the development of new anti-tumor therapies in the future. For instance, leukemia is a type of cancer that originates from the bone marrow hematopoietic

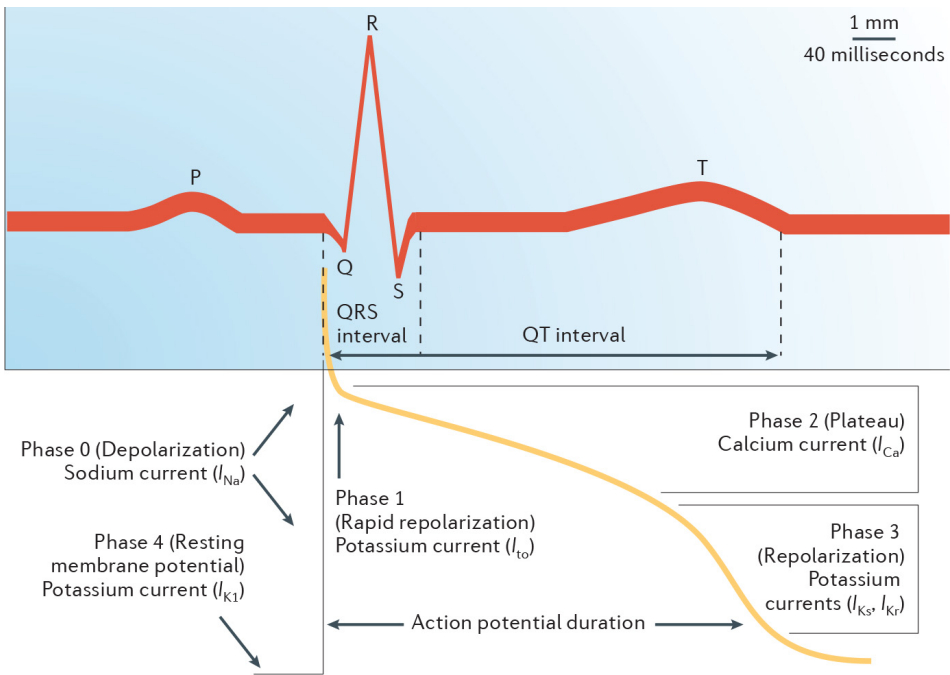


Figure 2. Standard model of the cardiomyocyte QT interval on an electrocardiogram (upper panel) and the corresponding action potential duration (lower panel). The QT interval is a measure of the duration of ventricular depolarization and subsequent repolarization.²²

stem cells. $K_v11.1$ channels are expressed in $CD34^+/CD38^-/CD123^{high}$ cells and induce significant proliferation of leukemia cells, whereas they are not detected in normal bone marrow cells.²⁵ Thus, a specific $K_v11.1$ blocker could be used to potentially prevent leukemia via reducing abnormal cell proliferation without affecting healthy cells that do not express the $K_v11.1$ channel. Taken together, the $K_v11.1$ channel may be used as a novel diagnostic and prognostic marker in human cancers as well as a new target for anti-neoplastic treatments.

Roles in schizophrenia

The contribution of the native $K_v11.1$ channel to the intrinsic electrical properties of neurons is poorly understood. $K_v11.1-3.1$ is the primate specific isoform of the $K_v11.1$ channel expressed in the CNS, and it has been associated with schizophrenia.²⁶ In this isoform the first 102 amino acids of the most abundant isoform $K_v11.1-1a$ are replaced with 6 amino acids, which results in faster channel deactivation but slower inactivation rates. Although both isomers are comparably expressed at the hippocampus and prefrontal cortex in a control group, the ex-

pression ratio of $K_v11.1-3.1$ to $K_v11.1-1a$ demonstrates an approximate 2.5-fold increase among patients with schizophrenia. Investigations on the $K_v11.1$ channel in neural cells may facilitate our understanding of the pathology of schizophrenia, and would provide a new solution for treating this mental disorder in the future.

Roles in smooth muscle related diseases

The $K_v11.1$ channel is pH sensitive, implying a molecular link for regulating electrical signaling through acidity of the gastrointestinal lumen. Several antibiotics like erythromycin display such adverse reactions as cramps and diarrhea, which might be caused by unintentional blockade of the $K_v11.1$ channel.²⁴ Akbarali *et al.* reported that the $K_v11.1$ channel fine-tuned the resting membrane potential of the circular smooth muscle cells in opossum esophagi, and channel blockers initiated the contraction of muscle segments by depolarization.²⁷ In human jejunum the $K_v11.1$ channel was immunohistochemically detected in circular and longitudinal smooth muscle cells, where it was assumed to have a fundamental role in controlling the motility patterns by modulating the electrical behavior of muscle cell.²⁸ Administration of methanesulfonanilide $K_v11.1$ blockers like E-4031 and MK-499 impacted the rhythmic contractions of jejunum. Altogether, these findings could help in the search for new targets for the treatment of gastro-esophageal reflux diseases, achalasia as well as intestinal motility disorders.

Human uterine contractions are triggered by an AP possessing a spike followed by prolonged depolarization.²⁹ Activation of the $K_v11.1$ channel results in the inactivation of the AP by suppressing the amplitude and duration of contraction before labor. In obese women, enhancement of the $K_v11.1$ activity by reducing the expression of β -inhibitory proteins shortened the duration of uterine APs and weakened contractions. This finding offers an explanation for the higher incidence of caesarian delivery in obesity, which should be further studied as it offers a new insight into the poor labor outcomes of obese women.

Roles in endocrine dysregulations

In human pancreatic islets, the $K_v11.1$ channel has been proven to contribute to the regulation of insulin secretion and the firing of β -cells.³⁰ Blockade of the $K_v11.1$ channel is sufficient to cause hyper-excitability during application of the insulin releasing drugs. This suggests that alterations in the channel function might be associated with some hyperinsulinemic conditions. The role of the $K_v11.1$ channel in hyperinsulinemic conditions is awaiting further elucidation that may lead to the discovery of more effective treatment for diabetes.

Roles in arrhythmia

Cardiac arrhythmias, anything from mild palpitations to severe conditions that have the potential to induce cardiac arrest or sudden death, are a major mortality cause in developed countries. The $K_v11.1$ channel has been suggested to play a particularly pivotal role in the suppression of arrhythmias, yet it has also been found to account for 30-40% of congenital LQTS cases and is the most common cause of drug-induced arrhythmias and cardiac death all over the world.^{31, 32}

The $K_v11.1$ channel as a target in arrhythmology

The short QT syndrome (SQTS) is a cardiac channelopathy associated with atrial fibrillation and sudden cardiac death.⁴ The SQTS type 1 variant (SQTS1) involves mutations at KCNH2 that encodes the α -subunit of the $K_v11.1$ channel.^{33, 34} Brugada *et al.* identified two different missense mutations at position 588 in the S5-P loop region (i.e. N588K) of the $K_v11.1$ channel, which were linked to the hereditary SQTS. These mutations resulted in a dramatic increase in I_{Kr} leading to a heterogeneous shortening of the APD and refractoriness.⁵ For this SQTS1, class III antiarrhythmic drugs, also known as $K_v11.1$ blockers, may be a therapeutic approach for controlling dysregulations of the cardiac rhythm by lengthening the APD and increasing the myocardial refractoriness without significantly altering the conduction velocity.³⁵ Notably, the sensitivity of SQTS1 to distinct $K_v11.1$ blockers differs in normalizing the shortening of QT intervals. For example, quinidine restored the shortened QT interval towards a normal range, whereby administration of sotalol and ibutilide in the same condition failed to normalize the abnormal QT interval.³⁶ This could be explained by the state-dependent inhibition of $K_v11.1$ blockers to the channel, as the N588K- $K_v11.1$ channel exhibits altered voltage-dependent inactivation kinetics compared to the wild type channel.

Missense mutations of the KCNH2 gene are also associated with LQTS type 2 variant (LQTS2) and an increased risk for sudden cardiac death. There are four classes of mechanisms determining the LQTS2 abnormalities, acting on $K_v11.1$ synthesis (class 1), intracellular transport or protein trafficking (class 2), channel gating (class 3) and potassium ion permeation (class 4). Anderson *et al.* performed two comprehensive analyses on 201 LQTS2-linked mutations in four structural domains (NH₂- and COOH-terminus, S1-S4 [VSD], S5-S6 [pore region], extracellular and intracellular linkers), and confirmed that the most common underlying mechanism for LQTS2 was the disturbance of protein trafficking (class 2).³⁷ Therefore, correction of the $K_v11.1$ trafficking deficiency could become a useful therapeutic principle in rescuing LQTS2. Most mutations causing trafficking defects can be pharmacologically amended by highly selective $K_v11.1$ blockers like

E-4031.³⁸ This compound displayed the highest chance to successfully correct the LQTS2 in channels expressing mutations at the NH_2 -terminus, followed by those in the pore domain and then C-linker.³⁷ Nevertheless, when the wild type $K_v11.1$ channel was co-expressed, the correction ability of E-4031 changed priorities to mutations in the pore domain followed by the ones in the NH_2 -terminus and finally these at the C-linker site. Additionally, $K_v11.1$ activators, which can augment the I_{Kr} , offer another novel anti-arrhythmic strategy for treatment of LQTS2. The first $K_v11.1$ activator RPR260243 was reported in 2005,³⁹ and only a limited number of such compounds have been available until now. Although these activators have shown pronounced antiarrhythmic effects in various *in silico*, *in vitro* and *in vivo* models, they are found to induce other proarrhythmic side effects such as increasing the APD dispersion³¹ and shortening the APD. Overall, activation of the $K_v11.1$ channel is a new research area, which remains to be exploited in the future.

$K_v11.1$ -related cardiotoxicity

As mentioned previously, mutations of the $K_v11.1$ channel affect heart conditions characterized by “loss-of-function” or “gain-of-function”, which are related to LQTS (**Figure 3A**) and SQTs (**Figure 3B**), respectively. A genetic heterogeneous disorder induced by “gain-of-function” mutations of the $K_v11.1$ channel is the congenital SQTs, which is identified by a shortened QT interval (< 330 ms) and episodes of syncope, paroxysmal atrial fibrillation or life-threatening arrhythmias.³⁶ On the other hand, the LQTS represents a cardiac clinical condition involving the $K_v11.1$ channel, which is characterized by “loss-of-function” of the channel. LQTS can be either congenital or acquired. Congenital LQTS is caused by mutations disrupting the channel functions as described previously. Mutations often lead to deficiencies in protein trafficking, which reduces the amounts of functional $K_v11.1$ channels located in the cell membrane.³⁶ Although mutations at other ion channels can also result in LQTS, the reported LQTSs are dominated by the $K_v11.1$ and $K_v7.1$ channels. Acquired LQTS refers to drug induced prolongation of the QT interval. This response may be induced by a specifically designed drug that blocks the cardiac repolarizing currents through binding to either the $K_v11.1$ channel (e.g., dofetilide, sotalolol, ibutilide) or to other ion channels involved in cardiac repolarization (e.g., alfuzosin to the sodium channel).⁴⁰ However, almost all drugs known to cause acquired LQTS appear to preferentially block the $K_v11.1$ channel. Furthermore, QT prolongation may arise as a side effect from compounds designed to act on non-cardiac targets. Drugs that belong to different chemical classes and possess various therapeutic indications are able to exert cardiotoxic effects by interfering with the $K_v11.1$ channel, such as antihistamines

(e.g., terfenadine), gastrointestinal prokinetic agents (e.g., cisapride), psychoactive agents (e.g., chlorpromazine) and antibiotics (e.g., cotrimoxazole).¹² To date, the most common cause of withdrawal from or restrictions of drugs in the market is related to their potential to cause QT prolongations and TdP via blockade of the $K_v11.1$ channel. This underlines the importance of early evaluation of possible blockade of the $K_v11.1$ channel for drug candidates, desirably in the early phase of drug development.

Several factors have been identified to account for the promiscuity of the $K_v11.1$ channel towards drug binding.^{6, 12, 41} Firstly, two aromatic residues Tyr652 and Phe656 are highly conserved in the $K_v11.1$ channel, and they are critical for the binding of structurally diverse drugs. A number of drugs can form a cation- π interaction between their positively charged nitrogen atoms and Tyr652 as well as a hydrophobic attraction of aromatic rings with Phe656. Secondly, the $K_v11.1$ channel lacks a PXP motif on the S6 helix leading to a large size of the inner cavity, which makes the channel accommodate a range of $K_v11.1$ blockers encompassing ample molecules. Lastly, multiple distinct binding sites for drugs at the $K_v11.1$ channel have been discovered, such as an intracellular binding pocket for dofetilide and an extracellular binding region for BeKm-1.⁴² This provides another reasonable explanation for the promiscuity of the $K_v11.1$ channel towards drug binding. Therefore, it is now common practice for pharmaceutical industry to screen for $K_v11.1$ liability in new chemical entities and conduct thorough clinical QT studies for potential drug candidates. In spite of the seriousness of $K_v11.1$ related-cardiotoxicity of drugs, the exact molecular and physiological interrelationships behind $K_v11.1$ blockade, QT prolongation and TdP remain to be explored. As shown in **Figure 2**, depolarization and repolarization of cardiac myocytes are complex processes that result from multiple competing and complementing ionic currents. For example, the potent $K_v11.1$ blocker verapamil does not display a repolarization liability due to its inhibition of the inward calcium current.^{40, 43} In this context, a Comprehensive *in vitro* Proarrhythmia Assay (CiPA) has been proposed as a novel safety screening proposal intended to replace the current regulatory guideline by July 2015.^{44, 45} Other strategies considering both affinity and kinetic indicators have also been proposed in order to improve the assessment of arrhythmic side effects for drug candidates.^{46, 47}

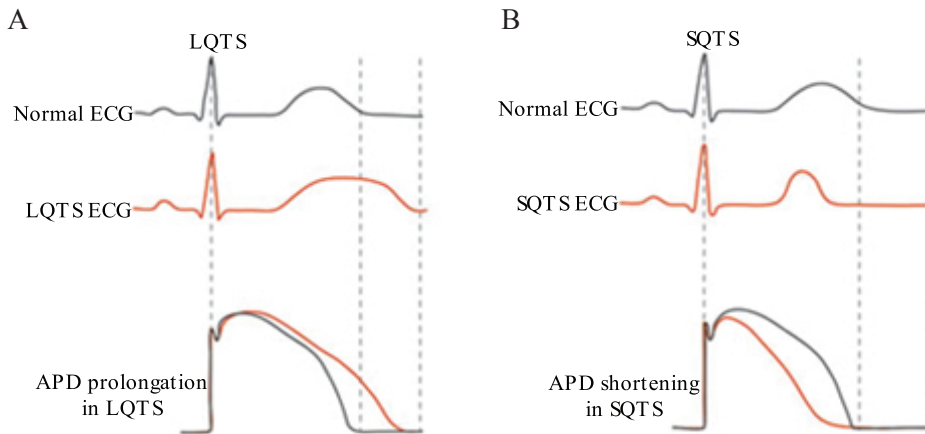


Figure 3. Schematic diagrams depicting the correlation of ventricular action potential duration (APD) to body-surface electrocardiogram (ECG) in normal, LQTS and SQTS patient groups. **(A)** Representation of an LQTS; **(B)** Representation of an SQTS.⁴⁸

Gating kinetics of the $K_v11.1$ channel

Voltage gated potassium channels regulate the selective conduction of K^+ across biological membranes by opening and closing the pore via structural rearrangement of the activation and/or inactivation gates. These gates are located at both intracellular and extracellular entrances of the SF, and the mediating process is referred to as gating kinetics.⁴⁹

The two gates of the $K_v11.1$ channel control the potassium flow through the channel. The activation gate is arranged at the intracellular side and formed by four S6 segments with slow movement to open and closed states, while the inactivation gate is located at the extracellular region of the pore and constituted by four SF segments with rapid movement to an inactivated state. The pore of the $K_v11.1$ channel is more stable in the open conformation compared to other voltage-gated potassium channels.⁵⁰ The voltage-sensor of the $K_v11.1$ channel consists of positively charged residues on the S4 domain and mediates the channel opening.⁵ Additionally, the $K_v11.1$ channel has three extra negative charges in the VSD, which makes it different from other voltage-gated potassium channels that possess only three negative charges on S2 and S3 segments.⁵¹ All these negative charges stabilize the positive charges on the S4 segment by forming salt bridges, influencing the movement of the S4 relative to other transmembrane segments during the gating.

Compared to most voltage-gated potassium channels, the gating kinetics of the $K_v11.1$ channel are unique: the transition rates of inactivation and recovery from inactivation are more rapid than the kinetics of activation and deactivation

(Figure 4).⁵¹ The time constant of inactivation for the $K_v11.1$ channel aligns from 6.5 to 2.2 ms in the voltage range of -10 to +30 mV, whereas its activation time constant is more than 50 ms at a voltage of +50 mV. By comparison, the durations of inactivation and activation at the same voltage ranges for the Shaker channel were approximately 2000 ms and less than 2 ms, respectively. The quick removal of inactivation at the depolarizing pulse as well as a slow deactivation leads to the formation of a “hook” (tail) current following repolarization, which is typical for the $K_v11.1$ channel and can be observed in various macroscopic I_{Kr} recordings.⁵²

Activation and deactivation

The activation and deactivation processes of the $K_v11.1$ channel are relatively slow compared to other voltage-gated potassium channels. The slow activation gating is caused by the slow movement of the VSD. The electrostatic interaction between Asp540 and Arg665 mediates the coupling between the VSD and S6 segment. Mutations on these residues were found to affect the activation and deactivation rates of the $K_v11.1$ channel, implicating that they play an important role in stabilizing the intermediate states in the activation process.⁵³ The slow deactivation kinetics is maintained by the unique cytosolic domains of the channel, in particular the proximal N-terminal domain.⁵⁴ Smith *et al.* confirmed that deleting the NH_2 terminus and adding a recombinant protein corresponding to the PAS domain accelerated the channel deactivation rate. Comparable to deletion of the entire NH_2 terminus, disruption of the α -helix at the NH_2 tail by substitutions of glycine or serine led to an increase of the $K_v11.1$ deactivation rate. Similarly, $K_v11.1$ channels, which have the N-terminal and PAS domains removed or Asp774, Glu788 and Asp803 mutated by arginine, exhibited much faster deactivation gating kinetics in contrast to the wild type channels.⁵⁵ However, this amendment did not alter the activation gating kinetics of the $K_v11.1$ channel. Of note, voltage dependency of activation and deactivation was insensitive to the potassium concentrations at the extracellular face of the channel.⁵²

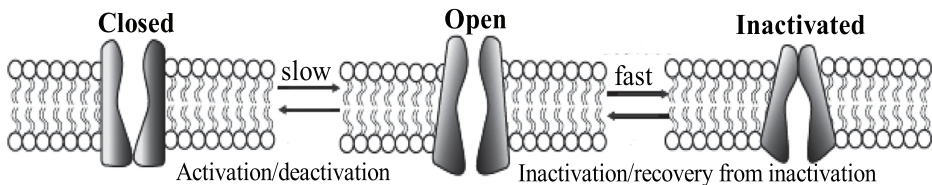


Figure 4. Different $K_v11.1$ channel conformations in the closed, open and inactivated states.⁵⁶

Inactivation and recovery from inactivation

Inactivation kinetics of the $K_v11.1$ channel comprise the forward (inactivation) and backward (recovery from inactivation) transitions between the open and inactivated states.^{32, 51} These procedures are extremely fast and voltage sensitive. At depolarized potentials the channel inactivation becomes faster than activation resulting in a steady-state rectification at positive voltages, whereas the channel deactivation is much slower compared to its recovery rate from inactivated state forming a hooked tail current that is specific for the $K_v11.1$ channel.^{5, 57} The $K_v11.1$ channel only demonstrates a C-type inactivation, which is different from the N-type inactivation existing for other voltage-gated ion channels. The N-type inactivation of potassium channels is induced by an occlusion of the ion-conducting pore by the intracellular N-terminal domain, while the C-type inactivation of the $K_v11.1$ channel permits the interconversion between two conformations of the stable conducting and non-conducting SFs. Kinetic analyses have underlied the early and late pore helix motions during the inactivation process of the $K_v11.1$ channel.⁵⁸ To date, the C-type inactivation of ion channels has been better understood than N-type inactivation.³²

Effect of gating kinetics on I_{Kr}

Ion conduction is highly dependent on the SF, which is composed of four peptides with a conformational arrangement pointing toward the pore axis of the $K_v11.1$ channel. The gating kinetics influence the contributions of I_{Kr} to the AP repolarization phases.⁵⁹ The $K_v11.1$ channel is activated during the AP upstroke and plateau phases, while a fast inactivation process of the channel greatly limits the amount of outward current at positive voltages (inward rectification). As the cell membrane repolarizes to negative voltages, the $K_v11.1$ channel recovers from inactivation and reenters the open state leading to an outward “resurgent” current that facilitates further repolarization. Thereafter, the outward I_{Kr} declines at the end of the AP due to the channel deactivation as well as a decreasing driving force for outward currents. The mechanism of $K_v11.1$ rectification is closely related to voltage-gated fast inactivation. Since the inactivation of channels takes place at a much faster rate than their activation, no significant outward currents are observable during the depolarization to a high membrane potential. The rapid inactivation of the $K_v11.1$ channel and the resulting rectification are partially responsible for the prolonged plateau phase which is typical of ventricular APs.⁷

Factors modulating $K_v11.1$ gating kinetics

Apart from voltage, the gating kinetics of the $K_v11.1$ channel are susceptible to many other factors such as temperature, extracellular pH, K^+ and Ca^{2+} concentrations.⁶⁰ An increase in temperature shifted the voltage dependence of activation to a hyperpolarizing direction, whereas that of inactivation was shifted towards a depolarizing direction.⁶¹ Moreover, the rates of activation and deactivation increase with higher temperatures, but less markedly than inactivation and the reverse recovery rates. In addition, Vandenberg *et al.* emphasized that the results obtained at room temperature could not be simply extrapolated to those of 37 °C by using a single temperature scale factor for the $K_v11.1$ channel due to the temperature dependence of gating kinetics.⁶¹ When it comes to the extracellular pH, the I_{Kr} amplitude was decreased and kinetics of activation and deactivation were increased when the external pH was lowered from 7.4 to 6.0, whereas activation was accelerated by alternations of the external pH from 7.4 to 8.0.⁶² Regarding the extracellular potassium concentrations, increasing the K^+ concentration from 4 to 10 mmol·L⁻¹ produced a +10 mV shift in voltage-dependent inactivation of the $K_v11.1$ channel and slowed the inactivation time course, while reducing the K^+ concentrations 4 to 1 mmol·L⁻¹ had little influence on inactivation voltage dependence, but accelerated the inactivation time course.⁶³ By contrast, an increase in Ca^{2+} concentration from 1.8 to 10 mM did not significantly influence the inactivation kinetics of the $K_v11.1$ channel, whereby it resulted in a reduction of I_{Kr} amplitude and activation kinetics but increased the deactivation rate.⁶⁴ Thus, Ca^{2+} may interact with externally accessible channel residues and further alter the membrane potential sensitivity of the voltage-sensor responsible for activation and deactivation, while this interaction does not change the inactivation gating mechanism.

Influences of ligands on $K_v11.1$ gating kinetics

$K_v11.1$ activators are able to increase the ventricular I_{Kr} , which can be used to treat LQTS associated ventricular arrhythmias. These activators act primarily on the C-type inactivation mechanism that is strictly related to the inward rectification. Based on different action modes, $K_v11.1$ activators are classified into type 1 and 2 groups.¹⁵ The type 1 activators enhance the $K_v11.1$ function by attenuating the C-type inactivation and slowing down the deactivation rate of the channel. The study of RPR260242 revealed that this activator exerted a concentration-dependent effect on reducing the deactivation rate of the $K_v11.1$ channel and also produced a positive shift in the voltage dependent inactivation, leading to an increase in I_{Kr} amplitude.⁶⁵ RPR260242 was found to interact with two clusters

of residues located on separate domains of the channel. The first cluster had its residues located in regions S5 (L553 and F557) and S6 (N658 and V659). Interaction with this cluster affects the channel's rearrangements that are associated with the deactivation and inactivation gating of the channel. On the other hand, residues for the second cluster are located in the S4-S5 linker (V549 and L550) and S6 (I662, L666 and Y667) segment. Binding of RPR260242 to this cluster is essential to mediate the slow deactivation kinetics induced by its interaction with the first cluster residues. Type 2 $K_v11.1$ activators augment the channel activity by primarily attenuating its C-type inactivation via slowing down the rapid onset of inactivation and shifting the half maximal inactivation voltage to more depolarized potentials. Perry *et al.* reported that PD-118057 shifted the half-point for inactivation of the $K_v11.1$ channel by +19 mV and increased the peak outward current of the $K_v11.1$ channel by 136%.⁶⁶ Scanning mutagenesis and molecular modeling suggested that PD-118057 bound to a hydrophobic pocket on two different channel subunits: L646 in the S6 domain for one subunit and L622 and F619 in the pore helix for an adjacent subunit.^{15, 66}

Apart from these activators, a number of $K_v11.1$ blockers alter the gating kinetics of the $K_v11.1$ channel. Based on the existence of distinct binding regions for ligands at the channel, $K_v11.1$ blockers can be divided into small molecules and peptide analogs which interact with intracellular and extracellular binding pockets, respectively. The anesthetic drug midazolam was recently unraveled to inhibit I_{Kr} by binding to the same classical binding site within the channel pore as that for prototypical blockers.⁶⁷ This compound resulted in a small negative shift of the activation curve of the $K_v11.1$ channel, while it did not significantly impact the channel's steady-state inactivation. On the other hand, BeKm-1 is a peptide inhibitor interacting with the extracellular amino acid residues close to the external pore region of the $K_v11.1$ channel.⁴² Zhang *et al.* found that BeKm-1 drastically shifted the midpoint of the activation curve towards positive voltages, decreased the activation rate but accelerated the deactivation rate.⁶⁸ These effects can be explained by the fact that binding of the BeKm-1 molecule to the channel contacted with the S5-P linker, impacting activation and deactivation kinetics of the $K_v11.1$ channel.

Binding and corresponding kinetics of ligands at the $K_v11.1$ channel

Methods for measurements

Patch clamp technique

Voltage-gated ion channels are primarily studied using the voltage clamp/patch clamp technique, which enables the clamping of the cell membrane potential to particular voltages using square or more complex waveforms that allows the measurement of specific activities in the ion channels.⁶⁹ Since this method allows a direct and real-time measurement of ion channel activity, it has been regarded as the golden standard in performing electrophysiological investigations on ion channels. There are various patch clamp techniques and systems available, different from one another but relying on the same principle.

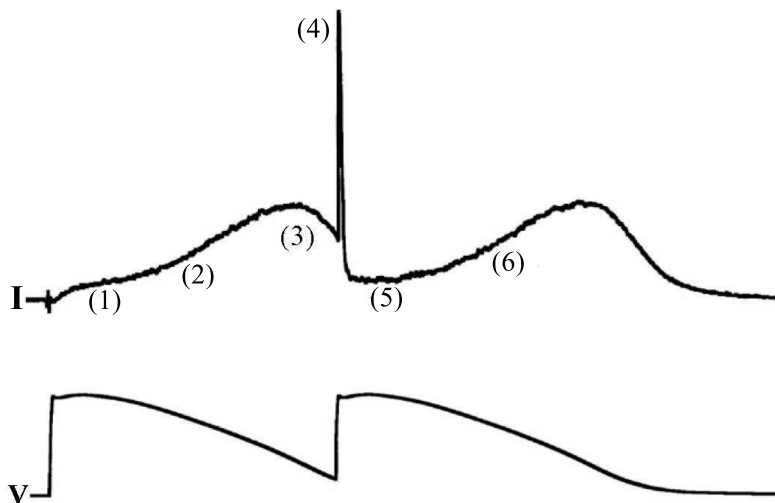


Figure 5. Example of a so-called action potential voltage clamp applied to transfected CHO cells expressing $K_v11.1$ channels ($CHOK_v11.1$ cells). Two pre-recorded action potentials from paced isolated ventricular myocytes (APs, lower panel) were used as the command voltage waveform for whole cell patch clamping the $CHOK_v11.1$ cells. The first AP in this example is followed by a second one elicited by a premature stimulus after 90% repolarization of the first AP. The resulting $K_v11.1$ currents recorded from the $CHOK_v11.1$ cells closely resemble the behavior of I_{Kr} in the native myocytes during the first and second AP (K^+ -current, upper panel).¹²

As shown in **Figure 5**,¹² the profile of current flow (upper panel) through the channel can be split into six phases: (1) the initial phase is characterized by a slow opening and fast inactivation of the $K_v11.1$ channel, limiting the current flow; (2) decreasing the voltage enables the channels to recover from inactivation, increasing the current flow; (3) a diminishment in current flow is determined by the slow deactivation and a decrease in driving force for potassium ions. At this phase, many of the channels are still in open states but pass little current; (4) applying a premature stimulus induces an increase in outward current; (5) the outward current has a rapid decay due to the rapid channel inactivation at depo-

larized potentials; (6) similar to the first phase, the large outward current in phase 6 opposes the cellular depolarization and suppresses the propagation of a premature beat. The advantage of this AP voltage clamp technique is that one can study the behavior of a single type of ion channel currents during APs without being hampered by other (often larger) ion currents that are also activated during an AP in native cells. Herein, the AP voltage clamp example implicates a mechanism foundation for other standard patch clamp recordings on the $K_v11.1$ channel.

The major difference between the $K_v11.1$ channel and other voltage-gated potassium channels is the presence of a very prominent tail current during the repolarization phase. **Figure 6** shows an example for the application of a standard voltage patch clamp assay in determining the concentration-dependent effects of cisapride on the $K_v11.1$ channel in transfected CHO cells.⁷⁰ From a holding potential of -80 mV, the cell is shortly clamped at -50 mV to test a leak current at this potential when all $K_v11.1$ channels are in closed states. Since this potential is not enough to activate the $K_v11.1$ channel, this recording is performed to correct for small background currents that do not originate from the $K_v11.1$ channel. The recorded current at -50 mV is referred to as a baseline step or leak current. This step is followed by a depolarization to +40 mV, where the $K_v11.1$ channels are alternating between the open and non-conductive, inactivated states. When repolarizing back to -50 mV, the I_{Kr} reaches its highest peak also known as the “peak tail current” due to the fast recovery of inactivated ion channels. Afterwards, the channels slowly close (de-activate). A cell responding to this voltage clamp protocol (**Figure 6A**) with a typical current signature shown in **Figure 6B** is regarded to express the $K_v11.1$ channel.

The drug concentration required to inhibit 50% of the tail current (IC_{50}) is usually determined by fitting the Hill equation to the compiled dose-response data. After the channels are exposed to compounds, a subsequent washout experiment is performed to characterize the reversibility of the inhibition. The patch clamp technique is able to identify the activity of moderately potent $K_v11.1$ blockers which could otherwise have been ignored in other assays leading to false negative results. Although the patch clamp technique is considered to be the “golden standard” in investigating the affinity and kinetic parameters of drugs at the $K_v11.1$ channel, there are several limitations to this technique. For instance, Hill *et al.* identified a limitation of any kinetic studies on drug blockade at the $K_v11.1$ channel, which is the lag time associated with drug application and washout.¹⁰ Most systems used for kinetic investigations support a lag time between 10 to 40 milliseconds that still allows recording slow time constants but causes difficulties with capturing fast time constants. Thus, drugs having low affinity and faster unblock time constants at the $K_v11.1$ channel, demonstrate more inaccurate estimates of

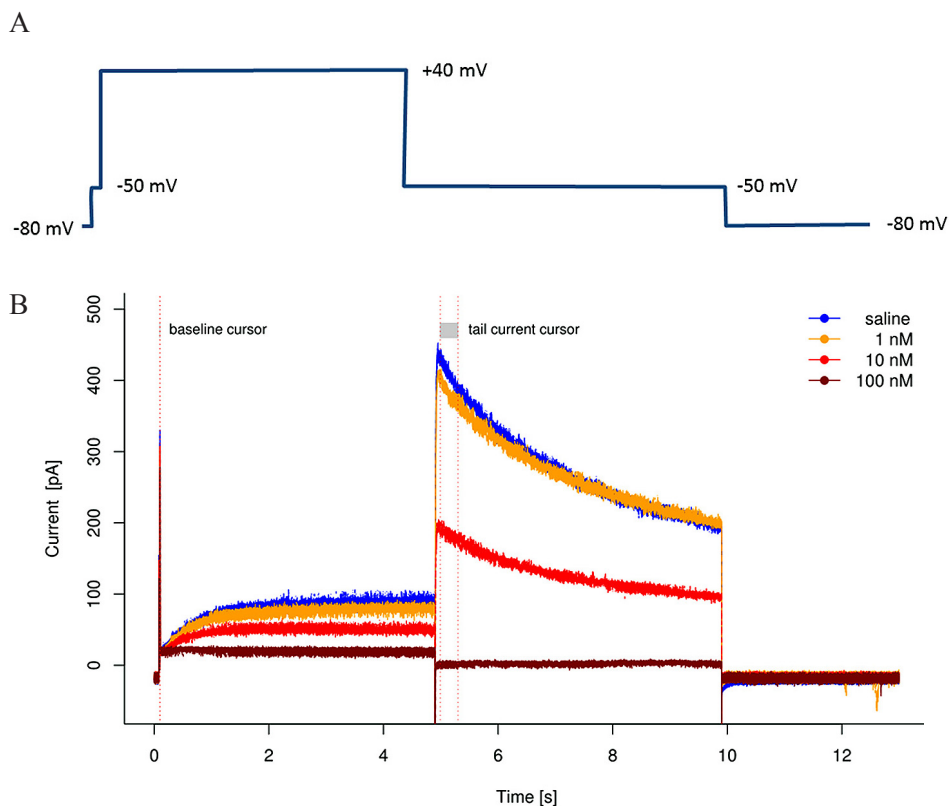


Figure 6. Example of $K_v11.1$ recordings showing the concentration-dependent effect (0–100 nM) of cisapride: **(A)** the voltage clamp protocol for I_{Kr} measurements; **(B)** I_{Kr} recordings after administration of different dosages of cisapride and saline (0 nM cisapride).⁷⁰

their fast components. Additionally, this technique is low throughput and requires a skilled operator, which hamper profiling of large compound series.⁷¹ Therefore, higher throughput assays are warranted to characterize the binding parameters of drugs candidates at the $K_v11.1$ channel in the early phase of drug development. Recently, automated patch techniques have revolutionized the research field of experimental electrophysiology, and enabled a substantial increase in throughput without compromising the data quality.^{70, 72} Moreover, the throughput of patch clamp screening can be further improved by introducing the patch clamp electrophysiology robots.⁷⁰

Radioligand binding assay

Since radioligand binding assays can provide reasonably accurate and efficient estimates of $K_v11.1$ affinity for compounds, they have become a different *in vitro* screening tools used by the pharmaceutical industries.⁵ These assays rely on

competitive binding of test ligands with a high-affinity, radiolabelled blocker to study the affinity and kinetics of unlabeled ligands at the receptor. Up to now, radioligand binding assays at the $K_v11.1$ channel have been developed for several specific and potent $K_v11.1$ blockers including [3H]dofetilide, [3H]astemizole, [3H]MK-499 and [3H]BeKm-1. In the [3H]dofetilide binding assay, the radioligand is used in conjunction with cell lines or membrane preparations expressing the $K_v11.1$ channel followed by incubation with the test compound which then competes for the binding site that is occupied by [3H]dofetilide.⁷³ This can yield the experimenter a wealth of information whether the screened compound competitively displaces [3H]dofetilide, its relative potency and, with further experimentation outlined in this thesis, the ligand's kinetics of interaction with that binding site. Diaz *et al.* demonstrated that the binding K_i values for 22 $K_v11.1$ blockers obtained in a [3H]dofetilide binding assay correlated well with their functional IC_{50} values derived from whole cell patch clamp studies.⁷⁴ Chiu *et al.* found that all their selected $K_v11.1$ blockers inhibited the binding of [3H]astemizole in a competitive manner, and consequently, developed a [3H]astemizole binding assay that they claimed to be robust with adequate sensitivity.⁷⁵ This assay is comparable to [3H]dofetilide binding experiments in terms of measured binding affinity (K_i and K_d values), with only 2- to 5-fold variations. Competitive radioligand binding assays apparently provide a rapid and highly predictive tool, which can be utilized together with electrophysiological studies to identify compounds that inhibit the $K_v11.1$ channel. Nevertheless, the binding assays have the disadvantage of being prone to produce false negative outcomes, for instance when the examined ligand binds to the channel at an allosteric site. Additionally, these assays may also provide false positives as channel modulation may need more than compound-channel binding. Accordingly, the role of radioligand binding assays in screening the $K_v11.1$ liability of drug candidates is still under discussion, and more researches should be conducted to improve the predictability of these assays.

Ion flux assay

Radioactive ion flux assay

Radiotracers are used to quantitate the flux of ions moving in or out of a cell through ion channels present on the cell membrane.⁷¹ The radiotracers of ions are specific for each class of ion channels, and $^{86}Rb^+$ is commonly used for the voltage-gated potassium channels. However, $^{86}Rb^+$ flux assays are heterogeneous, and also very slow due to the inconvenient radiotracer loading and wash steps. Furthermore, the radioactive tracers can only be applied to measure the steady-

state functions of ion channels. Additionally, an incomplete removal of extracellular tracers after loading or a continuous leak of the tracers out of cells results in a low signal-to-noise ratio for this kind of assays. Hence, although radioactive ion flux assays have been used for more than 30 years in ion channel investigations, their application for screening drug activity at ion channels like the $K_v11.1$ channel has become limited.

Non-radioactive ion flux assay

Ion flux assays with non-radioactive ion tracers using atomic adsorbance spectrometry (AAS) have been explored for a variety of voltage-gated ion channels.⁷¹ For this analysis, non-radioactive tracer ions are loaded into cells expressing the targeted ion channels (i.e. the $K_v11.1$ channel). Ion flux is initiated after channel activation performed by depolarizing the cell membrane with a high K^+ concentration buffer. Then, the concentration of the tracer ions in the supernatants and/or cells is measured, and the percentage of ion efflux (or influx) is calculated. This screening method has a moderate throughput, and it has been predominantly focused on potassium channels (e.g., Rb^+ efflux assay for the $K_v11.1$ channel).⁷⁶ The non-radioactive Rb^+ efflux assay is a high-capacity method for functional analysis of the $K_v11.1$ channel, which is particularly useful for the identification and characterization of $K_v11.1$ blockers and activators. Since this efflux assay is a direct measure of the channel activity, it is likely not prone to disturbances that usually occur in other indirect procedures, such as false positives in radioligand binding assays. Tang *et al.* compared the IC_{50} values of five known $K_v11.1$ inhibitors (dofetilide, terfenadine, cisapride, sertindole and astemizole) obtained from both the Rb^+ efflux assay and patch clamp technique.⁷⁷ The former displayed 5- to 20-fold higher IC_{50} values than the latter, yet the rank order of measured IC_{50} values for these compounds was identical in these two different experiments. This illustrates the capacity of the Rb^+ efflux assay to rank unknown compounds that block the $K_v11.1$ channel by their potency, meeting the requirements for compound profiling. In addition, Chaudhary *et al.* used the Rb^+ efflux assay to evaluate the $K_v11.1$ liability of astemizole, E-4031, cisapride, terfenadine, risperidone, quinidine and sotalol, and compared the results to those acquired in the patch clamp technique and [3H]dofetilide binding assay.⁷⁸ IC_{50} values of test ligands gathered with the efflux assay were increased compared with those from the electrophysiological technique, while the Rb^+ efflux assay was less sensitive in determining the potency of compounds but had a higher throughput to identify potent $K_v11.1$ blockers than the radioligand binding assay. Hence, the Rb^+ efflux assay allows for the rapid screening of compounds in a non-invasive manner. However, this nonradioactive ion flux assay has a low temporal resolution indicative of less

information compared to the voltage clamp assay. Meanwhile, a high expression level of $K_v11.1$ channels is necessary to achieve an acceptable signal-to-noise ratio for this technique.⁷⁹ Additionally, Rb^+ appeared to inhibit the inactivation of the $K_v11.1$ channel resulting in an underestimation of potency for most drugs, which impairs its application in drug screening for $K_v11.1$ liability.⁷⁶

Other techniques

The electrophysiological properties of cardiomyocytes expressing various ion channels can also be investigated by micro-electrode arrays (MEAs). This novel technology is based on the integration of cardiac cell cultures or vibratome slices from cardiac tissues on microchips in order to monitor the changes in extracellular electrograms.⁸⁰ The detected field potential durations (FPDs) correlate well with the APDs of cardiomyocytes from patch clamp assays as well as with QT intervals in clinical ECGs, while the measured beat frequencies are in agreement with the heart rates.^{81, 82} Moreover, MEAs utilizing networks of cells demonstrate a higher complexity, which circumvents the danger of retrieving false positives encountered by single-cell based assays.⁸² In addition, the non-invasive nature of MEAs allows the study of drug effects on beating rate and rhythm, and enables the detection of arrhythmia.⁸¹ However, the MEA devices are not suitable for stimulating and recording the electrophysiological parameters of single cells compared to patch clamp techniques. Furthermore, implantation of a micro-electrode array might have negative effects on the measurements due to various biological responses of cells upon the external insertion.⁸³ Altogether, screening compounds in cardiomyocytes, in particular human induced pluripotent stem cell-derived cardiac myocytes (hiPSC-CMs), with the MEAs technology is still awaiting optimization and will make a substantial contribution to safety pharmacology, which provides a promising means for preliminary drug profiling in the drug discovery pipeline.^{80, 84}

xCELLigence Real-Time Cell Analyzer (RTCA) Cardio System is another innovative label-free real-time platform, which can be utilized to measure the beating functions of cardiomyocytes like hiPSC-CMs based on impedance measurement.⁸⁵ This assay is performed using specially designed microtiter plates with interdigitated golden electrodes to dynamically monitor the impedance changes of cardiomyocyte layers during rhythmic contractions.^{85, 86} This new technology displays a higher throughput than patch clamping, allowing for screening the cardiotoxic liability of compounds earlier during the drug research process. Furthermore, the xCELLigence system enables the monitoring of ligand influences on cardiac functions in real time over prolonged intervals, which supports its application in revealing compounds that cause arrhythmia via inhibiting the

protein trafficking of ion channels.^{85, 87} In addition to such advantages, there are several challenges for the application of xCELLigence RTCA Cardio System in preclinical cardiac safety assessment.⁸⁷ For example, the predictive values of proarrhythmic drugs derived from the extracted parameters in this technology are not explicit, and are required to be further elucidated in the future.

Factors affecting the measurements

All the methods used for investigating the affinity and kinetic parameters of ligands at the $K_v11.1$ channel are influenced by a range of external factors. Herein, we mainly focus on the impacts of assay conditions, species diversity and temperature on the data interpretation for the $K_v11.1$ channel.

The patch clamp technique is a highly flexible method that can be performed in a variety of configurations and modes, providing a direct, precise and detailed measurement of the activity for an ion channel.⁷⁹ Specific bath and pipette solutions, voltage and current protocols based on research aims are essential to obtain reliable results. For instance, Kirsch *et al.* found that there was a 2-fold underestimation of the potency for pimozone at the $K_v11.1$ channel when the step-pulse protocol was changed from 2 s to 0.5 s at 35 °C.⁸⁸ In radioligand binding assays, BSA concentration in the assay buffers might considerably reduce the speed of filtration and further result in the loss of a low affinity binding component for the $K_v11.1$ blockers. Consequently, variability amongst the results acquired in different laboratories may stem, in part, from the varied assay conditions.

Species diversity is another common factor that influences the ligands' activity at the $K_v11.1$ channel in all techniques. Different binding and kinetic parameters of drugs at the $K_v11.1$ channel could be observed with cells from different species or tissues. There have been reported differences in IC_{50} values between the patch clamp measurements in *Xenopus* oocytes versus transfected mammalian cell cultures (i.e. HEK293 and native $K_v11.1$ channel in cardiomyocytes).⁸⁹ Next to protocol variations, these are also attributed to the restricted drug diffusion at the oocytes surface membrane and yolk sac absorption, which does not occur in mammalian cells. Moreover, even when the $K_v11.1$ channel is assessed in the same species but in different cell cultures, variations might be noticeable in the activity and functionality of the channel. This could be related to the varied contents or isoforms of the $K_v11.1$ proteins in different cell cultures. In this circumstance, tissue linearity experiments can be conducted to standardize the distinct results from different cell cultures.⁷⁵

Temperature is the most important factor that impacts the interpretation of data from different assays. Physiological temperature is supposed to be more

suitable to determine drug safety at the $K_v11.1$ channel, since channel gating, receptor binding and drug accumulation might be temperature-dependent. In the patch clamp study the measured IC_{50} values of sotalol and erythromycin at 35 °C were decreased by 2.9- and 7.1-fold respectively compared to these determined at room temperature.⁸⁸ Furthermore, the binding kinetics of ligands at the ion channel can be remarkably affected by the temperature. For instance, erythromycin had an extremely slow onset of block and the time required to reach half-maximal effect was 156 s at 22 °C, whereas the same compound displayed a much faster onset of block and the time needed to approach half-maximal effect was 18 s at 35 °C.⁸⁸ The incubation temperature affects the time for ion exchange in ion flux assays,⁹⁰ and also plays a paramount role in measuring the affinity and kinetic parameters of ligands in radioligand binding assays.⁹¹

Binding of ligands and their kinetics at the $K_v11.1$ channel

Small molecules that act at the intracellular side

Astemizole, desmethylastemizole and norastemizole

Astemizole is a second generation histamine H_1 -receptor antagonist.⁸⁹ In addition to antihistamine effects, it causes a QT interval prolongation and cardiac arrhythmia due to the unintended blockade of the $K_v11.1$ channel. Oxidative *O*- and *N*-demethylations of astemizole generate two metabolites desmethylastemizole and norastemizole, respectively. Desmethylastemizole and astemizole initiated equipotent blockade of the $K_v11.1$ channel, while norastemizole had weaker potency at the channel.⁸⁹ Taglialatela *et al.* investigated the concentration-dependent effect of astemizole on *Xenopus* oocytes transfected with the $K_v11.1$ channel by an extracellular perfusion, and calculated its IC_{50} as 480 nM.⁹² This value was 10 times higher than that previously reported by Suessbrich *et al.*,⁹³ which was explained by a longer incubation time in the latter study leading to higher intracellular drug concentrations and thus stronger potency. Binding of the parent drug and its metabolites occurs primarily in the open and inactivated states of the channel with a minimal block in the closed state.⁸⁹ Blockade of astemizole and desmethylastemizole occurred faster at higher action frequencies. Recovery from astemizole blockade was minimal, while a partial recovery for desmethylastemizole was observed after a washout period of 30 minutes. However, the inhibition of norastemizole was incomplete and only occurred at high concentrations after channel activation. Astemizole and norastemizole were found to bind in the open state of the channel in the region of the hydrophobic inner vestibule after the assembly of the channel tetramers.⁹⁴ A mutation to cysteine at the F656 pore

residue lining in the inner vestibule dramatically reduced the blockade of these two compounds.

Clozapine

Hill *et al.* performed the first study on directly measuring the binding and unbinding kinetics of the typical antipsychotic clozapine at the $K_v11.1$ channel expressed in CHO cells using the patch clamp technique with a Dynaflo automated compound delivery system.¹⁰ They revealed two kinetically distinct blocking effects consistent with different binding kinetics to the open and inactivated states of the channel, while the binding affinity of clozapine for the two different states were almost identical. The block and unblock time courses of clozapine were not monophasic, which encompassed a fast and a slow phase. The fast component of block was related to the fast component of unblock, and vice versa. The current recovery rate from clozapine block during the washout experiment was independent of the drug dosages applied in the system, whereas it was exposure time dependent with a slower recovery rate after a longer application of the drug. The molecular mechanism of clozapine blockade at the $K_v11.1$ channel has not been elucidated. However, it is believed that clozapine binds at the pore site towards the lumen on residues Tyr652 and Phe656 of the S6 domain, which is comparable to other prototypical $K_v11.1$ blockers.⁹⁵

Clofilium and ibutilide

Clofilium and ibutilide, which are two structurally related class III antiarrhythmic drugs, were found to have different time-dependent kinetics of block at the $K_v11.1$ channel in whole cell voltage clamped *Xenopus* oocytes.¹⁸ The binding potency of ibutilide at the channel showed an IC_{50} value of 28 nM, while a precise measurement of the IC_{50} value for clofilium was difficult due to its extraordinarily slow onset of block. The steady-state inhibition of clofilium to the $K_v11.1$ channel was not approached even after a prolonged exposure to more than 1 hour. Nevertheless, the onset of block was reported to be faster when clofilium was applied from the intracellular side of excised membranes in excised patch clamp experiments. Regarding the unblock rate, the inhibition of ibutilide was almost completely recovered after a 10-minute washout, whereby only 19% I_{Kr} was restored from clofilium block within the same washout period. This ultra-slow recovery rate of clofilium from $K_v11.1$ blockade is similar to the findings for other potent channel blockers which demonstrate slow unbinding profiles because of drug trapping within the central cavity of the channel after closure of the activated gate upon membrane repolarization.^{96, 97} To investigate the trapping hypothesis,

both clofilium and ibutilide were tested at the $K_v11.1$ D540K mutant that permits untrapping at a hyperpolarized state by allowing the gate to remain open.¹⁸ Again, recovery from $K_v11.1$ blockade in the case of ibutilide was almost complete, yet little current recovery from clofilium inhibition to the channel was observed. This ruled out the possibility of drug tapping within the channel cavity, also known as a “foot in the door” mechanism, for clofilium. The binding sites of clofilium and ibutilide at the $K_v11.1$ channel were the same by alanine-scanning mutagenesis of Tyr652, Phe656, Thr623, Ser624 and Val625 residues. The S624A mutant located at the base of the pore helix of the $K_v11.1$ channel was the only one that was found to enable the rapid I_{Kr} recovery from clofilium blockade.

Terfenadine

Terfenadine is a potent blocker of the $K_v11.1$ channel in the open state. The IC_{50} of terfenadine in *Xenopus* oocytes expressing the $K_v11.1$ channel was 350 nM at 22 °C.⁹³ Extracellular potassium concentrations significantly altered the $K_v11.1$ potency of terfenadine with an IC_{50} of 3.5 mM at 96 mM K^+ reduced to 350 nM in 2 mM K^+ .⁹⁸ The steady-state block of the $K_v11.1$ channel by terfenadine was approached within 7 minutes superfusion of Ringer’s solution containing terfenadine, and the blockade was frequency-, voltage- and use-independent. The recovery of terfenadine from block at the closed state took place after a washout period of more than 30 minutes, which can be explained by drug trapping inside of the central cavity of the $K_v11.1$ channel.⁹⁹ Unlike clofilium, the closure-deficient $K_v11.1$ D540K mutant was experimentally confirmed to facilitate the I_{Kr} recovery from terfenadine block at the $K_v11.1$ channel. Focusing on the molecular binding perspective, terfenadine interacts with S624, Y652, F656 and T632 residues, while amino acids Y652 and F656 are the most important determinants for the $K_v11.1$ sensitivity to terfenadine.⁹⁹

Cisapride

Cisapride, a prokinetic agent, is a potent $K_v11.1$ blocker.⁹⁹ The IC_{50} value of cisapride at the $K_v11.1$ channel on the *Xenopus* oocytes was 630 nM. The onset of block of cisapride was rapid and the recovery from block was complete within approximate 2 minutes.¹⁰⁰ Mutation studies for the binding site of cisapride at the $K_v11.1$ channel implicated that π - π interactions with Y652 and F656 residues and additional hydrophobic interactions with Y652 were essential for the channel sensitivity to cisapride.¹⁰¹

Propafenone

Witchel *et al.* used a concentration of 50 mM propafenone to induce a profound $K_v11.1$ channel blockade.¹⁰² The tail current was blocked by 96% at -70 mV while the blockade dropped to 5% in the F656A mutant in *Xenopus* oocytes. This indicates that the F656 residue is a critical determinant for the blockade of propafenone at the $K_v11.1$ channel, similar to other methanesulfonanilides like dofetilide and MK-499. Recovery of the $K_v11.1$ channel from propafenone blockade was very rapid in the open state, whereas it was virtually undetectable in the time scale tested in the closed state. A further study performed by Windisch *et al.* revealed that propafenone derivatives with short side chains were trapped in the closed channel and displayed a very slow unblock rate at the $K_v11.1$ channel, which was in contrast to the long side chain analogues displaying insignificant trapping.⁹⁶ Altogether, the study provides direct evidence for a “foot in the door” type blockade of ligands at the $K_v11.1$ channel.

Peptides that act at the extracellular side

APETx1 and Saxitoxin

APETx1 is a peptide purified from sea anemone, which acts as a gate modifier of the $K_v11.1$ channel.¹⁰³ APETx1 inhibited the I_{Kr} in a heterologous system with an IC_{50} value of 34 nM at room temperature, while the inhibition was maximal at 300 nM leaving 20% current unblocked even at concentrations up to 1 μ M in COS-7 cells transfected with $K_v11.1$ channels. Its kinetics of block profile were characterized by a rapid onset of block, and the steady-state inhibition was reached within 1 minute. The block of APETx1 to the $K_v11.1$ channel was totally reversible upon a washout period of 100 s. Similar to the binding sites for gating modifier toxins of other voltage-gated potassium channels, mutations in the S3 region of the $K_v11.1$ channel like G514C and E518C had dramatic impact on the responsiveness of the channel to APETx1.¹⁰⁴

Saxitoxin inhibited the I_{Kr} by more than 90% at 3 μ M in HEK293 cells expressing the $K_v11.1$ channel at 36 ± 1 °C.¹⁰⁵ Current reduction reached steady state quickly, and the block was reversible upon washout with dissociation characteristics opposing the simple first-order process. The concentration-dependency of saxitoxin alongside its kinetics of block onset and recovery suggested a complex binding of multiple molecules of saxitoxin to the extracellular side of the $K_v11.1$ channel. Co-administration of methanesulfonanilide MK-499 showed that the $K_v11.1$ inhibition effects of the two drugs were additive, further indicating that saxitoxin did not bind to the intracellular side of the channel as MK-499.

BeKm-1

BeKm-1 is a scorpion toxin, which selectively blocked the I_{Kr} current with an IC_{50} value of 3.3 nM in a patch clamp study in transfected HEK93 cells at room temperature.¹⁰⁶ The current block and unblock rates of wild type BeKm-1 at the $K_v11.1$ channel were $2.5 \times 10^6 \text{ M}^{-1} \cdot \text{s}^{-1}$ and 0.017 s^{-1} , respectively.¹⁰⁷ In radioligand binding assays the association and dissociation kinetics of [^{125}I]-BeKm-1 were extremely fast at room temperature, while its on- and off-rate constants at 0 °C were $3.8 \times 10^7 \text{ M}^{-1} \cdot \text{s}^{-1}$ and 0.00051 s^{-1} , separately.¹⁰⁷ Additionally, wild-type BeKm-1 displaced the binding of [^{125}I]-BeKm-1 with a half-maximal inhibitory concentration of 44 pM at 0 °C.¹⁰⁷ Collectively, discrepancies exist between quantitative results acquired in patch clamp and radioligand binding assays, albeit to the comparable rank orders of measured parameters from these two different techniques. BeKm-1 preferentially inhibited the I_{Kr} current through a closed state channel blockade mechanism,¹⁰⁸ and interacted with the $K_v11.1$ channel at the extracellular site.⁴²

Conclusions

The $K_v11.1$ channel is a voltage-gated potassium channel that shares structural characteristics with the voltage-gated potassium channel family but displays unique gating kinetics. It is involved in a number of physiological conditions, and has the potential to become a new biomarker and therapeutic target for cancer, schizophrenia and other important diseases due to its high expression in diseased cells instead of normal cells. More importantly, the $K_v11.1$ channel plays an important role in maintaining cardiac stability under normal conditions being the target of class III antiarrhythmic drugs, but at the same time, when dysregulated, causes notorious side effects of severe arrhythmias. A surprisingly diverse group of drugs including cardiac and non-cardiac medications have been withdrawn from or restricted for use in the market due to their blockade of the $K_v11.1$ channel. Therefore, it is routine practice for pharmaceutical companies to screen the $K_v11.1$ liability of drug candidates before they are approved to enter the market by regulatory agencies.

In this review, we summarized the generation, degradation, structure and function of the $K_v11.1$ channel, and its corresponding intentional and unintentional roles in drug development. This provides valuable information and theoretical foundations for investigations on the $K_v11.1$ channel as well as a comprehensive overview of the channel.

The unique gating kinetics of the $K_v11.1$ channel contribute to its important

functions in physiological conditions. Almost all $K_v11.1$ ligands affect the gating kinetics of the channel during their interaction with the channel. We reviewed the closed, open and inactivated states of the channel and also the transitions among these different states. Moreover, the impact of several assay conditions and $K_v11.1$ ligands on the channel kinetics was discussed. This emphasizes the importance of considering the gating kinetics of the $K_v11.1$ channel in seeking for $K_v11.1$ activators and compounds with less $K_v11.1$ -related cardiotoxicity. In addition, the differences between laboratories in evaluating the $K_v11.1$ ligands should be standardized by taking distinct assay conditions into consideration.

Currently, the estimation of the risk of a drug to cause LQTS is only based on its IC_{50} value at the $K_v11.1$ channel. When a drug or drug candidate exhibits an IC_{50} value 30-fold higher than its effective therapeutic plasma concentration, this drug is considered to have a safe cardiac profile. Although this rule ensures the exclusion of potentially harmful drugs, it could also lead to the preliminary withdrawal of certain drug candidates that may be unproblematic. Furthermore, drug inhibition of the $K_v11.1$ channel is a dynamic process in which binding and unbinding events occur over time. Therefore, we also examined in this review the binding and corresponding kinetics of different series of ligands to the $K_v11.1$ channel. Different techniques used to determine the binding and kinetic parameters of these ligands at the channel were summarized as well. All in all, we strongly plea for incorporation of kinetic assessment into ligand affinity at the channel in order to better predict the proarrhythmic propensities of $K_v11.1$ blockers. To date, the roles of binding (association) and unbinding (dissociation) of ligands with respect to their $K_v11.1$ cardiac side effects have not been well elucidated, and thus, more attention should be paid to the studies on these kinetics in the future.

Overall, a thorough analysis of the $K_v11.1$ channel, in particular the gating kinetics and ligand binding kinetics, enables the improvement of drug targeted design and reduction of unwanted arrhythmic side effects on this channel. The outcome of these investigations would also substantially contribute to the development of homology and mathematical models for better predicting the interactions of $K_v11.1$ ligands with the channel, which could effectively facilitate the investigations on the $K_v11.1$ channel in the near future.

References

1. Trebak, M.; Parekh, A. B. Ion channels in patho-physiology. *J. Physiol.* **2012**, *590*, 1347-1347.
2. Overington, J. P.; Al-Lazikani, B.; Hopkins, A. L. How many drug targets are there?

Nat. Rev. Drug Discov. **2006**, *5*, 993-996.

3. Gutman, G. A.; Chandy, K. G.; Grissmer, S.; Lazdunski, M.; Mckinnon, D.; Pardo, L. A.; Robertson, G. A.; Rudy, B.; Sanguinetti, M. C.; Stühmer, W. International union of pharmacology. LIII. Nomenclature and molecular relationships of voltage-gated potassium channels. *Pharmacol. Rev.* **2005**, *57*, 473-508.
4. Castle, N. A. Pharmacological modulation of voltage-gated potassium channels as a therapeutic strategy. *Expert Opin. Ther. Pat.* **2010**, *20*, 1471-1503.
5. Vandenberg, J. I.; Perry, M. D.; Perrin, M. J.; Mann, S. A.; Ke, Y.; Hill, A. P. hERG K^+ channels: Structure, function, and clinical significance. *Physiol. Rev.* **2012**, *92*, 1393-1478.
6. Sanguinetti, M. C.; Tristani-Firouzi, M. hERG potassium channels and cardiac arrhythmia. *Nature* **2006**, *440*, 463-469.
7. Sasano, T.; Ueda, K.; Orikabe, M.; Hirano, Y.; Kawano, S.; Yasunami, M.; Isobe, M.; Kimura, A.; Hiraoka, M. Novel C-terminus frameshift mutation, 1122fs/147, of hERG in LQT2: Additional amino acids generated by frameshift cause accelerated inactivation. *J. Mol. Cell. Cardiol.* **2004**, *37*, 1205-1211.
8. Anderson, C. L.; Delisle, B. P.; Anson, B. D.; Kilby, J. A.; Will, M. L.; Tester, D. J.; Gong, Q.; Zhou, Z.; Ackerman, M. J.; January, C. T. Most LQT2 mutations reduce $K_v11.1$ (hERG) current by a class 2 (trafficking-deficient) mechanism. *Circulation* **2006**, *113*, 365-373.
9. Romero, L.; Trenor, B.; Yang, P.; Saiz, J.; Clancy, C. E. *In silico* screening of the impact of hERG channel kinetic abnormalities on channel block and susceptibility to acquired long QT syndrome. *J. Mol. Cell. Cardiol.* **2014**, *72*, 126-137.
10. Hill, A. P.; Perrin, M. J.; Heide, J.; Campbell, T. J.; Mann, S. A.; Vandenberg, J. I. Kinetics of drug interaction with the $K_v11.1$ potassium channel. *Mol. Pharmacol.* **2014**, *85*, 769-776.
11. Nogawa, H.; Kawai, T. hERG trafficking inhibition in drug-induced lethal cardiac arrhythmia. *Eur. J. Pharmacol.* **2014**, *741*, 336-339.
12. Vandenberg, J. I.; Walker, B. D.; Campbell, T. J. hERG K^+ channels: Friend and foe. *Trends Pharmacol. Sci.* **2001**, *22*, 240-246.
13. Abbott, G. W.; Sesti, F.; Splawski, I.; Buck, M. E.; Lehmann, M. H.; Timothy, K. W.; Keating, M. T.; Goldstein, S. A. MiRP1 forms I_{Kr} potassium channels with hERG and is associated with cardiac arrhythmia. *Cell* **1999**, *97*, 175-187.
14. Mannhold, R.; Kubinyi, H.; Folkers, G.; Vaz, R.; Klabunde, T. Antitargets: Prediction and Prevention of Drug Side Effects. John Wiley & Sons: 2008; Vol. 38.
15. Perry, M.; Sanguinetti, M.; Mitcheson, J. Symposium review: Revealing the structural basis of action of hERG potassium channel activators and blockers. *J. Physiol.* **2010**, *588*, 3157-3167.
16. Saenen, J.; Labro, A.; Raes, A.; Snyders, D. Modulation of hERG gating by a charge

- cluster in the N-terminal proximal domain. *Biophys. J.* **2006**, *91*, 4381-4391.
17. Milnes, J. T.; Crociani, O.; Arcangeli, A.; Hancox, J. C.; Witchel, H. J. Blockade of hERG potassium currents by fluvoxamine: Incomplete attenuation by S6 mutations at F656 or Y652. *Br. J. Pharmacol.* **2003**, *139*, 887-898.
 18. Perry, M.; de Groot, M. J.; Helliwell, R.; Leishman, D.; Tristani-Firouzi, M.; Sanguinetti, M. C.; Mitcheson, J. Structural determinants of hERG channel block by clofilium and ibutilide. *Mol. Pharmacol.* **2004**, *66*, 240-249.
 19. Asher, V.; Sowter, H.; Shaw, R.; Bali, A.; Khan, R. Eag and hERG potassium channels as novel therapeutic targets in cancer. *World J. Surg. Oncol.* **2010**, *8*, 113-121.
 20. Nerbonne, J. M.; Kass, R. S. Molecular physiology of cardiac repolarization. *Physiol. Rev.* **2005**, *85*, 1205-1253.
 21. Pinnell, J.; Turner, S.; Howell, S. Cardiac muscle physiology. *Continuing Education in Anaesthesia, Critical Care & Pain* **2007**, *7*, 85-88.
 22. Chi, K. R. Revolution dawning in cardiotoxicity testing. *Nat. Rev. Drug Discov.* **2013**, *12*, 565-567.
 23. Babcock, J. J.; Li, M. hERG channel function: Beyond long QT. *Acta Pharmacol. Sin.* **2013**, *34*, 329-335.
 24. Jehle, J.; Schweizer, P.; Katus, H.; Thomas, D. Novel roles for hERG K⁺ channels in cell proliferation and apoptosis. *Cell Death Dis.* **2011**, *2*, e193.
 25. Li, H.; Liu, L.; Guo, L.; Zhang, J.; Du, W.; Li, X.; Liu, W.; Chen, X.; Huang, S. hERG K⁺ channel expression in CD34⁺/CD38⁻/CD123^{high} cells and primary leukemia cells and analysis of its regulation in leukemia cells. *Int. J. Hematol.* **2008**, *87*, 387-392.
 26. Heide, J.; Mann, S. A.; Vandenberg, J. I. The schizophrenia-associated K_v11.1-3.1 isoform results in reduced current accumulation during repetitive brief depolarizations. *Plos One* **2012**, *7*, e45624.
 27. Akbarali, H. I.; Thatte, H.; He, X. D.; Giles, W. R.; Goyal, R. K. Role of hERG-like K⁺ currents in opossum esophageal circular smooth muscle. *Am. J. Physiol. Cell Physiol.* **1999**, *277*, C1284-C1290.
 28. Farrelly, A.; Ro, S.; Callaghan, B.; Khoyi, M.; Fleming, N.; Horowitz, B.; Sanders, K.; Keef, K. Expression and function of KCNH2 (hERG) in the human jejunum. *Am. J. Physiol. Gastrointest. Liver Physiol.* **2003**, *284*, G883-G895.
 29. Parkington, H. C.; Stevenson, J.; Tonta, M. A.; Paul, J.; Butler, T.; Maiti, K.; Chan, E.-C.; Sheehan, P. M.; Brennecke, S. P.; Coleman, H. A.; Smith, R. Diminished hERG K⁺ channel activity facilitates strong human labour contractions but is dysregulated in obese women. *Nat. Commun.* **2014**, *5*.
 30. Rosati, B.; Marchetti, P.; Crociani, O.; Lecchi, M.; Lupi, R.; Arcangeli, A.; Olivetto, M.; Wanke, E. Glucose-and arginine-induced insulin secretion by human pancreatic β -cells: the role of hERG K⁺ channels in firing and release. *FASEB J.* **2000**, *14*, 2601-2610.

31. Grunnet, M.; Hansen, R. S.; Olesen, S.-P. hERG1 channel activators: A new anti-arrhythmic principle. *Prog. Biophys. Mol. Biol.* **2008**, *98*, 347-362.
32. Perry, M. D.; Ng, C. A.; Mann, S. A.; Sadrieh, A.; Imtiaz, M.; Hill, A. P.; Vandenberg, J. I. Getting to the heart of hERG K⁺ channel gating. *J. Physiol.* **2015**.
33. McPate, M. J.; Duncan, R. S.; Milnes, J. T.; Witchel, H. J.; Hancox, J. C. The N588K-hERG K⁺ channel mutation in the 'short QT syndrome': Mechanism of gain-in-function determined at 37 °C. *Biochem. Biophys. Res. Commun.* **2005**, *334*, 441-449.
34. Brugada, R.; Hong, K.; Dumaine, R.; Cordeiro, J.; Gaita, F.; Borggrefe, M.; Menendez, T. M.; Brugada, J.; Pollevick, G. D.; Wolpert, C.; Burashnikov, E.; Matsuo, K.; Sheng Wu, Y.; Guerchicoff, A.; Bianchi, F.; Giustetto, C.; Schimpf, R.; Brugada, P.; Antzelevitch, C. Sudden death associated with short-QT syndrome linked to mutations in hERG. *Circulation* **2004**, *109*, 30-35.
35. Taglialatela, M.; Castaldo, P.; Pannaccione, A.; Giorgio, G.; Annunziato, L. Human ether-à-go-go related gene (hERG) K⁺ channels as pharmacological targets: Present and future implications. *Biochem. Pharmacol.* **1998**, *55*, 1741-1746.
36. Raschi, E.; Vasina, V.; Poluzzi, E.; De Ponti, F. The hERG K⁺ channel: Target and antitarget strategies in drug development. *Pharmacol. Res.* **2008**, *57*, 181-195.
37. Anderson, C. L.; Kuzmicki, C. E.; Childs, R. R.; Hintz, C. J.; Delisle, B. P.; January, C. T. Large-scale mutational analysis of K_v11.1 reveals molecular insights into type 2 long QT syndrome. *Nat. Commun.* **2014**, *5*.
38. Zhou, Z.; Gong, Q.; January, C. T. Correction of defective protein trafficking of a mutant hERG potassium channel in human long QT syndrome pharmacological and temperature effects. *J. Biol. Chem.* **1999**, *274*, 31123-31126.
39. Kang, J.; Chen, X.; Wang, H.; Ji, J.; Cheng, H.; Incardona, J.; Reynolds, W.; Viviani, F.; Tabart, M.; Rampe, D. Discovery of a small molecule activator of the human ether-à-go-go-related gene (hERG) cardiac K⁺ channel. *Mol. Pharmacol.* **2005**, *67*, 827-836.
40. Perrin, M. J.; Subbiah, R. N.; Vandenberg, J. I.; Hill, A. P. Human ether-à-go-go related gene (hERG) K⁺ channels: Function and dysfunction. *Prog. Biophys. Mol. Biol.* **2008**, *98*, 137-148.
41. Aronov, A. M. Predictive *in silico* modeling for hERG channel blockers. *Drug Discov. Today* **2005**, *10*, 149-155.
42. Qu, Y.; Fang, M.; Gao, B.; Chui, R. W.; Vargas, H. M. BeKm-1, a peptide inhibitor of human ether-à-go-go-related gene potassium currents, prolongs QTc intervals in isolated rabbit heart. *J. Pharmacol. Exp. Ther.* **2011**, *337*, 2-8.
43. Ko, E. A.; Park, W. S.; Son, Y. K.; Ko, J.-H.; Choi, T.-H.; Jung, I. D.; Park, Y.-M.; Hong, D. H.; Kim, N.; Han, J. Calcium channel inhibitor, verapamil, inhibits the voltage-dependent K⁺ channels in rabbit coronary smooth muscle cells. *Biol. Pharm. Bull.* **2010**, *33*, 47-52.
44. Cavero, I.; Holzgrefe, H. Comprehensive *in vitro* proarrhythmia assay, a novel *in*

- vitro/in silico* paradigm to detect ventricular proarrhythmic liability: A visionary 21st century initiative. *Expert Opin. Drug Saf.* **2014**, *13*, 745-758.
45. Cavero, I. 13th annual meeting of the safety pharmacology society: Focus on novel technologies and safety pharmacology frontiers. *Expert Opin. Drug Saf.* **2014**, *13*, 1271-1281.
 46. Townsend, C. Is there a need to add another dimension (time) to the evaluation of the arrhythmogenic potential of new drug candidates *in vitro*? *Circulation* **2014**, *130*, 219-220.
 47. Di Veroli, G. Y.; Davies, M. R.; Zhang, H.; Abi-Gerges, N.; Boyett, M. R. hERG inhibitors with similar potency but different binding kinetics do not pose the same proarrhythmic risk: Implications for drug safety assessment. *J. Cardiovasc. Electrophysiol.* **2014**, *25*, 197-207.
 48. Giudicessi, J. R.; Ackerman, M. J. Potassium-channel mutations and cardiac arrhythmias-diagnosis and therapy. *Nat. Rev. Cardiol.* **2012**, *9*, 319-332.
 49. Ader, C.; Schneider, R.; Hornig, S.; Velisetty, P.; Vardanyan, V.; Giller, K.; Ohmert, I.; Becker, S.; Pongs, O.; Baldus, M. Coupling of activation and inactivation gate in a K⁺-channel: Potassium and ligand sensitivity. *EMBO J.* **2009**, *28*, 2825-2834.
 50. Jiang, Y.; Lee, A.; Chen, J.; Cadene, M.; Chait, B. T.; MacKinnon, R. The open pore conformation of potassium channels. *Nature* **2002**, *417*, 523-526.
 51. Zhang, M.; Liu, J.; Tseng, G.-N. Gating charges in the activation and inactivation processes of the hERG channel. *J. Gen. Physiol.* **2004**, *124*, 703-718.
 52. Shibasaki, T. Conductance and kinetics of delayed rectifier potassium channels in nodal cells of the rabbit heart. *J. Physiol.* **1987**, *387*, 227-250.
 53. Tristani-Firouzi, M.; Chen, J.; Sanguinetti, M. C. Interactions between S4-S5 linker and S6 transmembrane domain modulate gating of hERG K⁺ channels. *J. Biol. Chem.* **2002**, *277*, 18994-19000.
 54. Osterbur, M. L.; Zheng, R.; Marion, R.; Walsh, C.; McDonald, T. V. An interdomain KCNH2 mutation produces an intermediate long QT syndrome. *Hum. Mutat.* **2015**.
 55. Ng, C. A.; Phan, K.; Hill, A. P.; Vandenberg, J. I.; Perry, M. D. Multiple interactions between cytoplasmic domains regulate slow deactivation of K_v11.1 channels. *J. Biol. Chem.* **2014**, *289*, 25822-25832.
 56. Zhou, P.; Babcock, J.; Liu, L.; Li, M.; Gao, Z.-b. Activation of human ether-à-go-go related gene (hERG) potassium channels by small molecules. *Acta Pharmacol. Sin.* **2011**, *32*, 781-788.
 57. Bett, G. C.; Zhou, Q.; Rasmusson, R. L. Models of hERG gating. *Biophys. J.* **2011**, *101*, 631-642.
 58. Perry, M. D.; Ng, C. A.; Vandenberg, J. I. Pore helices play a dynamic role as integrators of domain motion during K_v11.1 channel inactivation gating. *J. Biol. Chem.* **2013**, *288*, 11482-11491.

59. Tseng, G.-N. I_{Kr} : The hERG channel. *J. Mol. Cell. Cardiol.* **2001**, 33, 835-849.
60. Perry, M. D.; Wong, S.; Ng, C. A.; Vandenberg, J. I. Hydrophobic interactions between the voltage sensor and pore mediate inactivation in K_v11.1 channels. *J. Gen. Physiol.* **2013**, 142, 275-288.
61. Vandenberg, J. I.; Varghese, A.; Lu, Y.; Bursill, J. A.; Mahaut-Smith, M. P.; Huang, C. L.-H. Temperature dependence of human ether-à-go-go-related gene K⁺ currents. *Am. J. Physiol. Cell Physiol.* **2006**, 291, C165-C175.
62. Bérubé, J.; Chahine, M.; Daleau, P. Modulation of hERG potassium channel properties by external pH. *Pflugers Arch.* **1999**, 438, 419-422.
63. Melgari, D.; Du, C.; El Harchi, A.; Zhang, Y.; Hancox, J. C. Suppression of the hERG potassium channel response to premature stimulation by reduction in extracellular potassium concentration. *Physiol. Rep.* **2014**, 2, e12165.
64. Johnson, J.; Mullins, F. M.; Bennett, P. B. Human ether-à-go-go-related gene K⁺ channel gating probed with extracellular Ca²⁺ evidence for two distinct voltage sensors. *J. Gen. Physiol.* **1999**, 113, 565-580.
65. Perry, M.; Sachse, F. B.; Sanguinetti, M. C. Structural basis of action for a human ether-a-go-go-related gene 1 potassium channel activator. *Proc. Natl. Acad. Sci. U.S.A.* **2007**, 104, 13827-13832.
66. Perry, M.; Sachse, F. B.; Abbruzzese, J.; Sanguinetti, M. C. PD-118057 contacts the pore helix of hERG1 channels to attenuate inactivation and enhance K⁺ conductance. *Proc. Natl. Acad. Sci. U.S.A.* **2009**, 106, 20075-20080.
67. Vonderlin, N.; Fischer, F.; Zitron, E.; Seyler, C.; Scherer, D.; Thomas, D.; Katus, H. A.; Scholz, E. P. Anesthetic drug midazolam inhibits cardiac human ether-à-go-go-related gene channels: Mode of action. *Drug Des. Devel. Ther.* **2015**, 9, 867-877.
68. Zhang, M.; Korolkova, Y. V.; Liu, J.; Jiang, M.; Grishin, E. V.; Tseng, G.-N. BeKm-1 is a hERG-specific toxin that shares the structure with ChTx but the mechanism of action with ErgTx1. *Biophys. J.* **2003**, 84, 3022-3036.
69. Long, Y.; Li, Z. Drug screening and drug safety evaluation by patch clamp technique. *Intech open access publisher*: 2012.
70. Danker, T.; Möller, C. Early identification of hERG liability in drug discovery programs by automated patch clamp. *Front. Pharmacol.* **2014**, 5, 1-11.
71. Zheng, W.; Spencer, R. H.; Kiss, L. High throughput assay technologies for ion channel drug discovery. *Assay Drug Dev. Technol.* **2004**, 2, 543-552.
72. Polonchuk, L. Industrializing electrophysiology: HT automated patch clamp on Syn-croPatch® 96 using instant frozen cells. In *Patch-Clamp Methods and Protocols*, Springer: 2014; pp 81-92.
73. Finlayson, K.; Pennington, A. J.; Kelly, J. S. [³H]Dofetilide binding in SHSY5Y and HEK293 cells expressing a hERG-like K⁺ channel? *Eur. J. Pharmacol.* **2001**, 412, 203-212.

74. Diaz, G. J.; Daniell, K.; Leitza, S. T.; Martin, R. L.; Su, Z.; McDermott, J. S.; Cox, B. F.; Gintant, G. A. The [³H]dofetilide binding assay is a predictive screening tool for hERG blockade and proarrhythmia: Comparison of intact cell and membrane preparations and effects of altering [K⁺]_o. *J. Pharmacol. Toxicol. Methods* **2004**, *50*, 187-199.
75. Chiu, P. J.; Marcoe, K. F.; Bounds, S. E.; Lin, C.; Feng, J.; Lin, A.; Cheng, F.; Crumb, W. J.; Mitchell, R. Validation of a [³H]astemizole binding assay in HEK293 cells expressing hERG K⁺ channels. *J. Pharmacol. Sci.* **2004**, *95*, 311-319.
76. Rezazadeh, S.; Hesketh, J. C.; Fedida, D. Rb⁺ flux through hERG channels affects the potency of channel blocking drugs: correlation with data obtained using a high-throughput Rb⁺ efflux assay. *J. Biomol. Screen* **2004**, *9*, 588-597.
77. Tang, W.; Kang, J.; Wu, X.; Rampe, D.; Wang, L.; Shen, H.; Li, Z.; Dunnington, D.; Garyantes, T. Development and evaluation of high throughput functional assay methods for hERG potassium channel. *J. Biomol. Screen* **2001**, *6*, 325-331.
78. Chaudhary, K. W.; O'Neal, J. M.; Mo, Z.; Fermi, B.; Gallavan, R. H.; Bahinski, A. Evaluation of the rubidium efflux assay for preclinical identification of hERG blockade. *Assay Drug Dev. Technol.* **2006**, *4*, 73-82.
79. Xu, J.; Wang, X.; Ensign, B.; Li, M.; Wu, L.; Guia, A.; Xu, J. Ion-channel assay technologies: Quo vadis? *Drug Discov. Today* **2001**, *6*, 1278-1287.
80. Yeung, C.; Sommerhage, F.; Wrobel, G.; Offenhäusser, A.; Chan, M.; Ingebrandt, S. Drug profiling using planar microelectrode arrays. *Anal. Bioanal. Chem.* **2007**, *387*, 2673-2680.
81. Navarrete, E. G.; Liang, P.; Lan, F.; Sanchez-Freire, V.; Simmons, C.; Gong, T.; Sharma, A.; Burrige, P. W.; Patlolla, B.; Lee, A. S.; Wu, H.; Beygui, R. E.; Wu, S. M.; Robbins, R. C.; Bers, D. M.; Wu, J. C. Screening drug-induced arrhythmia using human induced pluripotent stem cell-derived cardiomyocytes and low-impedance micro-electrode arrays. *Circulation* **2013**, *128*, S3-S13.
82. Meyer, T.; Boven, K.-H.; Günther, E.; Fejtl, M. Micro-electrode arrays in cardiac safety pharmacology. *Drug Saf.* **2004**, *27*, 763-772.
83. Chhatbar, P. Y.; von Kraus, L. M.; Semework, M.; Francis, J. T. A bio-friendly and economical technique for chronic implantation of multiple microelectrode arrays. *J. Neurosci. Methods* **2010**, *188*, 187-194.
84. Guo, L.; Abrams, R.; Babiarz, J. E.; Cohen, J. D.; Kameoka, S.; Sanders, M. J.; Chiao, E.; Kolaja, K. L. Estimating the risk of drug-induced proarrhythmia using human induced pluripotent stem cell derived cardiomyocytes. *Toxicol. Sci.* **2011**, *123*, 281-289.
85. Xi, B.; Wang, T.; Li, N.; Ouyang, W.; Zhang, W.; Wu, J.; Xu, X.; Wang, X.; Abassi, Y. A. Functional cardiotoxicity profiling and screening using the xCELLigence RTCA Cardio System. *JALA Charlottesv Va* **2011**, *16*, 415-421.
86. Himmel, H. M. Drug-induced functional cardiotoxicity screening in stem cell-derived human and mouse cardiomyocytes: Effects of reference compounds. *J. Pharmacol.*

Toxicol. Methods **2013**, 68, 97-111.

87. Abassi, Y. A.; Xi, B.; Li, N.; Ouyang, W.; Seiler, A.; Watzele, M.; Kettenhofen, R.; Bohlen, H.; Ehlich, A.; Kolossov, E.; Wang, X.; Xu, X. Dynamic monitoring of beating periodicity of stem cell-derived cardiomyocytes as a predictive tool for preclinical safety assessment. *Br. J. Pharmacol.* **2012**, 165, 1424-1441.

88. Kirsch, G. E.; Trepakova, E. S.; Brimecombe, J. C.; Sidach, S. S.; Erickson, H. D.; Kochan, M. C.; Shyjka, L. M.; Lacerda, A. E.; Brown, A. M. Variability in the measurement of hERG potassium channel inhibition: effects of temperature and stimulus pattern. *J. Pharmacol. Toxicol. Methods* **2004**, 50, 93-101.

89. Zhou, Z.; Vorperian, V. R.; Gong, Q.; Zhang, S.; January, C. T. Block of hERG potassium channels by the antihistamine astemizole and its metabolites desmethylastemizole and norastemizole. *J. Cardiovasc. Electrophysiol.* **1999**, 10, 836-843.

90. Terstappen, G. C. Functional analysis of native and recombinant ion channels using a high-capacity nonradioactive rubidium efflux assay. *Anal. Biochem.* **1999**, 272, 149-155.

91. Hulme, E. C.; Trevethick, M. A. Ligand binding assays at equilibrium: Validation and interpretation. *Br. J. Pharmacol.* **2010**, 161, 1219-1237.

92. Taglialatela, M.; Pannaccione, A.; Castaldo, P.; Giorgio, G.; Zhou, Z.; January, C. T.; Genovese, A.; Marone, G.; Annunziato, L. Molecular basis for the lack of hERG K⁺ channel block-related cardiotoxicity by the H₁ receptor blocker cetirizine compared with other second-generation antihistamines. *Mol. Pharmacol.* **1998**, 54, 113-121.

93. Suessbrich, H.; Waldegger, S.; Lang, F.; Busch, A. Blockade of hERG channels expressed in *Xenopus* oocytes by the histamine receptor antagonists terfenadine and astemizole. *FEBS Lett.* **1996**, 385, 77-80.

94. Ficker, E.; Obejero-Paz, C. A.; Zhao, S.; Brown, A. M. The binding site for channel blockers that rescue misprocessed human long QT syndrome type 2 ether-à-go-go-related gene (hERG) mutations. *J. Biol. Chem.* **2002**, 277, 4989-4998.

95. Lee, S.-Y.; Kim, Y.-J.; Kim, K.-T.; Choe, H.; Jo, S.-H. Blockade of hERG human K⁺ channels and I_{Kr} of guinea-pig cardiomyocytes by the antipsychotic drug clozapine. *Br. J. Pharmacol.* **2006**, 148, 499-509.

96. Windisch, A.; Timin, E.; Schwarz, T.; Stork-Riedler, D.; Erker, T.; Ecker, G.; Hering, S. Trapping and dissociation of propafenone derivatives in hERG channels. *Br. J. Pharmacol.* **2011**, 162, 1542-1552.

97. Sánchez-Chapula, J. A.; Navarro-Polanco, R. A.; Culberson, C.; Chen, J.; Sanguinetti, M. C. Molecular determinants of voltage-dependent human ether-à-go-go-related gene (hERG) K⁺ channel block. *J. Biol. Chem.* **2002**, 277, 23587-23595.

98. Roy, M.-L.; Dumaine, R.; Brown, A. M. hERG, a primary human ventricular target of the nonsedating antihistamine terfenadine. *Circulation* **1996**, 94, 817-823.

99. Kamiya, K.; Niwa, R.; Morishima, M.; Honjo, H.; Sanguinetti, M. C. Molecular

- determinants of hERG channel block by terfenadine and cisapride. *J. Pharmacol. Sci.* **2008**, *108*, 301.
100. Stork, D.; Timin, E.; Berjukow, S.; Huber, C.; Hohaus, A.; Auer, M.; Hering, S. State dependent dissociation of hERG channel inhibitors. *Br. J. Pharmacol.* **2007**, *151*, 1368-1376.
 101. Fernandez, D.; Ghanta, A.; Kauffman, G. W.; Sanguinetti, M. C. Physicochemical features of the hERG channel drug binding site. *J. Biol. Chem.* **2004**, *279*, 10120-10127.
 102. Witchel, H. J.; Dempsey, C. E.; Sessions, R. B.; Perry, M.; Milnes, J. T.; Hancox, J. C.; Mitcheson, J. S. The low-potency, voltage-dependent hERG blocker propafenone-molecular determinants and drug trapping. *Mol. Pharmacol.* **2004**, *66*, 1201-1212.
 103. Diochot, S.; Loret, E.; Bruhn, T.; Béress, L.; Lazdunski, M. APETx1, a new toxin from the sea anemone *Anthopleura elegantissima*, blocks voltage-gated human ether-à-go-go-related gene potassium channels. *Mol. Pharmacol.* **2003**, *64*, 59-69.
 104. Zhang, M.; Liu, X.-S.; Diochot, S.; Lazdunski, M.; Tseng, G.-N. APETx1 from sea anemone *Anthopleura elegantissima* is a gating modifier peptide toxin of the human ether-à-go-go-related potassium channel. *Mol. Pharmacol.* **2007**, *72*, 259-268.
 105. Wang, J.; Salata, J. J.; Bennett, P. B. Saxitoxin is a gating modifier of hERG K⁺ channels. *J. Gen. Physiol.* **2003**, *121*, 583-598.
 106. Korolkova, Y. V.; Kozlov, S. A.; Lipkin, A. V.; Pluzhnikov, K. A.; Hadley, J. K.; Filippov, A. K.; Brown, D. A.; Angelo, K.; Strøbæk, D.; Jespersen, T.; Olesen, S.-P.; Jensen, B. S.; Grishin, E. V. An ERG channel inhibitor from the scorpion *Buthus eupeus*. *J. Biol. Chem.* **2001**, *276*, 9868-9876.
 107. Angelo, K.; Korolkova, Y. V.; Grunnet, M.; Grishin, E. V.; Pluzhnikov, K. A.; Klaerke, D. A.; Knaus, H.-G.; Möller, M.; Olesen, S.-P. A radiolabeled peptide ligand of the hERG channel, [¹²⁵I]-BeKm-1. *Pflugers Arch.* **2003**, *447*, 55-63.
 108. Milnes, J. T.; Dempsey, C. E.; Ridley, J. M.; Crociani, O.; Arcangeli, A.; Hancox, J. C.; Witchel, H. J. Preferential closed channel blockade of hERG potassium currents by chemically synthesised BeKm-1 scorpion toxin. *FEBS letters* **2003**, *547*, 20-26.

Chapter 3

Allosteric modulators of the K_v11.1 (hERG) channel

Radioligand binding assays reveal allosteric characteristics of dofetilide analogues

Zhiyi Yu
Elisabeth Klaasse
Laura H. Heitman
Adriaan P. IJzerman

Adapted from Toxicol. Appl. Pharmacol. 2014, 274, 78-86.

Abstract

Drugs that block the cardiac $K_v11.1$ channel encoded by the human ether-à-go-go gene (hERG) have been associated with QT interval prolongation leading to proarrhythmia, and in some cases, sudden cardiac death. Because of special structural features of the $K_v11.1$ channel, it has become a promiscuous target that interacts with pharmaceuticals of widely varying chemical structures and a reason for concern in the pharmaceutical industry. The structural diversity suggests that multiple binding sites are available on the channel with possible allosteric interactions between them. In the present study, three reference compounds and nine compounds of a previously disclosed series were evaluated for their allosteric effects on the binding of [3H]astemizole and [3H]dofetilide to the $K_v11.1$ channel. LUF6200 was identified as an allosteric inhibitor in dissociation assays with both radioligands, yielding similar EC_{50} values in the low micromolar range. However, potassium ions increased the binding of the two radioligands in a concentration-dependent manner, and their EC_{50} values were not significantly different, indicating that potassium ions behaved as allosteric enhancers. Furthermore, addition of potassium ions resulted in a concentration-dependent leftward shift of the LUF6200 response curve, suggesting positive cooperativity and distinct allosteric sites for them. In conclusion, our investigations provide evidence for allosteric modulation of the $K_v11.1$ channel, which is discussed in the light of findings on other ion channels.

Introduction

The $K_v11.1$ channel, encoded by the hERG gene¹, is responsible for the rapid delayed rectifier K^+ current (I_{Kr}) that plays a critical role in the repolarization of cardiomyocytes during the cardiac action potential². It is made up of large intracellular N- and C-terminal domains^{3,4} and four identical α -subunits, each of which is formed by six α -helical transmembrane domains and a looping “pore region”^{5,6}. In humans, blockade of the $K_v11.1$ channel by drugs can cause excessive lengthening of the action potential, which is reflected by a QT interval prolongation in the electrocardiogram (ECG)^{7,8}. The excessive action potential prolongation may combine to produce and sustain Torsade de Pointes (TdP), which can be self-limiting or degenerate into ventricular fibrillation rapidly leading to death^{6,8}. Therefore, it has become a routine practice in the pharmaceutical industry to test compounds for their $K_v11.1$ liability during early preclinical safety assessments according to FDA guidelines⁹. In recent years, most attention has been paid to assess the affinity for the $K_v11.1$ channel of potential drug candidates in order to avoid and discard modest-to-high affinity compounds during the lead finding and optimization process¹⁰. However, allosteric modulation of the $K_v11.1$ channel as an alternative way of interaction has not been studied in any details until now.

With regard to G protein-coupled receptors (GPCRs), successful drugs that mediate their effects through the allosteric modulation of target activity have already reached the market, also in view of their potential greater selectivity, potency and/or safety profile when compared to orthosteric ligands^{11,12}. Radioligand binding assays, in particular kinetic radioligand dissociation assays, have been widely utilized to quantify the allosteric effects of GPCR ligands¹³. As for ion channels, allosteric modulators have been reported for ligand-gated ion channels in particular. For example, GW791343 might be applied to treat inflammatory disorders and pain due to its allosteric inhibition of the $P2X_7$ receptor^{14,15}. A negative allosteric modulator of the nicotinic acetylcholine receptor, UCI-30002, had been reported to have significant benefits as a strategy for treating nicotine addiction because of its high subtype-selectivity¹⁶. It has also become increasingly apparent that new potent and selective allosteric modulators of the GABA-A receptor and 5-HT₃ receptor may replace conventional antagonists and agonists for these targets^{17,18}. Allosteric modulation of voltage-gated ion channels such as several types of calcium, sodium and potassium channels and their possible clinical applications has been investigated as well, but to a lesser extent. As an example, a novel quinazolinone ligand (TTA-Q4) showed a positive allosteric interaction with the T-Type calcium channel since it enhanced radioligand binding, increased affinity in a saturable manner and slowed dissociation¹⁹.

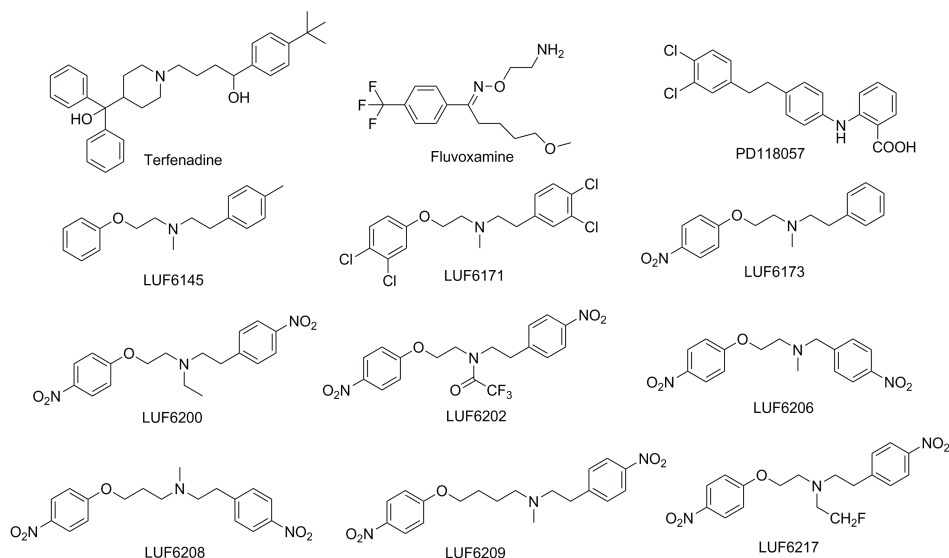


Figure 1. Compounds evaluated in this study. Terfenadine is a high-affinity reference $K_v11.1$ blocker, fluvoxamine is a low-affinity reference $K_v11.1$ blocker, PD118057 is a reference $K_v11.1$ activator, and all the other LUF compounds are members of a previously disclosed compound series interacting with the $K_v11.1$ channel.

Radioligand binding assays as a means of studying the $K_v11.1$ channel have been developed over the years. Two radioligands, [3H]astemizole and [3H]dofetilide, have mostly been used^{20–22}. The purpose of the present study was to identify and investigate allosteric modulators of the $K_v11.1$ channel using these two radioligands. The anti-depressant fluvoxamine²³ and the channel opener PD118057^{24, 25} (**Figure 1**), reported to have binding sites different from conventional $K_v11.1$ blockers, were selected as representative reference compounds. We identified a number of dofetilide analogues (**Figure 1**) displaying allosteric modulation in a pilot experiment and these were further investigated as were the allosteric effects of potassium ions in the same binding assays. Our findings suggest potential applications for such allosteric modulators, which might provide novel solutions for drug cardiotoxicity due to blockade of the $K_v11.1$ channel.

Materials and methods

Chemicals and reagents

Astemizole, terfenadine, fluvoxamine and PD118057 were purchased from Sigma Aldrich (Zwijndrecht, The Netherlands). Dofetilide and all the LUF compounds were synthesized in our own laboratory, as published previously²⁶. [3H]

Astemizole (specific activity 78.9 Ci·mmol⁻¹) and [³H]dofetilide (specific activity 70.0 Ci·mmol⁻¹) were purchased from Perkin Elmer (Groningen, The Netherlands). Bovine serum albumin (BSA, fraction V) was purchased from Sigma (St. Louis, MO). G418 was obtained from Stratagene (Cedar Creek, USA). All the other chemicals were of analytical grade and obtained from standard commercial sources. HEK293 cells stably expressing the K_v11.1 channel (HEK293K_v11.1) were kindly provided by Dr. Eckhard Ficker (University of Cleveland, USA).

Cell culture

HEK293K_v11.1 cells were cultured in a humidified atmosphere at 37 °C and 7% CO₂ in DMEM, containing 10% fetal calf serum, 50 IU mL⁻¹ penicillin, 50 µg·mL⁻¹ streptomycin and 1.25 µg·mL⁻¹ G418 for selection. Cells were subcultured twice a week (1:8). Then, the cells were subcultured 1:10 and transferred to large 15-cm diameter plates for membrane preparation.

Membrane preparation

HEK293K_v11.1 cells were grown to 80-90% confluence and detached from the plates by scraping them into 5 mL of PBS. Then, the detached cells were collected and centrifuged at 250 g for 10 min. The cell pellets were pooled and resuspended in 50 mM ice-cold Tris-HCl buffer containing 2 mM MgCl₂, pH 7.4. An UltraTurrax (Heidolph Instruments, Schwabach, Germany) was used to homogenize the cell suspension. Membranes and the cytosolic fraction were separated by centrifugation at 100,000 g in an Optima LE-80K ultracentrifuge (Beckman Coulter, Fullerton, CA) at 4 °C for 20 min. The pellets were resuspended in the Tris-HCl buffer, and the homogenization and centrifugation steps were repeated. The resulting pellets were resuspended in ice-cold incubation buffer (10 mM HEPES, 130 mM NaCl, 60 mM KCl, 0.8 mM MgCl₂, 1 mM EGTA, 10 mM glucose, 0.1% BSA, pH 7.4) using the UltraTurrax. Aliquots (125 or 250 µL) were stored at -80 °C. The protein concentration of the membranes was measured using the BCA method²⁷.

Kinetic radioligand association and dissociation assays

The incubation temperature and protein concentration were optimized for the kinetic studies. Three different temperatures (4, 15 and 25 °C) and five protein amounts (10, 15, 20, 30 and 50 µg) were investigated at the beginning of our research program. The optimal conditions for [³H]astemizole kinetic studies proved to be using 30 µg of membrane protein at an incubation temperature of 15 °C. The

association experiments of [^3H]astemizole were performed by incubating membrane aliquots containing 30 μg protein in a total volume of 100 μL incubation buffer at 15 $^{\circ}\text{C}$ for 90 min with 2 nM [^3H]astemizole. The amounts of radioligand bound to the receptor were measured at various time intervals during the incubation. The dissociation experiments were conducted by preincubating membrane aliquots containing 30 μg protein in a total volume of 100 μL incubation buffer at 15 $^{\circ}\text{C}$ for 90 min with 2 nM [^3H]astemizole. After preincubation, dissociation was initiated by addition of 10 μM astemizole for a total period of 60 min. The amounts of [^3H]astemizole still bound to the receptor were also measured at various time intervals. Separation of bound from free radioligand was performed by rapid filtration through Whatman GF/B filters using a Brandel harvester. Filters were subsequently washed six times with 2 mL ice-cold wash buffer (25 mM Tris-HCl, 130 mM NaCl, 60 mM KCl, 0.8 mM MgCl_2 , 0.05 mM CaCl_2 , 0.05% BSA, pH 7.4). Filter-bound radioactivity was determined by scintillation spectrometry using a liquid Scintillation Analyzer (Tri-Carb 2900TR) after addition of 3.5 mL Packard Emulsifier Safe and 2 h extraction.

For the kinetic studies of [^3H]dofetilide binding we used 20 μg of membrane protein at an incubation temperature of 25 $^{\circ}\text{C}$ with 5 nM [^3H]dofetilide. The association experiments were performed for 120 min, whereas the dissociation assays were induced by 10 μM dofetilide after a total period of 120 min preincubation and followed for another 60 min. Incubations were terminated, and samples were obtained and analyzed as described for [^3H]astemizole.

Kinetic radioligand dissociation assays-allosteric modulation

Single point dissociation assays

Dissociation experiments were mainly performed as described in the above paragraph. After preincubation, dissociation was initiated by addition of 10 μM astemizole or dofetilide in the absence (control) or presence of 10 μM of other ligands. After 10 min of dissociation, samples were separated by rapid filtration through a 96-well GF/B filter plate using a Perkin Elmer Filtermate-harvester (Perkin Elmer, Groningen, The Netherlands). Filters were subsequently washed twelve times with ice-cold wash buffer. The filter-bound radioactivity was determined by scintillation spectrometry using the 1450 Microbeta Wallac Trilux scintillation counter (Perkin Elmer) after addition of 37.5 μL Microscint and 2 h extraction. The binding of [^3H]astemizole or [^3H]dofetilide in the control was set as 100%.

Dissociation assays

After preincubation, dissociation was initiated by addition of 10 μ M astemizole or dofetilide in the absence (control) or presence of 10 μ M of possible allosteric modulators for a total period of 60 min. The amounts of radioligand still bound to the receptor were measured at various time intervals. Incubations were terminated, and samples were obtained as described in “*Single point dissociation assays*”.

Concentration dependency of allosteric modulators

In this setup the dissociation assay of [3 H]dofetilide was performed at 15 °C and the preincubation time to achieve radioligand association was 180 min; the dissociation assay for [3 H]astemizole was the same as described in “*Kinetic radioligand association and dissociation assays*”. After preincubation, dissociation was initiated by addition of 10 μ M astemizole or dofetilide in the absence (control) or presence of different concentrations of allosteric modulators. Incubations were terminated after 10 min of dissociation, and samples were obtained as described in “*Single point dissociation assays*”.

Equilibrium radioligand binding assays

The [3 H]astemizole and [3 H]dofetilide equilibrium binding assays for the K_v 11.1 channel were performed as described before^{20-22, 28} with minor modifications. In short, membrane aliquots containing 30 μ g protein for [3 H]astemizole or 20 μ g protein for [3 H]dofetilide were incubated in a total volume of 100 μ l incubation buffer at 25 °C for 60 min. Binding experiments were performed using a series of concentrations of potassium ions in the presence of 2 nM [3 H]astemizole or 5 nM [3 H]dofetilide. Nonspecific binding was determined in the presence of 10 μ M astemizole and represented approximately 15% of the total binding. [3 H]astemizole and [3 H]dofetilide did not show specific binding to membranes prepared from HEK293 cells lacking the expressed K_v 11.1 channel. The binding of [3 H]astemizole and [3 H]dofetilide in the presence of 100 mM KCl was set at 100% in all experiments, whereas nonspecific binding was set at 0%. Incubations were terminated by dilution with ice-cold wash buffer, and samples were obtained as described in “*Kinetic radioligand association and dissociation assays*”.

Cooperativity between different allosteric modulators

The dissociation assay of [3 H]dofetilide in the presence of different concentrations of KCl (2, 5, 10 and 60 mM) was performed as described in “*Concentra-*

tion dependency of allosteric modulators". After preincubation, dissociation was initiated by addition of 10 μM dofetilide in the absence (control) or presence of different concentrations of LUF6200. Incubations were terminated after 6 min of dissociation, and samples were obtained as described in "Single point dissociation assays".

Data analysis

All data of radioligand binding assays were analyzed with Prism v. 5.0 (Graph-Pad, San Diego, CA, USA). EC_{50} values for potassium ions were directly obtained from the non-linear regression concentration-effect curves. Dissociation rate constants, k_{off} , were obtained by computer analysis of the exponential decay of [^3H]astemizole or [^3H]dofetilide bound to the receptor. Association rate constants, k_{on} , were calculated according to the equation $k_{\text{on}} = (k_{\text{obs}} - k_{\text{off}})/[\text{L}^*]$, where the k_{obs} was obtained by computer analysis of the exponential association of [^3H]astemizole or [^3H]dofetilide bound to the receptor and $[\text{L}^*]$ was the amount of radioligand used for the association experiments. EC_{50} values from the dissociation experiments were calculated by non-linear regression analysis of concentration-effect curves of dissociation in the presence of different concentrations of unlabeled ligands. The differences of binding parameters between compounds and control were analyzed by an unpaired student t test. Significance was determined as $P < 0.05$. All values obtained are means of at least three independent experiments performed in duplicate.

Results

Optimization of assay conditions for [^3H]astemizole and [^3H]dofetilide kinetic study

Assay conditions were optimized according to a general radioligand binding protocol in our laboratory²⁹. Firstly, displacement assays for [^3H]astemizole and [^3H]dofetilide were performed at five different amounts of HEK293K_v11.1 membranes (10, 15, 20, 30 and 50 μg). A suitable window of specific [^3H]astemizole binding was obtained using 30 μg of membrane protein, whereas 20 μg of protein was required for [^3H]dofetilide binding to achieve a similar window. These membrane protein concentrations were also selected for the further kinetic study of two radioligands. Then, since it has been reported that compounds like AICAR or phenformine can also inhibit the K_v11.1 currents via activating AMP-dependent protein kinase³⁰, the binding of [^3H]astemizole and [^3H]dofetilide at membranes

prepared from HEK293 cells lacking the expressed $K_v11.1$ channel were determined. Neither of the two radioligands showed any specific binding here, indicating the direct binding of astemizole and dofetilide to the $K_v11.1$ channel. Subsequently, the association and dissociation of [3H]astemizole and [3H]dofetilide were determined at three different temperatures (4, 15 and 25 °C). The optimal incubation temperature was found to be 15 °C for [3H]astemizole and 25 °C for [3H]dofetilide concerning the appropriate on- and off-rates and the practical convenience of the experiments. Nevertheless, these findings were not applied too stringently as concentration-dependent effects of allosteric modulators of [3H]astemizole and [3H]dofetilide binding to the $K_v11.1$ channel were later conducted at 15 °C and concentration-effect curves for K^+ ions were recorded at 25 °C in order to obtain comparable results between the two radioligand binding assays.

Association and dissociation of [3H]astemizole from the HEK-293 $K_v11.1$ membranes

Because association and dissociation of [3H]astemizole from the HEK293 $K_v11.1$ membranes were both very fast at 25 °C, the kinetic study of [3H]astemizole binding was performed at 15 °C using 30 μ g HEK293 $K_v11.1$ membrane protein. The data were best described by non-linear regression using a mono-exponential model. As is shown in **Figure 2A** and **Table 1**, the binding equilibrium was reached within 90 min with a k_{on} value of $0.068 \pm 0.010 \text{ nM}^{-1} \cdot \text{min}^{-1}$. The dissociation rate and half-life time of [3H]astemizole were $0.055 \pm 0.010 \text{ min}^{-1}$ and $11 \pm 1.4 \text{ min}$, respectively (**Figure 2B** and **Table 1**). The dissociation of [3H]astemizole at 10 min was almost half of the total binding, so the 10-min dissociation time was selected for assessing the allosteric effects of compounds on the $K_v11.1$ channel in the follow-up experiments.

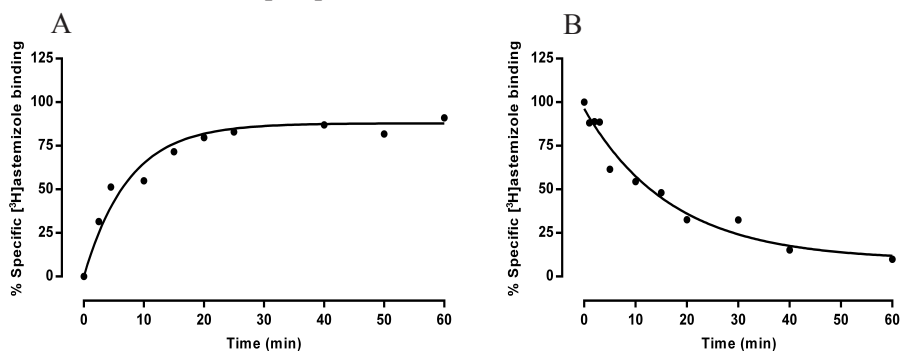


Figure 2. Association and dissociation curves of [3H]astemizole binding to the $K_v11.1$ channel. (**A**: Association curve; **B**: Dissociation curve) Dissociation was started by addition of 10 μ M astemizole after 90 min preincubation. Experiments were performed at 15

°C using 30 µg of HEK293K_v11.1 membrane protein.

Table 1. The association rate (k_{on}), dissociation rate (k_{off}) and the kinetically derived K_d of [³H]astemizole and [³H]dofetilide binding to the K_v11.1 channel.

	k_{on} (nM ⁻¹ ·min ⁻¹)	k_{off} (min ⁻¹)	K_d (nM)
Astemizole^a	0.068 ± 0.010	0.055 ± 0.010	0.85 ± 0.045
Dofetilide^b	0.032 ± 0.0026	0.20 ± 0.026	6.4 ± 1.3

Values are means (± S.E.M.) of at least three independent assays performed in duplicate.

^aThe association and dissociation assays of [³H]astemizole were performed at 15 °C.

^bThe association and dissociation assays of [³H]dofetilide were conducted at 25 °C.

Association and dissociation of [³H]dofetilide from the HEK-293K_v11.1 membranes

As is depicted in **Figure 3**, the association of [³H]dofetilide reached equilibrium at around 30 min, and it completely dissociated from the K_v11.1 channel within 60 min after addition of 10 µM dofetilide. By analyzing association and dissociation curves using a mono-exponential model, the k_{on} , k_{off} and $t_{1/2}$ values were 0.032 ± 0.0026 nM⁻¹·min⁻¹ and 0.20 ± 0.026 min⁻¹, respectively (**Table 1**). Similar to [³H]astemizole binding assay, a 10-min dissociation time point was chosen for the further study of allosteric modulators of the K_v11.1 channel.

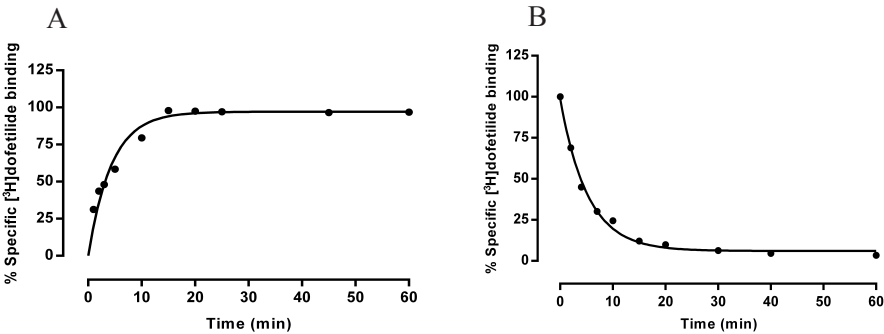


Figure 3. Association and dissociation curves of [³H]dofetilide binding to the K_v11.1 channel. (A: Association curve; B: Dissociation curve) Dissociation was started by addition of 10 µM dofetilide after 120 min preincubation. Experiments were performed at 25 °C using 20 µg of HEK293K_v11.1 membrane protein.

Screening for allosteric modulators of [³H]astemizole and [³H]dofetilide binding

Table 2. The specific binding of [³H]astemizole and [³H]dofetilide to the K_v11.1 channel after 10 min of dissociation in the absence (B_{control}) or presence of 10 μM unlabelled ligands (B).

Compound	%B/B _{control} of [³ H]astemizole	%B/B _{control} of [³ H]dofetilide
Control	100 ± 0	100 ± 0
Terfenadine	98 ± 1	93 ± 7
Fluvoxamine	129 ± 13 *	95 ± 12
PD118057	133 ± 14 *	109 ± 2 *
LUF6145	109 ± 5	93 ± 2
LUF6171	102 ± 6	104 ± 3
LUF6173	97 ± 8	71 ± 5 *
LUF6200	39 ± 4 ***	50 ± 1 ***
LUF6202	70 ± 2 ***	62 ± 4 *
LUF6206	86 ± 2 ***	70 ± 7 *
LUF6208	36 ± 6 ***	47 ± 5 **
LUF6209	39 ± 2 ***	43 ± 8 *
LUF6217	53 ± 4 ***	54 ± 5 *

Values are means (± S.E.M.) of three independent assays performed in duplicate. (* P < 0.05; ** P < 0.01; *** P < 0.001 versus control)

We screened three reference ligands and an in-house library of K_v11.1 blockers (LUF compounds) to identify their allosteric effects on [³H]astemizole binding to the K_v11.1 channel using a single point dissociation assay. This protocol resulted in several compounds that potentially increased (allosteric enhancers) and decreased (allosteric enhancers) the dissociation of the radioligand. All the data are listed in **Table 2** and shown in **Figure 4**. Fluvoxamine and PD118057 appeared to increase the specific binding of [³H]astemizole by 29 and 33% above control after 10 min, suggesting that they might behave as allosteric enhancers of [³H]astemizole binding. On the contrary, some of the compounds synthesized in our laboratory including LUF6200, LUF6208, LUF6209 and LUF6217 substantially reduced the binding of [³H]astemizole, supporting their role as allosteric inhibitors by accelerating the dissociation of the radioligand. Among them, LUF6200, 6208 and LUF6209 were the most potent allosteric inhibitors with only 39 ± 4, 36 ± 6 and 39 ± 2% specific binding left compared with 100% for the control. In ad-

dition, LUF6202 and LUF6206 also displayed significant allosteric inhibition effects, but to a lesser extent. Other compounds (terfenadine, LUF6145, LUF6171 and LUF6173) had no significant allosteric modulatory effects in this experiment.

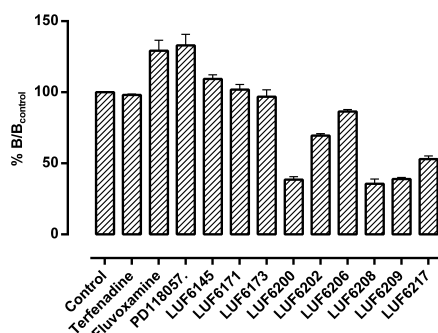


Figure 4. Bar graphs of the percentage specific binding of [³H]astemizole to the K_v11.1 channel after 10 min of dissociation induced by 10 μM astemizole in the absence (control) or presence of 10 μM of different compounds. The specific binding of [³H]astemizole in the absence of compounds was set as 100%. Experiments were performed at 15 °C using 30 μg HEK293K_v11.1 membrane protein.

The effects of the same compounds in the single point dissociation experiments of [³H]dofetilide binding to the K_v11.1 channel are shown in **Figure 5** and **Table 2**. The results obtained from this assay were almost the same as those derived from the [³H]astemizole binding assay. The only two exceptions were that fluvoxamine exerted no allosteric enhancement here and that LUF6173 now showed significant allosteric inhibition of [³H]dofetilide binding.

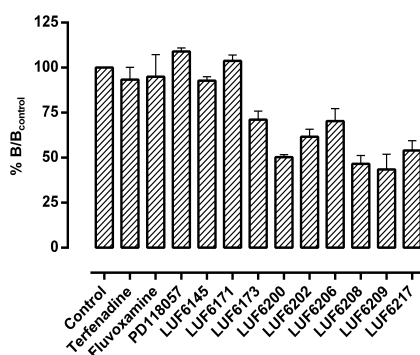


Figure 5. Bar graphs of the percentage specific binding of [³H]dofetilide to the K_v11.1 channel after 10 min of dissociation induced by 10 μM dofetilide in the absence (control) or presence of 10 μM of different compounds. The specific binding of [³H]dofetilide in the absence of compounds was set as 100%. Experiments were performed at 25 °C using 20 μg HEK293K_v11.1 membrane protein.

Subsequently, fluvoxamine, PD118057 and one potent representative allosteric inhibitor (LUF6200) were selected for the further experiments to validate their allosteric modulation effects.

Dissociation of [³H]astemizole from the K_v11.1 channel: effects of fluvoxamine, PD118057 and LUF6200

The dissociation of [³H]astemizole from the the K_v11.1 channel was induced by 10 μM astemizole in the absence (control) or presence of 10 μM of fluvoxamine, PD118057 or LUF6200 during a 60-min time course at 15 °C. The results are depicted in **Figure 6**. The dissociation rates of [³H]astemizole in the presence of fluvoxamine and PD118057 were $0.040 \pm 0.0091 \text{ min}^{-1}$ and $0.055 \pm 0.0053 \text{ min}^{-1}$, respectively, which were not significantly different from the control ($k_{\text{off}} = 0.055 \pm 0.010 \text{ min}^{-1}$). Moreover, the three curves in the absence or presence of fluvoxamine and PD118057 practically overlapped with each other. Thus, in this more detailed experiment, we verified that fluvoxamine and PD118057 did not allosterically enhance [³H]astemizole binding at a concentration of 10 μM. Interestingly, LUF6200 increased the dissociation rate of radioligand binding notably to a k_{off} value of $0.21 \pm 0.011 \text{ min}^{-1}$ ($P = 0.0005$), which corresponded to a 3.7-fold increase in the dissociation rate found for [³H]astemizole alone.

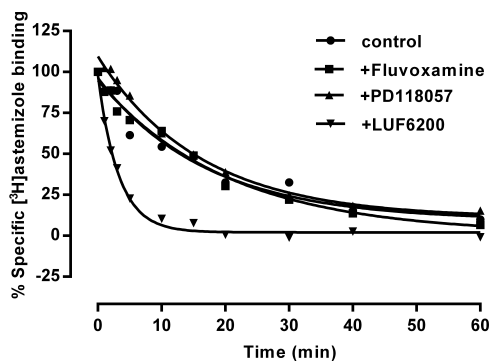


Figure 6. Dissociation curves of [³H]astemizole induced by 10 μM astemizole in the absence (control) or presence of 10 μM fluvoxamine, PD118057 and LUF6200. Experiments were performed at 15 °C using 30 μg HEK293K_v11.1 membrane protein.

Dissociation of [³H]dofetilide from the K_v11.1 channel: effects of PD118057 and LUF6200

Since fluvoxamine was found to have no allosteric capacity in both the [³H]astemizole and [³H]dofetilide binding assays described above, only PD118057 and

LUF6200 were tested for their allosteric effects on [3 H]dofetilide binding to the $K_v11.1$ channel (**Figure 7**). The results demonstrated that LUF6200 accelerated the dissociation rate of [3 H]dofetilide from $0.20 \pm 0.026 \text{ min}^{-1}$ to $1.5 \pm 0.17 \text{ min}^{-1}$ ($P = 0.0016$), while the k_{off} of [3 H]dofetilide in the presence of $10 \mu\text{M}$ PD118057 was $0.20 \pm 0.015 \text{ min}^{-1}$, displaying no enhancement effects on the binding of [3 H]dofetilide. This further proved that LUF6200 was an allosteric inhibitor but that PD118057 was not an allosteric enhancer of the binding of $K_v11.1$ radioligands.

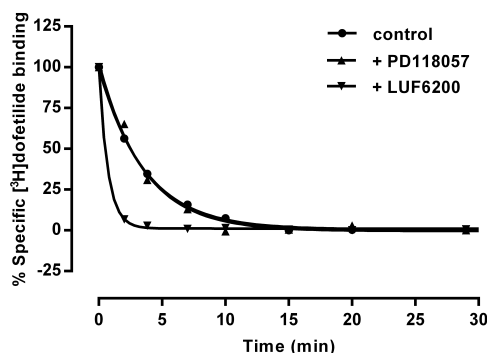


Figure 7. Dissociation curves of [3 H]dofetilide by $10 \mu\text{M}$ dofetilide in the absence (control) or presence of $10 \mu\text{M}$ PD118057 and LUF6200. Experiments were performed at 25°C using $20 \mu\text{g}$ HEK293 $K_v11.1$ membrane protein.

Concentration dependence of allosteric effects of LUF6200 on [3 H]astemizole and [3 H]dofetilide binding

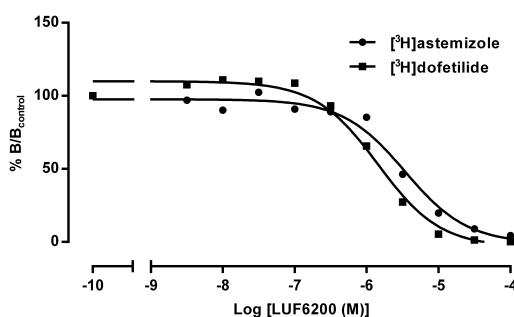


Figure 8. Concentration dependence curves of LUF6200 for accelerating the [3 H]astemizole or [3 H]dofetilide dissociation from the $K_v11.1$ channel. Membranes were first pre-equilibrated with [3 H]astemizole or [3 H]dofetilide, then the dissociation was induced by $10 \mu\text{M}$ astemizole or dofetilide in the absence (control) or presence of different concentrations of LUF6200 and the reaction was terminated after 10 min. The results are expressed as the ratio of the specific binding of [3 H]astemizole or [3 H]dofetilide in the

presence of 10 μM astemizole or dofetilide plus various concentrations of LUF6200 (B) over that in the presence of 10 μM astemizole or dofetilide alone (B_{control}). Experiments were performed at 15 $^{\circ}\text{C}$ using 30 μg HEK293K_v11.1 membrane protein for [^3H]astemizole and 20 μg membrane protein for [^3H]dofetilide binding.

The influence of increasing concentrations of LUF6200 on the dissociation of [^3H]astemizole and [^3H]dofetilide induced by 10 μM astemizole or dofetilide is shown in **Figure 8**. After 10 min of dissociation, the process was terminated by washing and rapid filtration. LUF6200 accelerated the dissociation of [^3H]astemizole and [^3H]dofetilide in a concentration-dependent manner with similar, not statistically significantly different, EC_{50} values of 4.9 ± 0.52 and 3.4 ± 0.97 μM , respectively ($P = 0.45$).

Concentration dependent effects of potassium ions on [^3H]astemizole and [^3H]dofetilide binding

To assess the influence of increasing concentrations of potassium ions on the binding of [^3H]astemizole and [^3H]dofetilide, we determined the specific binding of [^3H]astemizole and [^3H]dofetilide at different concentrations of KCl after 60 min preincubation at 25 $^{\circ}\text{C}$. The results are shown in **Figure 9**. The binding of both [^3H]astemizole and [^3H]dofetilide were elevated with increasing concentrations of potassium ions and reached a plateau as of a concentration of 30 mM. The mean EC_{50} values in the two different radioligand binding assays were 7.2 ± 0.60 mM and 8.1 ± 0.47 mM for [^3H]astemizole and [^3H]dofetilide, respectively, which were not significantly different ($P = 0.30$). It is also worth noting that when no potassium ions were added to incubation mixture, the specific binding of [^3H]astemizole and [^3H]dofetilide was negligible (data not shown).

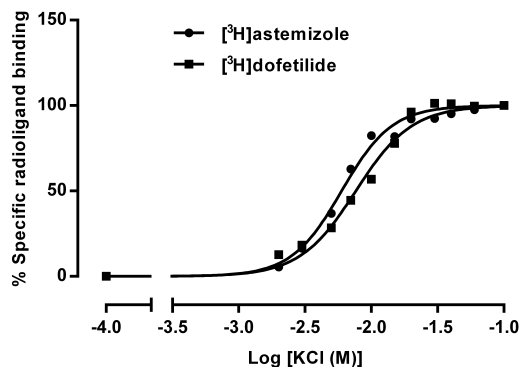


Figure 9. Dose-response curves of the specific binding of [^3H]astemizole and [^3H]dofetilide at different concentrations of potassium ions. Experiments were performed at 25 $^{\circ}\text{C}$

using 30 μg HEK293K_v11.1 membrane protein for [³H]astemizole binding and 20 μg membrane protein for [³H]dofetilide binding.

Effects of potassium ions on the acceleration of the [³H]dofetilide dissociation rate induced by LUF6200

In order to investigate whether the two modulators described above acted at different sites to produce these effects, the concentration-dependent effect of LUF6200 on [³H]dofetilide dissociation was studied in the presence of four different concentrations of KCl (**Figure 10**). The data obtained are represented in two formats. **Figure 10A** shows that addition of potassium ions decreased the dissociation, whereas LUF6200 dose-dependently enhanced that dissociation. **Figure 10B** demonstrates that addition of potassium ions resulted in a concentration-dependent leftward shift of the LUF6200 concentration-effect curve. The EC₅₀ values of LUF6200 in the presence of 2, 5, 10 and 60 mM potassium ions were 11 ± 1.7 , 6.4 ± 0.74 , 4.7 ± 0.53 and 3.5 ± 0.12 μM , respectively. This indicates that LUF6200 and potassium ions act at distinct allosteric sites on the K_v11.1 channel, and that potassium ions enhanced the allosteric effect of LUF6200.

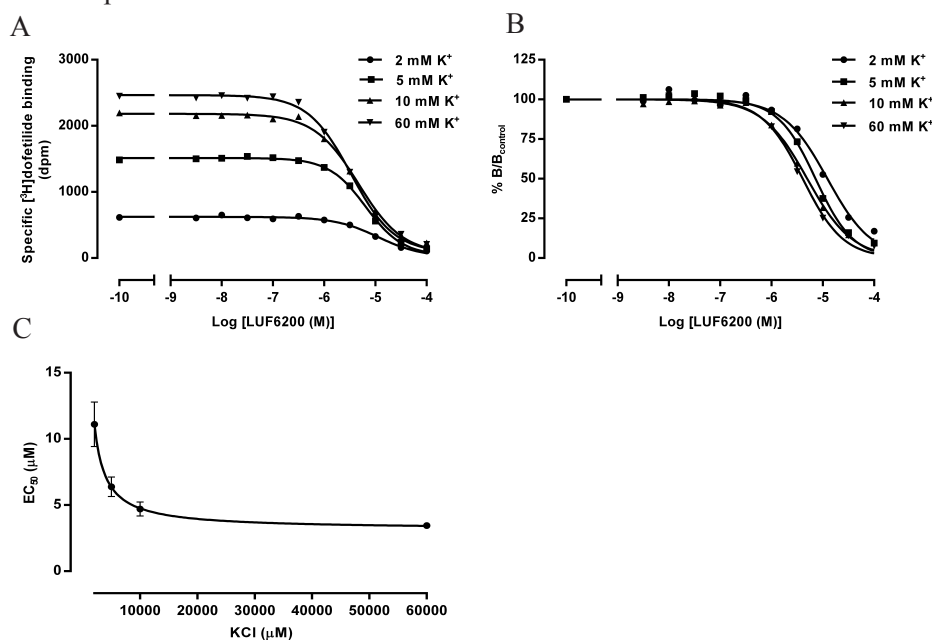


Figure 10. Concentration-effect curves of LUF6200 for accelerating the [³H]dofetilide dissociation from the K_v11.1 at 2, 5, 10 and 60 mM potassium ions before (**A**) and after normalization (**B**), and the positive cooperativity effect of potassium ions on LUF6200 in enhancing [³H]dofetilide dissociation (**C**). Membranes were first pre-equilibrated with [³H]dofetilide at different concentrations of potassium ions, then the dissociation was in-

duced by 10 μM dofetilide in the absence (control) or presence of different concentrations of LUF6200 and the reaction was terminated after 6 min. The results in **B** are expressed as the ratio of the specific binding of [^3H]dofetilide in the presence of 10 μM dofetilide plus various concentrations of LUF6200 (B) over that in the presence of 10 μM dofetilide alone (B_{control}). Experiments were performed at 15 $^{\circ}\text{C}$ using 20 μg HEK293K $_{\text{v}}$ 11.1 membrane protein. The experimental data of different concentrations of potassium ions affecting the modulating potency of LUF6200 are exhibited with standard error of the mean from three independent experiments (**C**).

Last, the cooperativity between LUF6200 and potassium ions was further analyzed according to a cooperativity model studied by us previously³¹, and the curve connecting all the data is displayed in **Figure 10C**. We discriminated three possible situations³¹, in which two compounds showed positive ($\delta > 1$), neutral ($\delta = 1$) or negative cooperativity ($\delta < 1$). In the present study, our data points complied with $\delta > 1$, thus further supporting a positive cooperativity between the binding of LUF6200 and potassium ions.

Discussion

In the present study, we evaluated the allosteric effects of a series of compounds with diverse chemical structures on the K $_{\text{v}}$ 11.1 channel using both [^3H]astemizole and [^3H]dofetilide binding assays, and also addressed the influence of potassium ions on the binding of two radioligands. To the best of our knowledge, this study is the first time to utilize radioligand binding assays for the characterization of allosteric modulators for the K $_{\text{v}}$ 11.1 channel. From these initial results, one potent allosteric inhibitor (LUF6200) was identified and several other compounds including LUF6208, LUF6209, LUF6217, LUF6202 and LUF6206 were also shown to possess allosteric inhibitory effects in two radioligand binding assays. Moreover, potassium ions increased the binding of [^3H]astemizole and [^3H]dofetilide to the K $_{\text{v}}$ 11.1 channel. Additionally, fluvoxamine and PD118057, known to have binding sites distinct from most other K $_{\text{v}}$ 11.1 blockers, exhibited no allosteric effects in this investigation.

A common binding site for a wide spectrum of K $_{\text{v}}$ 11.1 blockers, including astemizole and dofetilide, has been implied through different methods^{32, 33}. However, the amino acid residues involved in the interaction of these structurally diverse compounds may be different³². Therefore, in this study two different radioligands ([^3H]astemizole and [^3H]dofetilide) were adopted in order to study, validate and compare the behavior of putative allosteric modulators. Since an altered dissociation rate is unequivocally indicative of an allosteric interaction³⁴, [^3H]astemizole and [^3H]dofetilide dissociation assays were firstly developed and then performed

to reveal the allosteric effects of different ligands. The results in this paper show that both [^3H]astemizole and [^3H]dofetilide exhibit fast association rates and dissociate from the $\text{K}_{\text{v}}11.1$ channel after addition of an excess of unlabelled astemizole or dofetilide, indicative of the reversible binding of the two ligands. Additionally, both the association and dissociation curves of the two radioligands are better fitted with a single-site than a two-site model, which is different from the two binding sites model for [^3H]dofetilide reported by Duff et al.³⁵ However, the latter experiments were performed on intact cells instead of membrane preparations used in our study. The diffusion into and possible trapping of [^3H]dofetilide inside the intact cells might affect the association and dissociation of the radioligand significantly.

Subsequently, single time point dissociation assays were conducted to screen for allosteric modulators of the $\text{K}_{\text{v}}11.1$ channel. LUF6200 was selected as a representative allosteric inhibitor from the screening experiments due to its potent effects on both [^3H]astemizole and [^3H]dofetilide binding. Besides, terfenadine, which occupies the same binding site as astemizole and dofetilide³⁶, did not display allosteric effects in either of the two radioligand screening assays, suggesting the validity and accuracy of our methods. To further characterize the allosteric effects of LUF6200, a full radioligand dissociation assay was performed in the presence of this compound. LUF6200 caused a 3.7- and 7.5-fold increase in the dissociation rates of [^3H]astemizole and [^3H]dofetilide, respectively. This further supports the notion that LUF6200 is an allosteric inhibitor of conventional $\text{K}_{\text{v}}11.1$ blockers binding to the $\text{K}_{\text{v}}11.1$ channel. The EC_{50} values from the two different radioligand dissociation assays were almost the same and in the micromolar range, which suggests that astemizole and dofetilide occupy the same binding site on the $\text{K}_{\text{v}}11.1$ channel. In a previous study from our laboratory, LUF6200 displaced [^3H]astemizole binding from the $\text{K}_{\text{v}}11.1$ channel under equilibrium conditions with a very low K_{i} value of $1.2 \pm 0.6 \text{ nM}$ ²⁶. As is evident from **Figure 8**, there is little or negligible allosteric inhibition observed for LUF6200 at a concentration lower than $0.1 \mu\text{M}$. Taken together, we conclude that LUF6200 interacts with the $\text{K}_{\text{v}}11.1$ channel in a complicated fashion: it behaves as an orthosteric blocker at lower concentrations and as an allosteric inhibitor at higher concentrations.

Two major binding regions have been hypothesized for the $\text{K}_{\text{v}}11.1$ channel, one in the transmembrane region, the other extracellularly^{37, 38}. Most $\text{K}_{\text{v}}11.1$ blockers bind to the central transmembrane cavity of the channel, whereas agents described as facilitators, activators or enhancers of the $\text{K}_{\text{v}}11.1$ channel usually interact with a region facing away from the inner cavity³⁷. For instance, A-935142 has recently been stated to possess a binding site responsible for $\text{K}_{\text{v}}11.1$ current enhancement which is different from the pore binding site for traditional

K_v11.1 blockers³⁹. The binding sites of several peptide blockers like saxitoxin and BeKm-1 are located in the extracellular parts of the K_v11.1 channel^{40, 41} and some metal ions bind to different regions of the pore of the channel in comparison to most other K_v11.1 blockers^{42, 43}. Additionally, it has been reported that a few nontoxin K_v11.1 blockers are unlikely to fit within the inner cavity and must bind elsewhere^{23, 44}. Thus, multiple binding sites of these diverse compounds or ions at the K_v11.1 channel imply the plausible allosteric modulation between them. They might allosterically increase (allosteric inhibitors/negative allosteric modulators) or decrease (allosteric enhancers/positive allosteric modulators) the dissociation rates of typical K_v11.1 blockers from the channel. The current study does not allow determining the location of the putative binding site of LUF6200. Its nanomolar potency as a classical blocker suggests that it interacts with the central cavity; for its allosteric property a different binding site or different conformation of the channel may play a role, and further studies such as cross linker and western blotting experiments are required to elucidate the exact binding sites of this compound.

The results in this paper also show that fluvoxamine does not behave as an allosteric modulator when tested in a rigorous kinetic assay. However, it has been reported that the binding of fluvoxamine to the K_v11.1 channel did not involve amino acids such as Y652 and F656 that are crucial to the binding of other general K_v11.1 blockers^{45, 46}; hence, it was suggested that fluvoxamine probably binds to an extracellular site at the outer mouth of the channel²³. In addition, the activator PD118057 did not exert allosteric enhancement in both [³H]astemizole and [³H]dofetilide dissociation assays. PD118057 has been identified to bind to a hydrophobic binding pocket instead of the shared binding site for K_v11.1 blockers at the channel⁴⁷. The results obtained for these two compounds suggest that even though a compound binds to a distinct region of the K_v11.1 channel, its allosteric effects on the binding of other K_v11.1 blockers are still uncertain and need to be validated in more detailed experiments.

Since it has been reported that the extracellular potassium concentration affected the binding of [³H]dofetilide to neonatal mouse myocytes⁴⁸, we also studied the allosteric effects of potassium ions and found that these monovalent cations increase both [³H]astemizole and [³H]dofetilide binding in a concentration-dependent manner with very similar EC₅₀ values. In earlier studies on a variety of ion channels, it was reported that metal ion binding to the pore of an ion channel may affect the occupancy of the binding site for other ligands and thus decrease their binding^{42, 49}. This is in contrast to the observation in our study. Thus, we assume that K⁺ ions possibly function as an allosteric enhancer of K_v11.1 blockers by changing the conformation of their binding site rather than competitively oc-

cupying their binding site. Since two distinct allosteric sites on the human GnRH receptor³¹ and three different allosteric sites on the dopamine D₄ receptor⁵⁰ have been reported, we wondered whether LUF6200 and potassium ions exert their effect through two distinct allosteric sites on the K_v11.1 channel as well. Potassium ions both enhance the allosteric effect of LUF6200 and shift the LUF6200 dose–response curve to the left, supporting that the two modulators are indeed acting at different binding sites at the K_v11.1 channel. Furthermore, a curve described in **Figure 10C** indicated a positive cooperativity between LUF6200 and potassium ions. Taken together, we anticipate that there are at least two different sites of allosteric modulation for K_v11.1 blockers at the channel and that they interact with each other as well.

It is hypothesized that the ceiling effect of allosteric modulators of ligand-gated ion channels has important advantages over classic orthosterically acting compounds or open channel blockers, because it offers a much larger safety margin when it comes to drug administration and patient compliance⁵¹. A similar scenario may also be feasible for the K_v11.1 channel. For allosteric inhibitors one might argue that when non-cardiovascular drugs (e.g., astemizole) are combined with allosteric inhibitors of the K_v11.1 channel, their cardiac side effects might be diminished. On the other hand, when allosteric enhancers are administered together with antiarrhythmic drugs such as dofetilide whose desired target is the K_v11.1 channel, the therapeutic dose might be lowered, thereby possibly preventing adverse drug reactions such as TdP. Taken together, the discovery of allosteric modulators for the K_v11.1 channel might open new avenues for treating clinical conditions related to the K_v11.1 channel as well as potentially reducing K_v11.1 cardiotoxicity of other non-cardiovascular drugs by combination therapy.

In summary, the present study provides evidence for the allosteric effects of dofetilide analogues on the binding of K_v11.1 blockers to the K_v11.1 channel using both [³H]astemizole and [³H]dofetilide binding assays. LUF6200 emerges as an allosteric inhibitor with micromolar potency. Potassium ions allosterically enhance the binding of typical K_v11.1 blockers in concentrations that are physiologically relevant. Moreover, LUF6200 and potassium ions act at distinct allosteric sites on the K_v11.1 channel, and these binding sites show positive cooperativity. In addition, neither fluvoxamine nor PD118057 exhibit significant allosteric effects on the binding of two radioligands. This new information may be relevant for a further analysis of K_v11.1-related cardiotoxicity and provide novel solutions for proarrhythmic side effects induced by K_v11.1 blockers.

References

1. Keating, M. T.; Sanguinetti, M. C. Molecular and cellular mechanisms review of cardiac arrhythmias. *Cell* **2001**, *104*, 569-580.
2. Hoppe, U. C.; Marbán, E.; Johns, D. C. Distinct gene-specific mechanisms of arrhythmia revealed by cardiac gene transfer of two long QT disease genes, hERG and KCNE1. *Proc. Natl. Acad. Sci. U S A* **2001**, *98*, 5335-5340.
3. Schönherr, R.; Heinemann, S. H. Molecular determinants for activation and inactivation of hERG, a human inward rectifier potassium channel. *J. Physiol.* **1996**, *493*, 635-642.
4. Ng, C. A.; Hunter, M. J.; Perry, M. D.; Mobli, M.; Ke, Y.; Kuchel, P. W.; King, G. F.; Stock, D.; Vandenberg, J. I. The N-terminal tail of hERG contains an amphipathic α -helix that regulates channel deactivation. *PLoS One* **2011**, *6*, e16191.
5. Finlayson, K.; Witchel, H. J.; McCulloch, J.; Sharkey, J. Acquired QT interval prolongation and hERG: Implications for drug discovery and development. *Eur. J. Pharmacol.* **2004**, *500*, 129-142.
6. Sanguinetti, M. C.; Tristani-Firouzi, M. hERG potassium channels and cardiac arrhythmia. *Nat.* **2006**, *440*, 463-469.
7. Vandenberg, J. I.; Walker, B. D.; Campbell, T. J. hERG K⁺ channels: Friend and foe. *Trends Pharmacol. Sci.* **2001**, *22*, 240-246.
8. Hancox, J. C.; McPate, M. J.; El Harchi, A.; Zhang, Y. h. The hERG potassium channel and hERG screening for drug-induced torsades de pointes. *Pharmacol. Ther.* **2008**, *119*, 118-132.
9. Sanguinetti, M. C.; Mitcheson, J. S. Predicting drug-hERG channel interactions that cause acquired long QT syndrome. *Trends Pharmacol. Sci.* **2005**, *26*, 119-124.
10. Gintant, G. An evaluation of hERG current assay performance: Translating preclinical safety studies to clinical QT prolongation. *Pharmacol. Ther.* **2011**, *129*, 109-119.
11. May, L. T.; Leach, K.; Sexton, P. M.; Christopoulos, A. Allosteric modulation of G protein-coupled receptors. *Annu. Rev. Pharmacol. Toxicol.* **2007**, *47*, 1-51.
12. IJzerman, A. P.; Wijngaarden, I. v.; Soudijn, W. Allosteric modulation of G-protein-coupled receptors. *Expert Opin. Ther. Pat.* **2001**, *11*, 1889-1904.
13. Christopoulos, A. Allosteric binding sites on cell-surface receptors: Novel targets for drug discovery. *Nat. Rev. Drug. Discov.* **2002**, *1*, 198-210.
14. Michel, A.; Clay, W.; Ng, S.; Roman, S.; Thompson, K.; Condreay, J.; Hall, M.; Holbrook, J.; Livermore, D.; Senger, S. Identification of regions of the P2X₇ receptor that contribute to human and rat species differences in antagonist effects. *Br. J. Pharmacol.* **2008**, *155*, 738-751.
15. Michel, A.; Chambers, L.; Walter, D. Negative and positive allosteric modulators of the P2X₇ receptor. *Br. J. Pharmacol.* **2008**, *153*, 737-750.

16. Yoshimura, R. F.; Hogenkamp, D. J.; Li, W. Y.; Tran, M. B.; Belluzzi, J. D.; Whittemore, E. R.; Leslie, F. M.; Gee, K. W. Negative allosteric modulation of nicotinic acetylcholine receptors blocks nicotine self-administration in rats. *J. Pharmacol. Exp. Ther.* **2007**, *323*, 907-915.
17. Sancar, F.; Czajkowski, C. Allosteric modulators induce distinct movements at the GABA-binding site interface of the GABA-A receptor. *Neuropharmacology* **2011**, *60*, 520-528.
18. Trattnig, S. M.; Harpsøe, K.; Thygesen, S. B.; Rahr, L. M.; Ahring, P. K.; Balle, T.; Jensen, A. A. Discovery of a novel allosteric modulator of 5-HT₃ receptors-inhibition and potentiation of Cys-loop receptor signaling through a conserved transmembrane intersubunit site. *J. Biol. Chem.* **2012**, *287*, 25241-25254.
19. Uebele, V.; Nuss, C.; Fox, S.; Garson, S.; Cristescu, R.; Doran, S.; Kraus, R.; Santarelli, V.; Li, Y.; Barrow, J.; Yang, Z.-Q.; Schlegel, K.-A.; Rittle, K.; Reger, T.; Bednar, R.; Lemaire, W.; Mullen, F.; Ballard, J.; Tang, C.; Dai, G.; McManus, O.; Koblan, K.; Renger, J. Positive allosteric interaction of structurally diverse T-type calcium channel antagonists. *Cell Biochem. Biophys.* **2009**, *55*, 81-93.
20. Chiu, P. J.; Marcoe, K. F.; Bounds, S. E.; Lin, C.; Feng, J.; Lin, A.; Cheng, F.; Crumb, W. J.; Mitchell, R. Validation of a [³H]astemizole binding assay in HEK293 cells expressing hERG K⁺ channels. *J. Pharmacol. Sci.* **2004**, *95*, 311-319.
21. Chadwick, C. C.; Ezrin, A. M.; O'Connor, B.; Volberg, W. A.; Smith, D. I.; Wedge, K. J.; Hill, R. J.; Briggs, G. M.; Pagani, E. D.; Silver, P. J. Identification of a specific radioligand for the cardiac rapidly activating delayed rectifier K⁺ channel. *Circ. Res.* **1993**, *72*, 707-714.
22. Finlayson, K.; Pennington, A. J.; Kelly, J. S. [³H]Dofetilide binding in SHSY5Y and HEK293 cells expressing a hERG-like K⁺ channel? *Eur. J. Pharmacol.* **2001**, *412*, 203-212.
23. Mitcheson, J. S. Drug binding to hERG channels: Evidence for a 'non-aromatic' binding site for fluvoxamine. *Br. J. Pharmacol.* **2003**, *139*, 883-884.
24. Perry, M.; Sachse, F. B.; Abbruzzese, J.; Sanguinetti, M. C. PD-118057 contacts the pore helix of hERG1 channels to attenuate inactivation and enhance K⁺ conductance. *Proc. Natl. Acad. Sci. U S A* **2009**, *106*, 20075-20080.
25. Zhou, J.; Augelli-Szafran, C. E.; Bradley, J. A.; Chen, X.; Koci, B. J.; Volberg, W. A.; Sun, Z.; Cordes, J. S. Novel potent human ether-à-go-go-related gene (hERG) potassium channel enhancers and their in vitro antiarrhythmic activity. *Mol. Pharmacol.* **2005**, *68*, 876-884.
26. Shaguftha; Guo, D.; Klaasse, E.; de Vries, H.; Brussee, J.; Nalos, L.; Rook, M. B.; Vos, M. A.; van der Heyden, M. A.; IJzerman, A. P. Exploring chemical substructures essential for hERG K⁺ channel blockade by synthesis and biological evaluation of dofetilide analogues. *ChemMedChem* **2009**, *4*, 1722-1732.

27. Smith, P.; Krohn, R. I.; Hermanson, G.; Mallia, A.; Gartner, F.; Provenzano, M.; Fujimoto, E.; Goeke, N.; Olson, B.; Klenk, D. Measurement of protein using bicinchoninic acid. *Anal. Biochem.* **1985**, *150*, 76-85.
28. Diaz, G. J.; Daniell, K.; Leitza, S. T.; Martin, R. L.; Su, Z.; McDermott, J. S.; Cox, B. F.; Gintant, G. A. The [³H]dofetilide binding assay is a predictive screening tool for hERG blockade and proarrhythmia: Comparison of intact cell and membrane preparations and effects of altering [K⁺]_o. *J. Pharmacol. Toxicol. Methods* **2004**, *50*, 187-199.
29. Heitman, L. H.; Oosterom, J.; Bongers, K. M.; Timmers, C. M.; Wiegerinck, P. H.; IJzerman, A. P. [³H]Org 43553, the first low-molecular-weight agonistic and allosteric radioligand for the human luteinizing hormone receptor. *Mol. Pharmacol.* **2008**, *73*, 518-524.
30. Almilaji, A.; Munoz, C.; Elvira, B.; Fajol, A.; Pakladok, T.; Honisch, S.; Shumilina, E.; Lang, F.; Föller, M. AMP-activated protein kinase regulates hERG potassium channel. *Pflügers Arch. - Eur. J. Physiol.* **2013**, *465*, 1573-1582.
31. Heitman, L. H.; Ye, K.; Oosterom, J.; IJzerman, A. P. Amiloride derivatives and a nonpeptidic antagonist bind at two distinct allosteric sites in the human gonadotropin-releasing hormone receptor. *Mol. Pharmacol.* **2008**, *73*, 1808-1815.
32. Kamiya, K.; Niwa, R.; Mitcheson, J. S.; Sanguinetti, M. C. Molecular determinants of hERG channel block. *Mol. Pharmacol.* **2006**, *69*, 1709-1716.
33. Fernandez, D.; Ghanta, A.; Kauffman, G. W.; Sanguinetti, M. C. Physicochemical features of the hERG channel drug binding site. *J. Biol. Chem.* **2004**, *279*, 10120-10127.
34. Chen, F.; Larsen, M. B.; Neubauer, H. A.; Sánchez, C.; Plenge, P.; Wiborg, O. Characterization of an allosteric citalopram-binding site at the serotonin transporter. *J. Neurochem.* **2005**, *92*, 21-28.
35. Duff, H. J.; Feng, Z.; Sheldon, R. S. High-and low-affinity sites for [³H]dofetilide binding to guinea pig myocytes. *Circ. Res.* **1995**, *77*, 718-725.
36. Zünkler, B.; Friemel, A. Allosteric interactions between terfenadine and chlorbutanol on hERG channels. *Toxicol. Lett.* **2009**, *189*, S257.
37. Perry, M.; Sanguinetti, M.; Mitcheson, J. Symposium review: Revealing the structural basis of action of hERG potassium channel activators and blockers. *J. Physiol.* **2010**, *588*, 3157-3167.
38. Vargas, H. M.; Bass, A. S.; Breidenbach, A.; Feldman, H. S.; Gintant, G. A.; Harmer, A. R.; Heath, B.; Hoffmann, P.; Lagrutta, A.; Leishman, D.; McMahon, N.; Mittelstadt, S.; Polonchuk, L.; Pugsley, M. K.; Salata, J. J.; Valentin, J.-P. Scientific review and recommendations on preclinical cardiovascular safety evaluation of biologics. *J. Pharmacol. Toxicol. Methods* **2008**, *58*, 72-76.
39. Liu, X.; Limberis, J. T.; Su, Z.; Houseman, K.; Diaz, G. J.; Gintant, G. A.; Cox, B. F.; Martin, R. L. Characterization of A-935142, a hERG enhancer, in the presence and absence of standard hERG blockers. *Life Sci.* **2012**, *90*, 607-611.

40. Wang, J.; Salata, J. J.; Bennett, P. B. Saxitoxin is a gating modifier of hERG K⁺ channels. *J. Gen. Physiol.* **2003**, *121*, 583-598.
41. Milnes, J. T.; Dempsey, C. E.; Ridley, J. M.; Crociani, O.; Arcangeli, A.; Hancox, J. C.; Witchel, H. J. Preferential closed channel blockade of hERG potassium currents by chemically synthesised BeKm-1 scorpion toxin. *FEBS Lett.* **2003**, *547*, 20-26.
42. Reínés, A.; Zárate, S.; Peña, C.; de Lores Arnaiz, G. R. The effect of endogenous modulator endobain E on NMDA receptor is interfered by Zn²⁺ but is independent of modulation by spermidine. *Neurochem. Res.* **2004**, *29*, 819-825.
43. Elinder, F.; Århem, P. Metal ion effects on ion channel gating. *Q. Rev. Biophys.* **2003**, *36*, 373-427.
44. Milnes, J. T.; Crociani, O.; Arcangeli, A.; Hancox, J. C.; Witchel, H. J. Blockade of hERG potassium currents by fluvoxamine: Incomplete attenuation by S6 mutations at F656 or Y652. *Br. J. Pharmacol.* **2003**, *139*, 887-898.
45. Mitcheson, J. S.; Chen, J.; Lin, M.; Culberson, C.; Sanguinetti, M. C. A structural basis for drug-induced long QT syndrome. *Proc. Natl. Acad. Sci. USA* **2000**, *97*, 12329-12333.
46. Lees-Miller, J. P.; Duan, Y.; Teng, G. Q.; Duff, H. J. Molecular determinant of high-affinity dofetilide binding to hERG1 expressed in xenopus oocytes: Involvement of S6 sites. *Mol. Pharmacol.* **2000**, *57*, 367-374.
47. Zhou, P.; Babcock, J.; Liu, L.; Li, M.; Gao, Z. Activation of human ether-à-go-go related gene (hERG) potassium channels by small molecules. *Acta Pharmacol. Sin.* **2011**, *32*, 781-788.
48. Duff, H. J.; Feng, Z.; Fiset, C.; Wang, L.; Lees-Miller, J.; Sheldon, R. S. [³H]Dofetilide binding to cardiac myocytes: Modulation by extracellular potassium. *J. Mol. Cell. Cardiol.* **1997**, *29*, 183-191.
49. Demo, S. D.; Yellen, G. Ion effects on gating of the Ca²⁺-activated K⁺ channel correlate with occupancy of the pore. *Biophys. J.* **1992**, *61*, 639-648.
50. Schetz, J. A.; Sibley, D. R. The binding-site crevice of the D₄ dopamine receptor is coupled to three distinct sites of allosteric modulation. *J. Pharmacol. Exp. Ther.* **2001**, *296*, 359-363.
51. Hogg, R. C.; Buisson, B.; Bertrand, D. Allosteric modulation of ligand-gated ion channels. *Biochem. Pharmacol.* **2005**, *70*, 1267-1276.

Chapter 4

Allosteric modulation of $K_v11.1$ (hERG) channels protects against drug-induced ventricular arrhythmias

*Zhiyi Yu**

*Jia Liu**

Jacobus P. D. van Veldhoven

Adriaan P. IJzerman

Martin J. SchaliJ

Daniël A. Pijnappels

Laura H. Heitman

Antoine A. F. de Vries

**These authors contributed equally to this chapter.*

Abstract

Drug-induced ventricular arrhythmias (DiVAs) due to unintentional blockade of the $K_v11.1$ (hERG) channel are a major safety concern in drug development. In the past years, several highly prescribed drugs have been withdrawn for their ability to cause life-threatening arrhythmias. Here, we investigated whether the proarrhythmic risk of existing drugs could be reduced by $K_v11.1$ allosteric modulators. Using [3H]dofetilide binding assays with membranes of human $K_v11.1$ -expressing HEK293 cells, two existing compounds (VU0405601 and ML-T531) and a newly synthesized compound (LUF7244) were found to be negative allosteric modulators of dofetilide binding to the $K_v11.1$ channel with LUF7244 showing the strongest effect at 10 μM . The $K_v11.1$ affinity of typical blockers (i.e. dofetilide, astemizole, sertindole and cisapride) were significantly decreased by LUF7244. Treatment of neonatal rat ventricular myocyte (NRVM) monolayers with astemizole or sertindole caused heterogeneous prolongation of action potential (AP) duration and a high incidence of early afterdepolarizations upon 1-Hz electrical point stimulation, occasionally leading to unstable, self-terminating reentrant tachyarrhythmias. Pretreatment of NRVMs with LUF7244 prevented these proarrhythmic effects. NRVM monolayers treated with LUF7244 alone displayed electrophysiological properties indistinguishable from those of untreated NRVM cultures. Prolonged exposure of NRVMs to LUF7244 or LUF7244 plus astemizole did not affect their viability, excitability and contractility as assessed by molecular, immunological and electrophysiological assays. Conclusively, allosteric modulation of the $K_v11.1$ channel efficiently suppresses DiVAs *in vitro* by preventing potentially arrhythmogenic changes in AP characteristics, raising the possibility to resume the clinical use of unintended $K_v11.1$ blockers via pharmacological combination therapy.

Introduction

Drug-induced ventricular arrhythmias (DiVAs) are a frequently encountered clinical problem, which has resulted in the restricted use or market withdrawal of existing cardiac and non-cardiac drugs and still represents a major obstacle for the development of new drugs.¹ Inhibition of the rapid component of the delayed rectifier K^+ current (I_{Kr}) has been identified as the major culprit in the development of DiVAs. The consequential slowing of cardiac repolarization, manifested in the surface electrocardiogram as a prolongation of the QT interval, increases the likelihood of early afterdepolarizations (EADs), which may give rise to ectopic beats. Drug-induced I_{Kr} blockade also increases spatial dispersion of repolarization and refractoriness due to differences in relative I_{Kr} and I_{Ks} (the slow component of the delayed rectifier K^+ current) densities between cardiomyocytes in different regions of the ventricular wall.² Together these electrophysiological alterations promote the development of a special type of polymorphic ventricular arrhythmias known as “Torsades de Pointes” (TdPs), which mostly resolve spontaneously but occasionally degenerate into fatal ventricular fibrillation.³

The molecular correlate of I_{Kr} is the $K_v11.1$ protein encoded by the *KCNH2* gene (also known as ether-à-go-go-related gene 1 [ERG or ERG1]), possibly in combination with the MiRP1 or MinK protein, which are encoded by the *KCNE1* and *KCNE2* gene, respectively.⁴ $K_v11.1$ represents the pore-forming α subunit of the I_{Kr} channel, while MiRP1 and MinK are thought to be accessory β subunits involved in the modulation of its activity. Several structural features of $K_v11.1$ render the I_{Kr} channel particularly susceptible to blockade by a heterogeneous collection of chemical compounds including various non-cardiac drugs (e.g., astemizole, sertindole and cisapride).

An obvious strategy to reduce the proarrhythmic risk of drugs with unintended I_{Kr} blockade is by lowering their $K_v11.1$ affinity via chemical modifications. Alternatively, supplementary drugs that lessen the proarrhythmic risk of inadvertent $K_v11.1$ blockers can be developed potentially allowing the (i) reintroduction of medicines previously recalled from the market because of their $K_v11.1$ -related cardiotoxicity and (ii) admission of new drugs with fortuitous I_{Kr} -blocking effects. Paradoxically, screening of drugs for possible I_{Kr} -blocking side effects has resulted in the serendipitous discovery of various $K_v11.1$ activators.⁵ Besides their potential usefulness in treating inherited long QT syndrome (LQTS), these $K_v11.1$ activators may also be used to counteract $K_v11.1$ blockade-associated DiVAs. Indeed, Kang *et al.* showed that the action potential (AP) duration (APD)-prolonging effect of the I_{Kr} -blocking, class III antiarrhythmic drug dofetilide could be counterbalanced by the first identified synthetic $K_v11.1$ activator designated

RPR260243.⁶ However, due to the APD-shortening effect, $K_v11.1$ activators carry the risk of possibly inducing short QT syndrome.⁵ Recently, Potet *et al.* described a compound designated VU0405601 that upon pretreatment significantly reduced the APD-prolonging effect of dofetilide in Langendorff-perfused rabbit hearts and dose-dependently mitigated the $K_v11.1$ -blocking effects of seven different drugs in a fluorescence-based thallium flux assay performed with HEK293 cells stably overexpressing the human *KCNH2* gene (HEK293 $K_v11.1$ cells).⁷ VU0405601 exerted its effects on the $K_v11.1$ channel in whole-cell voltage clamp experiments using HEK293 $K_v11.1$ cells only when applied extracellularly. This suggests that VU0405601 binds to the extracellular domain of the $K_v11.1$ channel rather than to its central cavity leading us to hypothesize that VU0405601 counteracts the APD-prolonging effect of $K_v11.1$ blockers by an allosteric mechanism.

Allosteric modulators bind to their targets at a site topologically different from that of the endogenous ligand. Of note, since the $K_v11.1$ channel does not have an endogenous ligand, the authors refer to the site where typical blockers (i.e. dofetilide and astemizole) bind as the orthosteric site. From this so-called allosteric or regulatory site they generally display higher selectivity across receptor subtypes and thus provide a safer pharmacological profile than ligands binding to the orthosteric or active site.⁸ Whereas allosteric modulators targeting ligand-gated ion channels and G protein-coupled receptors have been well established as research tools and therapeutic agents,⁸⁻¹⁰ very little progress has been made in the discovery and clinical development of such compounds for voltage-gated ion channels, in particular the $K_v11.1$ channel.

In this study, different *in vitro* radioligand binding assays were used to investigate whether two previously reported compounds (i.e. VU0405601⁷ and ML-T531¹¹) and a new compound designated LUF7244 could allosterically modulate the binding of the potent $K_v11.1$ blocker dofetilide to the channel's central cavity.^{12,13} Radioligand binding assays were also employed to study LUF7244's influence on the interaction between (i) the $K_v11.1$ channel and three different blockbuster drugs (i.e. astemizole, sertindole and cisapride) that have been withdrawn from the market due to their $K_v11.1$ -related cardiotoxicity¹⁴ and (ii) astemizole and its intended target, the human histamine H_1 receptor (hH₁R). The radioligand binding assays were complemented with optical voltage mapping experiments in confluent monolayers of neonatal rat ventricular myocytes (NRVMs). These experiments were performed in the absence and presence of LUF7244 and/or any of the three blockbuster drugs. Electrophysiological parameters analyzed included conduction velocity (CV), APD at 40 and 90% repolarization (APD₄₀ and APD₉₀, respectively), APD dispersion and EAD incidence. In addition, the effects of LUF7244 alone and together with astemizole on the viability, excitability and

contractility of the NRVMs were investigated. The results of this study indicate that negative allosteric modulation of the $K_v11.1$ channel may provide a safe and effective means to prevent the proarrhythmic effects of I_{Kr} blockers that bind to the channel's central cavity.

Materials and methods

Materials

Dofetilide was synthesized in-house as previously described.¹⁵ Bovine serum albumin (BSA, fraction V) and the fortuitous $K_v11.1$ blockers astemizole, sertindole and cisapride were purchased from Sigma-Aldrich (St. Louis, MO). Tritium-labeled dofetilide (specific activity: 82.3 Ci·mmol⁻¹) and astemizole (specific activity: 78.4 Ci·mmol⁻¹) were obtained from PerkinElmer (Groningen, The Netherlands). The synthesis of VU0405601, ML-T531, as well as the design and synthesis of LUF7244 and its derivatives will be detailed elsewhere. G418 was purchased from Stratagene (Cedar Creek, TX). All other chemicals were of analytical grade and obtained from standard commercial sources. HEK293 $K_v11.1$ cells were kindly provided by Dr. Eckhard Ficker (Case Western Reserve University, Cleveland, OH).¹⁶ Expression plasmid pcDNA3.1-hH₁Rwt was a gift of Prof. Thue W. Schwartz (University of Copenhagen, Copenhagen, Denmark). All animal experiments were approved by the Animal Experiments Committee of Leiden University Medical Center and conformed to the Guide for the Care and Use of Laboratory Animals as stated by the US National Institutes of Health.

Radioligand binding assays

Cell culture and membrane preparations

HEK293 $K_v11.1$ cells were cultured and membranes were prepared and stored as described previously.¹⁷

HEK293 cells were cultured in a humidified atmosphere at 37 °C and 7% CO₂ in Dulbecco's modified Eagle's medium (DMEM; Sigma-Aldrich, D6546) supplemented with 10% fetal bovine serum (Sarstedt, Nümbrecht, Germany), 50 IU·mL⁻¹ penicillin (Sarstedt) and 50 µg·mL⁻¹ streptomycin (Sarstedt). When the cells had reached 50-60% confluence, the culture medium was refreshed and 500 µL of 150 mM NaCl containing 15 µg of pcDNA3.1-hH₁Rwt DNA and 45 µg of linear 25-kDa polyethylenimine (Polysciences Europe, Eppelheim, Germany) was added per 100-mm culture dish (Sarstedt). Cells were harvested 48 h after transfection. Membranes of HEK293 cells expressing hH₁R (HEK293hH₁R cells)

were prepared and stored as described for HEK293K_v11.1 cells except that incubation buffer I (50 mM Tris-HCl [pH 7.4]) was used instead of incubation buffer II (10 mM HEPES-NaOH [pH 7.4], 130 mM NaCl, 60 mM KCl, 0.8 mM MgCl₂, 1 mM EGTA, 10 mM glucose, 0.1% BSA).

Radioligand displacement assays

[³H]Dofetilide binding assays for the K_v11.1 channel were performed in incubation buffer II as described previously.¹⁷ Briefly, membrane aliquots containing 20 µg protein were incubated with 5 nM [³H]dofetilide in a total volume of 100 µl at 25 °C for 1 hour. Radioligand displacement experiments were carried out with various concentrations of the test compounds. Total binding was determined in the presence of unsupplemented incubation buffer II, whereas non-specific binding was evaluated in incubation buffer II containing 10 µM astemizole. Displacement experiments with different concentrations of dofetilide, astemizole, sertindole and cisapride were conducted in the absence (control) or presence of 10 µM LUF7244. Incubations were terminated by dilution with ice-cold wash buffer (25 mM Tris-HCl [pH 7.4], 130 mM NaCl, 60 mM KCl, 0.8 mM MgCl₂, 0.05 mM CaCl₂, 0.05% BSA). Free radioligand was separated from bound [³H]dofetilide by rapid filtration through a UniFilter-96 GF/B microplate using a PerkinElmer MicroBeta Filtermate-96 harvester. The radioactivity was determined using a Wallac 1450 MicroBeta TriLux liquid scintillation counter (PerkinElmer) after extraction with 25 µl MicroScint 20 (PerkinElmer).

[³H]Astemizole binding assays for the hH₁R were performed in incubation buffer I. Membrane aliquots containing 15 µg protein were incubated with 3.5 nM [³H]astemizole in a total volume of 100 µl at 25 °C for 3 h. Total binding was determined in the presence of unsupplemented incubation buffer I, whereas non-specific binding was evaluated in incubation buffer I containing 100 µM astemizole. LUF7244 displacement assays were carried out with various concentrations of this compound, while displacement assays with different concentrations of astemizole were conducted in the absence (control) or presence of 10 µM LUF7244. Incubations were terminated by dilution with ice-cold wash buffer II (50 mM Tris-HCl [pH 7.4]), and samples were obtained as mentioned above.

Kinetic dissociation assays

Kinetic dissociation assays of [³H]dofetilide were performed as described previously¹⁷ with the following modifications. Single-point dissociation experiments were conducted by addition of 10 µM dofetilide in the absence (control) or presence of 10 or 50 µM of the selected compounds after preincubating membranes

with [^3H]dofetilide at 25 °C for 2 h. After 6 min of dissociation, incubations were terminated and samples were obtained as described under “*Radioligand displacement assays*”. Traditional dissociation experiments were carried out with 10 μM dofetilide in the absence (control) or presence of 50 μM of the test compounds at 25 °C for a total period of 2 h after preincubation with the radioligand. The amounts of [^3H]dofetilide still bound to the receptor were measured at various time intervals. The concentration-dependent effect of LUF7244 was determined by addition of 10 μM dofetilide in the absence (control) or presence of different concentrations of LUF7244. After 6 min of dissociation, incubations were terminated and samples were obtained as described under “*Radioligand displacement assays*”.

Functional assays in NRVMs

Isolation and culture of NRVMs

NRVMs were isolated and cultured as described previously.¹⁸ Briefly, neonatal rats were anaesthetized with 4-5% isoflurane inhalation anesthesia. After adequate anesthesia had been confirmed by the absence of reflexes, the heart was quickly excised. Ventricles were separated from the remainder of the heart, cut into small pieces with a fine scissor and a scalpel and dissociated by collagenase type I (Worthington, Lakewood, NJ) digestion. The resulting cell suspension was applied to Primaria culture dishes (Corning Life Sciences, Amsterdam, The Netherlands) and incubated for 75 min at 37 °C in a humidified atmosphere of 5% CO_2 to allow preferential attachment of cardiac fibroblasts. The unattached cells (mainly cardiomyocytes) were collected, passed through a cell strainer (70- μm mesh pore size; BD Biosciences, Breda, The Netherlands) and applied at a density of 8×10^5 cells per well of a 24-well cell culture plate (Corning Life Sciences) to fibronectin (Sigma-Aldrich)-coated, round glass coverslips. Proliferation of residual cardiac fibroblasts (10-15%) was inhibited by incubating the cells for 2 h in culture medium containing 10 $\mu\text{g} \cdot \text{mL}^{-1}$ mitomycin C (Sigma-Aldrich) at 24 h after seeding (i.e. at day 1 of culture). Cells were subsequently maintained in a 1:1 mixture of DMEM (Life Technologies Europe, Bleiswijk, The Netherlands; catalog number: 22320) and Ham's F10 medium (Life Technologies Europe) supplemented with 5% horse serum (Life Technologies Europe), 2% BSA and sodium ascorbate to a final concentration of 0.4 mM. This so-called NRVM medium was replaced daily.

Immunocytochemical analyses

NRVMs were plated on fibronectin-coated, 15-mm diameter round glass coverslips at a density of 4×10^4 cells. At day 9 of culture, the cells were washed thrice with ice-cold phosphate-buffered saline (PBS), fixed for 30 min in buffered 4% formaldehyde (Added Pharma, Oss, The Netherlands) of 4 °C and permeabilized by a 10-minute incubation at room temperature (RT) with 0.1% Triton X-100 in PBS. Next, the cells were double-immunostained for K_v11.1 (rabbit polyclonal antibodies raised against the C terminus of human K_v11.1, Merck Millipore, Billerica, MA, catalog number: AB5930) and α -actinin (mouse monoclonal antibody, Sigma-Aldrich, clone: EA-53). Incubation with primary antibodies (diluted 1:200 in PBS-0.1% normal donkey serum) and corresponding donkey Alexa Fluor 488/568-conjugated secondary antibodies (1:400 dilution, Life Technologies Europe) lasted for 2 h. To visualize their nuclei, the cells were incubated for 10 min at RT with 10 $\mu\text{g} \cdot \text{mL}^{-1}$ Hoechst 33342 (Life Technologies Europe) in PBS. After each processing step, the cells were washed three times with PBS of RT. To minimize photobleaching, coverslips were mounted in VECTASHIELD mounting medium (Vector Laboratories, Burlingame, CA). Photomicrographs were obtained with the aid of a digital color camera-equipped fluorescence microscope (Nikon Eclipse 80i; Nikon Instruments Europe, Amstelveen, The Netherlands).

Reverse transcription-quantitative polymerase chain reaction (RT-qPCR) analyses

Cultures of NRVMs and of neonatal rat cardiac fibroblasts (NRCFs; maintained in NRVM medium) were washed once with ice-cold PBS after which the cells were lysed in TRIzol Reagent (Life Technologies Europe) and total RNA was isolated using the RNeasy Mini kit (QIAGEN Benelux, Venlo, The Netherlands). The RNA was reverse transcribed with the iScript cDNA synthesis kit (Bio-Rad, Hercules, CA) and the resulting cDNA was amplified by PCR using the Bioline SensiFAST SYBR No-ROX kit (GC biotech, Alphen aan den Rijn, The Netherlands). The forward and reverse primers for the amplification of rat *Kcnh2*-specific cDNA were localized in different exons and had the following sequences, respectively: 5' TAGCCTCCTCAACATCCC 3' and 5' CCATGTCTGCACTTAGCC 3'. For normalization purposes, rat 18S rRNA (*Rn18s*)-specific cDNA was amplified in parallel using the following forward and reverse primer, respectively: 5' GTAACCCGTTGAACCCCAT 3' and 5' CCATCCAATCGGTAGTAGCG 3'. PCR amplifications were carried out in a CFX96 Touch Real-Time PCR detection system (Bio-Rad) using a 2-step cycling protocol (20–40 cycles of 95 °C 10 sec, 60 °C 30 sec) after a 5-minute incubation at 95 °C. Quantitative analyses were

based on the $2^{-\Delta\Delta CT}$ method using CFX Manager software (Bio-Rad). For these analyses, PCRs were performed *in triplo* on three independent samples.

Optical mapping

APs were investigated on a whole-culture scale by optical mapping using the potentiometric dye di-4-ANEPPS (Life Technologies Europe) as described previously.¹⁹ The measurements were carried out at 37 °C on 9-day-old confluent NRVM monolayer cultures (see above). Optical signals were captured using a MiCAM ULTIMA-L imaging system (SciMedia, Costa Mesa, CA). To validate the experimental model, cells were incubated for 20 min in culture medium containing 0, 10, 30, 100 or 300 nM of the hH_1R antagonist and unintended $\text{K}_v11.1$ blocker astemizole and dimethylsulfoxide (DMSO) at a final concentration of 0.03%. In a subsequent experiment, NRVM cultures were first exposed for 30 min to 10 μM LUF7244 or its solvent (i.e. culture medium containing 0.1% DMSO). Next, astemizole (final concentration of 100 nM) or vehicle was added to the culture medium raising the DMSO concentration to 0.13%. Following an incubation period of 30 min at 37 °C, optical recordings were started in the continued presence of the appropriate vehicle/drug combinations (**Figure 4A**). Optical traces were analyzed using Brain Vision Analyzer 1208 software (Brainvision, Tokyo, Japan). To minimize noise artifacts, calculations were based on the average of the signals at a selected pixel and its eight nearest neighbors. CV, APD_{40} , APD_{90} and APD_{40} dispersion were determined using NRVM cultures showing uniform AP propagation and 1:1 capture after 1-Hz local stimulation. Each of these electrophysiological parameters was the average of values obtained from 6 different positions equally distributed across the cell cultures. The effects of LUF7244 on the $\text{K}_v11.1$ -inhibiting antipsychotic drug sertindole and gastroprokinetic agent cisapride were assessed in the same way as for astemizole expect that the final concentration of sertindole and cisapride was 1 μM .

To study the effects of long-term $\text{K}_v11.1$ allosteric modulation in the absence and presence of an unintended $\text{K}_v11.1$ blocker on cardiac excitability, confluent NRVM cultures were incubated for 3 days in culture medium containing 100 nM astemizole and/or 10 μM LUF7244 prior to potentiometric dye loading, short-term drug treatment (see above) and optical mapping in the continued presence of drug(s) at culture day 9. Confluent NRVM monolayers exposed to culture medium containing vehicle (i.e. DMSO at a final concentration of 0.13%) only, served as negative controls for this experiment. Just prior to optical mapping, movies of the cells were made using a Carl Zeiss Axiovert 40C microscope equipped with a LD A-Plan 20x/0.3 Ph1 objective (Zeiss Nederland, Slidrecht, The Netherlands) to record their contractions upon electrical field stimulation at 1 Hz and 8 V using

a 15-ms rectangular pulse.

Apoptosis assay

To investigate the effects of long-term $K_v11.1$ allosteric modulation in the absence or presence of simultaneous $K_v11.1$ blockade on cell viability, externalized phosphatidylserine (as early marker of apoptosis) was detected using Alexa-568-conjugated annexin V (Life Technologies Europe). NRVM cultures in 24-well plates were treated cells for 72 h with 100 nM astemizole and/or 10 μ M LUF7244 as described under “*Optical mapping*”. Mock-treated cells and cells incubated for 24 h in culture medium containing 1 μ M doxorubicin (Sigma-Aldrich) served as negative and positive controls, respectively. Next, the cells were washed once with ice-cold PBS and incubated for 15 min at RT with annexin V conjugate diluted 40-fold in binding buffer (10 mM HEPES-NaOH [pH 7.4], 140 mM NaCl, 2.5 mM CaCl_2) of 4 °C containing 10 $\mu\text{g}\cdot\text{mL}^{-1}$ Hoechst 33342. After a single wash with binding buffer of 4 °C, photomicrographs were taken using a Leica DMI6000 B inverted microscope equipped with a Leica DFC300 FX digital color camera (both from Leica Microsystems, Rijswijk, The Netherlands).

Data analysis

Data of the radioligand binding assays were analyzed with Prism 5.0 (Graph-Pad, San Diego, CA). Half maximal inhibitory concentrations (i.e. IC_{50} values) in displacement assays were directly obtained from non-linear regression analysis of dose-response curves. Apparent inhibitory binding constants (K_i values) were derived from the IC_{50} values according to the Cheng-Prusoff relationship²⁰: $K_i = \text{IC}_{50}/(1 + [\text{L}^*]/K_D)$, where $[\text{L}^*]$ is the concentration of radioligand and K_D is its dissociation constant determined by saturation assay²¹. Dissociation rate constants (k_{off}) were obtained by computer analysis of the exponential decay of [^3H] dofetilide bound to the $K_v11.1$ channel. Half maximal effective concentrations (i.e. EC_{50} values) from kinetic dissociation assays were calculated by non-linear regression analysis of concentration-effect curves of dissociation in the presence of different concentrations of unlabeled ligands. All values obtained from radioligand binding assays in this study are means of at least three independent experiments performed in duplicate. The number of samples per experimental group in the optical mapping experiments varied from 5 to 24 as indicated. Whenever appropriate, data are expressed as mean \pm standard error of the mean (SEM) or as mean \pm standard deviation (SD). Statistical analysis was performed with a two-tailed unpaired Student's t-test.

Results

Characterization of allosteric modulators of [³H]dofetilide binding to the K_v11.1 channel

The interaction of two previously reported ligands VU405601 and ML-T531 as well as the newly designed and synthesized compound LUF7244 (**Figure 1A**) with the human K_v11.1 channel was studied in different [³H]dofetilide binding assays. As shown in **Figure 1B** and **Table 1**, all three compounds reduced [³H]dofetilide binding at the K_v11.1 channel with relatively low affinity, i.e. with IC₅₀ values of $7.8 \pm 0.4 \mu\text{M}$, $12 \pm 1 \mu\text{M}$ and $3.9 \pm 0.7 \mu\text{M}$ for VU0405601 and ML-T531 and LUF7244, respectively. Moreover, all displacement curves demonstrated Hill coefficients significantly different from unity (data not shown), implying that VU0405601, ML-T531 and LUF7244 might not competitively displace [³H]dofetilide from the K_v11.1 channel but may occupy distinct binding pockets in the channel protein to allosterically modulate binding of the radioligand.

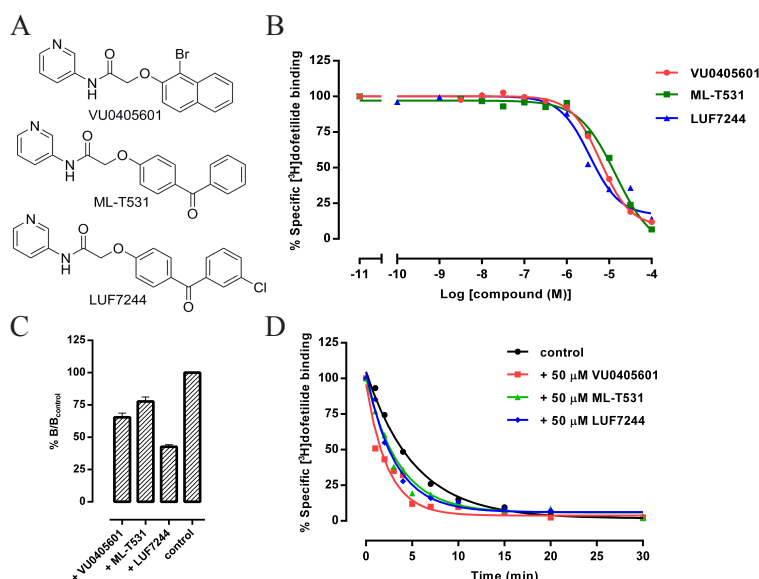


Figure 1. Characterization of allosteric modulators of dofetilide binding to the K_v11.1 channel in a [³H]dofetilide binding assay performed with membranes of HEK293K_v11.1 cells. **(A)** Chemical structures of VU0405601, ML-T531 and LUF7244. **(B)** Displacement curves of VU0405601, ML-T531 and LUF7244. **(C)** Percentage specific binding of [³H]dofetilide to the K_v11.1 channel after 6 min of dissociation induced by 10 μM dofetilide in the absence (control) or presence of 10 μM of VU0405601, ML-T531 or LUF7244. The specific binding of [³H]dofetilide in the absence of the test compounds was set as B_{control} , while the specific binding in their presence was set as B . **(D)** Time-dependent dissociation

of [^3H]dofetilide induced by 10 μM dofetilide in the absence (control) or presence of 50 μM VU0405601, ML-T531 or LUF7244. Experiments were performed at 25 $^{\circ}\text{C}$ using 20 μg of HEK293K $_{\text{v}}$ 11.1 membrane protein.

Subsequently, single-point dissociation assays were performed to screen for allosteric effects of these compounds on the binding of [^3H]dofetilide to the K $_{\text{v}}$ 11.1 channel. The results are summarized in **Figure 1C** and **Table 1**. At a concentration of 10 μM , VU0405601, ML-T531 and LUF7244 significantly increased the dissociation of [^3H]dofetilide from the K $_{\text{v}}$ 11.1 channel, indicating that these compounds are negative allosteric modulators of dofetilide binding to the channel. LUF7244 appeared to be the most potent negative allosteric modulator with $43 \pm 2\%$ dofetilide binding left compared to control conditions, while 10 μM VU0405601 and ML-T531 reduced dofetilide binding to $66 \pm 3\%$ and $78 \pm 3\%$, respectively.

The allosteric effects of VU0405601, ML-T531 and LUF7244 on the K $_{\text{v}}$ 11.1 channel were further investigated in traditional radioligand dissociation experiments to determine whether co-administration of these compounds with an excess unlabeled dofetilide would change the dissociation rate of [^3H]dofetilide from the K $_{\text{v}}$ 11.1 channel. In order to obtain larger effects, the three compounds were tested at a concentration of 50 μM instead of 10 μM as used in the single-point dissociation assay. As shown in **Figure 1D** and **Table 1**, all compounds significantly accelerated the dissociation of dofetilide, in line with the results from the single-point dissociation experiments. The off-rate of [^3H]dofetilide was allosterically increased 2.2-fold (from 0.22 ± 0.02 to $0.49 \pm 0.09 \text{ min}^{-1}$) with 50 μM VU0405601. The k_{off} value of [^3H]dofetilide rose to $0.33 \pm 0.03 \text{ min}^{-1}$ in the presence of 50 μM LUF7244, which was comparable to the effect of ML-T531 ($k_{\text{off, dofetilide}} = 0.30 \pm 0.02 \text{ min}^{-1}$).

Table 1. The half maximal inhibitory concentrations (IC_{50}), percentage specific binding of [^3H]dofetilide to the K $_{\text{v}}$ 11.1 channel after 6 minutes of dissociation in the absence or presence of 10 μM of the indicated compounds ($\%B/B_{\text{control}}$), and dissociation rates (k_{off}) of [^3H]dofetilide in the absence or presence of 50 μM of the indicated compounds.

	IC_{50} (nM)	$\%B/B_{\text{control}}$	k_{off} (min^{-1})
Dofetilide	-	100 ± 0	0.22 ± 0.02
+ VU0405601	7757 ± 350	66 ± 3 (***)	0.49 ± 0.09 (**)
+ ML-T531	12000 ± 1213	78 ± 3 (***)	0.30 ± 0.02 (**)
+ LUF7244	3855 ± 724	43 ± 2 (***)	0.33 ± 0.03 (**)

Values are means (\pm SEM) of at least three independent assays performed in duplicate. (** $P < 0.01$ versus control; *** $P < 0.001$ versus control)

Effects of LUF7244 on the binding of typical K_v11.1 blockers to the channel

Since LUF7244 was the most potent amongst the three allosteric modulators at the lower test concentration of 10 μ M and may therefore have the best safety profile, its potency to increase the dissociation of [³H]dofetilide from the K_v11.1 channel was investigated. The corresponding concentration-effect curve is shown in **Figure 2A**. From this graph, the modulatory potency (i.e. the EC₅₀) of LUF7244 was calculated to be 4.6 ± 0.8 μ M. Notably, LUF7244 could not completely abrogate [³H]dofetilide binding by accelerating its dissociation from the K_v11.1 channel.

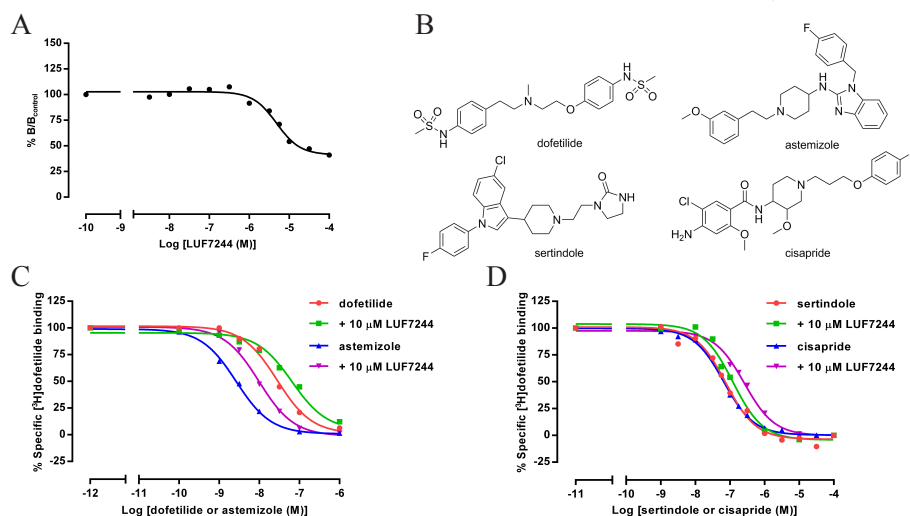


Figure 2. Assessment of the effects of LUF7244 on the binding of K_v11.1 blockers to the channel in a [³H]dofetilide binding assay performed with membranes of HEK293K_v11.1 cells. **(A)** Effect of different concentrations of LUF7244 on the dofetilide-induced dissociation of [³H]dofetilide from the K_v11.1 channel. After preincubating of HEK293K_v11.1 cell membranes with [³H]dofetilide, radioligand dissociation was induced by 10 μ M dofetilide in the absence or presence of different concentrations of LUF7244 and the incubation was terminated after 6 min. The results are expressed as the ratio of the specific binding of [³H]dofetilide in the presence of 10 μ M dofetilide plus various concentrations of negative allosteric modulators (*B*) over that in the presence of 10 μ M dofetilide alone (*B*_{control}). **(B)** Chemical structures of dofetilide, astemizole, sertindole and cisapride. **(C)** Displacement curves of dofetilide and astemizole in the absence or presence of 10 μ M LUF7244. **(D)** Displacement curves of sertindole and cisapride in the absence or presence of 10 μ M LUF7244. Experiments were performed at 25 °C using 20 μ g of HEK-293K_v11.1 membrane protein.

To investigate the effects of LUF7244 on the binding affinity of other com-

pounds besides dofetilide to the $K_v11.1$ channel, three additional $K_v11.1$ blockers (i.e. astemizole, sertindole and cisapride) from distinct therapeutic classes were selected (**Figure 2B**). As shown in **Figure 2C** and **2D**, the [3 H]dofetilide displacement curves of all four drugs were shifted rightwards in the presence of 10 μ M LUF7244, implicating that their $K_v11.1$ affinity were diminished by this negative allosteric modulator. The K_i values of dofetilide, astemizole, sertindole and cisapride in the absence or presence of 10 μ M LUF7244 are listed in **Table 2**. LUF7244 most strongly modulated cisapride binding to the $K_v11.1$ channel, increasing its K_i value by 4.0-fold from 21 ± 1 to 85 ± 7 nM. Similarly, the $K_v11.1$ affinity of astemizole, dofetilide and sertindole were reduced by 3.2-, 2.6- and 2.1-fold in the presence of LUF7244. Thus, the negative allosteric effect of LUF7244 on the $K_v11.1$ channel significantly lowered the channel's affinity for several chemically and therapeutically distinct $K_v11.1$ blockers.

Table 2. The $K_v11.1$ affinity (K_i) of dofetilide, astemizole, sertindole and cisapride in the absence (control) or presence of 10 μ M LUF7244.

	K_i (nM)	$K_{i, + 10 \mu\text{M LUF7244}}$ (nM)	Fold Change
Dofetilide	6.0 ± 0.5	16 ± 4 (**)	2.6
Astemizole	1.2 ± 0.2	3.7 ± 0.1 (***)	3.2
Sertindole	20 ± 2	40 ± 4 (**)	2.1
Cisapride	21 ± 1	85 ± 7 (***)	4.0

Values are means (\pm SEM) of at least three independent assays performed in duplicate. (** $P < 0.01$ versus control; *** $P < 0.001$ versus control)

Effects of LUF7244 on the binding of [3 H]astemizole to the hH_1R

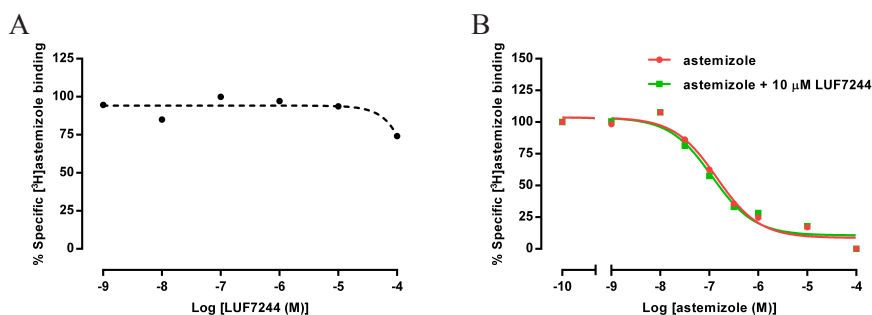


Figure 3. Assessment of the effects of LUF7244 on the binding of astemizole to the hH_1R in a [3 H]astemizole binding assay performed with membranes of HEK293 hH_1R cells. **(A)** Displacement curve of LUF7244. **(B)** Displacement curves of astemizole in the absence or presence of 10 μ M LUF7244. Experiments were performed at 25 $^{\circ}$ C using 15 μ g of HEK293 hH_1R membrane protein.

To be of practical use in preventing DiVAs, LUF7244 should not interfere with the desired activities of unintended $K_v11.1$ blockers. We therefore tested whether LUF7244 affected binding of the antihistamine drug astemizole to the hH_1R . As displayed in **Figure 3A**, LUF7244 did not decrease the binding of [3H]astemizole to the hH_1R . Furthermore, the displacement curve of astemizole binding to the hH_1R was not significantly shifted rightwards by LUF7244 (**Figure 3B**). Thus, LUF7244 reduces the affinity of the $K_v11.1$ channel for astemizole without affecting the binding of astemizole to its intended target receptor (i.e. the hH_1R).

Analysis of $K_v11.1$ protein expression in NRVMs

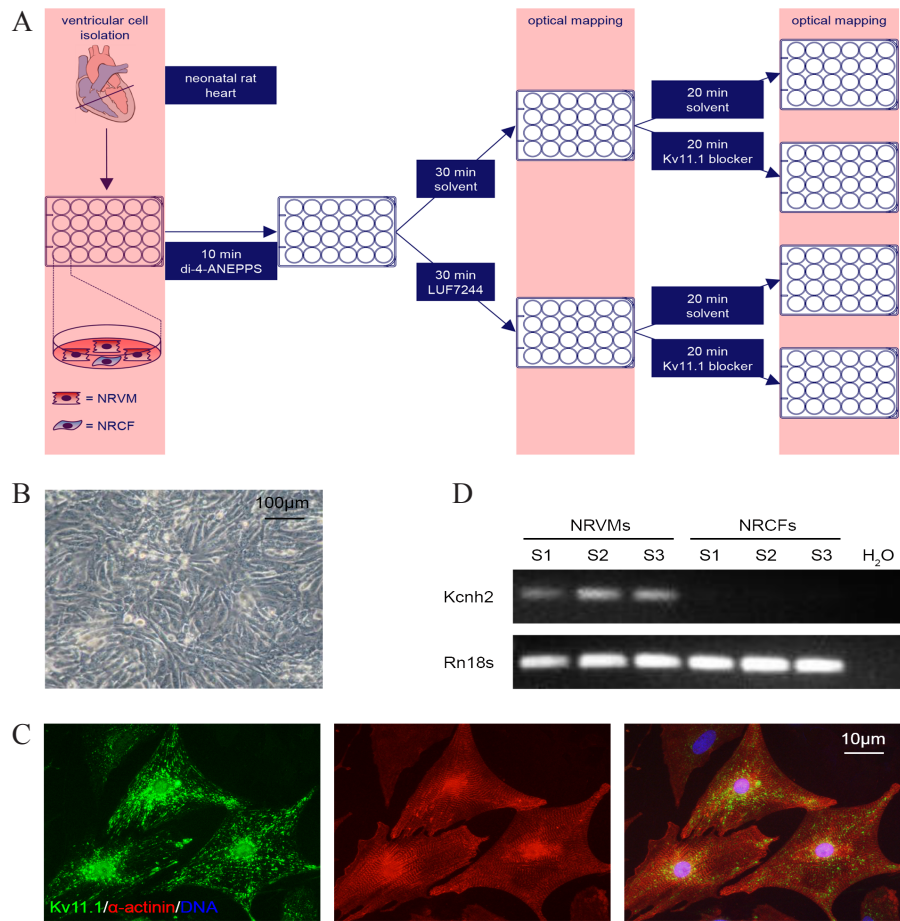


Figure 4. Biochemical characterization of the NRVM model. **(A)** Basic experimental set-up of the optical voltage mapping experiments. **(B)** Phase-contrast image of a typical confluent NRVM monolayer used for optical voltage mapping. **(C)** Immunocytochemical analysis of $K_v11.1$ protein expression in NRVM cultures. The $K_v11.1$ protein (green) is mainly located around the nucleus (blue) and at the sarcolemma of the α -actinin (red)-positive

NRVMs and hardly detectable in the α -actinin-negative non-cardiomyocytes. **(D)** Analysis of *Kcnh2* mRNA levels in NRVMs and NRCFs by RT-PCR.

Next, the electrophysiological consequences of allosteric modulation of the binding of typical $K_v11.1$ blockers at the channel by LUF7244 (see **Figure 4A**) was examined in confluent monolayer cultures of NRVMs (**Figure 4B**) as relevant *in vitro* model for studying cardiac arrhythmias.²² Double immunostaining for $K_v11.1$ and sarcomeric α -actinin showed that all cardiomyocytes in the NRVM cultures expressed the $K_v11.1$ protein (**Figure 4C**). The $K_v11.1$ signal had a punctate or linear appearance and was concentrated around nuclei and along the sarcolemma (**Figure 4C**). No significant $K_v11.1$ protein expression was observed in the low percentage of α -actinin⁺ cells (mainly NRCFs) present in the NRVM cultures. Consistently, comparison of *Kcnh2* transcript levels between NRVMs and NRCFs by RT-qPCR demonstrated 39-fold higher ($n=3$, $P < 0.01$) *Kcnh2* mRNA expression in NRVMs than in NRCFs (**Figure 4D**).

Electrophysiological consequences of $K_v11.1$ blockade by astemizole in NRVMs

Due to its relatively high specificity for the $K_v11.1$ channel,²³ astemizole was selected to study the electrophysiological consequences of $K_v11.1$ blockade by optical voltage mapping. NRVMs treated with astemizole displayed a concentration-dependent lengthening of APD and EAD incidence (**Figure 5** and **Figure 6**). As displayed in **Figure 5A** and **5B**, the APD_{40} and APD_{90} values of NRVMs were increased from 112 ± 16 and 295 ± 62 ms in vehicle-treated cultures ($n = 24$) to 156 ± 39 and 355 ± 66 ms in cultures containing 100 nM astemizole ($n = 24$, $P < 0.001$ and $P < 0.01$), respectively. Furthermore, exposure to 100 nM astemizole resulted in the occurrence of EADs in 25% of the NRVM cultures, whereas no EADs were observed under control conditions (**Figure 5C** and **5D**). Intriguingly, results presented in **Figure 5E** and **5F** demonstrated that the APD_{40} dispersion between NRVMs in the presence of 100 nM astemizole was significantly higher than that in its absence (39 ± 11 versus 16 ± 5 ms; $n = 24$, $P < 0.001$), indicative of aggravated repolarization heterogeneity due to the inhibition of I_{Kr} by astemizole. Occasionally, the astemizole-induced EADs resulted in short episodes of reentrant excitation (**Figure 7**) reminiscent of spontaneously terminating TdP episodes. Nonetheless, as indicated by the activation maps shown in **Figure 5G** and corresponding quantitative analysis depicted in **Figure 5H**, the CV in NRVM cultures was not significantly influenced by 100 nM astemizole (20 ± 4 cm·s⁻¹ vs 21 ± 3 cm·s⁻¹ in control cultures; $n = 10$, $P = 0.48$). Overall, these data validate the utility of NRVM cultures as an *in vitro* model for investigating the AP-prolonging

and associated proarrhythmic effects of $K_v11.1$ blockers like astemizole.

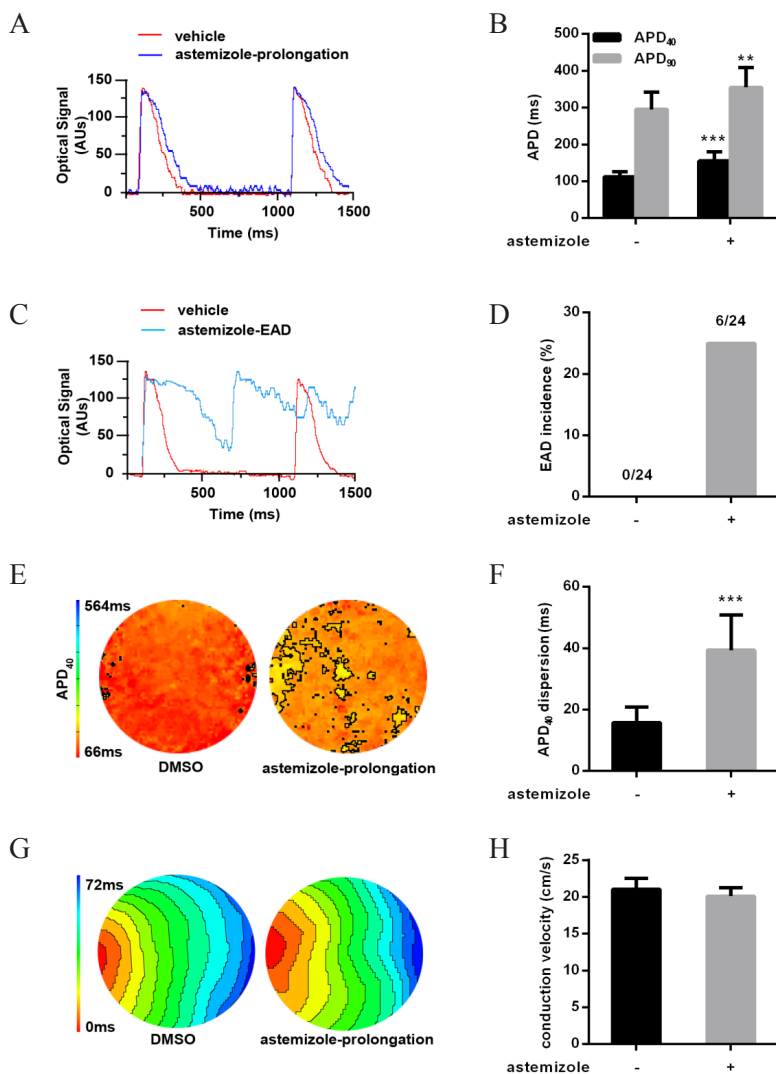


Figure 5. Electrophysiological characterization of the NRVM model by optical voltage mapping following 1-Hz electrical stimulation. Representative filtered optical signal traces (A and C), corresponding APD dispersion and activation maps (E and G, respectively) and quantitative analyses (bar graphs in B, D, F and H) of NRVM cultures exposed for 30 min to 100 nM astemizole or vehicle (control) and subjected to optical voltage mapping immediately afterwards. Astemizole treatment resulted in APD prolongation (APD₄₀ and APD₉₀, A and B), the occurrence of EADs (C and D) and an increase in APD₄₀ dispersion (E and F) but did not significantly alter CV (G and H). ** $P < 0.01$ and *** $P < 0.001$.

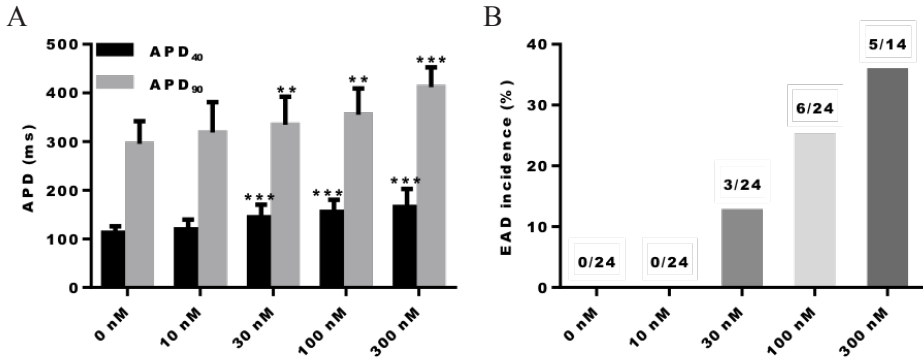


Figure 6. Assessment by optical voltage mapping of the effect of different concentrations of astemizole on the APD (APD₄₀ and APD₉₀, **A**) and EAD incidence (**B**) in NRVM monolayers. ** $P < 0.01$ and *** $P < 0.001$.

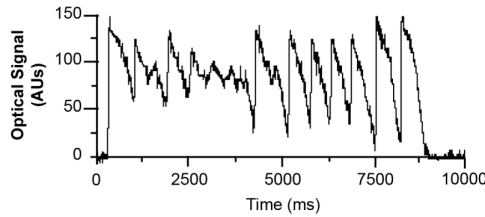


Figure 7. Optical voltage trace showing an unstable, self-terminating tachyarrhythmia in an astemizole-treated NRVM culture following 1-Hz electrical point stimulation.

Effects of LUF7244 on K_v11.1 blockade-associated proarrhythmic changes in NRVM cultures

To investigate the functional consequences of negative allosteric modulation of K_v11.1's interaction with typical K_v11.1 blockers, di-4-ANNEPS-loaded NRVM cultures were incubated for 20 min in culture medium containing 10 μ M LUF7244 before addition of astemizole, sertindole or cisapride. Since the K_i values of sertindole and cisapride for K_v11.1 are more than 10 times higher than that of astemizole (**Table 2**), these drugs were tested at a final concentration of 1 μ M instead of 100 nM as was used for astemizole. After incubation for 30 min, the NRVMs were optically mapped. As shown in **Figure 8A**, the APD-prolonging and EAD-promoting effects of astemizole were effectively suppressed by LUF7244. The APD₄₀ and APD₉₀ were significantly shortened from 156 ± 39 ms to 118 ± 18 ms ($n = 24$, $P < 0.001$) and from 355 ± 66 ms to 282 ± 63 ms ($n = 24$, $P < 0.01$), respectively, i.e. LUF7244 was able to reduce APD₄₀ and APD₉₀ to control values (**Figure 8B**). Moreover, in the presence of 10 μ M LUF7244 EADs were no longer observed in NRVM cultures exposed to 100 nM astemizole (**Figure 8C**).

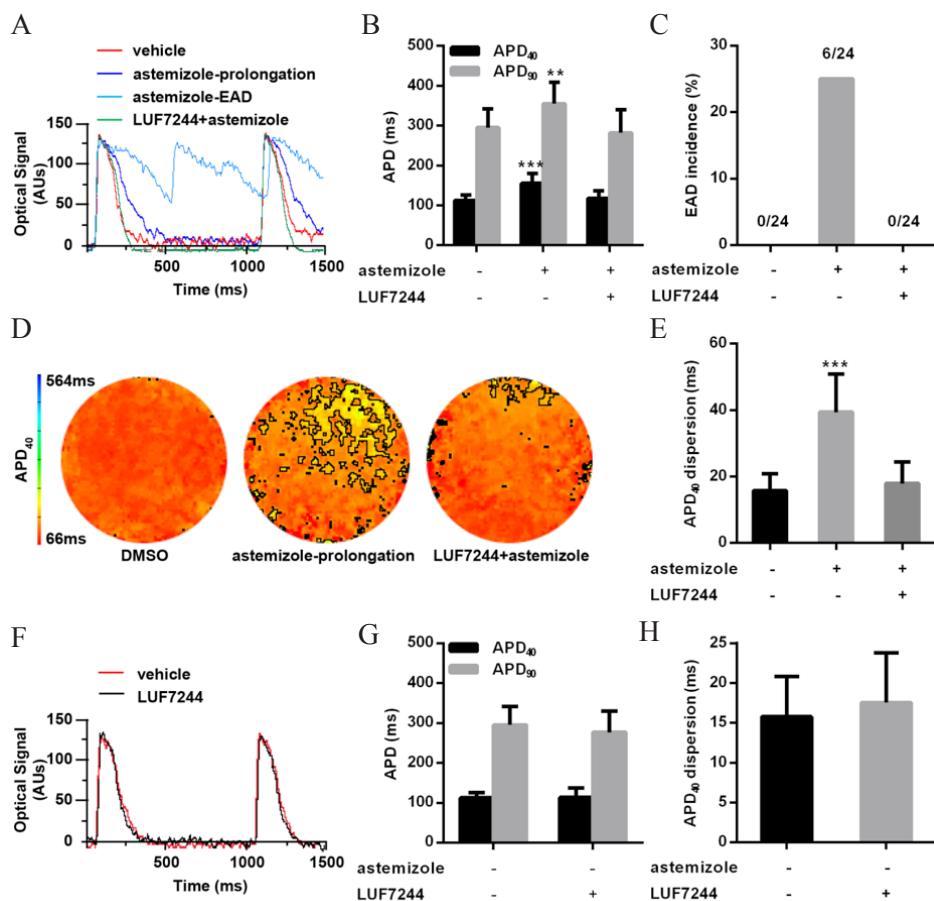


Figure 8. Assessment by optical voltage mapping of the ability of LUF7244 to counteract the proarrhythmic effects of astemizole on NRVMs. Representative filtered optical signal traces (A and F), APD dispersion maps (D) and quantitative analysis (bar graphs in B, C, E, G and H) of control NRVM cultures and of NRVM cultures that had been treated with 100 nM astemizole or with 10 μ M LUF7244 followed by 100 nM astemizole immediately before optical mapping. Pretreatment of NRVM cultures with LUF7244 completely prevented the astemizole-induced APD prolongation (APD₄₀ and APD₉₀, B), occurrence of EADs (C) and increase in APD₄₀ dispersion (D and E). Treatment of NRVM cultures with 10 μ M LUF7244 only did not change AP morphology (F), APD (G) or APD₄₀ dispersion (H). ** $P < 0.01$ and *** $P < 0.001$.

LUF7244 also prevented the increase in APD₄₀ dispersion caused by astemizole (Figure 8D and 8E). Reassuringly, the CVs in the NRVM cultures treated with vehicle, LUF7244, astemizole or LUF7244 plus astemizole did not significantly differ (data not shown). Also, at a final concentration of 10 μ M LUF7244 per se

did not reduce APD or significantly affect APD₄₀ dispersion (**Figure 8F-8H**), suggesting that this negative allosteric modulator poses very little, if any, risk for the development of arrhythmias associated with abnormal APD shortening. Very similar results of LUF7244 were obtained in NRVM cultures exposed to sertindole or cisapride (**Figure 9**). LUF7244 can thus suppress the proarrhythmic side effects of drugs from different therapeutic classes by allosteric modulation of the K_v11.1 channel without exerting, by itself, any obvious adverse electrophysiological effects on cardiomyocytes.

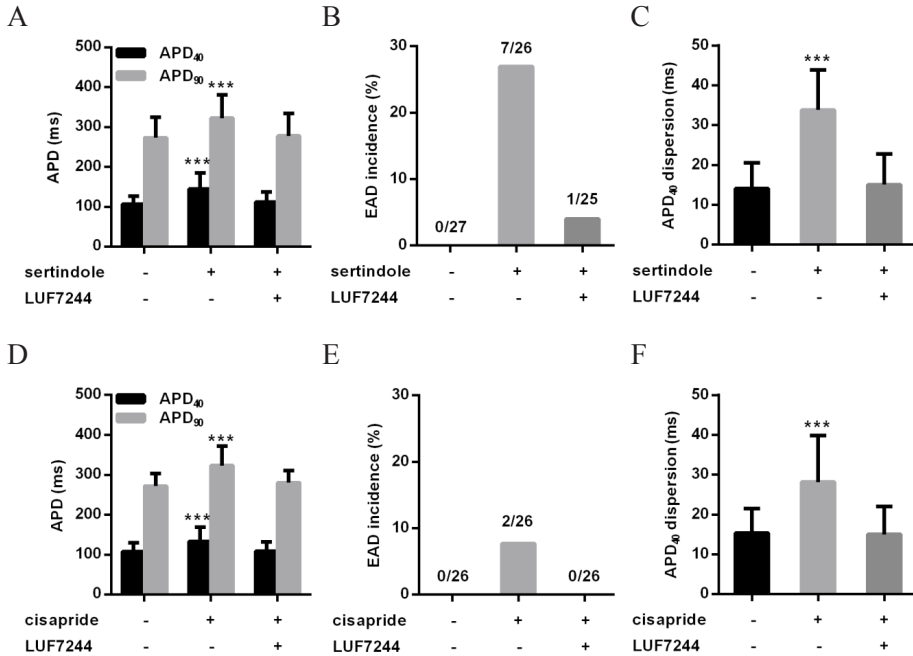


Figure 9. Assessment by optical voltage mapping of the ability of LUF7244 to counteract the proarrhythmic effects of sertindole and cisapride on NRVMs. Pretreatment of NRVM cultures with LUF7244 completely prevented the increase in APD (APD₄₀ and APD₉₀, **A** and **D**), EAD incidence (**B** and **E**) and APD₄₀ dispersion (**C** and **F**) induced by exposure of the cells to 1 μ M sertindole or cisapride. ** $P < 0.01$ and *** $P < 0.001$.

Effects of prolonged exposure of NRVMs to LUF7244 and/or astemizole on cell viability, excitability and contractility

To study the effects of prolonged allosteric modulation and/or blockade of the K_v11.1 channel on the viability of cardiomyocytes, 6-day-old NRVM cultures were incubated for 72 h in culture medium containing 10 μ M LUF7244 and/or 100 nM astemizole. Subsequent staining with fluorescently labeled annexin V to

detect cell surface-exposed phosphatidylserine yielded only very weak signals for cells exposed to vehicle, LUF7244, astemizole or LUF7244 plus astemizole, while NRVMs incubated for 24 h with the proapoptotic drug doxorubicin displayed strong annexin V fluorescence (**Figure 10A**). These results indicate that prolonged exposure to 10 μ M LUF7244 alone or in combination with 100 nM astemizole does not trigger programmed cell death.

Optical voltage mapping of 9-day-old NRVM cultures that had been mock-treated or treated for 72 h with 10 μ M LUF7244 and/or 100 nM astemizole produced very similar results as were obtained for cells that had only briefly been exposed to these compounds (compare **Figure 5** and **8** with **Figure 10B** and **10C**) and provided no indications for a drug-related reduction in excitability. Moreover, after electrical field stimulation cells in all four treatment groups displayed rhythmic contractions following the pacing frequency of 1 Hz (data not shown).

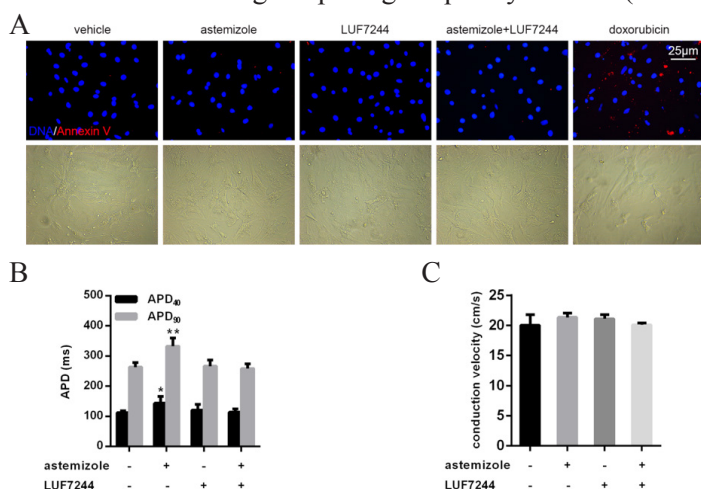


Figure 10. Effects of prolonged exposure of NRVMs to LUF7244 and/or astemizole on cell viability and excitability. **A:** Analysis by Alexa-568-conjugated annexin V staining of cell surface expression of phosphatidylserine as early marker of apoptosis. NRVM cultures exposed for 72 hours to vehicle, 10 μ M LUF7244, 100 nM astemizole or 10 μ M LUF7244 plus 100 nM astemizole showed very weak signals, while NRVMs incubated for 24 hours with 1 μ M of the proapoptotic drug doxorubicin displayed strong annexin V fluorescence. **B:** Quantitative comparison of APDs (APD₄₀ and APD₉₀) in NRVM cultures exposed for 72 hours to vehicle, 10 μ M LUF7244, 100 nM astemizole or 10 μ M LUF7244 plus 100 nM astemizole. **C:** Quantitative comparison of CV in NRVM cultures exposed for 72 hours to vehicle, 10 μ M LUF7244, 100 nM astemizole or 10 μ M LUF7244 plus 100 nM astemizole.

Discussion

Major findings

In radioligand binding assays the structurally related compounds VU0405601, ML-T531 and LUF7244 were found to weaken the interaction between the human $K_v11.1$ channel and the class III antiarrhythmic agent dofetilide as well as the unintended $K_v11.1$ blockers astemizole, sertindole and cisapride. VU0405601, ML-T531 and LUF7244 exerted their negative effects on the binding of typical $K_v11.1$ blockers to the channel's central cavity by an allosteric mechanism. Importantly, LUF7244 decreased the $K_v11.1$ affinity of astemizole without influencing its affinity at the hH_1R , being astemizole's intended target. Optical voltage mapping showed that incubation of NRVM monolayers with astemizole, sertindole or cisapride led to a significant increase in APD, APD dispersion and, except for cisapride, EAD incidence demonstrating the usefulness of this cellular model system for studying $K_v11.1$ blockade-related proarrhythmic risk. Pretreatment of the NRVMs with LUF7244 effectively prevented the proarrhythmic changes induced by astemizole, sertindole and cisapride without significantly shortening APD by itself and without adversely affecting NRVM viability, excitability and contractility. These findings provide a rationale for further exploring allosteric modulation as a strategy to prevent DiVAs.

NRVM monolayers as model for studying drug-induced LQTS

Many different methods have been exploited to assess drugs for their $K_v11.1$ blockade-associated arrhythmogenicity.^{3, 24} The interaction between a drug and the $K_v11.1$ channel is usually first investigated by computational and biochemical assays. Next, the $K_v11.1$ liability of suspicious drugs are typically evaluated by electrophysiological measurements on CHO or HEK293 cells expressing the human $K_v11.1$ channel. Despite their practical advantages, these non-excitable cellular models do not recapitulate the complex regulatory circuits governing $K_v11.1$ channel activity in cardiomyocytes and are unsuitable for studying AP generation and propagation. We hence employed NRVM monolayers to study the effects of LUF7244 on the proarrhythmic potential of three inadvertent $K_v11.1$ blockers. The reasons to specifically use NRVMs for this purpose are that these cells (i) can be relatively easily isolated and cultured, (ii) are well-characterized and (iii) do express functional $K_v11.1$ channels.²⁵ However, to the best of our knowledge, it is the first time that this model is being used to test compounds for their ability to prevent DiVAs resulting from unintended $K_v11.1$ blockade.

Although mechanistic insight into DiVAs is limited, there is broad consen-

sus about spatial dispersion of repolarization and EAD-induced triggered activity providing the substrate and trigger for the genesis of drug-induced TdP, respectively.² The EADs typically arise during phase 2 of the cardiac AP due to drug-dependent decreases in I_{Kr} causing increases of APD and QT interval. In support of the validity of our model, astemizole dose-dependently increased the APD and EAD incidence in monolayers of NRVMs (**Figure 6**). Also sertindole and cisapride had APD-prolonging effects (**Figure 9A** and **9D**) and each of the three fortuitous $K_v11.1$ blockers increased APD dispersion (**Figure 5F**, **Figure 9C** and **9F**). While 100 nM astemizole, 1 μ M sertindole and 1 μ M cisapride increased APD and APD dispersion to a similar extent, cisapride did not significantly increase EAD incidence in contrast to the other two drugs. This finding is in line with a previous study²⁶ and may be explained by cisapride's inhibitory effect on the $I_{Ca,L}$ in NRVMs.

Initially, EAD-dependent ectopic activity at multiple competing foci was thought to generate the undulating electrocardiographic patterns of TdP. Recently, meandering $I_{Ca,L}$ -mediated reentrant circuits initiated by EADs at single foci have been proposed as an alternative explanation for the highly characteristic electrocardiographic signature of TdP.^{27, 28} In support of the latter idea, exposure of NRVMs to $K_v11.1$ blockers occasionally gave rise to unstable, self-terminating reentrant tachyarrhythmias reminiscent of spontaneously terminating TdP episodes. Pretreatment with LUF7244 rendered NRVM monolayers unsusceptible to the $K_v11.1$ -blocking effects of astemizole, sertindole and cisapride. In the presence of LUF7244, these $K_v11.1$ blockers no longer caused heterogeneous APD prolongation and, due to the reduced opportunity for L-type Ca^{2+} channel reactivation, no longer gave rise to EADs. This raises the perspective to use LUF7244 as an antiarrhythmic additive to drugs with unintended I_{Kr} -suppressing effects. Thus, radioligand binding assays in combination with optical voltage mapping experiments of NRVM cultures offer convenient preclinical test systems for evaluating chemical entities that can potentially reduce $K_v11.1$ -related cardiotoxicity.

LUF7244's mode of action

The chemical structure of LUF7244 resembles those of ML-T531 and VU0405601. In a recent study, 10 μ M of ML-T531 was shown to reduce the APD of human induced pluripotent stem cells (hiPSC)-derived cardiomyocytes from an LQT1 patient to that of control cells by augmenting I_{Kr} .¹¹ However, the effects of ML-T531 on the APD of hiPSC-derived cardiomyocytes from a healthy individual and the ability of ML-T531 to inhibit the APD-prolonging effects of unintended $K_v11.1$ blockers were not investigated. Voltage clamp recordings of $K_v11.1$ -ex-

pressing CHO cells showed that ML-T531 reduces the deactivation rate of the $K_v11.1$ channel and causes a shift of its inactivation curve towards more positive voltages. Shortly after the discovery of ML-T531, VU0405601 was identified as a compound that, at a final concentration of 5 μM , protected Langendorff-perfused rabbit hearts from the proarrhythmic effects of exposure to 100 nM dofetilide.⁷ Although VU0405601 only partially reversed the dofetilide-dependent increase in APD, its administration prior to dofetilide strongly reduced the pacing-induced arrhythmia incidence from 42% to 4%, which was very close to the 2% of pacing-induced premature ventricular contractions observed in untreated hearts.⁷ Exposure of isolated rabbit ventricular myocytes to 5 μM of VU0405601 only marginally reduced APD, which is consonant with our finding that 10 μM LUF7244 did not noticeably affect the APD of NRVMs. However, at a final concentration of 50 μM , VU0405601 decreased the APD_{50} and APD_{90} of rabbit ventricular myocytes by $35 \pm 6\%$ and $32 \pm 4\%$, respectively. Patch clamp analysis of HEK293 $K_v11.1$ cells linked the APD-shortening effect of 50 μM VU0405601 to shifts in the $V_{1/2}$ of activation and inactivation and to changes in the kinetics of (de)activation and (de)inactivation causing an increase in I_{Kr} .

In this study, we found that VU0405601, ML-T531 and LUF7244 displayed comparatively low $K_v11.1$ affinity with Hill coefficients significantly different from unity for their [^3H]dofetilide displacement curves. This suggests that these ligands bind to the $K_v11.1$ channel at sites distinct from that of dofetilide, indicative of an allosteric mode of action.^{10, 29, 30} The binding of a drug to a receptor at an allosteric site (i.e. a site topologically distinct from that of the test ligand) triggers a conformational change within the receptor ultimately causing an alteration of the ligand's dissociation rate from its cognate (i.e. orthosteric) binding site.^{10, 31} Altered ligand dissociation rates have been found representative of allosteric interactions in various drug targets such as muscarinic and adenosine receptors.^{10, 32-34} Consistently, VU0405601, ML-T531 and LUF7244 significantly accelerated the dissociation of dofetilide from the $K_v11.1$ channel, strengthening the conclusion that they are negative allosteric modulators of dofetilide binding to the $K_v11.1$ channel. Our finding for VU0405601 is in agreement with the results of Potet *et al.*, who presented indirect evidence that VU0405601 binds from outside to the ectodomain of the $K_v11.1$ channel,⁷ while astemizole, cisapride, dofetilide and sertindole all bind to the channel's central cavity from inside³⁵⁻³⁷. In addition, the [^3H]dofetilide displacement curves of dofetilide, astemizole, sertindole and cisapride were shifted rightwards by LUF7244 (**Figure 2C and 2D**) providing further proof for its negative allosteric effect.^{10, 34} Collectively, the results of the different radioligand binding assays provide strong evidence that VU0405601, ML-T531 and LUF7244 are negative allosteric modulators of dofetilide binding

to the $K_v11.1$ channel. Binding of VU0405601, ML-T531 and LUF7244 likely alters the 3D structure of the $K_v11.1$ channel, which decreases its affinity for typical $K_v11.1$ blockers by increasing the dissociation rates of these blockers from the channel. Of note, the vast majority of fortuitous $K_v11.1$ blockers exert their effects by occupying the central cavity of the $K_v11.1$ channel and thereby obstructing the transport of K^+ ions through the channel's pore.³⁸ There are, however, also examples of drugs that reduce I_{Kr} by inhibiting, directly or indirectly, the trafficking of $K_v11.1$ to the plasma membrane.³⁹ Given their specific mode of action, it is unlikely that the I_{Kr} -inhibiting effects of these drugs can be abolished by LUF7244 or a related compound.

Since both VU0405601 and ML-T531 dose-dependently increased the $K_v11.1$ current density and given the structural similarity of these compounds with LUF7244, it is very likely that also LUF7244 can directly act as a (allosteric) $K_v11.1$ activator. Accordingly, the ability of LUF7244 to counteract astemizole-, sertindole- and cisapride-related arrhythmogenesis may be the combined result of its inhibitory effect on the binding of these unintended $K_v11.1$ blockers to the channel and of its direct enhancing effect on the $K_v11.1$ channel's activity. However, the fact that exposure of NRVMs to 10 μ M LUF7244 alone did not significantly change AP characteristics suggests that LUF7244's $K_v11.1$ -activating activity is not of critical importance for its ability to suppress the proarrhythmic effects of inadvertent $K_v11.1$ blockers. Moreover, possible effects of LUF7244 on other cardiac ion channels besides the $K_v11.1$ channel must be considered. The absence of a noticeable change in AP shape and duration following exposure of NRVMs to LUF7244 also argues against a possible effect of this allosteric modulator on cardiac ion channels different from the $K_v11.1$ channel. In keeping with this notion, $Na_v1.5$, I_{Ks} and $K_v1.5$ activities were not affected or only slightly reduced by 50 μ M VU0405601.⁷ Likewise, ML-T531 at a final concentration of 10 μ M had a minor suppressive effect on I_{Ks} and did not influence $Na_v1.5$, $Ca_v1.2$, $K_v4.3$ or $Kir2.1$ activities.¹¹ Thus, the antiarrhythmic propensity of LUF7244 is dominated by its negative allosteric impact on the binding of typical $K_v11.1$ blockers to the channel.

The fact that LUF7244 significantly decreased the $K_v11.1$ affinity of drugs with very different chemical structures (**Figure 2B**) in membrane radioligand binding assays and prevented these drugs from causing APD prolongation in NRVMs makes it likely that LUF7244 will be effective in reducing the cardiotoxicity of a broad range of $K_v11.1$ blockers. Further support for this notion comes from the fact that VU0405601, which was here shown to inhibit dofetilide interaction with the $K_v11.1$ channel by a similar mechanism to LUF7244, could abolish the blockade of $K_v11.1$ by seven different drugs.⁷ The different degree

to which LUF7244 increased the K_i values of dofetilide, astemizole, sertindole and cisapride suggests that the sensitivity of different $K_v11.1$ blockers to conformational changes in the $K_v11.1$ proteins differs. Accordingly, different LUF7244 concentrations may be required to abrogate the proarrhythmic effects of distinct $K_v11.1$ blockers.

Although at a final concentration of 50 μM LUF7244's ability to weaken the interaction between [^3H]dofetilide and the $K_v11.1$ channel was similar to those of VU0405601 and ML-T531 (**Figure 1D**), the new modulator was much more effective than the other two compounds at a final concentration of 10 μM (**Figure 1C**). Moreover, even 50 μM VU0405601 only modestly inhibited the APD-prolonging effect of 1 μM dofetilide (K_i for human $K_v11.1$: 6.0 nM) on rabbit ventricular myocytes,⁷ while 10 μM LUF7244 totally blocked the APD prolongation caused by exposure of NRVMs to 100 nM astemizole (K_i for human $K_v11.1$: 1.2 nM). These findings together with the substantial decrease in the APD of normal rabbit ventricular myocytes caused by 50 μM VU0405601 (see above), suggests that LUF7244 may possess a more favorable safety profile than VU0405601 or ML-T531.

Clinical applicability of allosteric $K_v11.1$ modulators

A major concern and obstacle for medicinal chemists involved in the development of drugs to remedy congenital and acquired LQTS is excessive APD shortening resulting in the short QT syndrome (SQTS).^{5, 40} For instance, at a concentration of 10 μM , the potent $K_v11.1$ activator ICA-105574 shortened the APD in Langendorff-perfused guinea pig hearts by 34% and induced non-TdP like ventricular arrhythmias in 2 out of 8 animals.⁴¹ Likewise, in a transgenic rabbit model of LQT1, shortening of the QTc interval by another $K_v11.1$ activator designated NS1643 was accompanied by an increased incidence of pacing-induced ventricular fibrillation.⁴² However, the fact that LUF7244 at a concentration that completely abolished the proarrhythmic effects of astemizole, sertindole and cisapride does not shorten the APD of NRVMs and therefore may not give rise to drug-induced short QT syndrome (SQTS) raises hope for its clinical applicability.

For the experiments in NRVM monolayers, the final astemizole concentration was 100 nM in most cases, while sertindole and cisapride were used at a final concentration of 1 μM . These concentrations are much higher than the therapeutic blood concentrations of these fortuitous $K_v11.1$ blockers, which are 2-50 $\mu\text{g}\cdot\text{L}^{-1}$ (i.e. 4.4-109 nM) for astemizole, 40-80 $\mu\text{g}\cdot\text{L}^{-1}$ (i.e. 86-172 nM) for cisapride and 50-100 $\mu\text{g}\cdot\text{L}^{-1}$ (i.e. 113-227 nM) for sertindole.⁴³ The proarrhythmic effects of these drugs on NRVMs were completely prevented by 10 μM (i.e. 3.7

mg·L⁻¹) LUF7244, a concentration that did not negatively influence the binding of astemizole to the hH₁R and did not noticeably affect the viability, contractility and excitability of the cardiomyocytes. Accordingly, blood LUF7244 concentrations well below 10 μM may suffice to counteract the proarrhythmic effects of unintended K_v11.1 blockers in humans. However, before LUF7244 or other allosteric modulators can be clinically applied as “co-drugs” or otherwise, they should be subjected to rigorous preclinical and clinical testing with appropriate pharmacokinetic and pharmacodynamics assessments to determine their benefit-risk profiles.

Limitations

Due to the difficulty to obtain and culture adult human ventricular myocytes, in this study NRVMs were used as 2D model system to investigate the effects of LUF7244 on K_v11.1 blockade-associated proarrhythmic changes in cardiac electrophysiology. However, adult human and neonatal rat ventricular myocytes have different AP morphologies because of qualitative and quantitative differences in the molecular components shaping the APs. Also, changes in cardiomyocyte electrophysiological properties may work out differently in a 2D cell layer than in the 3D heart. Nonetheless, studies on NRVM monolayers have greatly contributed to our current understanding of cardiac electrophysiology. Moreover, in spite of the differences in ventricular ion channel composition between humans and rats, their K_v11.1 proteins are very similar showing 95% amino acid identity for the largest isoforms. Consistently, the results of the radioligand binding assays, which were carried out with the human K_v11.1 protein, correlated very well with those of the optical mapping studies using NRVMs. Yet, ultimately, the ability of LUF7244 to counteract the proarrhythmic effects of unintended K_v11.1 blockers should be investigated in human subjects.

As mentioned above, LUF7244 did not inhibit the binding of astemizole to its intended target in radioligand binding assays and did not compromise the viability, excitability or contractility of NRVMs at a concentration sufficient to fully abrogate the proarrhythmic consequences of drug-induced K_v11.1 blockade in these cells. Despite these encouraging results, certainty about the lack of specific adverse/interfering effects of this negative allosteric modulator of K_v11.1 channel in humans can only be obtained through clinical studies. Moreover, now that the ability of LUF7244 to reduce the channel binding affinity of K_v11.1 blockers has been established, allosteric modulators with higher safety and/or efficacy than LUF7244 are likely to arise in the near future. The design of such compounds may benefit from the identification of the precise binding site of LUF7244 at the

K_v11.1 channel.

Conclusions

Allosteric modulators at the K_v11.1 channel could provide a new pharmacological treatment for drug-induced LQTS by preventing the potentially arrhythmogenic changes in AP characteristics caused by unintended K_v11.1 blockers. Through combined administration with a negative allosteric modulator, use of “old” drugs that have been banned because of their “K_v11.1 liability” may be resumed and new drugs with K_v11.1-blocking effects may not have to be excluded from clinical application.

References

1. Stockbridge, N.; Morganroth, J.; Shah, R. R.; Garnett, C. Dealing with global safety Issues. *Drug Saf.* **2013**, *36*, 167-182.
2. Antzelevitch, C. Ionic, molecular, and cellular bases of QT-interval prolongation and torsade de pointes. *Europace* **2007**, *9*, iv4-iv15.
3. Kannankeril, P.; Roden, D. M.; Darbar, D. Drug-induced long QT syndrome. *Pharmacol. Rev.* **2010**, *62*, 760-781.
4. Vandenberg, J. I.; Perry, M. D.; Perrin, M. J.; Mann, S. A.; Ke, Y.; Hill, A. P. hERG K⁺ channels: Structure, function, and clinical significance. *Physiol. Rev.* **2012**, *92*, 1393-1478.
5. Sanguinetti, M. C. hERG1 channel agonists and cardiac arrhythmia. *Curr. Opin. Pharmacol.* **2014**, *15*, 22-27.
6. Kang, J.; Chen, X.; Wang, H.; Ji, J.; Cheng, H.; Incardona, J.; Reynolds, W.; Viviani, F.; Tabart, M.; Rampe, D. Discovery of a small molecule activator of the human ether-à-go-go-related gene (hERG) cardiac K⁺ channel. *Mol. Pharmacol.* **2005**, *67*, 827-836.
7. Potet, F.; Lorinc, A. N.; Chaigne, S.; Hopkins, C. R.; Venkataraman, R.; Stepanovic, S. Z.; Lewis, L. M.; Days, E.; Sidorov, V. Y.; Engers, D. W.; Zou, B.; Afshartous, D.; George, A. L.; Campbell, C. M.; Balser, J. R.; Li, M.; Baudenbacher, F. J.; Lindsley, C. W.; Weaver, C. D.; Kupersmidt, S. Identification and characterization of a compound that protects cardiac tissue from human ether-à-go-go-related gene (hERG)-related drug-induced arrhythmias. *J. Biol. Chem.* **2012**, *287*, 39613-39625.
8. May, L. T.; Leach, K.; Sexton, P. M.; Christopoulos, A. Allosteric modulation of G protein-coupled receptors. *Annu. Rev. Pharmacol. Toxicol.* **2007**, *47*, 1-51.
9. Conn, P. J.; Christopoulos, A.; Lindsley, C. W. Allosteric modulators of GPCRs: A novel approach for the treatment of CNS disorders. *Nat. Rev. Drug Discov.* **2009**, *8*, 41-54.

10. Christopoulos, A.; Changeux, J.; Catterall, W. A.; Fabbro, D.; Burris, T. P.; Cidlowski, J. A.; Olsen, R. W.; Peters, J. A.; Neubig, R. R.; Pin, J.-P.; Sexton, P. M.; Kenakin, T. P.; Ehlert, F. J.; Spedding, M.; Langmead, C. J. International union of basic and clinical pharmacology. XC. multisite pharmacology: Recommendations for the nomenclature of receptor allosterism and allosteric ligands. *Pharmacol. Rev.* **2014**, *66*, 918-947.
11. Zhang, H.; Zou, B.; Yu, H.; Moretti, A.; Wang, X.; Yan, W.; Babcock, J. J.; Bellin, M.; McManus, O. B.; Tomaselli, G.; Nan, F.; Laugwitz, K. L.; Li, M. Modulation of hERG potassium channel gating normalizes action potential duration prolonged by dysfunctional KCNQ1 potassium channel. *Proc. Natl. Acad. Sci. U.S.A.* **2012**, *109*, 11866-11871.
12. Diaz, G. J.; Daniell, K.; Leitza, S. T.; Martin, R. L.; Su, Z.; McDermott, J. S.; Cox, B. F.; Gintant, G. A. The [³H]dofetilide binding assay is a predictive screening tool for hERG blockade and proarrhythmia: comparison of intact cell and membrane preparations and effects of altering [K⁺]_o. *J Pharmacol. Toxicol. Methods* **2004**, *50*, 187-199.
13. Ficker, E.; Jarolimek, W.; Kiehn, J.; Baumann, A.; Brown, A. M. Molecular determinants of dofetilide block of hERG K⁺ channels. *Circ. Res.* **1998**, *82*, 386-395.
14. Aronov, A. M. Predictive in silico modeling for hERG channel blockers. *Drug Discov. Today* **2005**, *10*, 149-155.
15. Shagufita; Guo, D.; Klaasse, E.; de Vries, H.; Brussee, J.; Nalos, L.; Rook, M. B.; Vos, M. A.; van der Heyden, M. A.; IJzerman, A. P. Exploring chemical substructures essential for hERG K⁺ channel blockade by synthesis and biological evaluation of dofetilide analogues. *ChemMedChem* **2009**, *4*, 1722-1732.
16. Ficker, E.; Dennis, A. T.; Wang, L.; Brown, A. M. Role of the cytosolic chaperones Hsp70 and Hsp90 in maturation of the cardiac potassium channel hERG. *Circ. Res.* **2003**, *92*, e87-e100.
17. Yu, Z.; Klaasse, E.; Heitman, L. H.; IJzerman, A. P. Allosteric modulators of the hERG K⁺ channel: Radioligand binding assays reveal allosteric characteristics of dofetilide analogs. *Toxicol. Appl. Pharmacol.* **2014**, *274*, 78-86.
18. Pijnappels, D. A.; Schali, M. J.; Ramkisoensing, A. A.; van Tuyn, J.; de Vries, A. A.; van der Laarse, A.; Ypey, D. L.; Atsma, D. E. Forced alignment of mesenchymal stem cells undergoing cardiomyogenic differentiation affects functional integration with cardiomyocyte cultures. *Circ. Res.* **2008**, *103*, 167-176.
19. Askar, S. F.; Ramkisoensing, A. A.; Schali, M. J.; Bingen, B. O.; Swildens, J.; van der Laarse, A.; Atsma, D. E.; de Vries, A. A.; Ypey, D. L.; Pijnappels, D. A. Antiproliferative treatment of myofibroblasts prevents arrhythmias *in vitro* by limiting myofibroblast-induced depolarization. *Cardiovasc. Res.* **2011**, *90*, 295-304.
20. Cheng, Y.; Prusoff, W. H. Relationship between the inhibition constant (K_i) and the concentration of inhibitor which causes 50 percent inhibition (I_{50}) of an enzymatic reaction. *Biochem. Pharmacol.* **1973**, *22*, 3099-3108.

21. Yu, Z.; IJzerman, A.; Heitman, L. K_v11.1 (hERG)-induced cardiotoxicity: A molecular insight from a binding kinetics study of prototypic K_v11.1 (hERG) inhibitors. *Br. J. Pharmacol.* **2015**, *172*, 940-945.
22. Himel, H. D.; Bub, G.; Lakireddy, P.; El-Sherif, N. Optical imaging of arrhythmias in the cardiomyocyte monolayer. *Heart Rhythm* **2012**, *9*, 2077-2082.
23. Redfern, W. S.; Carlsson, L.; Davis, A. S.; Lynch, W. G.; MacKenzie, I.; Palethorpe, S.; Siegl, P. K. S.; Strang, I.; Sullivan, A. T.; Wallis, R.; Camm, A. J.; Hammond, T. G. Relationships between preclinical cardiac electrophysiology, clinical QT interval prolongation and torsade de pointes for a broad range of drugs: Evidence for a provisional safety margin in drug development. *Cardiovasc. Res.* **2003**, *58*, 32-45.
24. Heijman, J.; Voigt, N.; Carlsson, L. G.; Dobrev, D. Cardiac safety assays. *Curr. Opin. Pharmacol.* **2014**, *15*, 16-21.
25. Korhonen, T.; Hänninen, S. L.; Tavi, P. Model of excitation-contraction coupling of rat neonatal ventricular myocytes. *Biophys. J.* **2009**, *96*, 1189-1209.
26. Davie, C.; Pierre-Valentin, J.; Pollard, C.; Standen, N.; Mitcheson, J.; Alexander, P.; Thong, B. Comparative pharmacology of guinea pig cardiac myocyte and cloned hERG (I_{Kr}) channel. *J. Cardiovasc. Electrophysiol.* **2004**, *15*, 1302-1309.
27. Murakawa, Y. Focal and reentrant mechanisms of torsades de pointes: EAD, reentry, or chimera? *J. Arrhythm.* **2011**, *27*, 28-37.
28. Chang, M. G.; Sato, D.; de Lange, E.; Lee, J.-H.; Karagueuzian, H. S.; Garfinkel, A.; Weiss, J. N.; Qu, Z. Bi-stable wave propagation and early afterdepolarization-mediated cardiac arrhythmias. *Heart Rhythm* **2012**, *9*, 115-122.
29. Pedigo, N.; Yamamura, H.; Nelson, D. L. Discrimination of multiple [³H]5-hydroxytryptamine binding sites by the neuroleptic spiperone in rat brain. *J. Neurochem.* **1981**, *36*, 220-226.
30. van den Nieuwendijk, A. M.; Pietra, D.; Heitman, L.; Göblyös, A.; IJzerman, A. P. Synthesis and biological evaluation of 2, 3, 5-substituted [1, 2, 4] thiadiazoles as allosteric modulators of adenosine receptors. *J. Med. Chem.* **2004**, *47*, 663-672.
31. Vauquelin, G.; Van Liefde, I. Radioligand dissociation measurements: Potential interference of rebinding and allosteric mechanisms and physiological relevance of the biological model systems. *Expert Opin. Drug Discov.* **2012**, *7*, 583-595.
32. Schober, D. A.; Croy, C. H.; Xiao, H.; Christopoulos, A.; Felder, C. C. Development of a radioligand, [³H]LY2119620, to probe the human M₂ and M₄ muscarinic receptor allosteric binding sites. *Mol. Pharmacol.* **2014**, *86*, 116-123.
33. Gao, Z.; Van Muijlwijk-Koezen, J. E.; Chen, A.; Müller, C. E.; IJzerman, A. P.; Jacobson, K. A. Allosteric modulation of A₃ adenosine receptors by a series of 3-(2-pyridinyl) isoquinoline derivatives. *Mol. Pharmacol.* **2001**, *60*, 1057-1063.
34. Dror, R. O.; Green, H. F.; Valant, C.; Borhani, D. W.; Valcourt, J. R.; Pan, A. C.; Arlow, D. H.; Canals, M.; Lane, J. R.; Rahmani, R.; Baell, J. B.; Sexton, P. M.; Chris-

- topoulos, A.; Shaw, D. E. Structural basis for modulation of a G protein-coupled receptor by allosteric drugs. *Nature* **2013**, *503*, 295-299.
35. Kamiya, K.; Niwa, R.; Mitcheson, J. S.; Sanguinetti, M. C. Molecular determinants of hERG channel block. *Mol. Pharmacol.* **2006**, *69*, 1709-1716.
36. Pearlstein, R. A.; Vaz, R. J.; Kang, J.; Chen, X.; Preobrazhenskaya, M.; Shchekotikhin, A. E.; Korolev, A. M.; Lysenkova, L. N.; Miroshnikova, O. V.; Hendrix, J.; Rampe, D. Characterization of hERG potassium channel inhibition using CoMSiA 3D QSAR and homology modeling approaches. *Bioorg. Med. Chem. Lett.* **2003**, *13*, 1829-1835.
37. García-Ferreiro, R. E.; Kerschensteiner, D.; Major, F.; Monje, F.; Stühmer, W.; Pardo, L. A. Mechanism of block of hEAG1 K⁺ channels by imipramine and astemizole. *J. Gen. Physiol.* **2004**, *124*, 301-317.
38. Perry, M.; Stansfeld, P. J.; Leaney, J.; Wood, C.; de Groot, M. J.; Leishman, D.; Sutcliffe, M. J.; Mitcheson, J. S. Drug binding interactions in the inner cavity of hERG channels: Molecular insights from structure-activity relationships of clofilium and ibutilide analogs. *Mol. Pharmacol.* **2006**, *69*, 509-519.
39. Nogawa, H.; Kawai, T. hERG trafficking inhibition in drug-induced lethal cardiac arrhythmia. *Eur. J. Pharmacol.* **2014**, *741*, 336-339.
40. Grunnet, M.; Hansen, R. S.; Olesen, S.-P. hERG1 channel activators: A new anti-arrhythmic principle. *Prog. Biophys. Mol. Biol.* **2008**, *98*, 347-362.
41. Meng, J.; Shi, C.; Li, L.; Du, Y.; Xu, Y. Compound ICA-105574 prevents arrhythmias induced by cardiac delayed repolarization. *Eur. J. Pharmacol.* **2013**, *718*, 87-97.
42. Bentzen, B. H.; Bahrke, S.; Wu, K.; Larsen, A. P.; Odening, K. E.; Franke, G.; Biermann, J.; Peng, X.; Koren, G.; Zehender, M.; Bode, C.; Grunnet, M.; Brunner, M. Pharmacological activation of K_v11.1 in transgenic long QT-1 rabbits. *J. Cardiovasc. Pharmacol.* **2011**, *57*, 223-230.
43. Schulz, M.; Iwersen-Bergmann, S.; Andresen, H.; Schmoldt, A. Therapeutic and toxic blood concentrations of nearly 1,000 drugs and other xenobiotics. *Critical Care* **2012**, *16*, R136.

Chapter 5

Synthesis and biological evaluation of negative allosteric modulators of the K_v11.1 (hERG) channel

*Zhiyi Yu
Jacobus P. D. van Veldhoven
Ingrid M. E. 't Hart
Adrian H. Kopf
Laura H. Heitman
Adriaan P. IJzerman*

Abstract

We synthesized and evaluated a series of compounds for their allosteric modulation at the $K_v11.1$ (hERG) channel. Most compounds were negative allosteric modulators of [3H]dofetilide binding to the channel, in particular **7f**, **7h-j** and **7p**. Compounds **7f** and **7p** were the most potent negative allosteric modulators amongst all ligands, dramatically increasing the dissociation rate of dofetilide in the radioligand kinetic binding assay, while remarkably reducing the affinity of dofetilide and astemizole in a competitive displacement assay. Additionally, both **7f** and **7p** displayed peculiar displacement characteristics with Hill coefficients significantly distinct from unity as shown by e.g., dofetilide, further indicative of their allosteric effects on dofetilide binding. Our findings in this investigation yielded several promising negative allosteric modulators for future functional and clinical research with respect to their antiarrhythmic propensities, either alone or in combination with known $K_v11.1$ blockers.

Introduction

The past decades have witnessed an emerging interest in the identification of allosteric modulators of G protein-coupled receptors (GPCRs), ligand-gated ion channels (LGICs) and enzymes.¹⁻³ Allosteric modulators are ligands that bind to a binding site on a target protein that is not overlapping with and spatially distinct from the so-called orthosteric binding site, i.e. the site where e.g., hormones and neurotransmitters bind.⁴ Negative allosteric modulators reduce receptor binding and/or function associated with orthosteric ligands, whereas positive allosteric modulators enhance these.^{2,4,5} The therapeutic potential of allosteric modulators has been demonstrated in clinical trials, with a number of such drugs now on the market. Allosterically acting ligands provide novel opportunities for drug discovery due to a possible higher subtype-selectivity (allosteric sites are usually less conserved than orthosteric binding sites) and fewer side effects compared with traditional orthosteric compounds due to their ‘ceiling’ effect.^{2,3} However, research on the allosteric modulation of voltage-gated ion channels (VGICs) is largely lacking, in particular for the $K_v11.1$ (hERG) channel.

The $K_v11.1$ channel, encoded by the human ether-à-go-go-related gene (hERG), plays a vital role in regulating cardiac repolarization of the action potential of human ventricular myocytes.^{6,7} Genetic dysfunction or pharmacological inhibition of the $K_v11.1$ channel leads to prolongation of the action potential duration (APD), QT interval lengthening, and the development of Torsades de Pointes (TdP). A staggering array of drugs including antiarrhythmic agents, antihistamines, antibiotics and antipsychotics are known to block the $K_v11.1$ channel via a common, promiscuous binding region within the aqueous inner cavity of the pore.^{8,9} More recently, a small number of compounds, referred to as $K_v11.1$ activators, have been proposed to remediate repolarization disorders in the heart, including acquired and congenital long QT syndromes, due to their up-regulation of $K_v11.1$ currents.^{7,10,11} These activators were found to bind at sites that are distinct from each other and also different from the binding residues of prototypical $K_v11.1$ blockers.⁹ For instance, RPR260243 ((3*R*,4*R*)-4-[3-(6-methoxyquinolin-4-yl)-3-oxopropyl]-1-[3-(2,3,5-trifluorophenyl)prop-2ynyl]piperidine-3-carboxylic acid) that was designated as a type 1 activator interacted with a putative binding site at the cytoplasmic end facing away from the inner cavity of the channel, while type 2 activators like NS1643 (1,3-bis[2-hydroxy-5-(trifluoromethyl)phenyl]urea) appeared to interact with residues located on the outer mouth of the pore.^{8,12,13} Furthermore, some of these activators were found to reduce the affinity and subsequently reverse the action potential prolongation produced by $K_v11.1$ blockers. Pretreatment of cells expressing the $K_v11.1$

channel with RPR260243 slightly reduced the affinity of the reference hERG blocker dofetilide (*N*-[4-(2-{[2-(4-methanesulfonamidophenoxy)ethyl](methyl)amino}ethyl)phenyl]methanesulfonamide), leading to a reduction of dofetilide's prolongation of the action potential.^{12, 14} Likewise, NS3623 (1-[4-bromo-2-(2*H*-tetrazol-5-yl)phenyl]-3-[3-(trifluoromethyl)phenyl]urea) produced a reversal of E-4031 (*N*-[4-[[1-[2-(6-Methyl-2-pyridinyl)ethyl]-4-piperidinyl]carbonyl]phenyl]methanesulfonamide dihydrochloride)-induced QT prolongation in both anaesthetized and conscious guinea pigs.¹⁵ In this sense, the so-called activators might be negative allosteric modulators of the action of $K_v11.1$ blockers, and so normalize the pharmacologically induced action potential prolongation. Indeed, the allosteric terminology at the $K_v11.1$ channel has been introduced in our previous study and a recent review.^{4, 16} Classic methods for screening allosteric modulators have been based on techniques used to identify $K_v11.1$ blockers, such as voltage-dependent fluorescence experiments and laborious patch clamp assays. However, these methods do not allow high throughput screening in the search for new hit and lead molecules.¹⁷ Moreover, although negative allosteric modulators of the $K_v11.1$ channel may be therapeutically promising, the current generation of modulators is not very potent and this raises concerns about their selectivity and liability for cardiac and non-cardiac side effects.^{9, 11} Therefore, it would be of particular importance to design and synthesize more novel allosteric modulators with higher potencies at the $K_v11.1$ channel.

Recently, Zhang *et al.* characterized a potent modulator (ML-T531, compound **7a** in this study) for the $K_v11.1$ channel after screening a large compound library using an automated electrophysiological technique, and found that it normalized APD prolongation induced by dysfunction of the $K_v7.1$ channel.¹⁸ This was the first experimental evidence that $K_v11.1$ modulators can prevent long QT type 1 (LQT1) in addition to type 2 (LQT2) syndrome. The concept that $K_v7.1$ and $K_v11.1$ activators can mutually rescue $K_v7.1$ -related LQT1 and $K_v11.1$ -induced LQT2 syndromes has been put forward previously, and was also validated by using a highly selective $K_v7.1$ modulator, R-L3 ((3*R*)-5-(2-fluorophenyl)-3-(1*H*-indol-3-ylmethyl)-1-methyl-3*H*-1,4-benzodiazepin-2-one)), which suppressed early afterdepolarizations initiated by the $K_v11.1$ blocker dofetilide in rabbit myocytes.^{17, 19, 20} Apart from ML-T531, a chemically similar compound (VU0405601, compound **7r**) was discovered in a fluorescence-based thallium influx assay, and this ligand allosterically diminished the affinity of dofetilide at the channel and relieved the arrhythmia induced by dofetilide.²¹ Altogether, negative allosteric modulators of the $K_v11.1$ channel could be beneficial in LQT syndromes induced by genetic loss-of-function or pharmacological inhibition of both $K_v11.1$ and $K_v7.1$ channels. In the present study, we selected ML-T531 and

VU0405601 as our starting point, and synthesized a series of new ligands with modifications at the three aromatic rings present in the basic scaffold of the lead compounds. Based on the results from a previously validated single point dissociation assay,¹⁶ their structure-activity relationships were analyzed. Subsequently, a selection of potent negative allosteric modulators were comprehensively characterized in [³H]dofetilide dissociation and displacement assays, and their influences on affinity of two specific K_v11.1 blockers (dofetilide and astemizole (1-[(4-fluorophenyl)methyl]-*N*-[1-[2-(4-methoxyphenyl)ethyl]-4-piperidyl]benzimidazol-2-amine)) were evaluated as well.

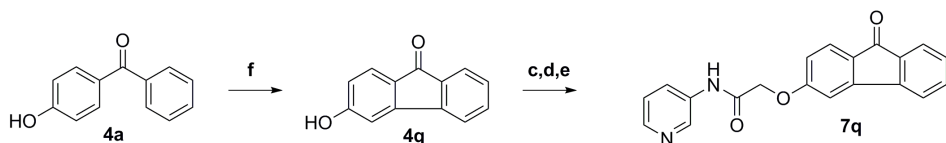
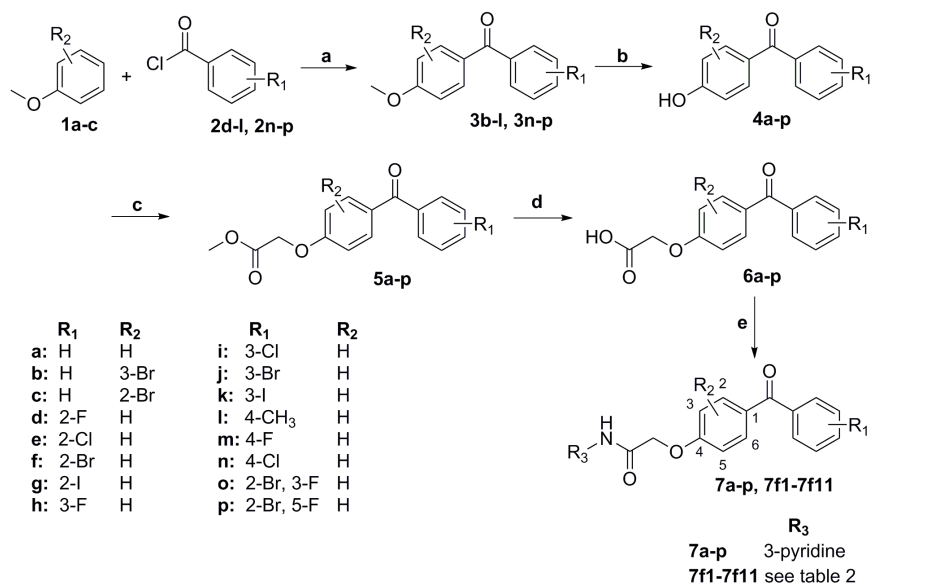
Results and discussion

Chemistry

The synthetic route of all final compounds is depicted in **Scheme 1** except that compound **7r** was synthesized as previously described.²¹ Small systematic chemical variations were made by introducing different functional groups at the three aromatic rings of the reference compound (ML-T531, **7a**). Compounds based on modifications at the two phenyl rings (**7a-p**) were synthesized as follows. Friedel-Crafts acylation of substituted anisols (**1a-c**) and benzoyl chlorides (**2d-l** and **2n-p**) resulted in the formation of different substituted-benzophenone derivatives (**3b-l** and **3n-p**).²² Apart from acid chlorides **2o** and **2p** that were synthesized from the corresponding carboxylic acids **8o** and **8p** (**Scheme 2**), all other intermediates were commercially available. Demethylation of the methoxy group for compounds **3b-l** and **3n-p** with AlCl₃ or BBr₃ in the case of **3c** led to **4b-l** and **4n-p** with high yields (65-97%).^{22, 23} Notably, demethylation of **3c** using AlCl₃ conditions resulted in the undesired debrominated product **4a**. Subsequently, reaction of **4a-p** with 2-methylbromoacetate and hydrolysis of **5a-p** with LiOH produced compounds **6a-p**. Eventually, final compounds **7a-p** were obtained via a peptide coupling, using EDCI*HCl (**7e** and **7l**) or the superior HATU, between the acids (**6a-p**) and 3-aminopyridine in yields of 23-98%.²¹ Fluorenone analogue **7q** was synthesized as follows: i) an oxidative dehydrogenative cyclization of benzophenone **4a** resulted in fluorenone intermediate **4q**, and ii) subsequent HATU peptide coupling conditions led to the formation of final compound **7q**.²⁴ To further investigate the influences of the 3-pyridine ring on the allosteric modulation capacities of ligands, a variety of substituted 3-aminopyridines (**7f1-f8**) and other nitrogen-containing heterocyclic rings (**7f9-f11**) were synthesized in a similar approach as described above. All intermediates were commercially available except intermediate **10f5**, which was synthesized from 5-bromo-3-methoxy-

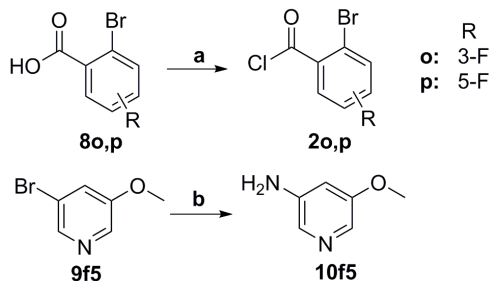
pyridine (**9f5**) through an amination using ammonia and copper sulphate pentahydrate (**Scheme 2**).²⁵

Scheme 1. Synthesis of compounds **7a-q** and **7f1-f11**.



a) AlCl_3 , DCM, 0 °C to r.t., 2 h; b) AlCl_3 , toluene, 130 °C, 2 h; c) 2-methylbromoacetate, K_2CO_3 , DMF, 65 °C, overnight; d) LiOH, THF, MeOH, 105 °C, 30 min; e) 3-aminopyridine, Et_3N , HATU or EDCI·HCl (**7e** and **7l**), DMF, overnight.

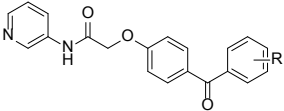
Scheme 2. Synthesis of intermediates (**2o**, **2p** and **10f5**)



a) SOCl_2 , 100 °C, 2h; b) NH_3 (aq), $\text{CuSO}_4 \cdot 5\text{H}_2\text{O}$, 140 °C, 20 h.

Structure-activity relationships

Initially, all synthesized compounds were tested for their abilities to increase or decrease the dissociation of [^3H]dofetilide from the HEK293K_v11.1 cell membrane preparations at 10 μM in a single point dissociation assay,¹⁶ and the results are summarized in **Table 1-3**. Compound **7a**, also referred to as ML-T531 in literature, has been reported to be the most potent K_v11.1 activator, which normalizes the prolonged APDs of patient-derived cardiomyocytes.¹⁸ Thus, a series of compounds with different substituents on the phenylcarbonyl ring were synthesized and evaluated for their allosteric modulation at the K_v11.1 channel (**Table 1**). Similar to compound **7a**, all compounds behaved as negative allosteric modulators of the K_v11.1 channel as they significantly increased the dissociation of dofetilide from the channel except **7l** and **7n**. The latter observation is in agreement with the previous finding that the effect of **7n** on K_v11.1 currents was insignificant and negligible,¹⁸ indicative of the reliability of our high-throughput single point dissociation assay. Introduction of halogens at the ortho position (**7d**, **7e** and **7g**) did not significantly impact the negative allosteric effect of the lead compound **7a**, whereas halogen substituents at the meta position (**7h-k**) displayed a more prominent enhancement of dofetilide dissociation compared to **7a**. Notably, introduction of a bromo substituent at the ortho position (**7f**) dramatically decreased the relative binding of dofetilide to $44 \pm 1\%$ from $78 \pm 3\%$ for **7a**, which implicated that ortho-bromo derivatives could be the starting point for designing more potent allosteric modulators of the K_v11.1 channel in the following step. With respect to the para position, methyl and chloro substituents (**7l** and **7n**) totally abolished the negative allosteric modulation properties of this series of compounds, while the 4-fluoro derivative slightly increased the allosteric effect (**7m** versus **7a**). The bigger size of the methyl and chloro substituents at the para-position may be the reason for this decrease in effect. Additionally, electron donating (**7l**) and withdrawing (**7n**) groups seemed to reduce the allosteric profiles of **7a** to the same extent, implying a negligible role of electronic effects in affecting allostery of compounds at the K_v11.1 channel. When bromo and fluoro substituents were simultaneously introduced to the ortho and meta positions, respectively, additional allosteric inhibition was observed for **7p** but **7o** exerted a much lower allosteric effect compared to compounds **7f** and **7h**. This confirms that steric hindrance at the phenyl ring might not be beneficial for the potency of these negative allosteric modulators.

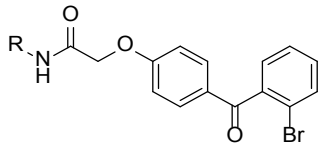
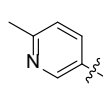
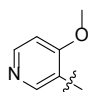
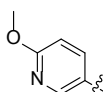
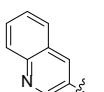
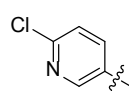
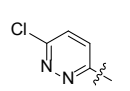
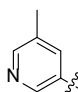
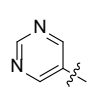
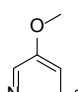
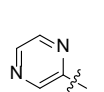
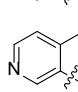
Table 1. Allosteric modulation of [³H]dofetilide binding at the K_v11.1 channel by 10 μM of compounds **7a** and **7d-p**.


Compd	R	%B/B _{control}	Compd	R	%B/B _{control}
7a	H	78 ± 3	7j	3-Br	57 ± 5
7d	2-F	85 ± 4	7k	3-I	62 ± 3
7e	2-Cl	71 ± 2	7l	4-CH ₃	97 ± 5
7f	2-Br	44 ± 1	7m	4-F	65 ± 2
7g	2-I	72 ± 2	7n	4-Cl	104 ± 2
7h	3-F	47 ± 2	7o	2-Br, 3-F	85 ± 1
7i	3-Cl	43 ± 2	7p	2-Br, 5-F	38 ± 3

Since compounds with a bromo substituent (**7f** and **7p**) at the ortho position of the phenylcarbonyl ring were among the most potent modulators, a variety of compounds with the same ortho-bromo substitution but different nitrogen-containing heterocyclic aromatic rings were designed to investigate the influences of the pyridine moiety on allosteric modulation of the K_v11.1 channel. As displayed in **Table 2**, none of these compounds showed more prominent negative allosteric activities than the starting compound **7f**. By contrast, introduction of methyl, methoxyl, chlorine and phenyl groups amongst 3-pyridyl analogues (**7f1-f8**) abrogated the negative allosteric effects, and compounds **7f2** and **7f4** even appeared to decrease the dissociation of dofetilide albeit not significantly. It is worth noting that substituents with opposite electronic effects such as **7f1** and **7f3** could not be distinguished with respect to their allosteric activities, which is in agreement with our earlier finding for derivatives **7l** and **7n** shown in **Table 1**. This further proves that electronic effects were not the determinants of allosteric characteristics for this series of ligands. In addition, replacement of the pyridine ring with chlorine-substituted diazine (**7f9**), pyrimidine (**7f10**) and pyrazine (**7f11**) moieties led to significant decreases of the negative allosteric effects on the K_v11.1 channel compared to **7f**. Altogether, a non-substituted pyridine moiety is preferred for binding to the allosteric sites at the K_v11.1 channel. As compound **7r** (VU0405601) was found to significantly increase the IC₇₀ value of dofetilide and thus prevent its K_v11.1 inhibition,²¹ substituents at the phenolic ring were also explored in **Table 3**. Introducing bromine at the phenolic ring wholly eliminated their allosteric effects (**7b-c** versus **7a**), whereby linkage of the two phenyl rings

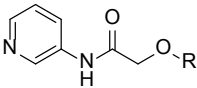
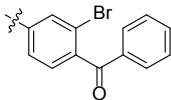
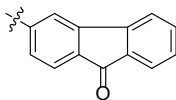
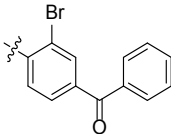
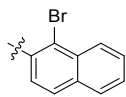
(**7q**) resulted in a comparably negative allosteric potency to the lead compound **7a**. Consistent with the previous publication,²¹ substitution of the general benzo-phenone moiety by a bromine-substituted naphthyl ring moderately increased the negative allosteric effect (**7r** versus **7a**).

Table 2. Allosteric modulation of [³H]dofetilide binding at the K_v11.1 channel by 10 μ M of compounds **7f1-f11**.

					
Compd	R	%B/B _{control}	Compd	R	%B/B _{control}
7f1		105 \pm 12	7f7		105 \pm 12
7f2		124 \pm 13	7f8		87 \pm 12
7f3		95 \pm 12	7f9		92 \pm 2
7f4		121 \pm 15	7f10		87 \pm 9
7f5		107 \pm 15	7f11		92 \pm 2
7f6		108 \pm 16			

Taken together, all three aromatic rings played critical roles in modifying the allosteric effects of this series of compounds at the K_v11.1 channel. In general, introducing halogen substituents with comparatively less steric hindrance at the phenylcarbonyl ring, and avoiding substituents at the pyridine and phenolic rings were favorable for enhancing the negative allosteric potencies of these modulators. Among all compounds shown in **Table 1-3**, **7f**, **7i** and **7p** were the most potent negative allosteric modulators by reducing [³H]dofetilide binding during dissociation to 44 \pm 1, 43 \pm 2 and 38 \pm 3% respectively, which demonstrated their higher potencies than reference compounds **7a** (78 \pm 3%) and **7r** (66 \pm 3%).

Table 3. Allosteric modulation of [³H]dofetilide binding at the K_v11.1 channel by 10 μM of compounds **7b**, **7c**, **7q** and **7r**.

					
Compd	R	%B/B _{control}	Compd	R	%B/B _{control}
7b		96 ± 1	7q		79 ± 6
7c		96 ± 7	7r		66 ± 3

Subsequently, several of the more potent allosteric modulators were selected in [³H]dofetilide dissociation and displacement assays to exploit their pharmacological characteristics at the K_v11.1 channel in more detail. Since the disintegration characteristics of a radioligand-receptor complex can only be altered by the binding of a compound to a site distinct from the radioligand binding site, the effects of these synthesized compounds on the dissociation rate of [³H]dofetilide can be unequivocally indicative of their allosteric actions.²⁶ In this respect, the dissociation behavior of [³H]dofetilide was investigated in the absence (control) or presence of potent modulators (**Figure 1** and **Table 4**). As concentration-dependent allosteric modulation has been observed in a plethora of receptors,^{5, 27-29} we evaluated a higher concentration (50 mM) of modulators in this assay, also to assess whether we could surpass the effects measured at 10 μM. The dissociation rate of the radioligand induced by an excess concentration of unlabeled dofetilide alone was 0.19 ± 0.01 min⁻¹, which was significantly increased by the selected compounds (**7f**, **7h-j** and **7p**), once more illustrating their negative allosteric modulation of the K_v11.1 channel. Compound **7p** was the most potent modulator that accelerated the k_{off} of dofetilide to 0.78 ± 0.20 min⁻¹, while **7j** was least efficacious with a dissociation rate of 0.27 ± 0.03 min⁻¹ for dofetilide. The ranking order of all five compounds in enhancing the dissociation rate of dofetilide was identical to the one obtained in the single point dissociation assay except for compound **7f**, which had a more prominent negative allosteric action in this assay. Next, the concentration-dependent effects of two representative compounds at increasing the dissociation of [³H]dofetilide from the K_v11.1 channel were assessed as in **Figure 2**, and the determined EC₅₀ values for **7f** and **7p** were 12 ± 2

and $4.6 \pm 0.4 \mu\text{M}$, respectively. This is in agreement with their activities in the other kinetic assays. It should be mentioned that a full concentration-effect curve of **7f** could not be recorded due to its limited solubility at higher concentrations. Furthermore, there was still 25% [^3H]dofetilide binding at the $\text{K}_{\text{v}}11.1$ channel left in the presence of $100 \mu\text{M}$ **7p**, which indicates that the binding of $\text{K}_{\text{v}}11.1$ blockers cannot be completely displaced via conformational changes of the channel caused by these negative allosteric modulators. More recently, curve-shifts that deviate from a simple competitive interaction at an equilibrium situation were revealed to be indicative of allostery.⁴ Consequently, we determined the effect of the potent modulators (**7f**, **7h-j** and **7p**) on the equilibrium affinity of two prototypical $\text{K}_{\text{v}}11.1$ blockers, dofetilide and astemizole (**Figure 3** and **Table 5**).

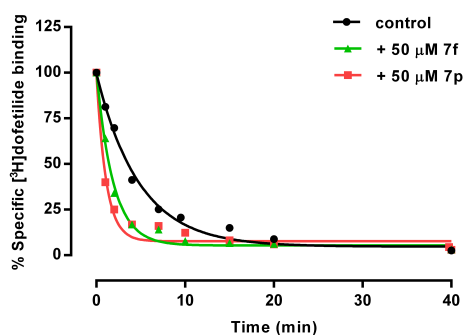


Figure 1. Dissociation curves of [^3H]dofetilide by $10 \mu\text{M}$ dofetilide in the absence (control) or presence of $50 \mu\text{M}$ **7f** and **7p**. Experiments were performed at 25°C with $20 \mu\text{g}$ HEK293 $\text{K}_{\text{v}}11.1$ membranes.

Table 4. Dissociation rates of [^3H]dofetilide in the absence (control) or presence of $50 \mu\text{M}$ **7f**, **7h-j** and **7p**, and EC_{50} values of two representative compounds (**7f** and **7p**) at accelerating dissociation of [^3H]dofetilide from the $\text{K}_{\text{v}}11.1$ channel.

Compd	$k_{\text{off, dofetilide}} (\text{min}^{-1})$	fold	$\text{EC}_{50} (\mu\text{M})$
control	0.19 ± 0.01	-	-
+ 7f	$0.57 \pm 0.05^{***}$	3.0	12 ± 2
+ 7h	$0.30 \pm 0.04^*$	1.6	-
+ 7i	$0.33 \pm 0.03^{**}$	1.7	-
+ 7j	$0.27 \pm 0.03^*$	1.4	-
+ 7p	$0.78 \pm 0.20^*$	4.1	4.6 ± 0.4

Values are means (\pm SEM) of at least three independent experiments performed in duplicate (* $P < 0.05$, ** $P < 0.01$, *** $P < 0.001$ versus control).

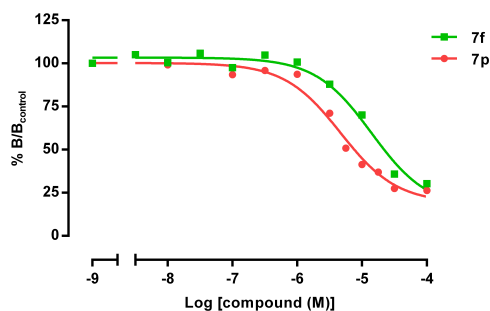


Figure 2. Concentration-dependent effects of **7f** and **7p** in accelerating dissociation of [^3H]dofetilide from the $\text{K}_{\text{v}}11.1$ channel. Membrane proteins were first pre-equilibrated with [^3H]dofetilide, then the dissociation was induced by $10\ \mu\text{M}$ dofetilide in the absence or presence of different concentrations of compounds and the incubation was terminated after 6 min. The results are expressed as the ratio of the specific binding of [^3H]dofetilide in the presence of $10\ \mu\text{M}$ dofetilide plus various concentrations of negative allosteric modulators (B) over that in the presence of $10\ \mu\text{M}$ dofetilide alone (B_{control}). Experiments were performed at $25\ ^\circ\text{C}$ with $20\ \mu\text{g}$ HEK293 $\text{K}_{\text{v}}11.1$ membranes.

As shown in **Figure 3A** and **3B**, the displacement curves of both dofetilide and astemizole were right-ward shifted by compound **7f** and **7p** at $10\ \mu\text{M}$, which is another indication of the negative allosteric properties of **7f** and **7p**. The affinity of dofetilide ($K_{\text{i}} = 4.8 \pm 0.5\ \text{nM}$) and astemizole ($K_{\text{i}} = 1.3 \pm 0.1\ \text{nM}$) were comparable to our previous findings,³⁰ and their apparent K_{i} values were increased in the presence of all tested compounds. The K_{i} values of dofetilide shifted to $6.8 \pm 0.5\ \text{nM}$ (**7j**) and $22 \pm 5\ \text{nM}$ (**7p**), while the values for astemizole were $1.8 \pm 0.5\ \text{nM}$ (**7j**) and $8.2 \pm 1.5\ \text{nM}$ (**7p**). Apart from compound **7f**, the fold increase in K_{i} values for dofetilide and astemizole by these modulators was very comparable, and fully in line with our findings in the other dissociation assays. This diminishing of the affinity of $\text{K}_{\text{v}}11.1$ blockers through negative allosteric modulation is very appealing and may even help in mitigating acquired LQT syndromes via relieving drug-induced $\text{K}_{\text{v}}11.1$ blockade. The [^3H]dofetilide equilibrium displacement curves of **7f** and **7p** shown in **Figure 4** were rather steep with pseudo Hill coefficients (-1.8 for both compounds) much larger than unity, further indicating their allosteric actions on dofetilide binding at the $\text{K}_{\text{v}}11.1$ channel.²⁹ For the sake of comparison, the displacement curve of dofetilide was also included in **Figure 4**, and the derived Hill slope was equal to -1.0 illustrating the competitive and ‘orthosteric’ binding of dofetilide and the reliability of this assay.

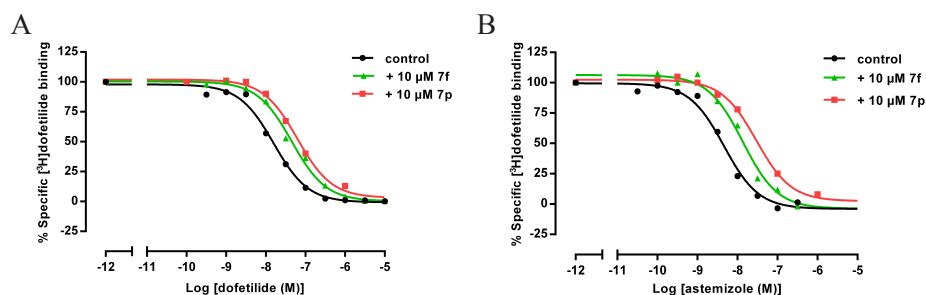


Figure 3. Displacement curves of dofetilide (**A**) and astemizole (**B**) in the absence (control) or presence of 10 μM **7f** and **7p** in a [^3H]dofetilide binding assay. Experiments were performed at 25 $^{\circ}\text{C}$ with 20 μg HEK293K_v11.1 membranes.

Table 5. The K_v11.1 affinities of dofetilide and astemizole in the absence (control) or presence of 10 μM **7f**, **7h-j** and **7p**.

Compd	K _{i, dofetilide} (nM)	fold	K _{i, astemizole} (nM)	fold
control	4.8 \pm 0.5	-	1.3 \pm 0.1	-
+ 7f	12 \pm 3*	2.5	5.3 \pm 1.3*	4.1
+ 7h	8.9 \pm 0.8*	1.9	2.5 \pm 0.9	1.9
+ 7i	16 \pm 4*	3.3	3.7 \pm 0.1***	2.8
+ 7j	6.8 \pm 0.5*	1.4	1.8 \pm 0.5	1.4
+ 7p	22 \pm 5*	4.6	8.2 \pm 1.5*	6.3

Values are means (\pm SEM) of at least three independent experiments performed in duplicate (* $P < 0.05$, *** $P < 0.001$ versus control).

K_v11.1 activators have been introduced as a new potential anti-arrhythmic strategy based on augmentation of the repolarization reserve of cardiomyocytes.³¹ In this context, reference compounds **7a** and **7r** have also been defined as activators.^{18, 21} Compound **7r** had been found to decrease the affinity of K_v11.1 blockers dofetilide and droperidol, and to reduce the action potential prolongation by dofetilide in isolated rabbit ventricular cardiomyocytes. In a similar fashion, RPR26024, the first known K_v11.1 activator, dose-dependently reversed the action potential-prolonging effects of dofetilide in guinea pig myocytes.¹² We hypothesized that the K_v11.1 activators might exert their antiarrhythmic effects through negative allosteric modulation of the binding of K_v11.1 blockers to the channel, and verified that this was the case for compound **7r**. Additionally, compound **7a** had been found to relieve APD prolonged by a genetic dysfunction of the K_v7.1 channel.¹⁸ Several negative allosteric modulators synthesized in this study displayed higher potencies than **7a** and **7r**, in particular **7f** and **7p**, which

implicates their roles as lead compounds in eventually treating patients with LQT syndromes induced by pharmacological blockade of the $K_v11.1$ channel or due to genetic defects of the potassium channels.

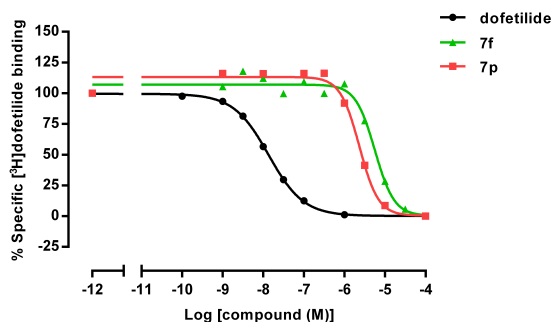


Figure 4. Displacement curves of $[^3\text{H}]$ dofetilide by dofetilide (control), **7f** and **7p**. Experiments were performed at 25 °C with 20 μg HEK293 $K_v11.1$ membranes.

Conclusion

In summary, modifications of the three aromatic rings of the basic scaffold from reference compounds **7a** and **7r** lead to a series of compounds comprising of novel negative allosteric modulators of dofetilide binding to the $K_v11.1$ channel. Structure-activity relationships demonstrate that all the three aromatic rings play pivotal roles in determining the allosteric effects of these ligands at the $K_v11.1$ channel. Introducing halogen substituents at the meta-position of phenylcarbonyl ring together with non-substituted pyridine and phenolic rings enhances the negative allosteric effects of these modulators. In the kinetic dissociation assays, these compounds significantly accelerate the dissociation of $[^3\text{H}]$ dofetilide from the $K_v11.1$ channel. Moreover, several potent modulators shift the displacement curves of prototypical $K_v11.1$ blockers (dofetilide and astemizole) to the right, and thus, diminish their $K_v11.1$ affinity at the channel. This is another indication of their negative allosteric properties, and also implicates their potential antiarrhythmic propensities in reducing acquired LQT syndromes induced by pharmacological blockade. Furthermore, these negative allosteric modulators may also become a new class of medicines for alleviating congenital LQT syndromes linked to both $K_v11.1$ and $K_v7.1$ channels like compound **7a**. Since compounds **7f** and **7p** are more potent than reference compounds **7a** and **7r**, they may serve as lead compounds for further optimization to relieve action potential prolongation through $K_v11.1$ channels or other potassium channels.

Experimental section

Chemistry

All solvents and reagents were purchased from commercial sources and were of analytical grade. Demineralised water is simply referred to as H₂O, as was used in all cases unless stated otherwise (i.e. brine). ¹H and ¹³C NMR spectra were recorded on a Bruker AV 400 liquid spectrometer (¹H NMR, 400 MHz; ¹³C NMR, 100 MHz) at ambient temperature. Chemical shifts are reported in parts per million (ppm), are designated by δ and are downfield to the internal standard tetramethylsilane (TMS) in CDCl₃. Coupling-constants are reported in Hz and are designated as J. Analytical purity of the final compounds was determined by high pressure liquid chromatography (HPLC) with a Phenomenex Gemini 3m C18 110A column (50 x 4.6 mm, 3 μ m), measuring UV absorbance at 254 nm. Sample preparation and HPLC method was - unless stated otherwise - as follows: 0.3-0.8 mg of compound was dissolved in 1 mL of a 1:1:1 mixture of CH₃CN/H₂O/tBuOH and eluted from the column within 15 minutes, with a three component system of H₂O/CH₃CN/1% TFA in H₂O, decreasing polarity of the solvent mixture in time from 80/10/10 to 0/90/10. All compounds showed a single peak at the designated retention time and are at least 95% pure. Liquid chromatography–mass spectrometry (LC-MS) analyses were performed using Thermo Finnigan Surveyor - LCQ Advantage Max LC-MS system and a Gemini C18 Phenomenex column (50 × 4.6 mm, 3 μ m). The sample preparation was the same as for HPLC analysis. The elution method was set up as follows: 1-4 min isocratic system of H₂O/CH₃CN/1% TFA in H₂O, 80:10:10, from the 4th min, a gradient was applied from 80:10:10 to 0:90:10 within 9 min, followed by 1 min of equilibration at 0:90:10 and 1 min at 80:10:10. Thin-layer chromatography (TLC) was routinely performed to monitor the progress of reactions, using aluminium coated Merck silica gel F254 plates. Purification by column chromatography was achieved by use of Grace Davison Davisil silica column material (LC60A 30-200 micron). Solutions were concentrated using a Heidolph laborota W8 2000 efficient rotary evaporation apparatus and by a high vacuum on a Binder APT line Vacuum Drying Oven. Microwave reactions were carried out in a Biotage Initiator using sealed tubes and at a set reaction temperature. The procedure for a series of similar compounds is given as a general procedure for all within that series, annotated by the numbers of the compounds.

Chlorination of bromo-fluoro-substituted-benzoic acids. To 2-bromo-5-fluorobenzoic acid **8p** (500 mg, 2.28 mmol) was added thionyl chloride (207 μ L, 2.85 mmol). The mixture was heated for 1.5 h at 100 °C (an additional

1 mL of SOCl_2 was added after 20 min). The thionyl chloride was evaporated and the product, **2-bromo-5-fluorobenzoyl chloride (2p)**, was used without further purification. 454 mg yield = 84%.

2-Bromo-3-fluorobenzoyl chloride (2o). Methode chlorination of bromo-fluoro-substituted-benzoic acids. Continued without further purification, 436 mg yield = 81%.

3-Amino-5-methoxy pyridine (10f5). 3-Bromo-5-methoxypyridine (**9f5**) (500 mg, 2.66 mmol), ammonium hydroxide (15 mL) and coppersulfate pentahydrate (33 mg, 0.13 mmol) were heated at 140 °C in the microwave in a closed tube for 20 h. The reaction mixture was cooled to room temperature and the crude material separated between ethyl acetate and water. The organic layer was washed with water (3 times) and brine, dried over MgSO_4 , filtered and concentrated *in vacuo* to give 84 mg, yield 25% of the desired product as solids. ^1H NMR (400 MHz, CDCl_3): δ 7.72 (d, J = 5.4 Hz, 2H), 6.51 (t, J = 2.4 Hz, 1H), 3.79 (s, 3H) ppm; HPLC-MS: m/z 125.0

General method for the Friedel Crafts acylation (**3b-l** and **3n-p**).

To a cooled mixture of the substituted benzoyl chloride **2b-l** and **2n-q** (5.71 mmol, 1.0 equiv.) and the (substituted)-anisole **1a-c** (7.14 mmol, 1.25 equiv.) in CH_2Cl_2 (0.2 M) or carbon disulfide (**3b**) was added AlCl_3 (7.14 mmol, 1.25 equiv.) in portions over 20 min under a nitrogen atmosphere. After 24 h at room temperature full conversion was observed with TLC (Pet. ether/EtOAc 19/1) and the reaction mixture was poured into a 3 M aq. HCl solution. The organics were extracted 3 times from the aqueous layer with CH_2Cl_2 , washed with water and brine, dried over MgSO_4 and concentrated *in vacuo*. The obtained crude material was triturated with petroleum ether to obtain the pure products as white solids.

(2-Bromo-4-methoxyphenyl)-phenylmethanone (3b). Started from 3-bromoanisole (**1b**) and benzoyl chloride. Yellow oil 2.20 g after column chromatography (2.5-5% EtOAc/Pet. ether), yield = 75%. ^1H NMR (400 MHz, CDCl_3): δ 7.80 (d, J = 7.2 Hz, 2H), 7.58 (d, J = 7.2 Hz, 1H), 7.45 (t, J = 8.0 Hz, 2H), 7.32 (d, J = 8.8 Hz, 1H), 7.19 (d, J = 2.0 Hz, 1H), 6.92 (dd, J = 8.6, 2.2 Hz, 1H), 3.86 (s, 3H) ppm. NMR in accordance with literature.³²

(3-Bromo-4-methoxyphenyl)-phenylmethanone (3c).³³ Started from 2-bromoanisole (**1c**) and benzoyl chloride. White solids 2.78 g, yield = 64%. ^1H NMR (400 MHz, CDCl_3): δ 8.07 (d, J = 2.0 Hz, 1H), 7.80 (dd, J = 8.4, 2.0 Hz, 1H), 7.77-7.73 (m, 2H), 7.60 (tt, J = 7.2, 1.2 Hz, 1H), 7.49 (t, J = 7.2 Hz, 2H), 6.96 (d, J = 8.8 Hz, 1H), 3.99 (s, 3H), 3.86 (s, 3H) ppm. NMR in accordance with literature data.³⁴

(2-Fluorophenyl)(4-methoxyphenyl)methanone (3d). Started from anisole

(**1a**) and 2-fluorobenzoyl chloride (**2d**). White solids 365 mg, yield = 34%. ^1H NMR (400 MHz, CDCl_3): δ 7.83 (d, J = 8.4 Hz, 2H), 7.52-7.46 (m, 2H), 7.25 (t, J = 7.6 Hz, 1H), 7.14 (t, J = 8.4 Hz, 1H), 6.94 (d, J = 8.4 Hz, 2H), 3.86 (s, 3H) ppm. NMR in accordance with literature data.³⁵

(2-Chlorophenyl)(4-methoxyphenyl)methanone (3e). Started from anisole (**1a**) and 2-fluorobenzoyl chloride (**2e**). Pinkish solids 2.43 g, yield = 66%. ^1H NMR (400 MHz, CDCl_3): δ 7.79 (dt, J = 8.8, 2.0 Hz, 2H), 7.47-7.38 (m, 2H), 7.36-7.33 (m, 2H), 6.94 (dt, J = 8.8, 2.0 Hz, 2H), 3.88 (s, 3H) ppm. NMR in accordance with literature data.³⁶

(2-Bromophenyl)(4-methoxyphenyl)methanone (3f). Started from anisole (**1a**) and 2-bromobenzoyl chloride (**2f**). White solids 586 mg, yield = 88%. ^1H NMR (400 MHz, CDCl_3): δ 7.79 (d, J = 8.4 Hz, 2H), 7.64 (d, J = 7.6 Hz, 1H), 7.41 (t, J = 7.6 Hz, 1H), 7.35-7.31 (m, 2H), 6.94 (d, J = 8.4 Hz, 2H), 3.88 (s, 3H) ppm. NMR in accordance with literature data.³⁶

(2-Iodophenyl)(4-methoxyphenyl)methanone (3g). Started from anisole (**1a**) and 2-iodobenzoyl chloride (**2g**). White solids 422 mg, yield = 66%. ^1H NMR (400 MHz, CDCl_3): δ 7.91 (d, J = 8.0 Hz, 1H), 7.78 (d, J = 8.8 Hz, 2H), 7.44 (t, J = 7.2 Hz, 1H), 7.28 (d, J = 6.8 Hz, 1H), 7.17 (t, J = 7.6 Hz, 1H), 6.94 (d, J = 8.8 Hz, 2H), 3.88 (s, 3H) ppm. NMR in accordance with literature data.³⁷

(3-Fluorophenyl)(4-methoxyphenyl)methanone (3h). Started from anisole (**1a**) and 3-fluorobenzoyl chloride (**2h**). White solids 576 mg, yield = 53%. ^1H NMR (400 MHz, CDCl_3): δ 7.82 (d, J = 8.8 Hz, 2H), 7.53 (d, J = 7.6 Hz, 1H), 7.47-7.42 (m, 2H), 7.28-7.24 (m, 1H), 6.97 (d, J = 8.8 Hz, 2H), 3.89 (s, 3H) ppm. NMR in accordance with literature data.³⁸

(3-Chlorophenyl)(4-methoxyphenyl)methanone (3i).³⁹ Started from anisole (**1a**) and 3-chlorobenzoyl chloride (**2i**). Pink solids 2.64 g, yield = 71%. ^1H NMR (400 MHz, CDCl_3): δ 7.80 (dt, J = 8.8, 2.0 Hz, 2H), 7.73 (t, J = 1.6 Hz, 1H), 7.62 (dt, J = 8.0, 1.2 Hz, 1H), 7.53 (dd, J = 8.0, 1.2 Hz, 1H), 7.41 (t, J = 8.0 Hz, 2H), 6.97 (dt, J = 9.2, 1.2 Hz, 2H), 3.89 (s, 3H) ppm.

(3-Bromophenyl)(4-methoxyphenyl)methanone (3j). Started from anisole (**1a**) and 3-bromobenzoyl chloride (**2j**). White solids 649 mg, yield = 49%. ^1H NMR (400 MHz, CDCl_3): δ 7.88 (t, J = 1.6 Hz, 1H), 7.80 (d, J = 8.8 Hz, 2H), 7.70-7.65 (m, 2H), 7.37 (t, J = 7.6, 1H), 6.97 (d, J = 8.8 Hz, 2H), 3.89 (s, 3H) ppm. NMR in accordance with literature data.³⁵

(3-Iodophenyl)(4-methoxyphenyl)methanone (3k). Started from anisole (**1a**) and 3-iodobenzoyl chloride (**2k**). White solids 300 mg, yield = 47%. ^1H NMR (400 MHz, CDCl_3): δ 8.08 (s, 1H), 7.90 (d, J = 8.0 Hz, 1H), 7.80 (d, J = 8.8 Hz, 2H), 7.70 (d, J = 7.6 Hz, 1H), 7.22 (t, J = 8.0 Hz, 1H), 6.98 (d, J = 8.8 Hz, 2H), 3.90 (s, 3H) ppm. NMR in accordance with literature data.⁴⁰

(4-Methoxyphenyl)(4-methylphenyl)methanone (3l). Started from anisole (**1a**) and 4-methylbenzoyl chloride (**2l**). White solids 2.31 g, yield = 68%. ^1H NMR (400 MHz, CDCl_3): δ 8.81 (dt, $J = 8.8, 2.0$ Hz, 2H), 7.67 (d, $J = 8.0$ Hz, 2H), 7.27 (d, $J = 8.4$ Hz, 2H), 6.96 (dt, $J = 8.8, 2.0$ Hz, 2H), 3.88 (s, 3H) ppm. NMR in accordance with literature data.³⁵

(4-Chlorophenyl)(4-methoxyphenyl)methanone (3n). Started from anisole (**1a**) and 4-chlorobenzoyl chloride (**2n**). White solids 1.02 g, yield = 73%. ^1H NMR (400 MHz, CDCl_3): δ 7.80 (dt, $J = 8.8, 2.0$ Hz, 2H), 7.71 (d, $J = 8.4$ Hz, 2H), 7.45 (d, $J = 8.2$ Hz, 2H), 6.96 (d, $J = 8.4$ Hz, 2H), 3.89 (s, 3H) ppm. NMR in accordance with literature data.³⁵

(2-Bromo-3-fluorophenyl)(4-methoxyphenyl)methanone (3o). Started from anisole (**1a**) and 2-bromo-3-fluorobenzoyl chloride (**2o**). White solids 316 mg, yield = 56%. ^1H NMR (400 MHz, CDCl_3): δ 7.78 (d, $J = 8.8$ Hz, 2H), 7.42-7.36 (m, 1H), 7.23 (td, $J = 8.2, 1.2$ Hz, 1H), 7.12 (dd, $J = 7.6, 0.4$ Hz, 1H), 6.95 (d, $J = 8.8$ Hz, 2H), 3.89 (s, 3H) ppm.

(2-Bromo-5-fluorophenyl)(4-methoxyphenyl)methanone (3p). Started from anisole (**1a**) and 2-bromo-5-fluorobenzoyl chloride (**2p**). White solids 438 mg, yield = 74%. ^1H NMR (400 MHz, CDCl_3): δ 7.79 (d, $J = 8.8$ Hz, 2H), 7.61-7.58 (m, 1H), 7.06 (d, $J = 7.6$ Hz, 2H), 6.95 (d, $J = 9.2$ Hz, 2H), 3.89 (s, 3H) ppm.

General method for demethylation of **3b**, **3d-l** and **3n-p** with aluminum trichloride (**4b**, **4d-l** and **4n-p**).²¹

AlCl_3 (2.5 equiv.) was slowly added to a solution of **3b**, **3d-l** and **3n-p** (1.0 equiv.) in toluene (0.15 M) under a N_2 atmosphere. The mixture was refluxed at 130 °C for 2 h and by TLC (Pet. ether/EtOAc 4/1) full conversion was shown. The cooled mixture was poured into an 3 M HCl (aq.) solution, the organics were extracted with ethyl acetate (3 times), washed with brine, dried over MgSO_4 and concentrated to give the desired 4-(benzoyl)phenols (**4b**, **4d-l** and **4n-p**) as solids.

(2-Bromo-4-hydroxyphenyl)-phenylmethanone (4b). Brownish solids 1.36 g, yield = 65%. ^1H NMR (400 MHz, CDCl_3): δ 7.81 (dd, $J = 8.4, 1.2$ Hz, 2H), 7.60 (t, $J = 7.4$ Hz, 1H), 7.46 (t, $J = 7.6$ Hz, 2H), 7.27 (d, $J = 6.8$ Hz, 1H), 7.16 (d, $J = 2.4$ Hz, 1H), 6.86 (dd, $J = 8.4, 2.4$ Hz, 1H), 6.36 (s br, 1H) ppm.

(2-Fluorophenyl)(4-hydroxyphenyl)methanone (4d).⁴¹ White solids 343 mg, yield = 100%. ^1H NMR (400 MHz, CDCl_3): δ 7.78 (d, $J = 8.4$ Hz, 2H), 7.51-7.48 (m, 2H), 7.26-7.24 (m, 1H), 7.18-7.12 (m, 1H), 6.91 (d, $J = 8.4$ Hz, 2H), 6.58 (s br, 1H) ppm.

(2-Chlorophenyl)(4-hydroxyphenyl)methanone (4e).⁴² White solids 2.17 g, yield = 95%. ^1H NMR (400 MHz, DMSO): δ 10.62 (s, 1H), 7.60-7.56 (m, 3H), 7.53 (td, $J = 8.4, 2.0$ Hz, 1H), 7.47 (td, $J = 8.4, 1.6$ Hz, 1H), 7.42 (dd, $J = 7.6, 1.6$

Hz, 1H), 6.88 (d, $J = 8.8$ Hz, 2H) ppm.

4-(2-Bromophenyl)(4-hydroxyphenyl)methanone (4f).⁴³ Brown oil, yield = quantitative. ¹H NMR (400 MHz, CDCl₃): δ 7.73 (d, $J = 8.4$ Hz, 2H), 7.63 (d, $J = 7.6$ Hz, 1H), 7.40 (t, $J = 7.6$ Hz, 1H), 7.33 (t, $J = 8.8$ Hz, 1H), 6.89 (d, $J = 8.4$ Hz, 2H), 6.69 (s br, 1H) ppm.

4-(4-Hydroxyphenyl)(2-iodophenyl)methanone (4g). White solids 393 mg, yield = 97%. ¹H NMR (400 MHz, CDCl₃): δ 7.90 (d, $J = 8.0$ Hz, 1H), 7.71 (d, $J = 8.8$ Hz, 2H), 7.43 (td, $J = 7.6, 0.8$ Hz, 1H), 7.27 (dd, $J = 7.6, 1.6$ Hz, 1H), 6.90 (d, $J = 8.8$ Hz, 2H) ppm. NMR data in accordance with literature.⁴⁴

4-(3-Fluorophenyl)(4-hydroxyphenyl)methanone (4h). White solids 172 mg, yield = 73%. ¹H NMR (400 MHz, CDCl₃): δ 7.77 (d, $J = 8.4$ Hz, 2H), 7.53 (d, $J = 8.0$ Hz, 1H), 7.48-7.43 (m, 2H), 7.30-7.18 (m, 1H), 6.95 (d, $J = 8.0, 0.8$ Hz, 2H) ppm. NMR data in accordance with literature.⁴⁵

4-(3-Chlorophenyl)(4-hydroxyphenyl)methanone (4i). Off white solids 2.35 g, yield = 95%. ¹H NMR (400 MHz, DMSO): δ 10.54 (s, 1H), 7.71-7.63 (m, 4H), 7.60-7.53 (m, 2H), 6.90 (dt, $J = 8.8, 2.0$ Hz, 2H) ppm. NMR data in accordance with literature.⁴⁶

4-(3-Bromophenyl)(4-hydroxyphenyl)methanone (4j). White solids 168 mg, yield = 88%. ¹H NMR (400 MHz, CDCl₃): δ 7.88 (t, $J = 1.6$ Hz, 1H), 7.77 (d, $J = 8.8$ Hz, 2H), 7.70 (dt, $J = 8.0, 1.2$ Hz, 1H), 7.66 (d, $J = 7.6$ Hz, 1H), 7.36 (t, $J = 8.0$ Hz, 1H), 6.93 (d, $J = 8.4$ Hz, 2H), 6.92 (s br, 1H) ppm. NMR data in accordance with literature.⁴⁷

4-(4-Hydroxyphenyl)(3-iodophenyl)methanone (4k). Brown solids 209 mg, yield = 73%. ¹H NMR (400 MHz, CDCl₃): δ 8.08 (s, 1H), 7.90 (d, $J = 8.0$ Hz, 1H), 7.77 (d, $J = 8.4$ Hz, 2H), 7.70 (d, $J = 7.6$ Hz, 1H), 7.22 (t, $J = 8.0$ Hz, 1H), 6.93 (d, $J = 8.8$ Hz, 2H), 5.74 (s br, 1H) ppm. NMR data in accordance with literature.⁴⁶

4-(4-Hydroxyphenyl)(4-methylphenyl)methanone (4l).⁴⁸ Brown solids 2.03 g, yield = 94%. ¹H NMR (400 MHz, DMSO): δ 10.39 (s, 1H), 7.64 (d, $J = 8.4$ Hz, 2H), 7.57 (d, $J = 8.0$ Hz, 2H), 7.33 (d, $J = 8.0$ Hz, 2H), 7.88 (d, $J = 8.8$ Hz, 2H), 2.39 (s, 3H) ppm.

4-(4-Chlorophenyl)(4-hydroxyphenyl)methanone (4n). Off white solids 821 mg, yield = 85%. ¹H NMR (400 MHz, CDCl₃): δ 7.76 (d, $J = 8.8$ Hz, 2H), 7.71 (d, $J = 8.8$ Hz, 2H), 7.46 (d, $J = 8.4$ Hz, 2H), 6.93 (d, $J = 8.8$ Hz, 2H), 6.15 (s br, 1H). NMR data in accordance with literature.⁴⁹

(2-Bromo-3-fluorophenyl)(4-hydroxyphenyl)methanone (4o). Off white solids 301 mg, yield = 100 %. ¹H NMR (400 MHz, CDCl₃): δ 8.32 (s br, 1H), 7.72 (dd, $J = 6.8, 2.0$ Hz, 2H), 7.41-7.35 (m, 1H), 7.22 (td, $J = 8.4, 2.0$ Hz, 1H), 7.11 (dd, $J = 7.6, 0.8$ Hz, 1H), 6.92 (dd, $J = 7.2, 1.6$ Hz, 2H) ppm.

(2-Bromo-5-fluorophenyl)(4-hydroxyphenyl)methanone (4p). White solids 236 mg, yield = 56%. ^1H NMR (400 MHz, CDCl_3): δ 8.49 (s br, 1H), 7.72 (dt, $J = 8.8, 2.4$ Hz, 2H), 7.60-7.57 (m, 1H), 7.09-7.04 (m, 2H), 6.93 (dd, $J = 8.8, 2.4$ Hz, 2H) ppm.

(3-Bromo-4-hydroxyphenyl)-phenylmethanone (4c). At -78°C **3c** (873 mg, 3.00 mmol, 1.0 equiv.) was dissolved in 20 mL of CH_2Cl_2 and a solution of BBr_3 in CH_2Cl_2 (1 M) (15 mL, 15 mmol, 5 equiv.) was added under a N_2 atmosphere. The mixture was stirred at room temperature and after 24 h cooled again to -78°C and quenched with water. The organics were extracted with CH_2Cl_2 (4 times) from the aqueous layer, dried over MgSO_4 and concentrated. The pure **4c** (584 mg of a yellowish solid yield = 70%) was obtained by column chromatography eluting with a gradient of CH_2Cl_2 to 2% MeOH in CH_2Cl_2 . ^1H NMR (400 MHz, CDCl_3): δ 8.03 (d, $J = 2.0$ Hz, 1H), 7.77-7.18 (m, 3H), 7.59 (tt, $J = 7.6, 1.6$ Hz, 1H), 7.50 (t, $J = 7.6$ Hz, 2H), 7.10 (d, $J = 8.4$ Hz, 1H), 6.00 (s, 1H) ppm.

General method for *O*-alkylation yielding compounds **5a-q**.

To a solution of **5a-q** (1.0 eq.) in DMF (0.2 M) was added K_2CO_3 (2.0 equiv.) and 2-methyl bromoacetate (2.0 equiv.). The mixture was stirred at 65°C for 24 h, after which it was cooled to room temperature and the mixture was separated between ethyl acetate and water. The organic layer was washed with water (3 times), brine, dried over MgSO_4 , and concentrated. This gave the desired *O*-alkylated products (**5a-q**) as one spot on TLC (1 EtOAc/4 Pet. ether) and used as crude material in the next reaction or purified as specified in the individual examples.

Methyl 2-(4-benzoylphenoxy)acetate (5a).⁵⁰ Recrystallized from EtOAc/Pet. ether. White solids 1.52 g, yield = 56%. ^1H NMR (400 MHz, CDCl_3): δ 7.83 (d, $J = 8.8$ Hz, 2H), 7.76 (d, $J = 8.0$ Hz, 2H), 7.57 (t, $J = 8.0$ Hz, 1H), 7.48 (t, $J = 8.0$ Hz, 2H), 6.97 (d, $J = 8.8$ Hz, 2H), 4.73 (s, 2H), 3.83 (s, 3H) ppm.

Methyl 2-(4-benzoyl-3-bromophenoxy)acetate (5b). Used as crude in the next reaction, yield = quantitative. ^1H NMR (400 MHz, CDCl_3): δ 7.79 (d, $J = 7.6$ Hz, 2H), 7.59 (t, $J = 7.2$ Hz, 1H), 7.46 (t, $J = 7.6$ Hz, 2H), 7.32 (d, $J = 8.4$ Hz, 1H), 7.20 (d, $J = 1.6$ Hz, 1H), 6.93 (dd, $J = 8.4, 1.6$ Hz, 1H), 4.69 (s, 2H), 3.83 (s, 3H) ppm.

Methyl 2-(4-benzoyl-2-bromophenoxy)acetate (5c). Started from **4c** (2.11 mmol) and this gave 606 mg of the product as a colorless oil after column chromatography using the gradient 1/1 Pet. ether/ CH_2Cl_2 to CH_2Cl_2 , yield = 82%. ^1H NMR (400 MHz, CDCl_3): δ 8.08 (d, $J = 2.0$ Hz, 1H), 7.78-7.74 (m, 3H), 7.60 (t, $J = 7.6$ Hz, 1H), 7.49 (t, $J = 7.6$ Hz, 2H), 6.83 (d, $J = 7.6$ Hz, 1H), 4.82 (s, 2H), 3.83 (s, 3H) ppm.

Methyl 2-(4-(2-fluorobenzoyl)phenoxy)acetate (5d). Used as crude in the next reaction, yield = quantitative. ^1H NMR (400 MHz, CDCl_3): δ 7.84 (d, J = 8.4 Hz, 2H), 7.54-7.48 (m, 2H), 7.28-7.24 (m, 1H), 7.16 (t, J = 9.2 Hz, 1H), 6.96 (d, J = 8.8 Hz, 2H), 4.72 (s, 2H), 3.82 (s, 3H) ppm.

Methyl 2-(4-(2-chlorobenzoyl)phenoxy)acetate (5e). Colorless oil 2.36 g, yield = 83%. ^1H NMR (400 MHz, DMSO): δ 7.76 (dt, J = 8.8, 1.6 Hz, 2H), 7.61-7.54 (m, 2H), 7.51-7.45 (m, 2H), 7.09 (dt, J = 8.8, 2.0 Hz, 2H), 4.94 (s, 2H), 3.70 (s, 3H) ppm.

Methyl 2-(4-(2-bromobenzoyl)phenoxy)acetate (5f). Colorless oil after column chromatography using the gradient 4/1 Pet. ether/EtOAc 341 mg, yield = 75%. ^1H NMR (400 MHz, CDCl_3): δ 7.79 (d, J = 8.8 Hz, 2H), 7.64 (d, J = 7.6 Hz, 1H), 7.41 (t, J = 7.2 Hz, 1H), 7.36-7.30 (m, 2H), 6.94 (d, J = 8.8 Hz, 2H), 4.71 (s, 2H), 3.82 (s, 3H) ppm.

Methyl 2-(4-(2-iodobenzoyl)phenoxy)acetate (5g). Used as crude material in the next reaction, brown oil 444 mg, yield = 93%. ^1H NMR (400 MHz, CDCl_3): δ 7.91 (d, J = 8.0 Hz, 1H), 7.78 (d, J = 8.8 Hz, 2H), 7.44 (t, J = 7.6 Hz, 1H), 7.27 (dd, J = 7.6, 1.2 Hz, 1H), 7.17 (td, J = 7.6, 1.6 Hz, 1H), 6.95 (d, J = 9.2 Hz, 2H), 4.73 (s, 2H), 3.81 (s, 3H) ppm.

Methyl 2-(4-(3-fluorobenzoyl)phenoxy)acetate (5h). Used as crude material in the next reaction, brown oil 244 mg, yield = quantitative. ^1H NMR (400 MHz, CDCl_3): δ 7.82 (dd, J = 8.8, 2.8 Hz, 2H), 7.52 (dd, J = 7.6, 0.8 Hz, 1H), 7.48-7.44 (m, 2H), 7.28 (d, J = 7.2 Hz, 1H), 6.98 (dd, J = 8.8, 2.4 Hz, 2H), 4.72 (s, 2H), 3.82 (s, 3H) ppm.

Methyl 2-(4-(3-chlorobenzoyl)phenoxy)acetate (5i). Washed crude mixture with Pet. ether, off white solids 2.86 g, yield = 93%. ^1H NMR (400 MHz, DMSO): δ 7.78-7.70 (m, 3H), 7.68 (t, J = 1.6 Hz, 1H), 7.62 (dt, J = 8.0, 1.6 Hz, 1H), 7.58 (t, J = 7.6 Hz, 1H), 7.11 (d, J = 8.8 Hz, 2H), 4.95 (s, 2H), 3.72 (s, 3H) ppm.

Methyl 2-(4-(3-bromobenzoyl)phenoxy)acetate (5j). Washed crude mixture with Pet. ether, off white solids 253 mg, yield = 99%. ^1H NMR (400 MHz, CDCl_3): δ 7.89 (t, J = 2.0 Hz, 1H), 7.81 (d, J = 8.8 Hz, 2H), 7.72-7.66 (m, 2H), 7.36 (t, J = 7.6 Hz, 1H), 6.98 (d, J = 8.8 Hz, 2H), 4.74 (s, 2H), 3.84 (s, 3H) ppm.

Methyl 2-(4-(3-iodobenzoyl)phenoxy)acetate (5k). Washed crude mixture with Pet. ether, off white solids 243 mg, yield = 99%. ^1H NMR (400 MHz, CDCl_3): δ 8.08 (t, J = 1.6 Hz, 1H), 7.90 (d, J = 7.6 Hz, 1H), 7.81 (dt, J = 8.2, 2.0 Hz, 2H), 7.70 (dt, J = 8.0, 1.2 Hz, 1H), 7.22 (t, J = 8.0 Hz, 1H), 6.98 (d, J = 8.8 Hz, 2H), 4.73 (s, 2H), 3.83 (s, 3H) ppm.

Methyl 2-(4-(4-methylbenzoyl)phenoxy)acetate (5l). Washed crude mixture with Pet. ether, off white solids 2.71 g, yield = 99%. ^1H NMR (400 MHz, CDCl_3): δ 7.80 (d, J = 8.4 Hz, 2H), 7.67 (d, J = 8.0 Hz, 2H), 7.27 (d, J = 8.0 Hz,

2H), 6.96 (d, $J = 8.4$ Hz, 2H), 4.72 (s, 2H), 3.83 (s, 3H), 2.44 (s, 3H) ppm.

Methyl 2-(4-(4-fluorobenzoyl)phenoxy)acetate (5m). Started from the commercially available **4m**. Washed crude mixture with Pet. ether, white solids 2.53 g, yield = 95%. ^1H NMR (400 MHz, DMSO): δ 7.80-7.76 (m, 2H), 7.73 (dt, $J = 8.8, 2.0$ Hz, 2H), 7.38 (tt, $J = 9.2, 2.4$ Hz, 2H), 7.09 (dt, $J = 8.8, 2.0$ Hz, 2H), 4.95 (s, 2H), 3.72 (s, 3H) ppm.

Methyl 2-(4-(4-chlorobenzoyl)phenoxy)acetate (5n). Used as crude material in the next reaction, yield was quantitative. ^1H NMR (400 MHz, CDCl_3): δ 7.80 (d, $J = 8.8$ Hz, 2H), 7.71 (d, $J = 8.4$ Hz, 2H), 7.46 (d, $J = 8.4$ Hz, 2H), 6.98 (d, $J = 8.8$ Hz, 2H), 4.73 (s, 2H), 3.83 (s, 3H) ppm.

Methyl 2-(4-(2-bromo-3-fluorobenzoyl)phenoxy)acetate (5o). Off white solids 275 mg, yield = 73%. ^1H NMR (400 MHz, CDCl_3): δ 7.77 (d, $J = 8.8$ Hz, 2H), 7.43-7.38 (m, 1H), 7.24 (td, $J = 8.4, 1.2$ Hz, 1H), 7.11 (d, $J = 7.6$ Hz, 1H), 6.95 (d, $J = 8.8$ Hz, 2H), 4.73 (s, 2H), 3.79 (s, 3H) ppm.

Methyl 2-(4-(2-bromo-5-fluorobenzoyl)phenoxy)acetate (5p). Used as crude material in the next reaction, yield = 98%. ^1H NMR (400 MHz, CDCl_3): δ 7.78 (d, $J = 8.4$ Hz, 2H), 7.62-7.57 (m, 1H), 7.10-7.04 (m, 2H), 6.96 (d, $J = 8.4$ Hz, 2H), 4.73 (s, 2H), 3.80 (s, 3H) ppm.

Methyl 2-((9-oxo-9H-fluoren-3-yl)oxy)acetate (5q). Started from **4b** (2.11 mmol) and this gave 309 mg as yellow solids after column chromatography using CH_2Cl_2 as an eluent, yield = 92%. ^1H NMR (400 MHz, CDCl_3): δ 7.64-7.60 (m, 2H), 7.48-7.45 (m, 2H), 7.33-7.27 (m, 1H), 7.07 (d, $J = 2.4$ Hz, 1H), 6.71 (dd, $J = 8.0, 2.0$ Hz, 1H), 4.74 (s, 2H), 3.84 (s, 3H) ppm.

General saponification procedure to obtain acids 6a-q.

To a solution of **5a-i** (1.0 eq.) in a mixture of equal amounts of THF and methanol (0.5 M solution) was added an aqueous 1 M solution of LiOH (5.0 eq.). After 1 hour at 100 °C the saponification of the esters **6a-q** was completed shown by TLC (EtOAc/Pet. ether 1/3). While the mixture was cooled on ice, the pH was adjusted to pH = 1 using a 2 M HCl solution (aq.). The resulting precipitate was collected by filtration, washed with water, Pet. ether and co-evaporated with acetone to dryness.

2-(4-Benzoylphenoxy)acetic acid (6a).⁵¹ White solids 1.37 g, yield = 95%. ^1H NMR (400 MHz, CDCl_3 + drop of DMSO): δ 9.50 (s br, 1H), 7.82 (d, $J = 8.4$ Hz, 2H), 7.75 (d, $J = 7.6$ Hz, 2H), 7.58 (t, $J = 7.6$ Hz, 1H), 7.47 (t, $J = 7.6$ Hz, 2H), 7.00 (d, $J = 8.8$ Hz, 2H), 4.69 (s, 2H) ppm.

2-(4-Benzoyl-2-bromophenoxy)acetic acid (6b). White solids 548 mg, yield = 95%. ^1H NMR (400 MHz, CDCl_3): δ 8.06 (d, $J = 2.0$ Hz, 1H), 7.77-7.34 (m, 3H), 6.60 (t, $J = 7.6$ Hz, 1H), 7.50 (t, $J = 8.0$ Hz, 2H), 6.89 (d, $J = 8.4$ Hz,

1H), 4.78 (s, 2H) ppm.

2-(4-Benzoyl-3-bromophenoxy)acetic acid (6c). Brown solids 1.28 g, yield = 78%. ¹H NMR (400 MHz, CDCl₃): δ 8.88 (s, br, 1H), 7.80 (d, *J* = 8.0 Hz, 2H), 7.63-7.58 (m, 1H), 7.50-7.44 (m, 2H), 7.34 (d, *J* = 8.4 Hz, 1H), 7.23 (d, *J* = 2.4 Hz, 1H), 6.96 (dd, *J* = 8.8, 2.4 Hz, 1H), 4.76 (s, 2H) ppm.

2-(4-(2-Fluorobenzoyl)phenoxy)acetic acid (6d). Off white solids 312 mg, yield = 67%. ¹H NMR (400 MHz, DMSO): δ 13.12 (s br, 1H), 7.73 (d, *J* = 8.4 Hz, 2H), 7.67-7.61 (m, 1H), 7.53 (td, *J* = 7.8, 1.2 Hz, 1H), 7.40-7.34 (m, 2H), 7.07 (d, *J* = 8.8 Hz, 2H), 4.82 (s, 2H) ppm.

2-(4-(2-Chlorobenzoyl)phenoxy)acetic acid (6e). White solids 1.77 g, yield = 79%. ¹H NMR (400 MHz, DMSO): δ 7.67 (dt, *J* = 8.8, 2.0 Hz, 2H), 7.62-7.53 (m, 2H), 7.51-7.43 (m, 2H), 7.05 (d, *J* = 9.2 Hz, 2H), 4.81 (s, 2H) ppm.

2-(4-(2-Bromobenzoyl)phenoxy)acetic acid (6f). Off white solids 8.60 g, yield = 86%. ¹H NMR (400 MHz, CDCl₃): δ 9.17 (s, br, 1H), 7.80 (d, *J* = 8.4 Hz, 2H), 7.63 (d, *J* = 8.0 Hz, 1H), 7.43-7.30 (m, 3H), 6.95 (d, *J* = 8.8 Hz, 2H), 4.75 (s, 2H) ppm.

2-(4-(2-Iodobenzoyl)phenoxy)acetic acid (6g). White solids 302 mg, yield = 71%. ¹H NMR (400 MHz, DMSO): δ 7.96 (d, *J* = 7.6 Hz, 1H), 7.64 (d, *J* = 8.8 Hz, 2H), 7.54 (t, *J* = 7.6 Hz, 1H), 7.35 (d, *J* = 7.6 Hz, 1H), 7.28 (t, *J* = 7.6 Hz, 1H), 7.06 (d, *J* = 8.8 Hz, 2H), 4.81 (s, 2H) ppm.

2-(4-(3-Fluorobenzoyl)phenoxy)acetic acid (6h). Brown solids 94 mg, yield = 45%. ¹H NMR (400 MHz, DMSO): δ 7.76 (d, *J* = 8.8 Hz, 2H), 7.63-7.56 (m, 1H), 7.52-7.46 (m, 3H), 7.08 (d, *J* = 9.2 Hz, 2H), 4.82 (s, 2H) ppm.

2-(4-(3-Chlorobenzoyl)phenoxy)acetic acid (6i). White solids 2.65 g, yield = 97%. ¹H NMR (400 MHz, DMSO): δ 7.75-7.69 (m, 3H), 7.67 (s, 1H), 7.61 (t, *J* = 7.6 Hz, 1H), 7.57 (t, *J* = 7.6 Hz, 1H), 7.04 (d, *J* = 8.8 Hz, 2H), 4.71 (s, 2H) ppm.

2-(4-(3-Bromobenzoyl)phenoxy)acetic acid (6j). White solids 146 mg, yield = 61%. ¹H NMR (400 MHz, DMSO): δ 7.86 (d, *J* = 8.0 Hz, 1H), 7.81 (s, 1H), 7.74 (d, *J* = 8.0 Hz, 2H), 7.67 (d, *J* = 7.2 Hz, 1H), 7.51 (t, *J* = 8.0 Hz, 1H), 7.08 (*J* = 8.0 Hz, 2H), 4.81 (s, 2H) ppm.

2-(4-(3-Iodobenzoyl)phenoxy)acetic acid (6k). White solids 118 mg, yield = 51%. ¹H NMR (400 MHz, DMSO): δ 8.01 (d, *J* = 7.6 Hz, 1H), 7.97 (s, 1H), 7.73 (d, *J* = 8.4 Hz, 2H), 7.67 (d, *J* = 7.6 Hz, 1H), 7.35 (t, *J* = 7.6 Hz, 1H), 7.08 (d, *J* = 8.8 Hz, 2H), 4.82 (s, 2H) ppm.

2-(4-(4-Methylbenzoyl)phenoxy)acetic acid (6l). Off white solids 2.16 g, yield = 81%. ¹H NMR (400 MHz, DMSO): δ 7.70 (d, *J* = 8.8 Hz, 2H), 7.60 (d, *J* = 8.0 Hz, 2H), 7.34 (d, *J* = 8.0 Hz, 2H), 7.04 (d, *J* = 9.2 Hz, 2H), 4.76 (s, 2H), 2.40 (s, 3H) ppm. NMR data in accordance with literature.⁵²

2-(4-(4-Fluorobenzoyl)phenoxy)acetic acid (6m). White solids after recryst-

tallization from MeOH 1.55 g, yield = 64%. ^1H NMR (400 MHz, DMSO): δ 13.20 (s br, 1H), 7.80-7.75 (m, 2H), 7.73 (d, J = 8.8 Hz, 2H), 7.37 (t, J = 8.8 Hz, 2H), 7.07 (d, J = 8.8 Hz, 2H), 4.81 (s, 2H) ppm.

2-(4-(4-Chlorobenzoyl)phenoxy)acetic acid (6n).⁵³ White solids 730 mg, yield 71%. ^1H NMR (400 MHz, DMSO): δ 7.73-7.70 (m, 4H), 7.61 (d, J = 7.6 Hz, 2H), 7.05 (d, J = 8.0 Hz, 2H), 4.74 (s, 2H) ppm.

2-(4-(2-Bromo-3-fluorobenzoyl)phenoxy)acetic acid (6o). White solids 225 mg, yield = 85%. ^1H NMR (400 MHz, CDCl_3): δ 8.89 (s br, 1H), 7.80 (d, J = 8.8 Hz, 2H), 7.43-7.37 (m, 1H), 7.25 (td, J = 8.4, 1.6 Hz, 1H), 7.12 (d, J = 7.2 Hz, 1H), 6.97 (d, J = 8.8 Hz, 2H), 4.77 (s, 2H) ppm.

2-(4-(2-Bromo-5-fluorobenzoyl)phenoxy)acetic acid (6p). White solid 231 mg, yield = 83%. ^1H NMR (400 MHz, CDCl_3): δ 10.07 (s, 1H), 7.78 (d, J = 8.8 Hz, 2H), 7.61-7.56 (m, 1H), 7.10-7.03 (m, 2H), 6.96 (d, J = 8.8 Hz, 2H), 4.75 (s, 2H) ppm.

2-((9-Oxo-9H-fluoren-3-yl)oxy)acetic acid (6q). Yellow solids 255 mg, yield = 87%. ^1H NMR (400 MHz, DMSO): δ 13.20 (br s, 1H), 7.81 (d, J = 7.6 Hz, 1H), 7.62-7.54 (m, 3H), 7.46 (s, 1H), 7.38 (t, J = 7.6 Hz, 1H), 6.84 (d, J = 6.8 Hz, 1H), 4.87 (s, 2H) ppm.

General peptide coupling method (7a-r and 7f1-f11).

To a solution of **6a-r** (1.0 equiv.) and Et_3N (1.5 equiv.) in DMF (0.125 M) was added 3-aminopyridine (1.1 equiv.) and HATU (1.1 equiv.) or EDCI*HCl (**7e** and **7l**). The mixture was stirred at room temperature for 20 h. The mixture was separated between ethyl acetate and water. The organic layer was washed with water twice, brine, dried over MgSO_4 and concentrated. Column chromatography using mixtures of 5% methanol/dichloromethane or EtOAc:Pet.ether 2:1 gave the pure desired products.

2-(4-Benzoylphenoxy)-N-(pyridin-3-yl)acetamide (7a).¹⁸ White solid, 211 mg, yield = 69%. ^1H NMR (400 MHz, CDCl_3): δ 8.70 (s br, 1H), 8.44 (s br, 1H), 8.40 (s br, 1H), 8.22 (d, J = 8.0 Hz, 1H), 7.89 (d, J = 8.4 Hz, 2H), 7.77 (d, J = 7.6 Hz, 2H), 7.60 (t, J = 7.6 Hz, 1H), 7.50 (t, J = 7.6 Hz, 2H), 7.34 (d, J = 7.2 Hz, 1H), 7.09 (d, J = 8.8 Hz, 2H), 4.74 (s, 2H) ppm; ^{13}C NMR (101 MHz, CDCl_3): δ 195.3, 166.4, 160.2, 137.4, 132.4, 132.2, 131.2, 129.5, 128.1, 127.8, 114.1, 67.2 ppm.; HPLC t_{R} = 7.28 min. purity 100%; ESI-MS: 333.13 $[\text{M}+\text{H}]^+$.

2-(4-Benzoyl-3-bromophenoxy)-N-(pyridin-3-yl)acetamide (7b). White solid, 158 mg, yield = 51%. ^1H NMR (400 MHz, CDCl_3): δ 8.71 (s, 1H), 8.43 (d, J = 4.8 Hz, 2H), 8.24 (d, J = 8.0 Hz, 1H), 7.80 (d, J = 7.6 Hz, 2H), 7.61 (t, J = 7.6 Hz, 1H), 7.47 (t, J = 7.8 Hz, 2H), 7.39-7.31 (m, 3H), 7.03 (d, J = 8.4 Hz, 1H), 4.71 (s, 2H) ppm; HPLC t_{R} = 7.15 min. purity 98%; ESI-MS: 411.13 $[\text{M}+\text{H}]^+$.

2-(4-Benzoyl-2-bromophenoxy)-*N*-(pyridin-3-yl)acetamide (7c). White solid, 293 mg, yield = 71%. ^1H NMR (400 MHz, CDCl_3): δ 8.80 (s, 1H), 8.74 (d, $J = 2.4$ Hz, 1H), 8.44 (d, $J = 4.8$ Hz, 1H), 8.27-8.23 (m, 1H), 8.15 (d, $J = 1.6$ Hz, 1H), 7.83 (dd, $J = 8.4, 2.0$ Hz, 1H), 7.80-7.74 (m, 2H), 7.63 (t, $J = 7.6$ Hz, 1H), 7.52 (t, $J = 7.6$ Hz, 2H), 7.35 (dd, $J = 8.4, 4.8$ Hz, 1H), 7.00 (d, $J = 8.8$ Hz, 1H), 4.78 (s, 2H) ppm; HPLC $t_R = 7.29$ min. purity 100%; ESI-MS: 411.07 $[\text{M}+\text{H}]^+$.

2-[4-(2-Fluorobenzoyl)phenoxy]-*N*-(pyridin-3-yl)acetamide (7d). White solid, 150 mg, yield = 78%. ^1H NMR (400 MHz, CDCl_3): δ 8.71 (s, 2H), 8.39 (d, $J = 3.6$ Hz, 1H), 8.20 (d, $J = 8.0$ Hz, 1H), 7.84 (d, $J = 8.4$ Hz, 2H), 7.55-7.49 (m, 2H), 7.31-7.24 (m, 2H), 7.15 (t, $J = 8.4$ Hz, 1H), 7.02 (d, $J = 9.2$ Hz, 2H), 4.70 (s, 2H) ppm; HPLC $t_R = 6.67$ min. purity 98%; ESI-MS: 351.13 $[\text{M}+\text{H}]^+$.

2-[4-(2-Chlorobenzoyl)phenoxy]-*N*-(pyridin-3-yl)acetamide (7e). Used EDCI*HCl instead of HATU. White solid, 72 mg, yield = 20%. ^1H NMR (400 MHz, CDCl_3): δ 8.70-8.60 (m, 2H), 8.39 (d, $J = 4.4$ Hz, 1H), 8.19 (d, $J = 8.0$ Hz, 1H), 7.81 (d, $J = 8.4$ Hz, 2H), 7.45-7.28 (m, 5H), 7.02 (d, $J = 8.4$ Hz, 2H), 4.71 (s, 2H) ppm; HPLC $t_R = 7.04$ min. purity 100%; ESI-MS: 367.13 $[\text{M}+\text{H}]^+$.

2-[4-(2-Bromobenzoyl)phenoxy]-*N*-(pyridin-3-yl)acetamide (7f). White solid, 9 mg, yield = 23%. ^1H NMR (400 MHz, CDCl_3): δ 8.68 (d, $J = 2.0$ Hz, 1H), 8.42 (d, $J = 4.4$ Hz, 1H), 8.36 (s, 1H), 8.22 (dt, $J = 8.4, 0.8$ Hz, 1H), 7.85 (d, $J = 8.8$ Hz, 2H), 7.65 (dd, $J = 7.6, 0.8$ Hz, 1H), 7.43 (td, $J = 7.4, 1.2$ Hz, 1H), 7.38-7.31 (m, 3H), 7.06 (d, $J = 8.8$ Hz, 2H), 4.72 (s, 2H) ppm; HPLC $t_R = 7.09$ min. purity 98%; ESI-MS: 411.07 $[\text{M}+\text{H}]^+$.

2-[4-(2-Iodobenzoyl)phenoxy]-*N*-(pyridin-3-yl)acetamide (7g). White solid, 113 mg, yield = 63%. ^1H NMR (400 MHz, CDCl_3): δ 8.68 (s, 1H), 8.43 (d, $J = 4.4$ Hz, 1H), 8.34 (s, 1H), 8.23 (d, $J = 8.4$ Hz, 1H), 7.93 (d, $J = 8.0$ Hz, 1H), 7.85 (d, $J = 8.4$ Hz, 2H), 7.46 (t, $J = 7.6$ Hz, 1H), 7.33 (dd, $J = 8.4$ Hz, 4.8 Hz, 1H), 7.29 (d, $J = 7.6$ Hz, 1H), 7.20 (td, $J = 7.6$ Hz, 1.2 Hz, 1H), 7.07 (d, $J = 8.8$ Hz, 2H), 4.73 (s, 2H) ppm; HPLC $t_R = 7.19$ min. purity 100%; ESI-MS: 459.00 $[\text{M}+\text{H}]^+$.

2-[4-(3-Fluorobenzoyl)phenoxy]-*N*-(pyridin-3-yl)acetamide (7h). White solid, 80 mg, yield = 67%. ^1H NMR (400 MHz, CDCl_3): δ 8.83 (s, 1H), 8.73 (d, $J = 2.4$ Hz, 1H), 8.39 (d, $J = 4.0$ Hz, 1H), 8.21 (d, $J = 8.8$ Hz, 1H), 7.82 (d, $J = 8.8$ Hz, 2H), 7.52-7.42 (m, 3H), 7.32-7.27 (m, 2H), 7.04 (d, $J = 8.8$ Hz, 2H), 4.73 (s, 2H) ppm; HPLC $t_R = 6.88$ min. purity 100%; ESI-MS: 351.13 $[\text{M}+\text{H}]^+$.

2-[4-(3-Chlorobenzoyl)phenoxy]-*N*-(pyridin-3-yl)acetamide (7i). White solid, 319 mg, yield = 87%. ^1H NMR (400 MHz, CDCl_3): δ 8.72 (d, $J = 2.0$ Hz, 1H), 8.44-8.40 (m, 2H), 8.27 (dd, $J = 8.4, 2.0$ Hz, 1H), 7.88 (d, $J = 8.8$ Hz, 2H), 7.74 (t, $J = 1.6$ Hz, 1H), 7.63 (dt, $J = 7.6, 1.6$ Hz, 1H), 7.58-7.55 (m, 1H), 7.44 (t, $J = 7.6$ Hz, 1H), 7.36 (dd, $J = 8.4, 4.8$ Hz, 1H), 7.11 (d, $J = 8.8$ Hz, 2H), 4.75 (s,

2H) ppm; HPLC t_R = 7.33 min. purity 100%; ESI-MS: 367.07 [M+H]⁺.

2-[4-(3-Bromobenzoyl)phenoxy]-N-(pyridin-3-yl)acetamide (7j). White solid, 63 mg, yield = 25%. ¹H NMR (400 MHz, DMSO): δ 10.42 (d, 1H), 8.79 (d, J = 2.0 Hz, 1H), 8.30 (d, J = 4.0 Hz, 1H), 8.07 (d, J = 8.4 Hz, 1H), 7.85 (d, J = 8.0 Hz, 1H), 7.81 (s, 1H), 7.78 (d, J = 8.8 Hz, 2H), 7.67 (d, J = 8.0 Hz, 1H), 7.51 (t, J = 7.6 Hz, 1H), 7.39-7.36 (m, 1H), 7.18 (d, J = 8.8 Hz, 2H), 4.90 (s, 2H) ppm; HPLC t_R = 7.42 min. purity 98%; ESI-MS: 411.13 [M+H]⁺.

2-[4-(3-Iodobenzoyl)phenoxy]-N-(pyridin-3-yl)acetamide (7k). White solid, 91 mg, yield = 71%. ¹H NMR (400 MHz, DMSO): δ 8.79 (d, J = 2.4 Hz, 1H), 8.30 (dd, J = 4.8, 1.2 Hz, 1H), 8.07 (dt, J = 8.0, 1.6 Hz, 1H), 8.01 (d, J = 8.0 Hz, 1H), 7.98 (t, J = 1.2 Hz, 1H), 7.77 (d, J = 8.8 Hz, 2H), 7.68 (d, J = 7.6 Hz, 1H), 7.39-7.33 (m, 2H), 7.17 (d, J = 8.8 Hz, 2H), 4.89 (s, 2H) ppm; HPLC t_R = 7.50 min. purity 98%; ESI-MS: 459.07 [M+H]⁺.

2-[4-(4-Methylbenzoyl)phenoxy]-N-(pyridin-3-yl)acetamide (7l). Used EDCI*HCl instead of HATU. White solid, 81 mg, yield = 26%. ¹H NMR (400 MHz, CDCl₃): δ 8.69 (d, J = 1.6 Hz, 1H), 8.45-8.38 (m, 2H), 8.23 (dd, J = 7.2, 1.2 Hz, 1H), 7.85 (d, J = 8.8 Hz, 2H), 7.68 (d, J = 8.0 Hz, 2H), 7.33 (dd, J = 8.4, 4.8 Hz, 1H), 7.28 (d, J = 7.2 Hz, 2H), 7.07 (d, J = 8.8 Hz, 2H), 4.73 (s, 2H), 2.45 (s, 3H) ppm; HPLC t_R = 7.09 min. purity 98%; ESI-MS: 347.13 [M+H]⁺.

2-(4-(4-Fluorobenzoyl)phenoxy)-N-(pyridin-3-yl)acetamide (7m). White solid, 187 mg, yield = 53%. ¹H NMR (400 MHz, CDCl₃): δ 8.72 (d, J = 2.4 Hz, 1H), 8.44-8.40 (m, 2H), 8.30-8.23 (m, 1H), 7.85 (d, J = 8.8 Hz, 2H), 7.83-7.77 (m, 2H), 7.35 (dd, J = 8.4, 4.8 Hz, 1H), 7.17 (t, J = 8.8 Hz, 2H), 7.09 (d, J = 8.8 Hz, 2H), 4.74 (s, 2H) ppm; HPLC t_R = 6.89 min. purity 99%; ESI-MS: 351.13 [M+H]⁺.

2-[4-(4-Chlorobenzoyl)phenoxy]-N-(pyridin-3-yl)acetamide (7n).¹⁸ White solid, 903 mg, yield = 98%. ¹H NMR (400 MHz, DMSO): δ 10.41 (s, 1H), 8.79 (d, J = 2.4 Hz, 1H), 8.30 (dd, J = 4.4, 1.2 Hz, 1H), 8.07 (dt, J = 8.0, 1.6 Hz, 1H), 7.77 (d, J = 8.8 Hz, 2H), 7.72 (dd, J = 8.8, 2.0 Hz, 2H), 7.62 (d, J = 8.4 Hz, 2H), 7.38 (dd, J = 8.4, 4.8 Hz, 1H), 7.17 (d, J = 8.8 Hz, 2H), 4.89 (s, 2H) ppm; HPLC t_R = 7.27 min. purity 100%; ESI-MS: 367.13 [M+H]⁺.

2-[4-(2-Bromo-3-fluorobenzoyl)phenoxy]-N-(5-methoxypyridin-3-yl)acetamide (7o). White solid, 69 mg, yield = 25%. ¹H NMR (400 MHz, CDCl₃): δ 8.68 (d, J = 2.0 Hz, 1H), 8.42 (d, J = 4.4 Hz, 1H), 8.37 (s, 1H), 8.22 (d, J = 8.4 Hz, 1H), 7.85 (d, J = 8.4 Hz, 2H), 7.44-7.39 (m, 1H), 7.33 (dd, J = 8.2, 4.8 Hz, 1H), 7.26 (t, J = 8.0 Hz, 1H), 7.13 (d, J = 7.6 Hz, 1H), 7.07 (d, J = 8.8 Hz, 2H), 4.72 (s, 2H) ppm; HPLC t_R = 7.25 min. purity 98%; ESI-MS: 429.07 [M+H]⁺.

2-[4-(2-Bromo-5-fluorobenzoyl)phenoxy]-N-(5-methoxypyridin-3-yl)acetamide (7p). White solid, 108 mg, yield = 39%. ¹H NMR (400 MHz, CDCl₃):

δ 8.67 (s, 1H), 8.43 (d, J = 4.4 Hz, 1H), 8.28 (s, 1H), 8.21 (d, J = 8.4 Hz, 1H), 7.86 (d, J = 8.8 Hz, 2H), 7.61 (dd, J = 8.4, 4.8 Hz, 1H), 7.33 (dd, J = 8.0, 4.8 Hz, 1H), 7.14-7.03 (m, 4H), 4.73 (s, 2H) ppm; HPLC t_R = 7.22 min. purity 100%; ESI-MS: 429.07 [M+H]⁺.

2-[(9-Oxo-9H-fluoren-3-yl)oxy]-N-(pyridin-3-yl)acetamide (7q). Started from **4q** and 3-aminopyridine. Yellow solid, 170 mg, yield = 51%. ¹H NMR (400 MHz, DMSO): δ 10.52 (s, 1H), 8.89 (d, J = 2.4 Hz, 1H), 8.37 (dd, J = 4.8, 1.2 Hz, 1H), 8.17 (d, J = 8.4 Hz, 1H), 7.81 (d, J = 7.2 Hz, 1H), 7.65-7.55 (m, 3H), 7.53-7.47 (m, 2H), 7.39 (t, J = 7.2 Hz, 1H), 6.95 (dd, J = 8.0, 2.0 Hz, 1H), 4.95 (s, 2H) ppm; HPLC t_R = 6.73 min. purity 99%; ESI-MS: 331.07 [M+H]⁺.

2-[(1-Bromonaphthalen-2-yl)oxy]-N-(pyridin-3-yl)acetamide (7r).²¹ White solid, 235 mg, yield = 74%. ¹H NMR (400 MHz, CDCl₃): δ 9.07 (s br, 1H), 8.77 (d, J = 2.4 Hz, 1H), 8.42 (dd, J = 4.8, 1.2 Hz, 1H), 8.28 (ddd, J = 8.4 Hz, 1.2, 1.2 Hz, 1H), 8.24 (d, J = 8.8 Hz, 1H), 7.89 (d, J = 8.8 Hz, 1H), 7.84 (d, J = 8.0 Hz, 1H), 7.65 (dd, J = 6.8, 0.8 Hz, 1H), 7.49 (dd, J = 7.2, 0.8 Hz, 1H), 7.34 (dd, J = 8.4, 3.6 Hz, 1H), 7.25 (d, J = 8.4 Hz, 1H), 4.83 (s, 2H); ¹³C NMR (101 MHz, CDCl₃): δ 166.2, 151.2, 145.9, 141.4, 134.0, 132.8, 130.6, 129.8, 128.4, 128.3, 127.0, 126.3, 125.5, 123.8, 114.7, 109.9, 69.0 ppm. HPLC t_R = 7.95 min. purity 99%; ESI-MS: 357.00 [M+H]⁺.

2-[4-(2-Bromobenzoyl)phenoxy]-N-(6-methylpyridin-3-yl)acetamide (7f1). Started from **6f** and 5-amino-2-methylpyridine. White solid, 47 mg, yield = 73%. ¹H NMR (400 MHz, CDCl₃): δ 8.54 (d, J = 2.4 Hz, 1H), 8.35 (s, 1H), 8.07 (dd, J = 8.4, 2.4 Hz, 1H), 7.84 (d, J = 8.8 Hz, 2H), 7.65 (d, J = 7.6 Hz, 1H), 7.43 (td, J = 7.2, 0.8 Hz, 1H), 7.37-7.33 (m, 2H), 7.17 (d, J = 8.4 Hz, 1H), 7.05 (d, J = 8.8 Hz, 2H), 4.70 (s, 2H), 2.54 (s, 3H) ppm; HPLC t_R = 7.09 min. purity 99%; ESI-MS: 425.07 [M+H]⁺.

2-[4-(2-Bromobenzoyl)phenoxy]-N-(6-methoxypyridin-3-yl)acetamide (7f2). Started from **6f** and 5-amino-2-methoxypyridine. White solid, 50 mg, yield = 94%. ¹H NMR (400 MHz, CDCl₃): δ 8.31-8.20 (m, 2H), 7.91 (dd, J = 7.8, 2.0 Hz, 1H), 7.83 (d, J = 8.4 Hz, 2H), 7.64 (d, J = 7.6 Hz, 1H), 7.42 (t, J = 7.2 Hz, 1H), 7.37-7.32 (m, 2H), 7.04 (d, J = 8.8 Hz, 2H), 6.75 (d, J = 8.8 Hz, 1H), 4.69 (s, 2H), 3.92 (s, 3H) ppm; HPLC t_R = 9.06 min. purity 98%; ESI-MS: 441.07 [M+H]⁺.

2-[4-(2-Bromobenzoyl)phenoxy]-N-(6-chloropyridin-3-yl)acetamide (7f3). Started from **6f** and 5-amino-2-chloropyridine. Yellow solid, 51 mg, yield = 82%. ¹H NMR (400 MHz, CDCl₃): δ 8.47 (d, J = 2.8 Hz, 1H), 8.30 (s, 1H), 8.21 (dd, J = 8.8, 2.8 Hz, 1H), 7.85 (d, J = 8.0 Hz, 2H), 7.65 (d, J = 8.0 Hz, 1H), 7.43-7.32 (m, 4H), 7.05 (d, J = 8.8 Hz, 2H), 4.71 (s, 2H) ppm; HPLC t_R = 9.65 min. purity 100%; ESI-MS: 445.07 [M+H]⁺.

2-[4-(2-Bromobenzoyl)phenoxy]-*N*-(5-methylpyridin-3-yl)acetamide (7f4). Started from **6f** and 3-amino-5-methylpyridine. White solid, 55 mg, yield = 86%. ¹H NMR (400 MHz, CDCl₃): δ 8.47 (d, *J* = 2.0 Hz, 1H), 8.40 (s, 1H), 8.24 (s, 1H), 8.04 (s, 1H), 7.83 (dd, *J* = 7.8, 2.0 Hz, 2H), 7.65 (dd, *J* = 7.2, 0.8 Hz, 1H), 7.43 (td, *J* = 7.0, 1.2 Hz, 1H), 7.37-7.33 (m, 2H), 7.05 (d, *J* = 8.8 Hz, 2H), 4.71 (s, 2H), 2.36 (s, 3H) ppm. HPLC *t*_R = 7.18 min. purity 99%; ESI-MS: 425.07 [M+H]⁺.

2-[4-(2-Bromobenzoyl)phenoxy]-*N*-(5-methoxypyridin-3-yl)acetamide (7f5). Started from **6f** and 3-amino-5-methoxypyridine. White solid, 274 mg, yield = 100%. ¹H NMR (400 MHz, CDCl₃): δ 8.78 (s, 1H), 8.23 (d, *J* = 1.6 Hz, 1H), 8.09 (d, *J* = 2.4 Hz, 1H), 7.90 (t, *J* = 2.4 Hz, 1H), 7.80 (dt, *J* = 9.2, 2.0 Hz, 2H), 7.63 (dd, *J* = 7.8, 1.2 Hz, 1H), 7.41 (td, *J* = 7.8, 1.2 Hz, 1H), 7.34 (td, *J* = 7.8, 2.0 Hz, 1H), 7.30 (dd, *J* = 7.6, 2.0 Hz, 1H), 7.02 (dt, *J* = 8.8, 2.4 Hz, 2H), 4.70 (s, 2H), 3.85 (s, 3H) ppm. HPLC *t*_R = 7.44 min. purity 99%; ESI-MS: 441.07 [M+H]⁺.

2-[4-(2-Bromobenzoyl)phenoxy]-*N*-(4-methylpyridin-3-yl)acetamide (7f6). Started from **6f** and 3-amino-4-methylpyridine. White solid, 90 mg, yield = 70%. ¹H NMR (400 MHz, CDCl₃): δ 8.92 (s, 1H), 8.34 (d, *J* = 4.4 Hz, 1H), 8.28 (s, 1H), 7.84 (d, *J* = 8.8 Hz, 2H), 7.64 (d, *J* = 7.6 Hz, 1H), 7.43 (td, *J* = 7.2, 0.8 Hz, 1H), 7.35 (td, *J* = 7.8, 2.0 Hz, 1H), 7.33 (dd, *J* = 7.4, 2.0 Hz, 1H), 7.16 (d, *J* = 4.8 Hz, 1H), 7.05 (d, *J* = 8.8 Hz, 2H), 4.76 (s, 2H), 2.25 (s, 3H) ppm. HPLC *t*_R = 7.05 min. purity 100%; ESI-MS: 425.13 [M+H]⁺.

2-[4-(2-Bromobenzoyl)phenoxy]-*N*-(4-methoxypyridin-3-yl)acetamide (7f7). Started from **6f** and 3-amino-4-methoxypyridine. Yellow solid, 35 mg, yield = 72%. ¹H NMR (400 MHz, CDCl₃): δ 9.48 (s, 1H), 8.66 (s, 1H), 8.33 (d, *J* = 5.2 Hz, 1H), 7.85 (d, *J* = 8.8 Hz, 2H), 7.65 (d, *J* = 8.0 Hz, 1H), 7.44-7.32 (m, 3H), 7.05 (d, *J* = 8.8 Hz, 2H), 6.85 (d, *J* = 5.6 Hz, 1H), 4.72 (s, 2H), 3.95 (s, 3H) ppm. HPLC *t*_R = 7.13 min. purity 99%; ESI-MS: 441.13 [M+H]⁺.

2-(4-(2-Bromobenzoyl)phenoxy)-*N*-(quinolin-3-yl)acetamide (7f8). Started from **6f** and 3-aminoquinoline. White solid, 44 mg, yield = 83%. ¹H NMR (400 MHz, CDCl₃): δ 8.85 (d, *J* = 2.4 Hz, 1H), 8.79 (s, 1H), 8.60 (s, 1H), 8.06 (d, *J* = 8.4 Hz, 1H), 7.86-7.81 (m, 3H), 7.68-7.63 (m, 2H), 7.55 (t, *J* = 8.0 Hz, 1H), 7.40 (t, *J* = 7.6 Hz, 1H), 7.37-7.31 (m, 2H), 7.07 (d, *J* = 7.6 Hz, 2H), 4.76 (s, 2H) ppm. HPLC *t*_R = 8.10 min. purity 99%; ESI-MS: 461.07 [M+H]⁺.

2-[4-(2-Bromobenzoyl)phenoxy]-*N*-(6-chloropyridazin-3-yl)acetamide (7f9). Started from **6f** and 3-amino-6-chloro-pyridazine. White solid, 32 mg, yield = 6%. ¹H NMR (400 MHz, CDCl₃): δ 9.49 (s, 1H), 8.57 (d, *J* = 8.8 Hz, 1H), 7.86 (d, *J* = 7.6 Hz, 2H), 7.65 (d, *J* = 8.0 Hz, 1H), 7.57 (d, *J* = 9.2 Hz, 1H), 7.43-7.30 (m, 3H), 7.07 (d, *J* = 7.1 Hz, 2H), 4.77 (s, 2H) ppm. HPLC *t*_R = 9.37 min.

purity 97%; ESI-MS: 445.93 [M+H]⁺.

2-[4-(2-Bromobenzoyl)phenoxy]-N-(pyrimidin-5-yl)acetamide (7f10). Started from **6f** and 5-aminopyrimidine. White solid, 24 mg, yield = 26%. ¹H NMR (400 MHz, CDCl₃): δ 9.08 (s, 2H), 9.03 (s, 1H), 8.45 (s, 1H), 7.81 (d, *J* = 8.8 Hz, 2H), 7.65 (d, *J* = 8.0 Hz, 1H), 7.43 (td, *J* = 7.4, 1.2 Hz, 1H), 7.39-7.31 (m, 2H), 7.05 (d, *J* = 8.8 Hz, 2H), 4.75 (s, 2H) ppm. HPLC *t*_R = 8.27 min. purity 99%; ESI-MS: 412.07 [M+H]⁺.

2-(4-(2-Bromobenzoyl)phenoxy)-N-(pyrazin-2-yl)acetamide (7f11). Started from **6f** and 2-aminopyrazine. White solid, 14 mg, yield = 53%. ¹H NMR (400 MHz, CDCl₃) δ 9.62 (s, 1H), 8.87 (s, 1H), 8.43 (s, 1H), 8.31 (s, 1H), 7.85 (dt, *J* = 8.8, 2.0 Hz, 2H), 7.65 (dd, *J* = 7.6, 0.8 Hz, 1H), 7.43 (td, *J* = 7.6, 1.2 Hz, 1H), 7.39-7.32 (m, 2H), 7.06 (dt, *J* = 9.2, 2.8 Hz, 2H), 4.75 (s, 2H) ppm. HPLC *t*_R = 8.68 min. purity 98%; ESI-MS: 412.00 [M+H]⁺.

Biology

Materials and methods

Dofetilide was synthesized in our own laboratory,⁵⁴ and astemizole was purchased from Sigma Aldrich (Zwijndrecht, The Netherlands). Tritium-labeled dofetilide (specific activity 82.3 Ci·mmol⁻¹) was purchased from PerkinElmer (Groningen, The Netherlands). Bovine serum albumin (BSA, fraction V) was purchased from Sigma (St. Louis, MO, USA). G418 was obtained from Stratagene (Cedar Creek, USA). All the other chemicals were of analytical grade and obtained from standard commercial sources. HEK293 cells stably expressing the K_v11.1 channel (HEK293K_v11.1) were kindly provided by Dr. Eckhard Ficker (University of Cleveland, USA).

Cell culture and membrane preparation

HEK293K_v11.1 cells were cultured, and membranes were prepared and stored as described previously.¹⁶

Radioligand kinetic dissociation assays

Kinetic dissociation assays of [³H]dofetilide were performed in incubation buffer (10 mM HEPES, 130 mM NaCl, 60 mM KCl, 0.8 mM MgCl₂, 1 mM EGTA, 10 mM glucose, 0.1% BSA, pH 7.4) as described previously with the following modifications.¹⁶ Single point dissociation experiments were conducted by addition of 10 μM dofetilide in the absence (control) or presence of 10 μM synthesized

compounds after preincubation at 25 °C for 2 h. After 6 minutes of dissociation, incubations were terminated by dilution with ice-cold wash buffer (25 mM Tris-HCl, 130 mM NaCl, 60 mM KCl, 0.8 mM MgCl₂, 0.05 mM CaCl₂, 0.05 % BSA, pH 7.4). Separation of bound from free radioligand was performed by rapid filtration through a 96-well GF/B filter plate using a PerkinElmer Filtermate-harvester (PerkinElmer, Groningen, The Netherlands). The filter-bound radioactivity was determined by scintillation spectrometry using the P-E 1450 Microbeta Wallac Trilux scintillation counter (PerkinElmer) after addition of 25 µL Microscint and extraction. Full dissociation assays were carried out with 10 µM dofetilide in the absence (control) or presence of 50 µM selected compounds for a total period of 2 h after preincubation. The amounts of radioligand still bound to the receptor were measured at various time intervals. Concentration-dependent effects of compounds **7f** and **7p** were determined by addition of 10 µM dofetilide in the absence (control) or presence of different concentrations of **7f** and **7p**. After 6 min of dissociation, the incubations were terminated and samples were obtained as described above.

Radioligand displacement assay

[³H]Dofetilide binding assays for the K_v11.1 channel were performed in incubation buffer as described previously.¹⁶ Briefly, membrane aliquots containing 20 µg protein were incubated with 5 nM [³H]dofetilide in a total volume of 100 µl incubation buffer at 25 °C for 1 h. Radioligand displacement experiments were carried out with various concentrations of tested compounds. Total binding was determined in the presence of incubation buffer, whereas nonspecific binding was evaluated with 10 µM astemizole. Incubations were terminated by dilution with ice-cold wash buffer, and samples were obtained as described in the “*radioligand kinetic dissociation assays*”. The displacement assays of dofetilide and astemizole were conducted in the absence (control) or presence of 10 µM **7f**, **7h-j** and **7p**.

Data analysis

All data of radioligand binding assays were analyzed with Prism v. 5.0 (Graph-Pad, San Diego, CA, USA). Dissociation rate constants, k_{off} , were obtained by computer analysis of the exponential decay of [³H]dofetilide bound to the K_v11.1 channel. EC₅₀ values from kinetic dissociation assays were calculated by non-linear regression analysis of concentration-effect curves of dissociation in the presence of different concentrations of unlabeled ligands. IC₅₀ values in displacement assays were directly obtained from non-linear regression analysis of dose-re-

sponse curves. Apparent inhibitory binding constants (K_i values) were derived from the IC_{50} values according to the Cheng-Prusoff relationship:⁵⁵ $K_i = IC_{50}/(1 + [L^*]/K_D)$, where $[L^*]$ is the concentration of radioligand and K_D its dissociation constant from the saturation assay.³⁰ All values obtained from radioligand binding assays in this study are means of at least three independent experiments performed in duplicate, and data are presented as mean \pm SEM. Statistical analysis was performed with a two-tailed unpaired Student's t-test.

References

1. May, L. T.; Leach, K.; Sexton, P. M.; Christopoulos, A. Allosteric modulation of G protein-coupled receptors. *Ann. Rev. Pharm. Toxicol.* **2007**, *47*, 1-51.
2. Hogg, R. C.; Buisson, B.; Bertrand, D. Allosteric modulation of ligand-gated ion channels. *Biochem. Pharmacol.* **2005**, *70*, 1267-1276.
3. Lewis, J. A.; Lebois, E. P.; Lindsley, C. W. Allosteric modulation of kinases and GPCRs: Design principles and structural diversity. *Curr. Opin. Chem. Biol.* **2008**, *12*, 269-280.
4. Christopoulos, A.; Changeux, J.-P.; Catterall, W. A.; Fabbro, D.; Burris, T. P.; Cidlowski, J. A.; Olsen, R. W.; Peters, J. A.; Neubig, R. R.; Pin, J.; Sexton, P. M.; Kenakin, T. P.; Ehlert, F. J.; Spedding, M.; Langmead, C. J. International union of basic and clinical pharmacology. XC. multisite pharmacology: Recommendations for the nomenclature of receptor allosterism and allosteric ligands. *Pharmacol. Rev.* **2014**, *66*, 918-947.
5. Davey, A. E.; Leach, K.; Valant, C.; Conigrave, A. D.; Sexton, P. M.; Christopoulos, A. Positive and negative allosteric modulators promote biased signaling at the calcium-sensing receptor. *Endocrinol.* **2011**, *153*, 1232-1241.
6. Sanguinetti, M. C.; Tristani-Firouzi, M. hERG potassium channels and cardiac arrhythmia. *Nature* **2006**, *440*, 463-469.
7. Vandenberg, J. I.; Perry, M. D.; Perrin, M. J.; Mann, S. A.; Ke, Y.; Hill, A. P. hERG K^+ channels: Structure, function, and clinical significance. *Physiol. Rev.* **2012**, *92*, 1393-1478.
8. Xu, X.; Recanatini, M.; Roberti, M.; Tseng, G.-N. Probing the binding sites and mechanisms of action of two human ether-à-go-go-related gene channel activators, 1,3-bis-(2-hydroxy-5-trifluoromethyl-phenyl)-urea (NS1643) and 2-[2-(3,4-dichloro-phenyl)-2,3-dihydro-1H-isoindol-5-ylamino]-nicotinic acid (PD307243). *Mol. Pharmacol.* **2008**, *73*, 1709-1721.
9. Perry, M.; Sanguinetti, M.; Mitcheson, J. Revealing the structural basis of action of hERG potassium channel activators and blockers. *J. Physiol. (Lond.)* **2010**, *588*, 3157-3167.
10. Ravens, U. Novel pharmacological approaches for antiarrhythmic therapy. *Naunyn*

Schmiedebergs Arch. Pharmacol. **2010**, 381, 187-193.

11. Grunnet, M.; Hansen, R. S.; Olesen, S.-P. hERG1 channel activators: A new anti-arrhythmic principle. *Prog. Biophys. Mol. Biol.* **2008**, 98, 347-362.
12. Kang, J.; Chen, X.; Wang, H.; Ji, J.; Cheng, H.; Incardona, J.; Reynolds, W.; Viviani, F.; Tabart, M.; Rampe, D. Discovery of a small molecule activator of the human ether-à-go-go-related gene (hERG) cardiac K⁺ channel. *Mol. Pharmacol.* **2005**, 67, 827-836.
13. Perry, M.; Sachse, F. B.; Sanguinetti, M. C. Structural basis of action for a human ether-à-go-go-related gene 1 potassium channel activator. *Proc. Natl. Acad. Sci. U.S.A.* **2007**, 104, 13827-13832.
14. Durdagi, S.; Guo, J.; Lees-Miller, J. P.; Noskov, S. Y.; Duff, H. J. Structure-guided topographic mapping and mutagenesis to elucidate binding sites for the human ether-à-go-go-related gene 1 potassium channel (KCNH2) activator NS1643. *J. Pharmacol. Exp. Ther.* **2012**, 342, 441-452.
15. Hansen, R. S.; Olesen, S.-P.; Rønn, L. C. B.; Grunnet, M. *In vivo* effects of the I_{Kr} agonist NS3623 on cardiac electrophysiology of the guinea pig. *J. Cardiovasc. Pharmacol.* **2008**, 52, 35-41.
16. Yu, Z.; Klaasse, E.; Heitman, L. H.; IJzerman, A. P. Allosteric modulators of the hERG K⁺ channel: Radioligand binding assays reveal allosteric characteristics of dofetilide analogs. *Toxicol. Appl. Pharmacol.* **2014**, 274, 78-86.
17. Seeböhm, G. Activators of cation channels: Potential in treatment of channelopathies. *Mol. Pharmacol.* **2005**, 67, 585-588.
18. Zhang, H.; Zou, B.; Yu, H.; Moretti, A.; Wang, X.; Yan, W.; Babcock, J. J.; Bellin, M.; McManus, O. B.; Tomaselli, G.; Nan, F.; Laugwitz, K. L.; Li, M. Modulation of hERG potassium channel gating normalizes action potential duration prolonged by dysfunctional KCNQ1 potassium channel. *Proc. Natl. Acad. Sci. U.S.A.* **2012**, 109, 11866-11871.
19. Diness, T. G.; Yeh, Y.-H.; Qi, X. Y.; Chartier, D.; Tsuji, Y.; Hansen, R. S.; Olesen, S.-P.; Grunnet, M.; Nattel, S. Antiarrhythmic properties of a rapid delayed-rectifier current activator in rabbit models of acquired long QT syndrome. *Cardiovasc. Res.* **2008**, 79, 61-69.
20. Xu, X.; Salata, J. J.; Wang, J.; Wu, Y.; Yan, G.; Liu, T.; Marinchak, R. A.; Kowey, P. R. Increasing I_{Ks} corrects abnormal repolarization in rabbit models of acquired LQT2 and ventricular hypertrophy. *Am. J. Physiol. Heart Circ. Physiol.* **2002**, 283, H664-H670.
21. Potet, F.; Lorinc, A. N.; Chaigne, S.; Hopkins, C. R.; Venkataraman, R.; Stepanovic, S. Z.; Lewis, L. M.; Days, E.; Sidorov, V. Y.; Engers, D. W.; Zou, B.; Afshartous, D.; George, A. L.; Campbell, C. M.; Balser, J. R.; Li, M.; Baudenbacher, F. J.; Lindsley, C. W.; Weaver, C. D.; Kupersmidt, S. Identification and characterization of a compound that protects cardiac tissue from human Ether-à-go-go-related gene (hERG)-related drug-induced arrhythmias. *J. Biol. Chem.* **2012**, 287, 39613-39625.

22. Ruenitz, P. C.; Bourne, C. S.; Sullivan, K. J.; Moore, S. A. Estrogenic triarylethylene acetic acids: Effect of structural variation on estrogen receptor affinity and estrogenic potency and efficacy in MCF-7 cells. *J. Med. Chem.* **1996**, *39*, 4853-4859.
23. Breyer, S.; Semmler, A.; Miller, T.; Hill, A.; Geissler, S.; Haberkorn, U.; Mier, W. Radioiodinated dechloro-4-iodofenofibrate: A hydrophobic model drug for molecular imaging studies. *Int. J. Pharm* **2012**, *431*, 78-83.
24. Li, H.; Zhu, R.; Shi, W.; He, K.; Shi, Z. Synthesis of fluorenone derivatives through Pd-catalyzed dehydrogenative cyclization. *Org. Lett.* **2012**, *14*, 4850-4853.
25. Li, B.; Magee, T. V.; Buzon, R. A.; Widlicka, D. W.; Bill, D. R.; Brandt, T.; Cao, X.; Coutant, M.; Dou, H.; Granskog, K. Process development of a novel azetidiny ketolide antibiotic. *Org. Process Res. Dev.* **2012**, *16*, 788-797.
26. Kostenis, E.; Mohr, K. Two-point kinetic experiments to quantify allosteric effects on radioligand dissociation. *Trends Pharmacol. Sci.* **1996**, *17*, 280-283.
27. Kalinichev, M.; Donovan-Rodriguez, T.; Girard, F.; Riguet, E.; Rouillier, M.; Bour-nique, B.; Haddouk, H.; Mutel, V.; Poli, S. Evaluation of peripheral versus central effects of GABA_B receptor activation using a novel, positive allosteric modulator of the GABA_B receptor ADX71943, a pharmacological tool compound with a fully peripheral activity profile. *Br. J. Pharmacol.* **2014**, *171*, 4941-4954.
28. Gao, Z.; Van Muijlwijk-Koezen, J. E.; Chen, A.; Müller, C. E.; IJzerman, A. P.; Jacobson, K. A. Allosteric modulation of A₃ adenosine receptors by a series of 3-(2-pyr-idinyl) isoquinoline derivatives. *Mol. Pharmacol.* **2001**, *60*, 1057-1063.
29. van den Nieuwendijk, A. M.; Pietra, D.; Heitman, L.; Göblyös, A.; IJzerman, A. P. Synthesis and biological evaluation of 2, 3, 5-substituted [1, 2, 4] thiadiazoles as al-losteric modulators of adenosine receptors. *J. Med. Chem.* **2004**, *47*, 663-672.
30. Yu, Z.; IJzerman, A.; Heitman, L. K_v11.1 (hERG)-induced cardiotoxicity: A molec-ular insight from a binding kinetics study of prototypic K_v11.1 (hERG) inhibitors. *Br. J. Pharmacol.* **2015**, *172*, 940-945.
31. Szabo, G.; Farkas, V.; Grunnet, M.; Mohacsi, A.; P Nanasi, P. Enhanced repolariza-tion capacity: New potential antiarrhythmic strategy based on HERG channel activation. *Curr. Med. Chem.* **2011**, *18*, 3607-3621.
32. Moorthy, J. N.; Samanta, S. Photoinduced C-Br homolysis of 2-bromobenzophe-ones and pschorr ring closure of 2-aryolaryl radicals to fluorenones. *J. Org. Chem.* **2007**, *72*, 9786-9789.
33. Shimizu, Y.; Izumi, S.; Takenaka, J.; Momoda, J. Chromene compound and curable composition. In Google Patents: 2012.
34. Babu, S. A.; Yasuda, M.; Baba, A. In (III)-mediated chemoselective dehydroge-native interaction of ClMe₂SiH with carboxylic acids: Direct chemo-and regioselective Friedel-Crafts acylation of aromatic ethers. *Org. Lett.* **2007**, *9*, 405-408.
35. Liao, Y.; Hu, Q. Aryl ketone synthesis via tandem orthoplatinated triarylphos-

- phite-catalyzed addition reactions of arylboronic acids with aldehydes followed by oxidation. *J. Org. Chem.* **2010**, *75*, 6986-6989.
36. Sui, Y.; Zhang, X.; Wu, J.; Li, S.; Zhou, J.; Li, M.; Fang, W.; Chan, A. S.; Wu, J. Cu^{II}-catalyzed asymmetric hydrosilylation of diaryl- and aryl heteroaryl ketones: Application in the enantioselective synthesis of orphenadrine and neobenodine. *Chem. Eur. J.* **2012**, *18*, 7486-7492.
 37. Aziz, J.; Frison, G.; Le Menez, P.; Brion, J.-D.; Hamze, A.; Alami, M. Gold versus palladium: A regioselective cycloisomerization of aromatic enynes. *Adv. Synth. Catal.* **2013**, *355*, 3425-3436.
 38. Wang, X.; Liu, F.; Tu, H.; Zhang, A. One-pot synthesis of diarylmethanones through palladium-catalyzed sequential coupling and aerobic oxidation of aryl bromides with acetophenone as a latent carbonyl donor. *J. Org. Chem.* **2014**, *79*, 6554-6562.
 39. Sarvari, M. H.; Sharghi, H. Solvent-free catalytic friedel-crafts acylation of aromatic compounds with carboxylic acids by using a novel heterogeneous catalyst System: *p*-Toluenesulfonic acid/Graphite. *Helv. Chim. Acta* **2005**, *88*, 2282-2287.
 40. Gan, Y.; Blank, D. H.; Ney, J. E.; Spencer, T. A. Nonsteroidal benzophenone-containing analogues of cholesterol. *J. Org. Chem.* **2006**, *71*, 5864-5869.
 41. Cowart, M.; Faghih, R.; Curtis, M. P.; Gfesser, G. A.; Bennani, Y. L.; Black, L. A.; Pan, L.; Marsh, K. C.; Sullivan, J. P.; Esbenshade, T. A.; Fox, G. B.; Hancock, A. A. 4-(2-[2-(2 (*R*)-methylpyrrolidin-1-yl)ethyl] benzofuran-5-yl) benzonitrile and related 2-aminoethylbenzofuran H₃ receptor antagonists potently enhance cognition and attention. *J. Med. Chem.* **2005**, *48*, 38-55.
 42. Böger, M.; Dürr, D.; Gsell, L.; Hall, R. G.; Karrer, F.; Kristiansen, O.; Maienfisch, P.; Pascual, A.; Rindlisbacher, A. Synthesis and structure-activity relationships of benzophenone hydrazone derivatives with insecticidal activity. *Pest Manag. Sci.* **2001**, *57*, 191-202.
 43. Williams, D. L.; Ronzion, A. R. A contribution to the total synthesis of alizarin¹. Synthesis of 1, 2-dihydroxy-9, 10-anthraquinone-9-C¹⁴. *J. Org. Chem.* **1953**, *18*, 489-495.
 44. Sasse, A.; Ligneau, X.; Sadek, B.; Elz, S.; Pertz, H. H.; Ganellin, C. R.; Arrang, J.-M.; Schwartz, J.-C.; Schunack, W.; Stark, H. Benzophenone derivatives and related compounds as potent histamine H₃-receptor antagonists and potential PET/SPECT ligands. *Arch. Pharm.* **2001**, *334*, 45-52.
 45. Bao, X.; Jin, Y.; Liu, X.; Liao, H.; Zhang, L.; Pang, T. Synthesis and biological evaluation of XB-1 analogues as novel histamine H₃ receptor antagonists and neuroprotective agents. *RSC Adv.* **2014**, *4*, 6761-6775.
 46. Sudha, B.; Shashikanth, S.; Ara Khanum, S. Synthesis of 5-(4'-aroyl)-aryloxy methyl-4*H*-(1, 2, 4)-triazolin-3-thiol and their biological activity. *Heterocycl. Comm.* **2004**, *10*, 85-88.
 47. Nakatani, K.; Dohno, C.; Saito, I. Synthesis of DNA oligomers containing modified

- uracil possessing electron-accepting benzophenone chromophore. *J. Org. Chem.* **1999**, *64*, 6901-6904.
48. Atkinson, G. E.; Fischer, P. M.; Chan, W. C. A versatile polymer-supported 4-(4-methylphenyl (chloro) methyl) phenoxy linker for solid-phase synthesis of pseudo-peptides. *J. Org. Chem.* **2000**, *65*, 5048-5056.
49. Sundstrom, G. Metabolic hydroxylation of the aromatic rings of 1, 1-dichloro-2, 2-bis (4-chlorophenyl) ethylene (p, p'-DDE) by the rat. *J. Agric. Food Chem.* **1977**, *25*, 18-21.
50. Soper, Q. F.; Whitehead, C. W.; Behrens, O. K.; Corse, J. J.; Jones, R. G. Biosynthesis of penicillins. VII.¹ Oxy-and mercaptoacetic acids. *J. Am. Chem. Soc.* **1948**, *70*, 2849-2855.
51. Giampietro, L.; Angelo, A.; Giancristofaro, A.; Ammazalorso, A.; De Filippis, B.; DiMatteo, M.; Fantacuzzi, M.; Linciano, P.; Maccallini, C.; Amoroso, R. Effect of stilbene and chalcone scaffolds incorporation in clofibric acid on PPAR α agonistic activity. *Med. Chem.* **2014**, *10*, 59-65.
52. Alewood, D.; Hopping, G.; Brust, A.; Reid, R. C.; Alewood, P. F. Benzhydrylamine linker grafting: A strategy for the improved synthesis of C-terminal peptide amides. *J. Pept. Sci.* **2010**, *16*, 551-557.
53. Massolini, G.; Carmellino, M.; Baruffini, A. Some derivatives of 4-(p. chlorobenzoyl) phenol were prepared and tested for phytoiatric antimycotic activity. *Farm. Ed. Sci.* **1986**, *41*, 381-387.
54. Shagufta; Guo, D.; Klaasse, E.; de Vries, H.; Brussee, J.; Nalos, L.; Rook, M. B.; Vos, M. A.; van der Heyden, M. A.; IJzerman, A. P. Exploring Chemical Substructures Essential for hERG K⁺ Channel Blockade by Synthesis and Biological Evaluation of Dofetilide Analogues. *ChemMedChem* **2009**, *4*, 1722-1732.
55. Cheng, Y.; Prusoff, W. H. Relationship between the inhibition constant (K_i) and the concentration of inhibitor which causes 50 percent inhibition (I_{50}) of an enzymatic reaction. *Biochem. Pharmacol.* **1973**, *22*, 3099-3108.

Chapter 6

K_v11.1 (hERG)-induced cardiotoxicity: a molecular insight from a binding kinetics study of prototypic K_v11.1 inhibitors

Zhiyi Yu
Adriaan P. IJzerman
Laura H. Heitman

Adapted from Br. J. Pharmacol. **2015**, 172, 940-945.

Abstract

Drug-induced arrhythmia due to blockade of the $K_v11.1$ channel (also known as the hERG K^+ channel) is a frequent side effect and arouses major safety concerns during the drug development process. Previous studies have primarily focused on equilibrium parameters, i.e. affinity or potency, of drug candidates at the channel. The aim of this study was to determine the kinetics of the interaction with the channel for a number of known $K_v11.1$ blockers and to explore a possible correlation with the affinity or physicochemical properties of these compounds. In this context, the affinity and kinetic parameters of fifteen prototypic $K_v11.1$ inhibitors were evaluated in a number of [3H]dofetilide binding assays. The lipophilicity ($\log K_{w-C8}$) and membrane partitioning ($\log K_{w-IAM}$) of these compounds were determined by means of HPLC analysis. Accordingly, a novel [3H]dofetilide competition association assay was set up and validated, which allowed us to determine the binding kinetics of the $K_v11.1$ blockers used in this study. Interestingly, the compounds' affinity (K_i values) were correlated to their association rates rather than dissociation rates. Overall lipophilicity or membrane partitioning of the compounds were not correlated to their affinity and rate constants for the channel. In conclusion, a compound's affinity for the $K_v11.1$ channel is determined by the rate of association with the channel, while overall lipophilicity and membrane affinity are not. In more general terms, our findings provide novel insights into the mechanism of action for a compound's activity at the $K_v11.1$ channel. This may yield further understanding in how $K_v11.1$ -induced cardiotoxicity is governed and how it can be circumvented in the future.

Introduction

The $K_v11.1$ channel, a voltage-gated potassium channel previously known as hERG (human ether-à-go-go related gene), encodes the pore-forming subunit of the rapid component of the delayed rectifier K^+ channel, I_{Kr} , which contributes to phase 3 repolarization in cardiac action potentials¹⁻⁴. Genetic defects or drug blockade of the $K_v11.1$ channel normally cause delayed repolarization of cardiac action potentials and Torsades de Pointes (TdP)⁵. In some cases, TdP can degenerate into ventricular fibrillation and lead to sudden death^{6,7}. Currently, a number of drugs have been withdrawn from the market due to their blockade of the $K_v11.1$ channel, including astemizole and cisapride⁸. In addition, either ‘black box’ warnings or significant restrictions have been rendered for several other drugs, such as droperidol and ibutilide⁸. Withdrawing or restricting drugs due to their $K_v11.1$ liability in less than 1% of the patient population causes unpredictable and huge costs to industry, and brings troubles for patients as well owing that some effective drugs would be beneficial for the vast majority of patients^{8,9}.

In the past decades, a series of techniques including whole cell patch-clamp technologies, radioligand binding assays and ion flux assays have been developed and used to screen for $K_v11.1$ liability of compounds^{5,10}. From these, equilibrium radioligand displacement assays have been suggested as a low-cost and high throughput technology alternative to other available methods and are widely employed to obtain the affinity of compounds at the $K_v11.1$ channel¹¹⁻¹³. These studies provide equilibrium parameters, such as IC_{50} or K_i values. For instance, a 30-fold margin between $K_v11.1$ IC_{50} and maximum free plasma concentration (C_{max}) has been recommended to assess drug safety with respect to arrhythmogenesis¹⁴. However, the kinetics of the interaction between a drug and the $K_v11.1$ channel may be equally, or even more, important. Knowledge of association and dissociation rate constants has already led to better insights in the action of drugs at other targets, such as enzymes and G protein-coupled receptors^{15,16}.

In the present study, we hypothesized that a slow association rate (k_{on}) to and/or a fast dissociation rate constant (k_{off}) from the channel may be beneficial to reduce or avoid $K_v11.1$ -related cardiovascular side effects. Hence, a detailed understanding of a ligand’s binding kinetics at the channel may provide clues to enable the optimization of its kinetic profiles, and potentially ‘rescue’ it from removal of the drug discovery pipeline. In this context, we describe the development and validation of a [3H]dofetilide competition association assay in HEK293 $K_v11.1$ cell membranes to determine the kinetic binding parameters of 15 unlabelled reference compounds from different “Redfern” categories¹⁴ (**Table 1**). We systematically investigated both equilibrium affinity and kinetic binding

data of those compounds, and compared these parameters with the compounds' physicochemical properties. Since the interaction of drugs with membrane phospholipids is not only driven by lipophilicity, but also electrostatic interactions with both acidic and basic moieties on phosphate head groups^{17, 18}, a regular column and an immobilized artificial membrane (IAM) column, were used to derive two hydrophobic parameters for these compounds, i.e. $\log K_{W-C8}$ and $\log K_{W-IAM}$, respectively. Finally, both hydrophobic parameters were compared with the compounds' affinity and kinetic data. Taken together, the present study provides a novel approach to study the kinetics of the interaction between a drug and the $K_v11.1$ channel, which may help to more precisely assess $K_v11.1$ liability of drug candidates in the future.

Methods

Materials

Astemizole, sertindole, terfenadine, moxifloxacin, amiodarone, chlorpromazine, ibutilide, clofilium, pimozone, cisapride, ranolazine, sotalol, thioridazine and all the solutes for HPLC determinations were purchased from Sigma Aldrich (Zwijndrecht, The Netherlands). Dofetilide and E-4031 were synthesized in our own laboratory^{19, 20}. Tritium-labeled dofetilide (specific activity 65~87 Ci·mmol⁻¹) was purchased from Perkin Elmer (Groningen, The Netherlands). Bovine serum albumin (BSA, fraction V) was purchased from Sigma (St. Louis, MO, USA). G418 was obtained from Stratagene (Cedar Creek, USA). The chemicals for HPLC were of HPLC grade; all the other chemicals were of analytical grade and achieved from standard commercial sources. HEK293 cells stably expressing the $K_v11.1$ channel (HEK293 $K_v11.1$) were kindly provided by Dr Eckhard Ficker (University of Cleveland, USA). The molecular target nomenclature ($K_v11.1$) conforms to 'The Concise Guide to PHARMACOLOGY 2013/14: Ion Channels'²¹.

Cell culture and membrane preparation

HEK293 $K_v11.1$ cells were cultured and membranes were prepared and stored as described previously²².

Table 1. Chemical structures and information on the use of 15 $K_v11.1$ blockers examined in this study.

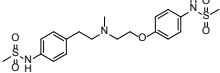
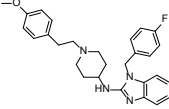
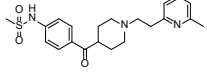
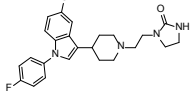
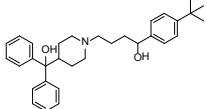
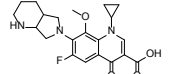
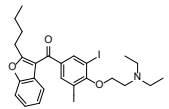
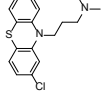
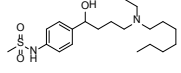
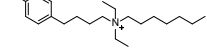
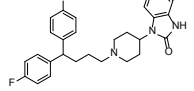
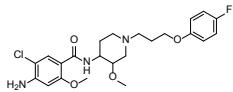
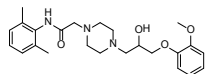
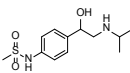
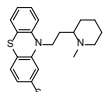
Name	Chemical structure	Therapeutic class	TdP ^a	Redfern category ^b	Status in the US ^a
Dofetilide		antiarrhythmic	++	1	restricted
Astemizole		antihistamine	++	2	withdrawn
E-4031		antiarrhythmic	++	1*	not approved
Sertindole		antipsychotic	+	2	not approved
Terfenadine		antihistamine	++	2	withdrawn
Moxifloxacin		antibacterial	++	3*	restricted
Amiodarone		antiarrhythmic	++	1	restricted
Chlorpromazine		antipsychotic	++	3*	restricted
Ibutilide		antiarrhythmic	++	1	restricted
Clofilium		antiarrhythmic	++	1*	not approved
Pimozide		antipsychotic	++	3	restricted

Table 1 continued

Name	Chemical structure	Therapeutic class	TdP ^a	Redfern category ^b	Status in the US ^a
Cisapride		gastroprokinetic	++	2	withdrawn
Ranolazine		antianginal	+	5*	restricted
Sotalol		antiarrhythmic	++	1	restricted
Thioridazine		antipsychotic	++	3	restricted

^a+ drugs with possible TdP risk, and ++ drugs with known TdP risk. Information on these compounds was retrieved from CredibleMeds[®] available at: <http://crediblemeds.org/> (accessed 10 April 2014).

^bRedfern categories for most compounds were derived from the literature (Redfern *et al.*, 2003); they are 1: Class Ia and III antiarrhythmics; 2: Withdrawn from market due to TdP; 3: Measurable incidence / numerous reports of TdP in humans; 4: Isolated reports of TdP in humans; 5: No reports of TdP in humans. * Redfern categories for these compounds were deduced according to the definition for different categories.

Radioligand saturation assay

Membrane aliquots containing 20 µg of protein were incubated in a total volume of 100 µL of incubation buffer (10 mM HEPES, 130 mM NaCl, 60 mM KCl, 0.8 mM MgCl₂, 1 mM EGTA, 10 mM Glucose, 0.1% BSA, pH 7.4) at 25 °C for 120 min to ensure that the equilibrium was reached at all concentrations of radioligand. Total binding was determined at a range of concentrations (0.2 ~ 22 nM) of [³H]dofetilide, whereas nonspecific binding was determined at three different concentrations of radioligand in the presence of 10 µM astemizole and analyzed by linear regression. Incubations were terminated by dilution with ice-cold wash buffer (25 mM Tris-HCl, 130 mM NaCl, 60 mM KCl, 0.8 mM MgCl₂, 0.05 mM CaCl₂, 0.05% BSA, pH 7.4). Separation of bound from free radioligand was performed by rapid filtration through Whatman GF/B filters using a Brandel harvester. Filters were subsequently washed 6 times with 2 mL ice-cold wash buffer. Filter-bound radioactivity was determined by scintillation spectrometry using a liquid Scintillation Analyzer (Tri-Carb 2900TR) after addition of 3.5 mL

of Packard Emulsifier Safe and 2 h extraction.

Radioligand association and dissociation assay

Kinetic association experiments were performed by incubating membrane aliquots containing 20 μg of protein in a total volume of 100 μL incubation buffer at 25 °C for 120 min with 16 different concentrations (0.7–16 nM) of [^3H]dofetilide. The amount of radioligand bound to the receptor was measured at various time intervals during the incubation. Incubations were terminated, and samples were obtained and analyzed as described in “*radioligand saturation assay*”. Further traditional association and dissociation assays were performed as described previously²².

Radioligand displacement assay

The [^3H]dofetilide binding assay for the $\text{K}_{\text{v}}11.1$ channel was performed as described previously²². In short, membrane aliquots containing 20 μg protein were incubated in a total volume of 100 μL incubation buffer at 25 °C for 60 min. Radioligand displacement experiments were conducted using 11 concentrations of the competing ligand in the presence of 5 nM [^3H]dofetilide. At this concentration, total radioligand binding did not exceed 10% of the radioligand added to prevent ligand depletion. Nonspecific binding was determined in the presence of 10 μM astemizole and represented approximately 15% of the total binding. [^3H]Dofetilide did not bind to membranes prepared from empty HEK293 cells lacking the $\text{K}_{\text{v}}11.1$ channel (data not shown). Total binding was determined in the presence of incubation buffer and was set at 100% in all experiments, whereas nonspecific binding was set at 0%. Incubations were terminated by dilution with ice-cold wash buffer. Separation of bound from free radioligand was performed by rapid filtration through a 96-well GF/B filter plate using a Perkin Elmer Filtermate-harvester (Perkin Elmer, Groningen, The Netherlands). Filters were subsequently washed 12 times with ice-cold wash buffer. The filter-bound radioactivity was determined by scintillation spectrometry using the P-E 1450 Microbeta Wallac Trilux scintillation counter (Perkin Elmer) after addition of 25 μL Microscint and 2 h extraction.

Radioligand competition association assay

The binding kinetics of unlabelled reference compounds were determined at 25 °C using the competition association assay according to a previously published method²³. In a standard assay, three different concentrations (0.3, 1- and 3-fold

of their K_i values) of unlabelled dofetilide, astemizole and E-4031 were tested. We assessed the binding kinetics of all other unlabelled reference compounds in a simplified one-concentration competition association assay based on Guo *et al.*²⁴. The experiments were initiated by incubating membrane aliquots containing 20 μg of protein in a total volume of 100 μL of incubation buffer in the absence (control) or presence of a certain concentration of unlabelled ligands at 25 °C for 120 min with 5 nM [^3H]dofetilide. The amounts of radioligand bound to the receptor were measured at various time intervals during the incubation. Incubations were terminated, and samples were obtained and analyzed as described in “*radioligand displacement assay*”.

Determination of $\log K_{\text{W-C8}}$ and $\log K_{\text{W-IAM}}$ parameters by HPLC

$\log K_{\text{W-C8}}$ values were measured on a Supelcosil LC-ABZ, 5 cm \times 4.6 mm, 5 μm column according to a methodology described previously^{25, 26}. In short, retention times of the compounds were determined at three different methanol percentages. These retention times were converted to k values by using the formula $k = (t_{\text{R}} - t_0)/t_{\text{R}}$ in which t_{R} is the retention time and t_0 the retention time of a “nondelayed” compound (pure methanol). The calculated $\log k$ values were plotted against the methanol concentrations and extrapolated to a 0% methanol situation yielding the $\log K_{\text{W-C8}}$ values for 15 reference compounds (intercept of y axis).

An isocratic method was applied to measure the $\log K_{\text{W-IAM}}$ values of all tested compounds on a 10 cm \times 4.6 mm, 10 μm Regis IAM PC DD2 column²⁷. Retention times of the compounds were determined at three different concentrations of acetonitrile. The k_{IAM} values were calculated by the equation $k_{\text{IAM}} = (t_{\text{R}} - t_0)/t_{\text{R}}$ in which t_{R} represents retention times of tested compounds, whereas t_0 is determined by injecting a sodium nitrate solution in the HPLC system. The $\log k_{\text{IAM}}$ values for a compound were plotted against the applied acetonitrile concentrations. The intercept with the Y -axis of the straight line through these data points yielded the extrapolated $\log K_{\text{W-IAM}}$ values for the 15 reference compounds.

Data analysis

All data of radioligand binding assays were analyzed using the non-linear regression curve fitting program Prism v. 5.1 (GraphPad, San Diego, CA, USA). K_{D} and B_{max} values of [^3H]dofetilide at HEK293K_v11.1 membranes were obtained by computational analysis of saturation curves. Apparent inhibitory binding constants (K_i values) were derived from the IC_{50} values according to the Cheng and Prusoff equation $K_i = \text{IC}_{50}/(1 + [\text{L}^*]/K_{\text{D}})$, where $[\text{L}^*]$ was the concentration of radioligand and K_{D} was its dissociation constant from the saturation assay²⁸. In

the kinetic association experiments, the on- and off-rates were derived from the linear regression analysis using the equation $k_{\text{obs}} = k_{\text{on}}[L^*] + k_{\text{off}}$, where the k_{obs} value was obtained by computer analysis of the exponential association of [^3H] dofetilide bound to the receptor with $[L^*]$ being the concentration of radioligand. The association and dissociation rates were used to calculate the kinetic K_D value using the following equation $K_D = k_{\text{off}}/k_{\text{on}}$. The association and dissociation rates for unlabelled compounds were calculated by fitting the data into the competition association model using “kinetics of competitive binding”²³:

$$K_A = k_1[L] + k_2$$

$$K_B = k_3[I] + k_4$$

$$S = \sqrt{(K_A - K_B)^2 + 4k_1k_3LI10^{-18}}$$

$$K_F = 0.5 (K_A + K_B + S)$$

$$K_S = 0.5 (K_A + K_B - S)$$

$$Q = \frac{B_{\text{max}}k_1L10^{-9}}{K_F - K_S}$$

$$Y = Q \left(\frac{k_4(K_F - K_S)}{K_F K_S} + \frac{k_4 - K_F}{K_F} e^{(-K_F X)} - \frac{k_4 - K_S}{K_S} e^{(-K_S X)} \right)$$

Where X is the time (min), Y the specific binding of [^3H]dofetilide, k_1 and k_2 are the k_{on} ($\text{M}^{-1} \cdot \text{min}^{-1}$) and k_{off} (min^{-1}) of [^3H]dofetilide obtained from the traditional association and dissociation assay, L the concentration of [^3H]dofetilide (nM), B_{max} the maximum specific binding (dpm) and I the concentration of the unlabelled compound (nM). Fixing these parameters allowed the following parameters to be calculated: k_3 , which is the k_{on} value ($\text{M}^{-1} \cdot \text{min}^{-1}$) of the unlabelled compound and k_4 , which is the k_{off} value (min^{-1}) of the unlabelled compound. $\text{Log}K_{\text{W-C8}}$ and $\text{log}K_{\text{W-IAM}}$ values were derived from linear regression analysis as mentioned above. The molecular weight (M.W.), logP and $\text{p}K_a$ values were calculated using a structure-based calculation plug-in provided by ChemAxon (Budapest, Hungary). All values obtained from radioligand binding assays in this study are means of at least three independent experiments performed in duplicate. Statistical analysis was performed with a two-tailed unpaired Student's t-test.

Results

[^3H]Dofetilide saturation assay

The binding of [^3H]dofetilide to HEK293K $_{\text{V}}$ 11.1 cell membranes was saturable and best described by a one-site binding model. A representative saturation curve and the averaged data of three independent experiments performed in duplicate are shown in **Figure 1** and **Table 2**, respectively. The K_{D} and B_{max} values obtained from this assay were 2.4 ± 0.1 nM and 1.6 ± 0.1 pmol \cdot mg $^{-1}$ protein, respectively. The K_{D} value for [^3H]dofetilide from this assay was used to calculate K_{i} rather than IC_{50} values from the displacement assay for 15 reference compounds.

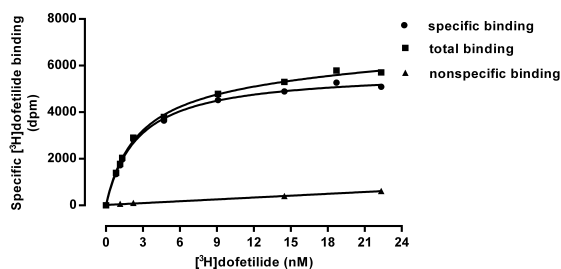


Figure 1. Saturation of [^3H]dofetilide binding to HEK293K $_{\text{V}}$ 11.1 membranes. Total binding was determined at increasing concentrations of [^3H]dofetilide. Nonspecific binding was determined at three concentrations of [^3H]dofetilide, and nonspecific binding at other concentrations of radioligand was extrapolated by linear regression. Specific binding was calculated as the difference between the total and nonspecific binding. The K_{D} value was 2.4 ± 0.1 nM, and the B_{max} value was 1.6 ± 0.1 pmol \cdot mg $^{-1}$ protein. Experiments were performed at 25 °C using 20 μg of HEK293K $_{\text{V}}$ 11.1 membrane protein.

[^3H]Dofetilide association and dissociation assay

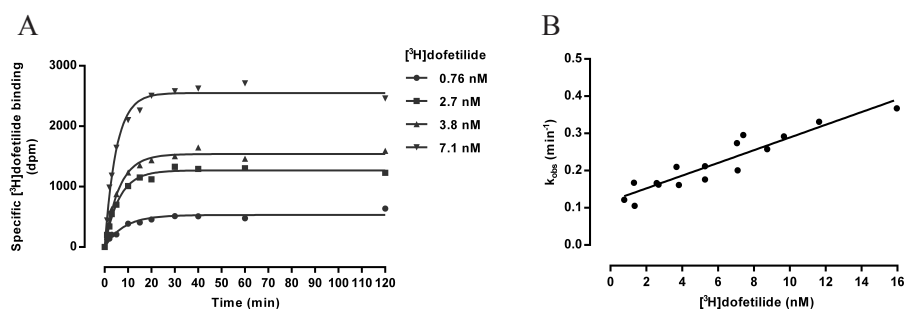


Figure 2: Characterization of the association and dissociation rates of [^3H]dofetilide to HEK293K $_{\text{V}}$ 11.1 membranes in the kinetic association assay. **(A)** Representative association curves of [^3H]dofetilide at four different concentrations; **(B)** A plot of k_{obs} values versus the concentration of [^3H]dofetilide. Experiments were performed at 25 °C using 20 μg of HEK293K $_{\text{V}}$ 11.1 membrane protein.

Initial experiments were performed to fully characterize the association and dissociation rates of [^3H]dofetilide to and from HEK293K $_{\text{V}}$ 11.1 membranes, respec-

tively. As the association rate of a ligand is dependent upon the concentration used, kinetic association experiments with a range of [^3H]dofetilide concentrations were conducted. In **Figure 2A**, curves are shown for four of such concentrations (0.76, 2.7, 3.8 and 7.1 nM). A plot of the k_{obs} values against more, including higher, concentrations of [^3H]dofetilide (**Figure 2B**) was consistent with a linear correlation ($r^2 = 0.86$, $P < 0.0001$), indicating that the binding of [^3H]dofetilide to the $K_v11.1$ channel followed the law of mass action for a simple bimolecular interaction and that the equation $k_{\text{on}} = (k_{\text{obs}} - k_{\text{off}})/[L^*]$ was applicable in this study. The k_{on} and k_{off} values obtained from this plot were $0.017 \text{ nM}^{-1} \cdot \text{min}^{-1}$ and 0.12 min^{-1} , respectively (**Table 2**). When k_{off} was divided by k_{on} , a kinetically derived K_D value of 7.1 nM was obtained. These values were in agreement with values for apparent on- and off-rates and kinetic K_D of [^3H]dofetilide assessed at one (5 nM) concentration ($k_{\text{on}} = 0.032 \pm 0.003 \text{ nM}^{-1} \cdot \text{min}^{-1}$, $k_{\text{off}} = 0.20 \pm 0.03 \text{ min}^{-1}$ and $K_D = 6.4 \pm 1.3 \text{ nM}$) derived from the traditional association and dissociation assays published previously²².

Table 2. Binding parameters of dofetilide from different equilibrium and kinetic binding assays.

Binding parameters	Saturation assay	Kinetic association assay ^a	Traditional association and dissociation assay ^b	Displacement assay	Competition association assay
$k_{\text{on}} (\text{nM}^{-1} \cdot \text{min}^{-1})$	-	0.017	0.032 ± 0.003	-	0.048 ± 0.011
$k_{\text{off}} (\text{min}^{-1})$	-	0.12	0.20 ± 0.03	-	0.13 ± 0.02
$K_D (\text{nM})$	2.4 ± 0.1	7.1 ^c	6.4 ± 1.3^c	-	2.7 ± 0.3^c
$K_i (\text{nM})$	-	-	-	5.4 ± 0.8	-

Values are means (\pm S.E.M.) of three independent assays performed in duplicate.

^aData were derived from linear regression of one independent association assay of [^3H]dofetilide at different concentrations.

^bData from our previous study²².

^cKinetic $K_D = k_{\text{off}}/k_{\text{on}}$.

[^3H]Dofetilide displacement assay

Competition binding assays were performed to generate K_i values for 15 reference compounds. Compounds were selected based on structural diversity and having a wide range of $K_v11.1$ binding affinity, and included both anti-arrhythmic drugs and drugs for other therapeutic areas (e.g., astemizole and terfenadine for the treatment of allergic conditions). All compounds produced a concentration-dependent inhibition of specific [^3H]dofetilide binding, and their displace-

ment curves were best described by a one-site competition model (**Figure 3**). All K_i values are listed in **Table 3**. Among the 15 compounds, clofilium had the highest affinity to the $K_v11.1$ channel, displacing [3 H]dofetilide with a K_i value of 0.55 ± 0.09 nM, whereas moxifloxacin exhibited the lowest affinity of 252 ± 121 μ M. Ranolazine and sotalol showed similar and relatively weak inhibition of the channel with K_i values of 21 ± 6 and 25 ± 1 μ M, respectively. Additionally, amiodarone, thioridazine and chlorpromazine displayed modest $K_v11.1$ blockade with K_i values from 0.3 to 3 μ M. All other compounds demonstrated relatively high affinity to the $K_v11.1$ channel, between 2.5 ± 0.2 nM (astemizole) and 63 ± 4 nM (terfenadine).

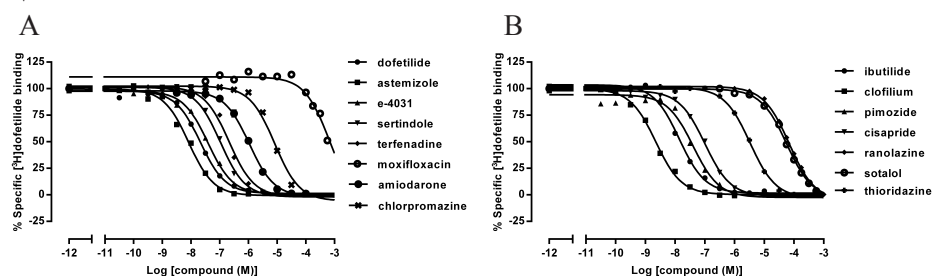


Figure 3. Displacement curves of [3 H]dofetilide from HEK293 $K_v11.1$ membranes by different known $K_v11.1$ channel blockers. **(A)** Dofetilide, astemizole, E-4031, sertindole, terfenadine, moxifloxacin, amiodarone and chlorpromazine; **(B)** Ibutilide, clofilium, pimozone, cisapride, ranolazine, sotalol and thioridazine. Experiments were performed at 25 °C using 20 μ g of HEK293 $K_v11.1$ membrane protein.

[3 H]Dofetilide competition association assay

With the k_{on} (k_1) and k_{off} (k_2) values of [3 H]dofetilide obtained from the traditional association and dissociation assays, it was possible to determine the k_{on} (k_3) and k_{off} (k_4) values of unlabelled compounds by performing so-called competition association experiments. Firstly, we validated the competition association assay at the $K_v11.1$ channel using three concentrations of ‘cold’ dofetilide equivalent to 0.3-, 1- and 3-fold of its K_i value. A representative experiment is shown in **Figure 4**. The k_{on} (k_3) and k_{off} (k_4) values for dofetilide determined in this assay were 0.048 ± 0.011 nM $^{-1}$ ·min $^{-1}$ and 0.13 ± 0.02 min $^{-1}$, respectively, and in good agreement with the kinetic parameters determined in the traditional association and dissociation assays, as shown in **Table 2**. Furthermore, the kinetic K_D value (2.7 ± 0.3 nM) derived from this assay was similar to the K_D value (2.4 ± 0.1 nM) obtained from the [3 H]dofetilide saturation assay. In addition, these K_D values were in the same range as dofetilide’s affinity constant that stemmed from the displacement assay ($K_i = 5.4 \pm 0.8$ nM) and the kinetically derived K_D values from kinetic association assay and traditional kinetic experiments (7.1 nM or 6.4

± 1.3 nM, respectively). Overall, the results presented here demonstrated that the competition association assay could be applied to determine the association and dissociation rates of other unlabeled ligands at the $K_v11.1$ channel. It is noteworthy that a good experimental window was achieved using a concentration of dofetilide at 1-fold its K_i value in the competition association assay, as displayed in **Figure 4**. Reassuringly, when astemizole and E-4031 were tested in this standard three-concentration assay, similar findings were observed as well (data not shown). Thus, the other unlabelled ligands were only tested at 1-fold their K_i values rather than three different concentrations in the further competition association experiments in order to improve the throughput of this method.

Table 3. The affinity constants and kinetic parameters of 15 compounds at the $K_v11.1$ channel obtained from the [3 H]dofetilide displacement and competition association assay.

Compound	K_i (nM) ^a	k_{on} (nM ⁻¹ ·min ⁻¹) ^b	k_{off} (min ⁻¹) ^b	K_D (nM) ^c
Dofetilide	5.4 ± 0.8	0.048 ± 0.011	0.13 ± 0.02	2.7 ± 0.3
Astemizole	2.5 ± 0.2	0.17 ± 0.03	0.083 ± 0.003	0.53 ± 0.07
E-4031	13 ± 0.7	0.026 ± 0.003	0.27 ± 0.02	10 ± 1
Sertindole	34 ± 5	0.048 ± 0.007	0.86 ± 0.17	18 ± 1
Terfenadine	63 ± 4	0.0071 ± 0.0025	0.25 ± 0.03	39 ± 7
Moxifloxacin	252347 ± 120995	$(4.7 \pm 1.0) \times 10^{-6}$	0.28 ± 0.06	64531 ± 10276
Amiodarone	308 ± 33	$(6.0 \pm 0.7) \times 10^{-4}$	0.23 ± 0.02	387 ± 37
Chlorpromazine	2518 ± 301	$(1.3 \pm 0.2) \times 10^{-4}$	0.36 ± 0.05	2714 ± 154
Ibutilide	5.1 ± 0.4	0.046 ± 0.006	0.20 ± 0.02	4.6 ± 1.1
Clofilium	0.55 ± 0.09	0.23 ± 0.07	0.10 ± 0.01	0.54 ± 0.17
Pimozide	28 ± 7	0.071 ± 0.020	0.22 ± 0.07	3.2 ± 0.4
Cisapride	54 ± 10	0.031 ± 0.009	0.59 ± 0.14	20 ± 2
Ranolazine	21379 ± 5776	$(1.5 \pm 0.4) \times 10^{-5}$	0.23 ± 0.04	16672 ± 1820
Sotalol	24663 ± 1379	$(1.7 \pm 0.3) \times 10^{-5}$	0.32 ± 0.03	19740 ± 1591
Thioridazine	1065 ± 41	$(2.3 \pm 0.4) \times 10^{-4}$	0.24 ± 0.05	1050 ± 48

Values are means (\pm S.E.M.) of three independent assays performed in duplicate.

^a K_i values were derived from the [3 H]dofetilide displacement assay.

^b k_{on} (k_3) and k_{off} (k_4) values of unlabelled compounds were determined in the [3 H]dofetilide competition association assay.

^cKinetic $K_D = k_{off}/k_{on}$.

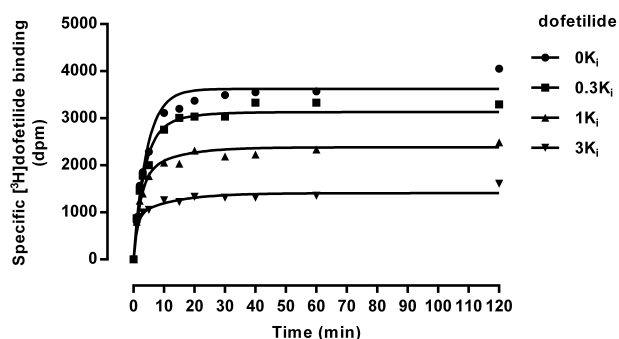


Figure 4. Competition association assay of [^3H]dofetilide in the absence (control) or presence of 0.3-, 1- and 3-fold of unlabeled dofetilide's K_i value. Experiments were performed at 25 °C using 20 μg of HEK293K $_{v11.1}$ membrane protein.

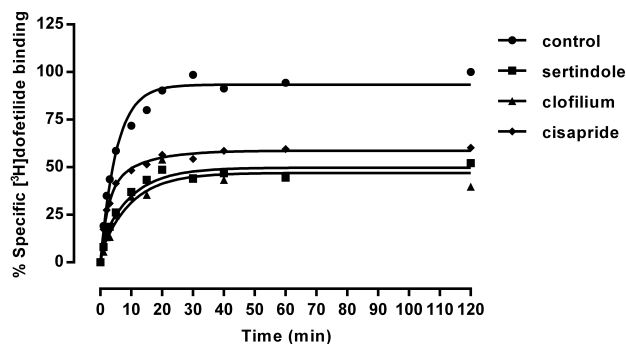


Figure 5. Representative competition association curves of [^3H]dofetilide in the absence (control) or presence of unlabelled sertindole, clofilium and cisapride at a concentration of 1-fold their K_i values. Experiments were performed at 25 °C using 20 μg of HEK-293K $_{v11.1}$ membrane protein.

Subsequently, kinetic parameters of 12 other known K $_{v11.1}$ blockers were evaluated and representative normalized curves for several compounds are depicted in **Figure 5**. The on- and off-rates of all compounds determined by these experiments are shown in **Table 3**. The association rates for all the compounds were quite distinct with k_{on} values ranging from $(4.7 \pm 1.0) \times 10^{-6} \text{ nM}^{-1} \cdot \text{min}^{-1}$ (moxifloxacin) to $0.23 \pm 0.07 \text{ nM}^{-1} \cdot \text{min}^{-1}$ (clofilium), i.e. an almost 50,000-fold difference between the fastest and slowest associating compounds. On the other hand, the dissociation rates of these 15 compounds were more similar, with the highest value of $0.86 \pm 0.17 \text{ min}^{-1}$ for sertindole and lowest k_{off} of $0.083 \pm 0.003 \text{ min}^{-1}$ for astemizole, i.e. only a 10-fold difference. Considering the kinetically-derived K_D values shown in **Table 3**, clofilium was the most potent inhibitor to

the $K_v11.1$ channel with a kinetic K_D value of 0.54 ± 0.17 nM, while moxifloxacin had the lowest affinity ($K_D = 65 \pm 10$ μ M) to the channel. These results were in the same rank order as the K_i values derived from the equilibrium displacement assay.

Correlations of equilibrium K_i with kinetic K_D , k_{on} , and k_{off} values

A plot of the logarithms of kinetic K_D values (i.e. k_{off}/k_{on}) derived from the [3 H] dofetilide competition association assays and the logarithms of equilibrium K_i values obtained from the displacement experiments was made, and a significant correlation (**Figure 6A**) was observed. This showed an excellent consistence of the results from two different methods and indicated a high reliability of the [3 H] dofetilide competition association assay. More interestingly, a significant inverse relationship was also found between pk_{on} and pK_i values for unlabelled compounds in **Figure 6B**. On the contrary, there was no significant linear relationship between pk_{off} and pK_i values ($r^2 = 0.15$, $P = 0.15$, data not shown). Together, this suggested that the [3 H]dofetilide competition association assay was successfully validated for assessing the kinetics of other unlabelled competitive compounds, and that the affinity of these compounds at the $K_v11.1$ channel was mainly controlled by their on-rates rather than off-rates.

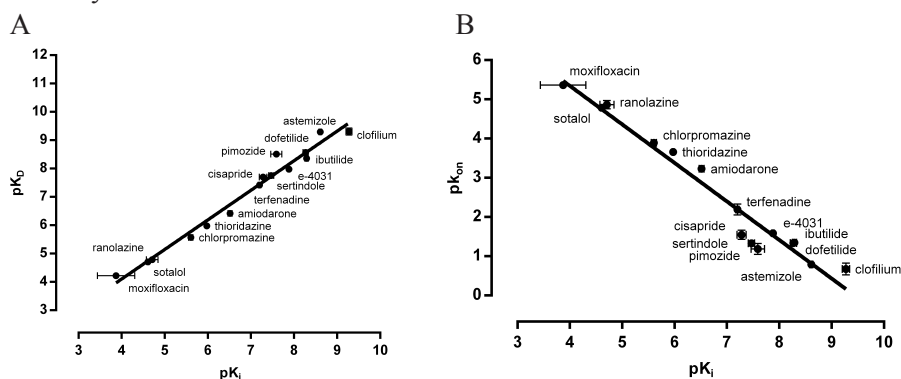


Figure 6. Correlations between the affinity constant (K_i) and (A) the kinetically derived equilibrium dissociation constants, K_D ($r^2 = 0.98$, $P < 0.0001$) and (B) the association rates, k_{on} for unlabelled ligands at the $K_v11.1$ channel ($r^2 = 0.95$, $P < 0.0001$). K_i , K_D and k_{on} values are listed in **Table 3**.

Lipophilicity ($\log K_{W-C8}$) and membrane partition coefficient ($\log K_{W-IAM}$) of $K_v11.1$ blockers

The isocratical $\log K_{W-C8}$ values ('lipophilicity') were evaluated at pH 7.4 and are detailed in **Table 4**. The lipophilicity of 15 reference compounds covered a wide numerical range, varying from 0.56 (sotalol) to 5.52 (amiodarone). We also calculated $\log P$ values as a measure for lipophilicity, and plotted these against the $\log K_{W-C8}$ data (**Table 4**). A significant correlation was found between them ($r^2 = 0.81$, $P < 0.0001$), which implied that for this series of compounds calculated $\log P$ values can be used interchangeably with the experimentally determined values.

Table 4. The lipophilicity, membrane partition coefficients and other physicochemical properties of 15 K_v11.1 blockers.

Compound	$\log K_{W-C8}$ ^a	$\log K_{W-IAM}$ ^b	M.W. ^c	$\log P$ ^c	pK_a ^c
Dofetilide	0.84	2.08	441.57	0.59	8.99
Astemizole	3.52	3.40	458.57	5.39	8.75
E-4031	1.29	1.98	401.52	1.73	8.01
Sertindole	3.97	3.38	440.94	3.77	8.59
Terfenadine	4.05	4.01	471.67	6.48	9.02
Moxifloxacin	1.12	1.57	401.43	1.97	9.42
Amiodarone	5.52	3.30	645.31	7.64	8.47
Chlorpromazine	3.39	3.36	318.86	4.54	9.20
Ibutilide	0.90	2.53	384.58	3.25	10.40
Clofilium	2.00	-0.35	338.98	2.91	n.a. ^d
Pimozide	4.69	3.80	461.55	5.83	8.38
Cisapride	3.12	2.66	465.95	2.49	8.24
Ranolazine	2.17	2.39	427.54	2.83	7.17
Sotalol	0.56	0.66	272.36	0.05	9.43
Thioridazine	3.53	3.80	370.58	5.47	8.93

^a $\log K_{W-C8}$ values were derived from HPLC experiments on a Supelcosil LC-ABZ, 5 cm × 4.6 mm, 5 μ m column.

^b $\log K_{W-IAM}$ values were derived from HPLC experiments on a 10 cm x 4.6 mm, 10 μ m Regis IAM PC DD2 column.

^cValues were derived from the structure-based calculation plug-in by ChemAxon.

^dn.a. not applicable; this compound is permanently charged.

To mimic the interactions of our ligands with membrane phospholipids, an IAM HPLC column that is a reflection of the lipid environment of a fluid cell membrane on a solid matrix was used to determine membrane partition coefficients ($\log K_{W-IAM}$) for all reference compounds. Their $\log K_{W-IAM}$ values were measured at pH 7.4 and are summarized in **Table 4**. Terfenadine had the highest $\log K_{W-IAM}$ value of 4.01, indicating that this compound possessed the highest affinity for membrane phospholipids. On the contrary, the $\log K_{W-IAM}$ for clofilium was only -0.35, most likely due to its quaternary ammonium moiety, which demonstrated that this compound hardly interacted with phospholipid membranes.

Subsequently, the possible correlation between $\log K_{W-C8}$ and $\log K_{W-IAM}$ was studied, and the result is shown in **Figure 7**. A significant linear relationship ($r^2 = 0.52$, $P < 0.0024$) was observed for these two parameters even when including the outlier clofilium. Obviously, a similar significant correlation was also found between calculated $\log P$ and $\log K_{W-IAM}$ values ($r^2 = 0.52$, $P = 0.0022$, data not shown). Next, the relationship between affinity constants or kinetic rate constants of the 15 $K_v 11.1$ inhibitors and their membrane interactions were investigated, as shown in **Figure 8A – 8C**. Apparently, no relationships were found for any of them ($P > 0.05$), demonstrating that membrane interactions did not affect affinity and binding kinetics of these ligands at the $K_v 11.1$ channel. Similarly, there were no correlations between $\log K_{W-C8}$ and pK_i , pK_{on} or pK_{off} values (data not shown).

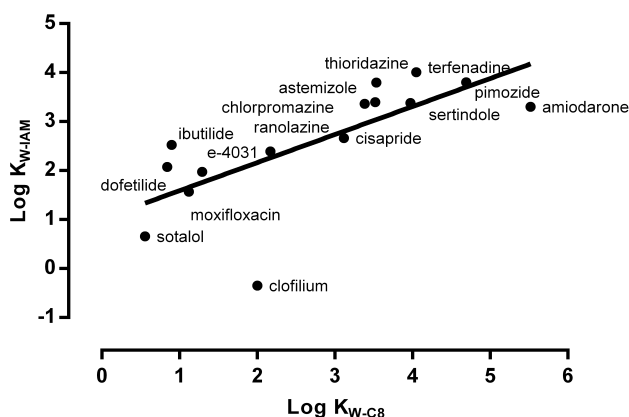


Figure 7. Correlation between $\log K_{W-C8}$ and $\log K_{W-IAM}$ values at pH 7.4 for 15 $K_v 11.1$ inhibitors ($r^2 = 0.52$, $P < 0.0024$). $\log K_{W-C8}$ and $\log K_{W-IAM}$ values are listed in **Table 4**.

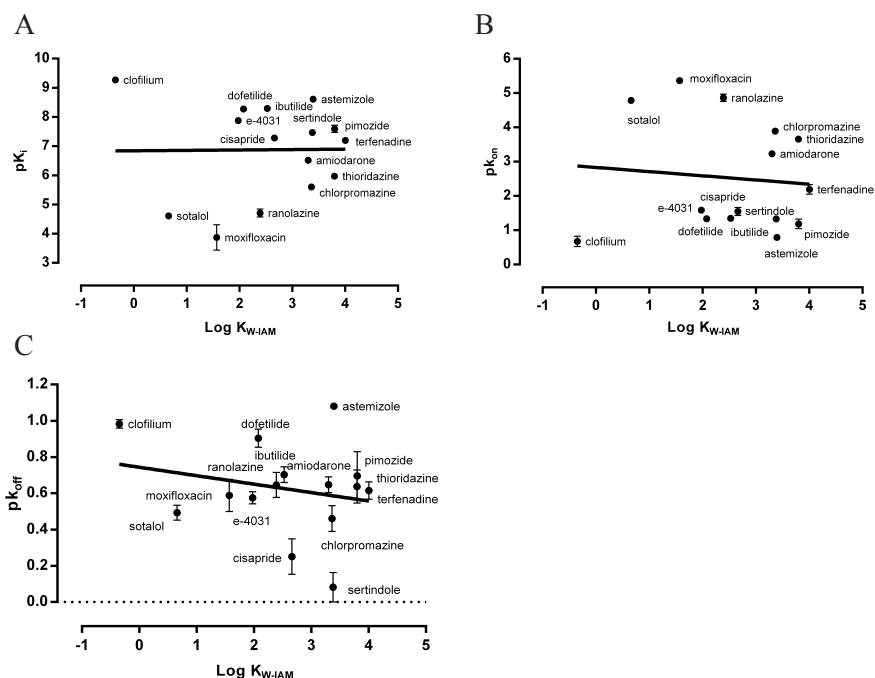


Figure 8. Correlation of $\log K_{w-IAM}$ values and binding parameters of 15 $K_{v11.1}$ inhibitors. No significant relationship between $\log K_{w-IAM}$ and values of (A) pK_i ($r^2 = 0.00011$, $P = 0.97$), (B) pK_{on} ($r^2 = 0.0087$, $P = 0.74$) or (C) pK_{off} was observed ($r^2 = 0.051$, $P = 0.42$). All data used in these plots are listed in **Table 3** and **Table 4**.

Role of other calculated physicochemical properties in ligand-receptor binding kinetics

Lastly, two other physicochemical properties of the unlabelled compounds, molecular weight (M.W.) and acid/base constant (pK_a) (**Table 4**), were compared with their on-/off- rates and dissociation constants. As depicted in **Figure 9**, no significant correlations were observed between the logarithms of on-rates of the compounds in this study and their molecular properties. Moreover, there were no obvious relationships between the logarithms of off-rates or equilibrium K_i values and these physicochemical properties either ($P > 0.05$, data not shown). These results implied that the binding kinetics of compounds at the $K_v11.1$ channel was not governed by their overall, macroscopic, physicochemical properties.

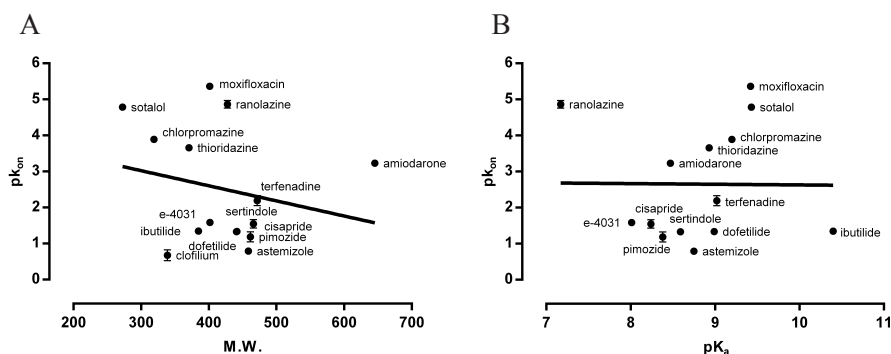


Figure 9. Lack of correlation between the association rates (pK_{on} values) of selected compounds and their physicochemical properties. **(A)** No significant correlation was observed with M.W. ($r^2 = 0.049$, $P = 0.43$); **(B)** No significant correlation was observed with pK_a ($r^2 = 0.000076$, $P = 0.98$). M.W. and pK_a values are shown in **Table 4**.

Discussion and conclusions

Since the introduction of the competition association assay²³, more and more researchers have utilized this method to study the binding kinetics of unlabelled ligands at their targets, such as muscarinic receptors and the adenosine A_{2A} receptor^{24, 29, 30}. In addition, a few examples in literature have been reported to apply this technique for the determination of ligand binding kinetics at ligand-gated ion channels³¹. To the best of our knowledge, the current study is the first to assess binding kinetics of ligands interacting with voltage-gated ion channels, in particular the $K_v11.1$ channel.

It might be argued that our study has some limitations. The stably-transfected HEK293 $K_v11.1$ cells lack the (co-)expression of two ancillary β -subunits, minK and MiRP1³. Discrepancies could also exist between membrane binding assays and whole cell experiments, which are more relevant to the channel's natural orientation. For instance, the kinetics of the drug- $K_v11.1$ interaction have been reported to be use- and frequency-dependent in whole cell patch clamp assays due to special gating kinetics of the channel^{32, 33}. In our membrane binding assays, we speculate that the channels maintain the same configurations, and thus the kinetic parameters in this investigation should resemble the actual binding process between $K_v11.1$ blockers and the channel. To perform straightforward and accurate kinetic determinations, experiments were carried out at 25 °C with membrane preparations of stably-transfected HEK293 $K_v11.1$ cells. We reason that all parameters obtained at 25 °C in this investigation lead to a similar compound rank order as those at physiological temperature. In fact, this has been shown for

another target based on van't Hoff and Eyring equations³⁴.

The linear plot of k_{obs} values obtained at increasing concentrations of [³H] dofetilide (**Figure 2B**) strongly supported a pseudo-first-order kinetic behavior of its binding to the $K_v11.1$ channel, which provided the theoretical foundation for all kinetic analyses in our present study. Other mechanisms of action such as induced-fit or conformational selection would have resulted in deviations from linearity; in such cases, the Motulsky and Mahan model and equations would not have been applicable^{35, 36}. All 15 reference compounds had a pseudo-Hill coefficient close to unity in the [³H]dofetilide displacement assay (data not shown), which indicated a competitive mode of inhibition with regard to the radioligand. This is another indication of the simple bimolecular interaction model and corroborated a pseudo-first-order kinetic behavior of the binding to the $K_v11.1$ channel. This finding was in accordance with previous studies describing the presence of a single affinity state for $K_v11.1$ inhibitors at the channel^{37, 38}. Subsequently, a newly developed [³H]dofetilide competition association assay was applied to study the binding kinetics of 15 unlabelled reference compounds with diverse chemical structures at the $K_v11.1$ channel (**Table 1**). The k_{on} , k_{off} and K_D values of dofetilide from this assay were comparable to the values derived from saturation and kinetic association experiments and traditional association and dissociation assays²², indicative of the accuracy and reliability of this new assay. Moreover, the excellent linear correlation between these kinetically derived K_D values of 15 reference compounds and their K_i values from the equilibrium displacement assay further supported the latter (**Figure 6A**). Taken together, this led us to conclude that a novel [³H]dofetilide competition association assay was successfully developed and validated.

Correlations between the affinity data (K_i) and the kinetic parameters (on- and off-rates) were also investigated in the present study. Surprisingly, there was a significant inverse correlation between pK_i and $p k_{\text{on}}$ values for reference compounds (**Figure 6B**), whereas no relationship was found between pK_i and $p k_{\text{off}}$ values (data not shown). Although this correlation between affinity and association rates has been shown to be the case for β_2 -adrenoceptor agonists³⁹ and OX_2 -receptor antagonists⁴⁰, this phenomenon is supposed to be unusual and counter-intuitive. Dogma has it that the collision theory sets the maximum value for k_{on} as the diffusion limit for a ligand and a target, which is about $10^8 \sim 10^9 \text{ M}^{-1} \cdot \text{s}^{-1}$ ⁴¹. In this view, there can only be small variations in the on-rate constants and thus the equilibrium affinity changes are mainly dictated by the off-rates of ligands^{15, 41, 42}. In contrast to these classical assumptions, association rates of our selected structurally diverse compounds varied around 50,000-fold, whereas their dissociation rates differed only 10-fold. This clearly indicated that apart from

off-rates, on-rates also play a pivotal role in regulating affinity of ligands to their targeted receptors, at least for the $K_v11.1$ channel.

Recently, it has been reported that drug-receptor association rates and corresponding affinity were enhanced due to concentrating effects and lateral diffusion of membrane associated β_2 -adrenoceptor ligands and k_{on} values were positively correlated to their lipophilicity and membrane interactions^{18, 43}. Furthermore, Sykes *et al.*¹⁸ observed that dissociation rates were much more correlated to the corrected 'true' affinity, which considers drug concentration gradients in the local environment due to membrane affinity, than the apparent affinity. Additionally, it was recommended that any prediction of pharmacodynamic properties should take membrane interactions as well as lipophilicity into account¹⁷. Hence, the potential influence of membrane affinity on ligand binding to the $K_v11.1$ channel was investigated by the determination of both $\log K_{w-C8}$ and $\log K_{w-IAM}$ values. However, when pK_i and pK_{on} were compared to $\log K_{w-C8}$ and $\log K_{w-IAM}$, no significant relationships were observed in our case (**Figure 8**). This indicated that membrane interactions of our ligands did not influence their association rates and binding affinity to the $K_v11.1$ channel, and that the apparent affinity of these reference compounds is their 'true' affinity. Interestingly, when $\log K_{w-C8}$ and $\log K_{w-IAM}$ were compared to each other, clofilium was observed to deviate from the significant linear correlation (**Figure 7**). Herein, we hypothesized that the lipophilic alkyl chains of clofilium compensated for its hydrophilic quaternary ammonium group and thus dominated its lipophilicity in the octanol-water system, while the positive charge at the nitrogen played a more critical role in the IAM system and weakened its membrane interactions. With regard to dissociation rates, no correlations were found to either $\log K_{w-C8}$ or $\log K_{w-IAM}$ values as well (data not shown). This was in accordance with previous findings^{18, 44} and demonstrated that the dissociation rate of a drug was not affected by its local concentrations and thus independent of membrane affinity. Of note, typical $K_v11.1$ inhibitors are known to bind to the inner cavity in the intracellular part of the channel³. However, all experiments in the present study were performed with HEK293 $K_v11.1$ membranes instead of intact cells and were thus independent of transmembrane transport of ligands. From **Figure 6B**, it follows that a significant relationship between affinity and association rates for 15 $K_v11.1$ inhibitors was found, which showed that ligand- $K_v11.1$ rather than ligand-membrane association controlled their affinity. Apparently, an aqueous entry pathway predominates the binding of $K_v11.1$ blockers to the channel, and an additional compartment induced by the lipid membranes does not play a significant role.

We questioned whether it would be possible to correlate other general physicochemical properties of these molecules to their biological profile (**Figure 9**).

This was not the case, since typical features such as molecular weight and the basicity of the $K_v11.1$ blockers were not correlated to any of the equilibrium or kinetic binding parameters tested. However, it has been stated previously that physicochemical properties of drugs are relevant for their kinetic parameters^{41, 45}. For instance, Miller *et al.*⁴⁶ reported that molecular weight was one of the most important factors to affect the dissociation kinetics of ligands from their biological targets including enzymes (kinases) and G protein-coupled receptors. From the present study, it follows that the effects of general molecular properties on the binding kinetics of a ligand to $K_v11.1$ channel are negligible compared to other targets.

Previous studies have also suggested that k_{off} values, or drug-target residence times (RTs, the reciprocal of k_{off}), play an important role in the duration of pharmacological effects^{15, 24, 42}. In other words, an increased drug–target RT could elicit an improved or prolonged drug effect⁴⁷. Nevertheless, when adverse effects result directly from drug occupancy at the pharmacological target, such as chlorpromazine binding to D_2 receptor or clopidogrel to $P2Y_{12}$ receptor, a long RT would result in so-called ‘on-target’ drug toxicity, and thus a short RT is favored⁴⁸. In our hands, however, the dissociation rates and hence residence times of selected 15 $K_v11.1$ inhibitors were very similar (**Table 3**). On the contrary, association rates of our reference compounds varied widely, and are therefore potentially more important to predict the safety of $K_v11.1$ inhibitors.

Previously, Redfern *et al.*¹⁴ have assigned drugs into five categories of torsadogenic propensity and proposed a “30-fold safety margin” between C_{max} and $K_v11.1$ IC_{50} values as a marker to predict TdP. However, it is known that TdP are not only induced by inhibition of the $K_v11.1$ channel but also regulated by other potassium channels, sodium and calcium channels^{14, 49}. Therefore, a Comprehensive *in vitro* Proarrhythmia Assay (CiPA) has recently been introduced to assess drug-induced proarrhythmic risk more efficiently and accurately^{49, 50}. The kinetics of drug block and unblock were suggested to be incorporated together with drug potency at ion channels in arrhythmia evaluation during the interpretation of this paradigm⁴⁹. Although the present study focuses on the $K_v11.1$ channel only, it provides a new medium throughput method to determine the association and dissociation rates of $K_v11.1$ blockers, which can be used subsequently for other ion channels as well, if a radioligand is available. Interestingly, Veroli *et al.*⁵¹ derived from mathematical models that fast binding $K_v11.1$ blockers in the untrapped configuration and trapped blockers induced greater action potential and QT prolongation. This strengthens the application of our method in the future, and suggests that using slow association and/or fast dissociation characteristics as a “novel marker” might be beneficial for reducing $K_v11.1$ cardiotoxicity of drug

candidates.

In conclusion, a novel [^3H]dofetilide competition association assay has been successfully developed and validated to characterize the kinetic binding parameters of unlabelled compounds at the $\text{K}_v11.1$ channel. Importantly, association rates of $\text{K}_v11.1$ blockers were divergent, i.e. not diffusion limited, and excellently correlated to their affinity values. In addition, membrane interactions and other molecular properties do not influence the affinity and kinetic binding parameters of ligands at the $\text{K}_v11.1$ channel. Altogether, this is quite unlike the mechanisms of interaction proposed for other drug target classes, such as kinases and G protein-coupled receptors. Hence, we postulate that association rates can be used to assess a compound's $\text{K}_v11.1$ liability, apart from its affinity. However, further studies involving compounds with a wide range of k_{off} values are required to assess the effect of residence time on drug-induced $\text{K}_v11.1$ cardiotoxicity. Overall, we believe that this research provides novel insights into the kinetic study of ion channels, which can hopefully help to avoid $\text{K}_v11.1$ -induced cardiotoxicity of drug candidates in the future.

References

1. Doyle, D. A.; Cabral, J. M.; Pfuetzner, R. A.; Kuo, A.; Gulbis, J. M.; Cohen, S. L.; Chait, B. T.; MacKinnon, R. The structure of the potassium channel: Molecular basis of K^+ conduction and selectivity. *Science* **1998**, *280*, 69-77.
2. Nerbonne, J. M. Molecular basis of functional voltage-gated K^+ channel diversity in the mammalian myocardium. *J. Physiol.* **2000**, *525*, 285-298.
3. Vandenberg, J. I.; Walker, B. D.; Campbell, T. J. hERG K^+ channels: Friend and foe. *Trends Pharmacol. Sci.* **2001**, *22*, 240-246.
4. Vandenberg, J. I.; Perry, M. D.; Perrin, M. J.; Mann, S. A.; Ke, Y.; Hill, A. P. hERG K^+ channels: Structure, function, and clinical significance. *Physiol. Rev.* **2012**, *92*, 1393-1478.
5. Hancox, J. C.; McPate, M. J.; El Harchi, A.; Zhang, Y. The hERG potassium channel and hERG screening for drug-induced torsades de pointes. *Pharmacol. Ther.* **2008**, *119*, 118-132.
6. Sanguinetti, M. C.; Tristani-Firouzi, M. hERG potassium channels and cardiac arrhythmia. *Nature* **2006**, *440*, 463-469.
7. Rampe, D.; Brown, A. M. A history of the role of the hERG channel in cardiac risk assessment. *J. Pharmacol. Toxicol. Methods* **2013**, *68*, 13-22.
8. Fitzgerald, P. T.; Ackerman, M. J. Drug-induced torsades de pointes: The evolving role of pharmacogenetics. *Heart Rhythm* **2005**, *2*, S30-S37.
9. Noble, D. Computational models of the heart and their use in assessing the actions

- of drugs. *J. Pharmacol. Sci.* **2008**, *107*, 107-117.
10. Heijman, J.; Voigt, N.; Carlsson, L. G.; Dobrev, D. Cardiac safety assays. *Curr. Opin. Pharmacol.* **2014**, *15*, 16-21.
 11. Krohn, K. A. The physical chemistry of ligand-receptor binding identifies some limitations to the analysis of receptor images. *Nucl. Med. Biol.* **2001**, *28*, 477-483.
 12. Chiu, P. J.; Marcoe, K. F.; Bounds, S. E.; Lin, C.; Feng, J.; Lin, A.; Cheng, F.; Crumb, W. J.; Mitchell, R. Validation of a [³H]astemizole binding assay in HEK293 cells expressing hERG K⁺ channels. *J. Pharmacol. Sci.* **2004**, *95*, 311-319.
 13. Diaz, G. J.; Daniell, K.; Leitza, S. T.; Martin, R. L.; Su, Z.; McDermott, J. S.; Cox, B. F.; Gintant, G. A. The [³H]dofetilide binding assay is a predictive screening tool for hERG blockade and proarrhythmia: Comparison of intact cell and membrane preparations and effects of altering [K⁺]_o. *J. Pharmacol. Toxicol. Methods* **2004**, *50*, 187-199.
 14. Redfern, W. S.; Carlsson, L.; Davis, A. S.; Lynch, W. G.; MacKenzie, I.; Palethorpe, S.; Siegl, P. K. S.; Strang, I.; Sullivan, A. T.; Wallis, R.; Camm, A. J.; Hammond, T. G. Relationships between preclinical cardiac electrophysiology, clinical QT interval prolongation and torsade de pointes for a broad range of drugs: Evidence for a provisional safety margin in drug development. *Cardiovasc. Res.* **2003**, *58*, 32-45.
 15. Copeland, R. A.; Pompliano, D. L.; Meek, T. D. Drug-target residence time and its implications for lead optimization. *Nat. Rev. Drug Discov.* **2006**, *5*, 730-739.
 16. Pan, A. C.; Borhani, D. W.; Dror, R. O.; Shaw, D. E. Molecular determinants of drug-receptor binding kinetics. *Drug discov. today* **2013**, *18*, 667-673.
 17. Taillardat-Bertschinger, A.; Carrupt, P.-A.; Barbato, F.; Testa, B. Immobilized artificial membrane HPLC in drug research. *J. Med. Chem.* **2003**, *46*, 655-665.
 18. Sykes, D.; Parry, C.; Reilly, J.; Wright, P.; Fairhurst, R.; Charlton, S. J. Observed drug-receptor association rates are governed by membrane affinity: The importance of establishing “micro PK/PD relationships” at the β₂-adrenoceptor. *Mol. Pharmacol.* **2014**, *85*, 608-617.
 19. Shaguftha; Guo, D.; Klaasse, E.; de Vries, H.; Brussee, J.; Nalos, L.; Rook, M. B.; Vos, M. A.; van der Heyden, M. A.; IJzerman, A. P. Exploring chemical substructures essential for hERG K⁺ channel blockade by synthesis and biological evaluation of dofetilide analogues. *ChemMedChem* **2009**, *4*, 1722-1732.
 20. Vilums, M.; Overman, J.; Klaasse, E.; Scheel, O.; Brussee, J.; IJzerman, A. P. Understanding of molecular substructures that contribute to hERG K⁺ channel blockade: Synthesis and biological evaluation of E-4031 analogues. *ChemMedChem* **2012**, *7*, 107-113.
 21. Alexander, S. P.; Benson, H. E.; Faccenda, E.; Pawson, A. J.; Sharman, J. L.; Catterall, W. A.; Spedding, M.; Peters, J. A.; Harmar, A. J. The concise guide to pharmacology 2013/14: Ion channels. *Br. J. Pharmacol.* **2013**, *170*, 1607-1651.
 22. Yu, Z.; Klaasse, E.; Heitman, L. H.; IJzerman, A. P. Allosteric modulators of the hERG K⁺ channel: Radioligand binding assays reveal allosteric characteristics of dofeti-

- lide analogs. *Toxicol. Appl. Pharmacol.* **2014**, 274, 78-86.
23. Motulsky, H. J.; Mahan, L. The kinetics of competitive radioligand binding predicted by the law of mass action. *Mol. Pharmacol.* **1984**, 25, 1-9.
24. Guo, D.; Mulder-Krieger, T.; IJzerman, A. P.; Heitman, L. H. Functional efficacy of adenosine A_{2A} receptor agonists is positively correlated to their receptor residence time. *Br. J. Pharmacol.* **2012**, 166, 1846-1859.
25. Heitman, L. H.; Narlawar, R.; de Vries, H.; Willemsen, M. N.; Wolfram, D.; Brussee, J.; IJzerman, A. P. Substituted terphenyl compounds as the first class of low molecular weight allosteric inhibitors of the luteinizing hormone receptor. *J. Med. Chem.* **2009**, 52, 2036-2042.
26. Lombardo, F.; Shalaeva, M. Y.; Tupper, K. A.; Gao, F. ElogDoct: A tool for lipophilicity determination in drug discovery. 2. Basic and neutral compounds. *J. Med. Chem.* **2001**, 44, 2490-2497.
27. Valko, K.; Du, C. M.; Bevan, C. D.; Reynolds, D. P.; Abraham, M. H. Rapid-gradient HPLC method for measuring drug interactions with immobilized artificial membrane: Comparison with other lipophilicity measures. *J. Pharm. Sci.* **2000**, 89, 1085-1096.
28. Cheng, Y.-C.; Prusoff, W. H. Relationship between the inhibition constant (K_i) and the concentration of inhibitor which causes 50 percent inhibition (I_{50}) of an enzymatic reaction. *Biochem. Pharmacol.* **1973**, 22, 3099-3108.
29. Schreiber, G.; Henis, Y. I.; Sokolovsky, M. Analysis of ligand binding to receptors by competition kinetics. Application to muscarinic antagonists in rat brain cortex. *J. Biol. Chem.* **1985**, 260, 8789-8794.
30. Dowling, M. R.; Charlton, S. J. Quantifying the association and dissociation rates of unlabelled antagonists at the muscarinic M₃ receptor. *Br. J. Pharmacol.* **2006**, 148, 927-937.
31. Hawkinson, J.; Casida, J. E. Binding kinetics of gamma-aminobutyric acidA receptor noncompetitive antagonists: Trioxabicyclooctane, dithiane, and cyclodiene insecticide-induced slow transition to blocked chloride channel conformation. *Mol. Pharmacol.* **1992**, 42, 1069-1076.
32. Stork, D.; Timin, E.; Berjukow, S.; Huber, C.; Hohaus, A.; Auer, M.; Hering, S. State dependent dissociation of hERG channel inhibitors. *Br. J. Pharmacol.* **2007**, 151, 1368-1376.
33. Windisch, A.; Timin, E.; Schwarz, T.; Stork-Riedler, D.; Erker, T.; Ecker, G.; Hering, S. Trapping and dissociation of propafenone derivatives in hERG channels. *Br. J. Pharmacol.* **2011**, 162, 1542-1552.
34. Mondal, K.; Regnstrom, K.; Morishige, W.; Barbour, R.; Probst, G.; Xu, Y.-Z.; Artis, D. R.; Yao, N.; Beroza, P.; Bova, M. P. Thermodynamic and kinetic characterization of hydroxyethylamine β -secretase-1 inhibitors. *Biochem. Biophys. Res. Commun.* **2013**, 441, 291-296.

35. Tummino, P. J.; Copeland, R. A. Residence time of receptor-ligand complexes and its effect on biological function. *Biochemistry* **2008**, *47*, 5481-5492.
36. Vogt, A. D.; Di Cera, E. Conformational selection or induced fit? A critical appraisal of the kinetic mechanism. *Biochemistry* **2012**, *51*, 5894-5902.
37. Finlayson, K.; Pennington, A. J.; Kelly, J. S. [³H]Dofetilide binding in SHSY5Y and HEK293 cells expressing a hERG-like K⁺ channel? *Eur. J. Pharmacol.* **2001**, *412*, 203-212.
38. Finlayson, K.; Turnbull, L.; January, C. T.; Sharkey, J.; Kelly, J. S. [³H]Dofetilide binding to hERG transfected membranes: A potential high throughput preclinical screen. *Eur. J. Pharmacol.* **2001**, *430*, 147-148.
39. Sykes, D. A.; Charlton, S. J. Slow receptor dissociation is not a key factor in the duration of action of inhaled long-acting β_2 -adrenoceptor agonists. *Br. J. Pharmacol.* **2012**, *165*, 2672-2683.
40. Mould, R.; Brown, J.; Marshall, F. H.; Langmead, C. Binding kinetics differentiates functional antagonism of orexin-2 receptor ligands. *Br. J. Pharmacol.* **2014**, *171*, 351-363.
41. Smith, G. F. Medicinal Chemistry by the Numbers: The physicochemistry, thermodynamics and kinetics of modern drug design. *Prog. Med. Chem.* **2009**, *48*, 1-29.
42. Lu, H.; Tonge, P. J. Drug-target residence time: Critical information for lead optimization. *Curr. Opin. Chem. Biol.* **2010**, *14*, 467-474.
43. Hanson, M. A.; Roth, C. B.; Jo, E.; Griffith, M. T.; Scott, F. L.; Reinhart, G.; Desale, H.; Clemons, B.; Cahalan, S. M.; Schuerer, S. C. Crystal structure of a lipid G protein-coupled receptor. *Science* **2012**, *335*, 851-855.
44. Mason, R. P.; Rhodes, D. G.; Herbette, L. G. Reevaluating equilibrium and kinetic binding parameters for lipophilic drugs based on a structural model for drug interactions with biological membranes. *J. Med. Chem.* **1991**, *34*, 869-877.
45. Shaikh, S. A.; Jain, T.; Sandhu, G.; Latha, N.; Jayaram, B. From drug target to leads-sketching a physicochemical pathway for lead molecule design in silico. *Curr. Pharm. Des.* **2007**, *13*, 3454-3470.
46. Miller, D. C.; Lunn, G.; Jones, P.; Sabnis, Y.; Davies, N. L.; Driscoll, P. Investigation of the effect of molecular properties on the binding kinetics of a ligand to its biological target. *MedChemComm* **2012**, *3*, 449-452.
47. Dahl, G.; Åkerud, T. Pharmacokinetics and the drug-target residence time concept. *Drug Discov. Today* **2013**, *18*, 697-707.
48. Copeland, R. A. The dynamics of drug-target interactions: Drug-target residence time and its impact on efficacy and safety. *Expert Opin. Drug Discov.* **2010**, *5*, 305-310.
49. Sager, P. T.; Gintant, G.; Turner, J. R.; Pettit, S.; Stockbridge, N. Rechanneling the cardiac proarrhythmia safety paradigm: A meeting report from the Cardiac Safety Research Consortium. *Am. Heart J.* **2014**, *167*, 292-300.

50. Cavero, I. 13th annual meeting of the safety pharmacology society: Focus on novel technologies and safety pharmacology frontiers. *Expert Opin. Drug Saf.* **2014**, *13*, 1271-1281.
51. Veroli, G. Y. D.; Davies, M. R.; Zhang, H.; Abi-Gerges, N.; Boyett, M. R. hERG inhibitors with similar potency but different binding kinetics do not pose the same proarrhythmic risk: Implications for drug safety assessment. *J. Cardiovasc. Electrophysiol.* **2014**, *25*, 197-207.

Chapter 7

Structure-affinity relationships (SARs) and structure-kinetics relationships (SKRs) of K_v11.1 (hERG) blockers

Zhiyi Yu
Jacobus P. D. van Veldhoven
Julien Louvel
Ingrid M. E. 't Hart
Martin B. Rook
Marcel A. G. van der Heyden
Laura H. Heitman
Adriaan P. IJzerman

Adapted from J. Med. Chem. **2015**, 58, 5916-5929.

Abstract

We explored structure-kinetics relationships and structure-affinity relationships in four series of $K_v11.1$ (hERG) blockers. We learned that despite dramatic differences in affinity and association rates, there were hardly any variations in the dissociation rate constants of these molecules with residence times (RTs) of a few minutes only. Hence, we synthesized sixteen novel molecules, in particular in the pyridinium class of compounds, to further address this peculiar phenomenon. We found molecules with very short RTs (< 1 min) and much longer RTs (> 100 min). This enabled us to construct a k_{on} - k_{off} - K_D kinetic map for all compounds, providing a possible framework for a further and more precise categorization of $K_v11.1$ blockers. Additionally, two representative compounds were tested in patch clamp assays, and their RTs were compared with patch clamp IC_{50} values. Our findings strongly suggest that the simultaneous study of ligand affinity and kinetic parameters may help to explain and predict $K_v11.1$ -mediated cardiotoxicity.

Introduction

Cardiac safety has become a major concern facing the pharmaceutical industries and regulatory agencies over the last several decades. A substantial number of drugs, including both cardiac and non-cardiac medications, have been restricted in their applications or withdrawn from the market due to their $K_v11.1$ -induced cardiotoxicity.^{1,2} The $K_v11.1$ channel, often referred to as the human ether-à-go-go-related gene (hERG) K^+ channel, mediates the most important component of phase 3 repolarization of human ventricular myocytes.³ Blockade of the $K_v11.1$ channel can lead to the prolongation of action potential durations (APDs) and an elevated risk of lethal arrhythmias such as Torsade de Pointes (TdP).⁴ As a consequence, measurement of $K_v11.1$ liability of drugs is a critical component of regulatory guidelines for preclinical QT studies.^{5,6} In this regard, a 30-fold safety margin between $K_v11.1$ IC_{50} and C_{max} values (maximum free plasma concentrations) has been proposed to define the cardiac safety of compounds.⁷ However, this approach of considering IC_{50} values solely is rather arbitrary and crude, which might explain unsatisfactory quantitative predictions and sometimes excludes useful medications that are not problematic.^{6,8,9} For instance, the IC_{50} value of ketoconazole (1-[4-(4-[(2*R*,4*S*)-2-(2,4-Dichlorophenyl)-2-(1*H*-imidazol-1-ylmethyl)-1,3-dioxolan-4-yl] methoxy}phenyl)piperazin-1-yl]ethan-1-one) at the $K_v11.1$ channel is relatively close to its effective therapeutic plasma concentration (11-fold difference), yet it has been proven to be a safe drug in clinical trials due to the fact that this drug has a slow binding rate and is not trapped into the channel.^{9,10} Therefore, knowledge of association and dissociation kinetics of drugs at the $K_v11.1$ channel may be important in defining their propensities to prolong the QT interval.

The concept of structure-affinity relationships (SARs) describing the interdependency between compound structures and binding affinity has been extensively explored over the past decades.^{11,12} However, similar studies illustrating the dependency between compound structures and binding kinetics, coined as structure-kinetics relationships (SKRs), have been less well investigated to date. Recently, drug-target kinetics, in particular receptor-ligand residence times (RTs), have been shown to also determine the therapeutic potential of drug candidates *in vivo*, and to be predictive of drug efficacy and safety.^{13,14} Consequently, there is an emerging awareness of the importance of measuring the kinetics of drug-target interactions. SKRs are now being reported and discussed for ligand binding to G protein-coupled receptors (GPCRs) and enzymes.^{11,15-17} With regard to ion channels, measuring the interaction kinetics of drugs with the $K_v11.1$ channel has already been recommended to be incorporated into Comprehensive *in vitro*

Proarrhythmia Assay (CiPA) strategies to hopefully provide significant improvements of proarrhythmic assessments.^{18, 19} Recent studies have demonstrated that $K_v11.1$ blockers with similar potency (IC_{50} values) but distinct binding kinetics can have markedly diverse proarrhythmic potential, suggesting the necessity to extend $K_v11.1$ inhibition assays with studies on investigating the dynamics of drug-channel interactions.^{1, 8, 9} In addition, particular interest has arisen in the so-called trapping phenomenon, characterized by capture of a drug within the $K_v11.1$ channel and thus a slow dissociation rate from the channel, which harbors an enhanced proarrhythmic risk caused by the drug.^{20, 21} Moreover, a substantial underestimation of cardiac risks has been observed in assessing the ventricular action potential due to neglecting drug-binding kinetics at cardiac $K_v11.1$ channels.⁸ Therefore, there is an urgent need to add the dimension of binding and unbinding kinetics to the more routinely determined affinity values in order to evaluate the arrhythmogenic potential of drug candidates *in vitro*.

In our previous studies, we have successfully validated a [3H]dofetilide competition association assay that can determine the association/dissociation rates and RTs of compounds accurately and efficiently.² In the present study a structurally diverse set of $K_v11.1$ blockers with four different scaffolds were newly synthesized or selected from our in-house library published previously,²²⁻²⁵ and their kinetic parameters (k_{on} , k_{off} , K_D and RTs) as well as affinity (K_i) were determined in [3H]dofetilide binding assays. A k_{on} - k_{off} - K_D ‘kinetic map’ was delineated for all compounds together with three reference compounds: astemizole (1-[(4-fluorophenyl)methyl]-N-[1-[2-(4-methoxyphenyl)ethyl]-4-piperidyl]benzimidazol-2-amine, a notorious $K_v11.1$ blocker), dofetilide (N-[4-(2-{[2-(4-methanesulfonamidophenoxy)ethyl] (methyl)amino}ethyl)phenyl]methanesulfonamide, a specific $K_v11.1$ blocker with restricted usage in the market) and ranolazine ((*RS*)-N-(2,6-dimethylphenyl)-2-[4-[2-hydroxy-3-(2-methoxyphenoxy)-propyl]pipe-razin-1-yl]acetamide, a safe $K_v11.1$ blocker).^{2, 26-28} Two compounds were further tested in a manual patch clamp assay. The SARs and SKRs derived for the compounds in this study reveal new features and aspects of the blockers’ interactions with the $K_v11.1$ channel. This information is expected to provide valuable information for circumventing $K_v11.1$ -induced cardiotoxicity during the preclinical stages of the drug discovery pipeline.

Results and discussion

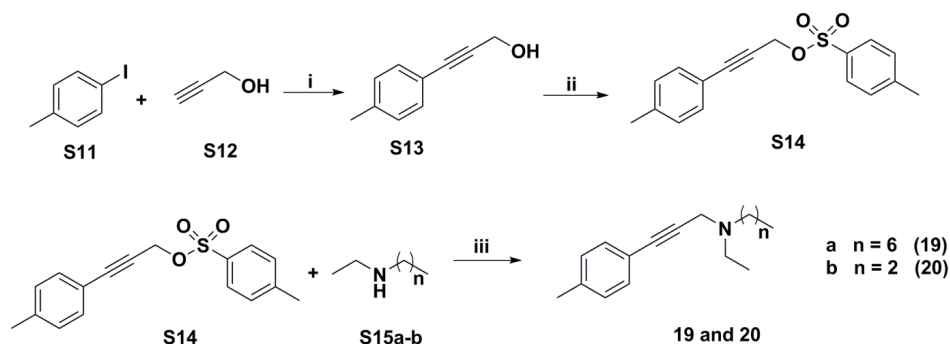
Chemistry

Compounds **19**, **20**, **24**, **25**, **27-30** and **39-46** were newly synthesized in order to

obtain compounds with various RT values besides a diverse range of K_i and k_{on} values. All other compounds were selected from our in-house library based on their distinct affinity and kinetic parameters, and synthesis of these compounds has been reported in our previously published studies.²²⁻²⁵

As shown in **Scheme 1**, clofilium (4-(4-Chlorophenyl)butyl-diethyl-heptylammonium) derivatives **19** and **20** were prepared from 4-iodotoluene in a 3-step sequence as following: Sonogashira cross-coupling of 4-iodotoluene and propargyl alcohol, formation of the corresponding tosylate and displacement of the tosylate with the corresponding secondary amine.²⁴

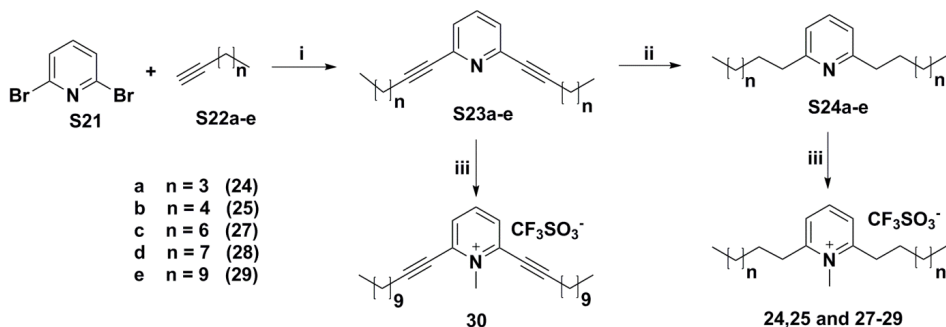
Scheme 1. Synthesis of clofilium derivatives (**19** and **20**)



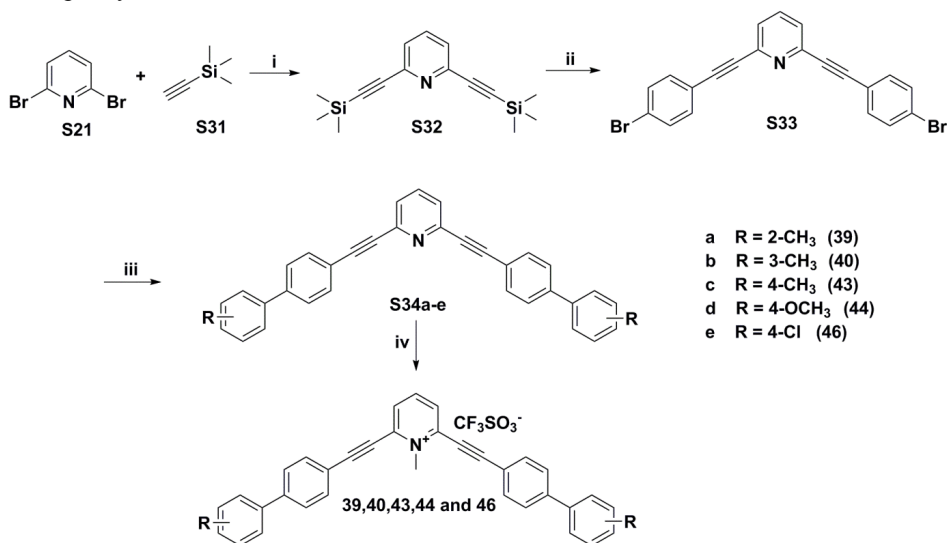
i) $\text{PdCl}_2(\text{PPh}_3)_2$, CuI , Et_3N , THF, r.t.; ii) tosyl chloride, KOH , Et_2O , 0°C to r.t.; iii) K_2CO_3 , DMF, r.t.

To investigate the effect of flexibility in the side chains of aliphatic pyridinium derivatives, several symmetrical 2,6-substituted *N*-methylated-pyridine compounds with different alkyl chain lengths (**24**, **25** and **27-30**) were synthesized according to **Scheme 2**. The first series of compounds (**S23a-e**) were derived from commercially available 2,6-dibromo-pyridine and 1-alkynes with various lengths via a Sonogashira coupling reaction.²⁵ The final compounds (**24**, **25** and **27-29**) were synthesized in relatively high yields by reduction of triple bonds to single bonds and methylation of neutral pyridines. **30** was obtained directly from **S23e** by methylation of the central nitrogen with a good yield of 94%.

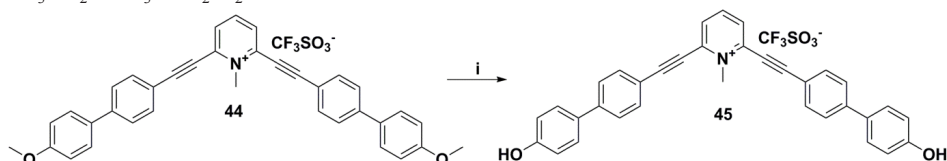
Next, influences of different substituents at the phenyl rings on affinity and kinetic parameters of K_v 11.1 blockers were explored, and a series of substituted biphenyl pyridines (**39-46**) were synthesized. As displayed in **Scheme 3**, compound **S32** was obtained by Sonogashira reaction of 2,6-dibromo-pyridine and ethynyltrimethylsilane with $\text{Pd}(\text{PPh}_3)_4$ and CuI as catalysts instead of $\text{PdCl}_2(\text{PPh}_3)_2$ and CuI displayed in **Scheme 2**.²⁹ After one-pot deprotection and Castro-Stephens coupling with 1-bromo-4-iodobenzene,³⁰ **S32** was converted to **S33** in a low yield that was probably caused by formation of undesired oxidative

Scheme 2. Synthesis of symmetrical 2,6-substituted *N*-methylated pyridines with various alkyl chain lengths

i) $\text{PdCl}_2(\text{PPh}_3)_2$, CuI , Et_3N , r.t.; ii) 10% Pd/C , H_2 , THF, MeOH, r.t.; iii) $\text{CF}_3\text{SO}_2\text{OCH}_3$, CH_2Cl_2 , 0 °C to r.t.

Scheme 3. Synthesis of symmetrical 2,6-substituted *N*-methylated pyridines with different biphenyl substituents

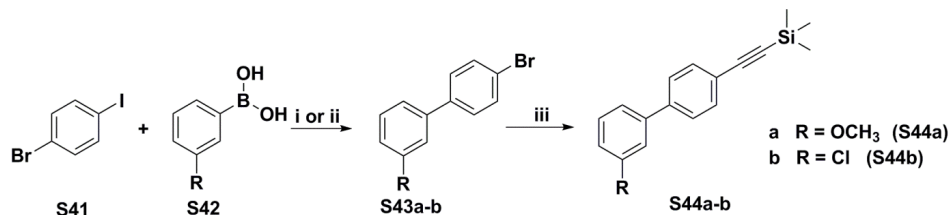
A) Synthesis of compounds **39**, **40**, **43**, **44** and **46**: i) $\text{Pd}(\text{PPh}_3)_4$, CuI , diisopropylamine, toluene, r.t.; ii) CuCl , PPh_3 , potassium benzoate, 1-bromo-4-iodobenzene, DMI, 120 °C; iii) $\text{Pd}(\text{PPh}_3)_4$, K_2CO_3 , toluene, ethanol, substituted-phenylboronic acid, 50 °C; iv) $\text{CF}_3\text{SO}_2\text{OCH}_3$, CH_2Cl_2 , 0 °C to r.t.



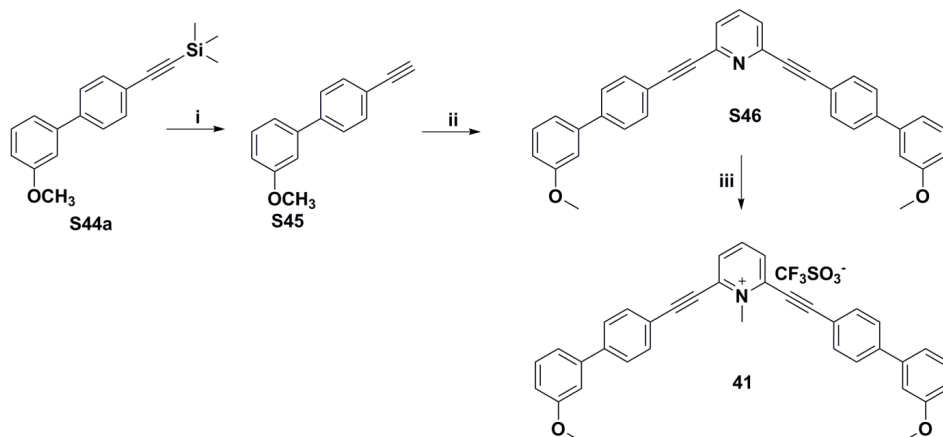
B) Synthesis of compound **45**: i) BBr_3 , CH_2Cl_2 , -78 °C to r.t.

Glaser homo-coupling and intra-polymerization of reacting molecules.³¹ Suzuki reactions were further performed with **S33** and different substituted phenylboronic acids to yield the neutral pyridine compounds (**S34a-e**),³² from which final compounds (**39**, **40**, **43**, **44** and **46**) were derived via methylation of the central nitrogen in moderate to high yields. Subsequently, demethylation of **44** with boron tribromide led to the formation of compound **45**. Notably, synthetic routes mentioned above were not suitable for producing neutral biphenyl pyridines with methoxy and chlorine substituents at the meta-position of the second benzene ring. Hence, **41** and **42** were synthesized by different methods shown in **Scheme 4**. In the first step, Suzuki reactions were applied between the substituted phenylboronic acid and 1-bromo-4-iodobenzene in the presence of different palladium catalysts to produce **S43a** and **S43b** in moderate yields of 27% and 40%, respectively. **S43a** and **S43b** further reacted with ethynyltrimethylsilane through Sonogashira reaction,³³ resulting in high yields of **S44a** and **S44b**. Compound **41** was eventually obtained from **S44a** with a yield of 36% through three steps: deprotection, Sonogashira reaction and methylation, whereas **42** was obtained from **S44b** via a one-pot Sonogashira reaction and methylation in a yield of 45%.

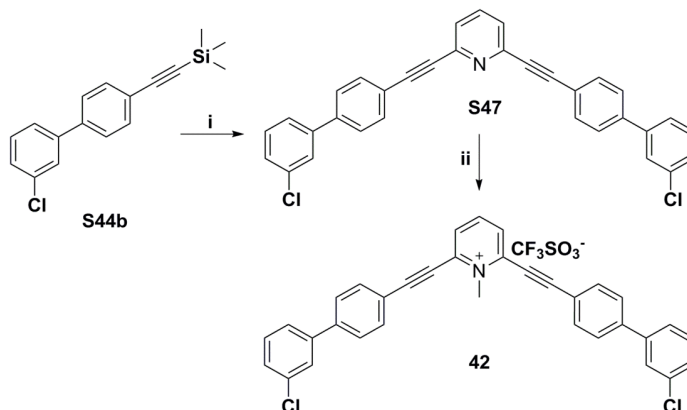
Scheme 4. Synthesis of symmetrical 2,6-substituted *N*-methylated pyridines (**41** and **42**)



A) Synthesis of compounds S44a-b: i) 2M K₂CO₃, Pd(PPh₃)₄, toluene, ethanol, 80 °C; ii) 2M K₂CO₃, Pd(OAc)₂, PPh₃, toluene, ethanol, 80 °C; iii) PdCl₂(PPh₃)₂, CuI, PPh₃, THF, piperidine, 120 °C.



B) Synthesis of compound 41: i) 2M NaOH, diethyl ether, methanol; ii) $\text{PdCl}_2(\text{PPh}_3)_2$, CuI, Et_3N , 2, 6-dibromo-pyridine; iii) $\text{CF}_3\text{SO}_2\text{OCH}_3$, CH_2Cl_2 , 0 °C to r.t.



C) Synthesis of compound 42: i) CuCl, PPh_3 , potassium benzoate, 2, 6-dibromo-pyridine, DMI, 120 °C; ii) $\text{CF}_3\text{SO}_2\text{OCH}_3$, CH_2Cl_2 , 0 °C to r.t.

Biology

The binding affinity and kinetic parameters of all compounds were determined in [^3H]dofetilide competitive displacement and competition association assays on HEK293 cell membranes stably transfected with the $\text{K}_{\text{v}}11.1$ channel (HEK-293 $\text{K}_{\text{v}}11.1$) as described previously by our group.² As shown in **Figure 1**, compounds with a wide range of IC_{50} values demonstrated a monophasic binding behavior instead of a biphasic pattern reported for a [^3H]astemizole binding assay,^{23, 25} indicating that the binding process of compounds followed a single-step bimolecular interaction scheme, and thus, fulfilled the theoretical requirements

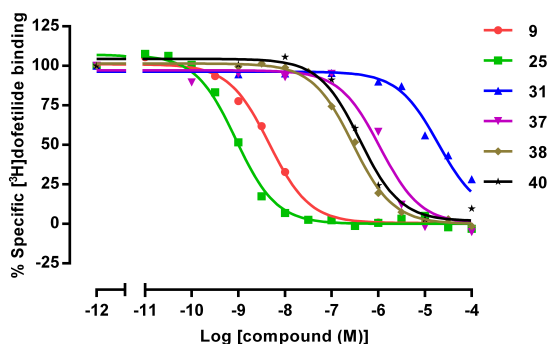


Figure 1. Representative displacement curves of specific [^3H]dofetilide binding by **9**, **25**, **31**, **37**, **38** and **40**. Experiments were performed at 25 °C using 20 μg of HEK293 $\text{K}_{\text{v}}11.1$ membrane protein.

for the Motulsky-Mahan approach to evaluate the binding kinetics of unlabeled ligands.³⁴ **Figure 2** shows the competition association assay for three representative compounds (**31**, **37** and **38**) with different binding kinetics, in particular varying RTs. Compound **37** had a shorter RT than [³H]dofetilide with an association curve slowly and monotonically approaching equilibrium versus time, whereas **38** possessed a longer RT compared to the radioligand, indicated by a typical ‘overshoot’ and then a decline in the association curve.¹⁵ Meanwhile, **31** exhibited a RT similar to dofetilide, evidenced by the same curve shape compared to the association curve of radioligand alone. As the K_i values of all tested compounds calculated from the IC_{50} values mentioned above,³⁵ were in good agreement with kinetically derived K_D data ($K_D = k_{off}/k_{on}$, **Figure 3A**), only K_i values were used to summarize the SARs in this study. The consistency of K_i and K_D values extended our previous finding to a more general observation,² proving the reliability of the [³H]dofetilide competition association assay in assessing the kinetics of unlabeled ligands at the K_v 11.1 channel. In addition, the k_{on} values for all ligands were significantly correlated to their K_i values ($P < 0.0001$, **Figure 3B**), which is in agreement with our published data.² In the same publication affinity and kinetic parameters of the parental compounds dofetilide, E-4031 and clofilium were also measured and reported.² Furthermore, a provisional k_{on} - k_{off} - K_D ‘kinetic map’ was constructed based on the compounds’ varying affinity and kinetic parameters in order to divide these compounds into four different groups (quadrants) of potentially negligible (quadrant **IV**), moderate (quadrant **I** and **III**) and high arrhythmic (quadrant **II**) side effects (**Figure 4**). Finally, we selected two compounds (**21** and **38**) with comparable binding affinity but distinct association and dissociation rates or RTs to be studied in a whole-cell patch clamp assay using the same HEK-293K_v11.1 cells (**Figure 5**).

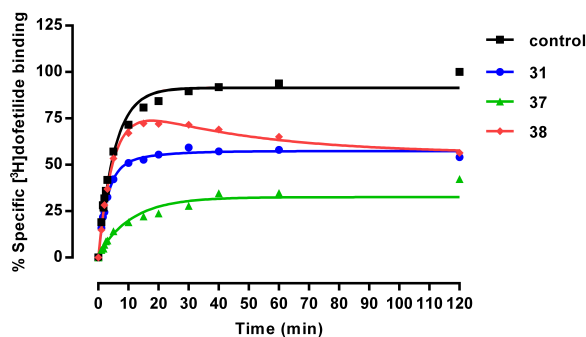


Figure 2. Representative competition association curves of [³H]dofetilide in the absence (control) or presence of unlabeled **31**, **37** and **38** at their IC_{50} value concentrations. Experiments were performed at 25 °C using 20 μ g of HEK293K_v11.1 membrane protein.

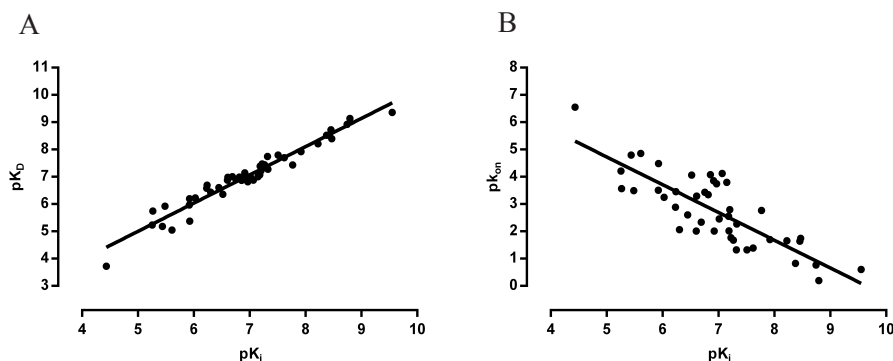


Figure 3. Correlation between pK_i and pK_D (A, $r^2 = 0.95$, $P < 0.0001$) or pK_{on} (B, $r^2 = 0.68$, $P < 0.0001$) values of all tested compounds as obtained from [3H]dofetilide competitive displacement experiments and competition association assays, respectively.

Structure-affinity relationships (SARs) and structure-kinetics relationships (SKRs)

Derivatives of dofetilide

First, we explored the effects of pK_a values of the central nitrogen on affinity, association rates and RTs of compounds **1-8** (Table 1), in which the pK_a values were taken from our previous publication.²² Briefly, increasing the pK_a values via different *N*-alkyl substituents resulted in an increase of affinity of these compounds (**1-5**, **7** and **8**) at the $K_v11.1$ channel. Association rates of these compounds were less sensitive to pK_a alterations but showed a similar trend as the affinity. For instance, compound **8** ($pK_a = -4.95$) displayed the lowest affinity and smallest k_{on} value, while **3** ($pK_a = 9.61$) had the highest affinity and fastest association rate at the channel. These changes corresponded rather well with the principle that reducing pK_a values of the central nitrogen of $K_v11.1$ blockers decreases the proportion of molecules in the protonated form at physiological pH and further make fewer active species available for the productive π -cation interactions with amino acid Tyr652 lining the inner cavity of the channel.^{36, 37} Additionally, zwitterionic compound **6** with a CH_2COOH substituent at the central nitrogen had a lower affinity and slower association rate than **8**, indicating that the negatively charged carboxylate group caused unfavorable interactions of the $K_v11.1$ blocker with the channel.³⁸ Overall, however, the RTs ($1/k_{off}$) of **1-8** were not much impacted by pK_a values of the central nitrogen and zwitterionic propensity of molecules, with values between 0.56 ± 0.06 (**7**) and 3.8 ± 1.0 min (**3**).

Table 1. Binding affinity and kinetic parameters of dofetilide derivatives

Compd	R ₁	R ₂	R ₃	n ₁	n ₂	K _i (nM)	k _{on} (nM ⁻¹ ·min ⁻¹)	k _{off} (min ⁻¹)	K _D (nM)	RT (min)
1	4-NO ₂	4-NO ₂	H	2	2	47±1	0.0054±0.0015	0.27±0.06	53±6	3.7±0.8
2	4-NO ₂	4-NO ₂	CH ₃	2	2	24±2	0.041±0.004	0.82±0.09	20±4	1.2±0.1
3	4-NO ₂	4-NO ₂	CH ₂ CH ₃	2	2	4.2±0.5	0.15±0.06	0.26±0.07	3.0±0.2	3.8±1.0
4	4-NO ₂	4-NO ₂	CH ₂ CH ₂ F	2	2	65±13	0.0096±0.0019	0.30±0.08	41±11	3.3±0.9
5	4-NO ₂	4-NO ₂	CH ₂ CN	2	2	203±6	0.0046±0.0012	0.40±0.05	99±26	2.5±0.3
6	4-NO ₂	4-NO ₂	CH ₂ COOH	2	2	588±31	0.0013±0.0001	0.35±0.10	260±52	2.9±0.8
7	4-NO ₂	4-NO ₂	COCH ₃	2	2	251±32	0.0098±0.0034	1.8±0.2	132±5	0.56±0.06
8	4-NO ₂	4-NO ₂	COCF ₃	2	2	355±14	0.0025±0.0003	0.61±0.09	247±27	1.6±0.3
9	4-NO ₂	4-NO ₂	CH ₃	4	2	1.6±0.3	0.64±0.29	0.26±0.05	0.73±0.39	3.8±0.7
10	4-NO ₂	4-NO ₂	CH ₃	4	1	66±6	0.0028±0.0008	0.22±0.05	85±7	4.5±1.0
11	3, 4-di-Cl	3, 4-di-Cl	CH ₃	2	2	5571±507	(6.2±3.0)×10 ⁻⁵	0.19±0.01	5807±228	5.3±0.2
12	H	4-OCH ₃	CH ₃	2	2	944±58	(5.6±0.9)×10 ⁻⁴	0.30±0.07	591±197	3.3±0.7

Next, the lengths of side alkyl linkers and substituents on the phenyl rings were investigated for the analysis of SARs and SKRs. Comparable to our own studies on distance-related flexibility,^{24, 39} elongation of the alkyl chain between the central nitrogen and phenoxy moiety enhanced the K_v11.1 affinity and association rates (**9** versus **2**), while shortening the other alkyl linker with the phenyl ring lowered the affinity and association rates (**10** versus **2** and **9**). Nonetheless, **9** (RT = 3.8 ± 0.7 min) and **10** (RT = 4.5 ± 1.0 min) demonstrated similar dissociation characteristics at the K_v11.1 channel compared to other compounds in **Table 1**, suggesting that varying chain lengths between the central nitrogen and the two peripheral aromatic rings exerted negligible effects on the dissociation process of this type of ligands from the K_v11.1 channel. In addition, replacement of NO₂ groups on the phenoxy and phenyl rings with 3,4-di-Cl or other groups like OCH₃ dramatically decreased the K_v11.1 affinity and association rates of ligands (**11** and **12** versus **2**). Compound **11** had the lowest affinity (K_i = 5571 ± 507 nM), slowest association rate (k_{on} = 6.2 ± 3.0) × 10⁻⁵ nM⁻¹·min⁻¹) but longest RT of 5.3 ± 0.2 min at the K_v11.1 channel amongst all dofetilide derivatives (**1-12**). This implies that addition of electron-withdrawing groups on the aromatic rings reduces the affinity and association kinetics of K_v11.1 blockers by hampering their π -stacking and hydrophobic interactions with Phe656 and Tyr652 residues lining the pore cavity of the K_v11.1 channel,^{36, 40} whereby this hindered interaction did not obviously disturb the dissociation of ligands. Overall, the association rates of this series of compounds were (negatively) correlated to their K_i values (see also **Figure 3B**), which is in full agreement with our previous finding that ligand affinity for the

K_v 11.1 channel are mainly regulated by the compounds' association rates.² Unlike the widely varying K_i and k_{on} values, RTs of these dofetilide analogues were largely similar.

Derivatives of E-4031

Benzoylpiperidine analogues (**13**, **14** and **16**) demonstrated comparable K_i and k_{on} values at the K_v 11.1 channel. This implicates that: i) electron withdrawing or donating groups at the two peripheral rings, ii) slightly lengthening the carbon chain between the central nitrogen atom and the phenyl ring and iii) permanent protonation of the basic nitrogen, had much smaller effects on K_v 11.1 affinity and association kinetics of E-4031 (N-[4-[1-[2-(6-Methylpyridin-2-yl)ethyl]piperidine-4-carbonyl]phenyl]) derivatives (**Table 2**) compared to the dofetilide series (**Table 1**). However, when the benzoylpiperidine was replaced by benzoylpiperazine (**15**), the K_i value was drastically increased to 5418 ± 374 nM and its association rate was substantially decreased to $(2.7 \pm 0.6) \times 10^{-4}$ nM⁻¹·min⁻¹. Distinct from the variations in affinity and association rates, all E-4031 derivatives displayed comparably short RTs between 2.0 ± 0.5 (**14**) and 2.9 ± 0.8 min (**16**) at the K_v 11.1 channel.

Table 2. Binding affinity and kinetic parameters of E-4031 derivatives

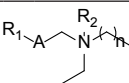
Compd	R ₁	R ₂	X	R ₃	n	K _i (nM)	k _{on} (nM ⁻¹ ·min ⁻¹)	k _{off} (min ⁻¹)	K _D (nM)	RT (min)
13	4-Cl	3, 4-di-Cl	CH	-	2	54±3	0.021±0.009	0.39±0.06	36±22	2.6±0.4
14	4-CH ₃	H	CH	-	3	60±2	0.017±0.003	0.49±0.12	34±14	2.0±0.5
15	H	H	N	-	2	5418±374	(2.7±0.6)×10 ⁻⁴	0.46±0.03	1812±313	2.2±0.1
16	4-Cl	H	CH	CH ₃	2	48±1	0.048±0.022	0.35±0.09	18±9	2.9±0.8

Derivatives of clofilium

Comparable to our own and other studies,^{24, 25, 41} increasing the rigidity by introduction of alkene and alkyne moieties in the chain between the phenyl ring and central nitrogen atom diminished the K_v 11.1 affinity and association rates of clofilium derivatives (**18** and **21** versus **17**, **Table 3**), whereby permanent protonation of the central nitrogen atom with a CH₂CH₃ group resulted in a dramatic enhancement of the affinity and association rate ($K_i = 1.8 \pm 0.2$ nM and $k_{on} = 0.17 \pm 0.07$ nM⁻¹·min⁻¹ for **22**). Therefore, rigidity and protonation play pivotal roles in determining the affinity and association rates of clofilium analogues at

the $K_v11.1$ channel. However, permanently protonating the central nitrogen obviously imposed more significant effects on $K_v11.1$ affinity and association rates, and thus compensated for the negative influences exerted by increasing rigidity via introduction of an alkyne bond (**22** versus **17**). According to different in-silico $K_v11.1$ models, protonation of the central nitrogen atom facilitates the π -cation interaction of ligands with the crucial binding residue (Tyr652) that faces into the S6 domain of the channel.^{36, 42–44} With regard to dissociation characteristics, compounds **17** and **18** had similar RTs at the $K_v11.1$ channel (2.7 ± 0.3 and 2.0 ± 0.5 min for **17** and **18**, respectively), while **21** and **22** having an alkyne moiety displayed longer RTs. Subsequently, two novel compounds with an alkyne group but different side chain lengths (**19** and **20**) were synthesized in order to obtain more variations in dissociation rate constants or RTs. Both compounds exhibited comparably low affinity and slow association rates at the $K_v11.1$ channel, indicating the flexibility adjusted by side chain lengths imposed insignificant effects on weakening $K_v11.1$ affinity and association kinetics of this series of ligands. Likewise, the dissociation rates of **19** and **20** were identical with comparatively longer RTs of 7.7 ± 1.6 and 6.7 ± 2.0 min, respectively. Altogether, introduction of an alkyne group in these clofilium analogues slightly increased their RTs at the $K_v11.1$ channel (**19–22** versus **17–18**). With all these clofilium derivatives (**Table 3**), their association rates illustrated the same overall tendency as the affinity shown in **Figure 3B**. Most importantly, compound **22** showed the highest affinity, fastest association rate and longest RT, implying a strong and prolonged inhibition of the $K_v11.1$ channel.

Table 3. Binding affinity and kinetic parameters of clofilium derivatives

									
Compd	R ₁	R ₂	A	n	K _i (nM)	k _{on} (nM ⁻¹ ·min ⁻¹)	k _{off} (min ⁻¹)	K _D (nM)	RT (min)
17	4-Cl-C ₆ H ₄ CH ₂	-	—CH ₂ CH ₂ —	6	31±5	0.048±0.019	0.37±0.04	16±10	2.7±0.3
18	C ₆ H ₅ CH ₂	-	—HC·CH—	6	119±2	0.0098±0.0042	0.50±0.12	86±45	2.0±0.5
19	4-CH ₃ -C ₆ H ₅	-	—C≡C—	6	3282±613	(3.2±2.0)×10 ⁻⁴	0.13±0.03	1188±122	7.7±1.6
20	4-CH ₃ -C ₆ H ₅	-	—C≡C—	2	1196±141	(3.1±0.7)×10 ⁻⁴	0.15±0.05	637±339	6.7±2.0
21	(C ₆ H ₅) ₂ CH	-	—C≡C—	6	97±13	0.0035±0.0008	0.27±0.06	100±52	3.7±0.8
22	4-Cl-C ₆ H ₅	CH ₂ CH ₃	—C≡C—	6	1.8±0.2	0.17±0.07	0.13±0.04	1.2±0.6	7.7±2.6

Derivatives of pyridinium

As compounds with high lipophilicity can bind to residue Phe656 of the $K_v11.1$ channel through hydrophobic van der Waals interactions as well, peripheral aro-

maticity is not essential for their $K_v11.1$ binding.^{25, 37} In this context, eight aliphatic pyridinium analogues with various side chains (**23-30**) were synthesized or selected to define their SARs and SKRs (**Table 4**). Several general observations can be made: i) permanently protonating the central nitrogen atom by a methyl substituent (**23** versus other compounds), and ii) increasing flexibility via stretching the side alkyl chain from $n = 3$ to $n = 6$ (**24** versus **25-27**) enhanced the $K_v11.1$ affinity of compounds. However, the binding affinity were decreased with iii) the continuous prolongation of side chains up to $n=7$ (**24** versus **28-29**) and iv) replacement of alkane with alkyne (**29** versus **30**). All these results are in excellent agreement with protonation and rigidity rules,⁴⁵ and with the fact that the large aperture at the bottom of the $K_v11.1$ channel cavity has boundaries that accommodate molecules with defined sizes.⁴⁶ Likewise, protonation, flexibility of side chains and rigidity by an alkyne moiety exerted the same overall effects on association rates of these aliphatic pyridines, which implicates that the affinity of aliphatic pyridinium blockers were correlated to their association rate constants at the $K_v11.1$ channel (see also for dofetilide, E-4031 and clofilium derivatives, **Figure 3B**). Intriguingly, RTs in this series of compounds tended to be longer and different from the three other compound classes mentioned above as well as from our previous data.² The newly synthesized compound **29** had the longest RT of 36 ± 2 min, whereas **24** showed the shortest RT with 4.3 ± 0.8 min. In addition, pyridines with *n*-octyl side chains (**23**, RT = 19 ± 1 min) presented a comparable RT to **26** (25 ± 1 min) and **28** (16 ± 4 min) at the $K_v11.1$ channel. Apparently, permanent protonation of the central nitrogen atom (**23** versus **26**) and prolongation of side alkyl chains (**28** versus **23** and **26**) had much less influence on RTs compared to their roles in overall affinity and association rates. It is noteworthy that more rigidity induced by an alkyne moiety diminished the RT to 8.3 ± 1.7 min for **30**. Altogether, increasing rigidity of aliphatic pyridine blockers can decrease their affinity, association rates and RTs simultaneously (**30** versus **29**), and thus, it may provide an efficient solution for circumventing $K_v11.1$ side effects of drug candidates. In a second series of pyridinium analogues (**31-33**), the $K_v11.1$ affinity and association rates were also increased by permanent protonation of the central nitrogen atom (**32** versus **31**) but decreased with an alkyne moiety (**33** versus **32**). However, the RTs of **31-33** were comparable between 7.7 ± 0.7 (**32**) and 9.1 ± 1.7 min (**33**), indicating different dissociation profiles of these compounds compared to aliphatic pyridinium analogues of which rigidity affected the RTs significantly.

Next, a series of biphenyl substituted pyridinium derivatives (**34**, **35** and **38-46**) together with their precursors (**36** and **37**) were synthesized or selected to achieve more variations in RTs. As shown in **Table 4**, permanent protonation and rigidification by alkyne imposed the same effects on $K_v11.1$ affinity as our

findings for other derivatives (**34** versus **35-46** and **35** versus **36-46**, respectively). Additionally, decreasing bulkiness via removal of the second benzene rings or replacing the aromatic phenyl rings close to the central nitrogen atom with cyclohexyl diminished the affinity of $K_v11.1$ blockers (**36-37** versus **38**), possibly caused by reduced π -stacking and hydrophobic interactions.³⁶ Furthermore, introduction of different groups at the second benzene rings lowered their $K_v11.1$ affinity compared to the non-substituted compound (**39-45** versus **38**), indicating a possible steric hindrance of these groups in ligand binding.^{22, 25} Although the k_{on} values showed a comparable decline to affinity because of the increased rigidity by an alkyne moiety (**35** versus **38-46**) and reduction of the aromatic rings (**36** versus **37**), the negative relationship between K_i and k_{on} values was not conspicuous for this series of compounds. For instance, compound **38** showed a smaller K_i value as well as slower association rate than **39**. On the contrary, the RTs of these compounds were significantly increased by replacing ethyl with alkyne (**35** versus **38-46**). Moreover, decreasing bulkiness of these pyridinium analogues led to shorter RTs (**36-37** versus **38-46**). Compound **36** and **37** showed the shortest RTs amongst all these derivatives, providing evidence that reduced bulkiness facilitates unbinding dynamics of $K_v11.1$ blockers at the channel. Our findings are contradictory to the classic ‘foot-in-door’ mechanism, in which bulky residues of $K_v11.1$ blockers prevent the closure of the channel gate and thus promote the channel recovery from blockade.²⁰ The explanation for our results is that less hydrophobic interactions and smaller sizes of molecules can accelerate the dissociation of such ligands from the channel. Compound **38** without any substituents on the benzene rings had the longest RT of 105 ± 4 min at the $K_v11.1$ channel, while substituents at the second benzene rings (**39-46**) often had distinct and lowering effects on RTs. While introducing CH_3 (**40**) and Cl (**42**) at the meta-position did not affect RTs significantly, a substituent at the ortho-position (**39**) of the benzene rings reduced the RT, like at the para-position (**43-46**) but to a lesser extent (**43** versus **39**). Secondly, a methoxy group at the meta-position of the second benzene rings was less favorable for maintaining long RTs (**41** versus **40** and **42**). A similar observation was made for the two compounds with 4- OCH_3 (**44**) and 4- OH (**45**) groups at the second benzene rings, of which RTs were decreased to 24 ± 4 and 19 ± 3 min, respectively, particularly when compared with **46** (63 ± 4 min) and **43** (30 ± 6 min). Collectively, we have successfully obtained compounds with divergent RTs (i.e. approx. 300-fold difference, between **37** and **38**) next to varied affinity and association rates, which provides the possibility to investigate the influence of RTs on *in vivo* cardiotoxicity of $K_v11.1$ blockers.

Table 4. Binding affinity and kinetic parameters of pyridinium analogues

Compd	A	R	n	K _i (nM)	k _{on} (nM ⁻¹ ·min ⁻¹)	k _{off} (min ⁻¹)	K _D (nM)	RT (min)
23	—CH ₂ CH ₂ —	-	5	36870±10861	(2.8±0.4)×10 ⁻⁷	0.052±0.002	190546±27585	19±1
24	—CH ₂ CH ₂ —	CH ₃	3	12±1	0.020±0.005	0.23±0.04	12±0	4.3±0.8
25	—CH ₂ CH ₂ —	CH ₃	4	0.28±0.01	0.25±0.08	0.10 ± 0.02	0.44±0.05	10± 2
26	—CH ₂ CH ₂ —	CH ₃	5	3.5±0.3	0.023±0.004	0.040±0.002	1.9±0.5	25±1
27	—CH ₂ CH ₂ —	CH ₃	6	3.4±0.9	0.018±0.003	0.069±0.005	4.0±0.6	14±1
28	—CH ₂ CH ₂ —	CH ₃	7	17±3	0.0017±0.0002	0.064±0.015	37±5	16±4
29	—CH ₂ CH ₂ —	CH ₃	9	108±10	(1.8±0.2)×10 ⁻⁴	0.028±0.001	153±10	36±2
30	—C≡C—	CH ₃	9	1179±297	(3.3±1.1)×10 ⁻⁵	0.12±0.02	4258±1139	8.3±1.7

Compd	A	R	K _i (nM)	k _{on} (nM ⁻¹ ·min ⁻¹)	k _{off} (min ⁻¹)	K _D (nM)	RT (min)
31	—CH ₂ CH ₂ —	-	3654±81	(1.6±0.3)×10 ⁻⁵	0.11±0.01	6631±536	9.1±0.8
32	—CH ₂ CH ₂ —	CH ₃	6.0±0.5	0.022±0.003	0.13±0.01	6.1±1.2	7.7±0.7
33	—C≡C—	CH ₃	2460±262	(1.4±0.4)×10 ⁻⁵	0.11±0.02	8877±1904	9.1±1.7

Compd	R ₁	A	R ₂	B	K _i (nM)	k _{on} (nM ⁻¹ ·min ⁻¹)	k _{off} (min ⁻¹)	K _D (nM)	RT (min)
34	-	—C≡C—	C ₆ H ₅	C ₆ H ₄	>100 μM	n.d.	n.d.	n.d.	n.d.
35	CH ₃	—CH ₂ CH ₂ —	C ₆ H ₅	C ₆ H ₄	63±9	0.0016±0.0003	0.098±0.021	60±4	10±2
36	CH ₃	—C≡C—	H	C ₆ H ₁₀	1208±36	(3.3±1.2)×10 ⁻⁴	0.30±0.05	1074±268	3.3±0.6
37	CH ₃	—C≡C—	H	C ₆ H ₄	498±107	0.0086±0.0020	2.9±0.3	368±61	0.34±0.04
38	CH ₃	—C≡C—	C ₆ H ₅	C ₆ H ₄	86±12	(7.5±1.0) ×10 ⁻⁵	0.0095±0.0003	132±19	105±4
39	CH ₃	—C≡C—	2-CH ₃ -C ₆ H ₅	C ₆ H ₄	577±41	(3.5±0.3)×1 ⁻⁴	0.071±0.004	203±19	14±1
40	CH ₃	—C≡C—	3-CH ₃ -C ₆ H ₅	C ₆ H ₄	122±15	(1.4±0.2)×10 ⁻⁴	0.010±0.003	72±18	100±30
41	CH ₃	—C≡C—	3-OCH ₃ -C ₆ H ₅	C ₆ H ₄	176±10	(3.7±0.4)×10 ⁻⁴	0.047±0.009	125±13	21± 4
42	CH ₃	—C≡C—	3-Cl-C ₆ H ₅	C ₆ H ₄	139±20	(8.3±0.9)×10 ⁻⁵	0.011±0.002	135±14	91±17
43	CH ₃	—C≡C—	4-CH ₃ -C ₆ H ₅	C ₆ H ₄	303±49	(8.6±1.0)×10 ⁻⁵	0.033±0.006	440±78	30±6
44	CH ₃	—C≡C—	4-OCH ₃ -C ₆ H ₅	C ₆ H ₄	247±44	(4.5±0.2)×10 ⁻⁴	0.042±0.007	105±16	24± 4
45	CH ₃	—C≡C—	4-OH-C ₆ H ₅	C ₆ H ₄	153±32	(5.1±0.7)×10 ⁻⁴	0.053±0.008	103±3	19±3
46	CH ₃	—C≡C—	4-Cl-C ₆ H ₅	C ₆ H ₄	71±9	(1.6±0.2)×10 ⁻⁴	0.016±0.001	100±10	63±4

n.d.: not detectable.

Kinetic map

Using the kinetic data in **Tables 1-4**, we plotted the dissociation rates (pk_{off} , y axis) against association rates (pk_{on} , x axis) of all our compounds together with three reference compounds (astemizole, dofetilide and ranolazine) into a kinetic map (**Figure 4**). The parallel diagonal dashed lines represent the kinetically derived K_D values. In this $k_{\text{on}}-k_{\text{off}}-K_D$ map, compounds with the same affinity or association rates may have divergent dissociation rates or RTs, and vice versa. Therefore, risk assessment and possible mitigation of inhibitory efficacies of $K_v11.1$ blockers should take association rates (k_{on}) and RTs into account rather than affinity alone. In this context, all ligands were divided into four quadrants (**I**, **II**, **III** and **IV**) according to our hypothesis that high affinity, fast association rates and slow dissociation rates (long RTs) contribute together to serious $K_v11.1$ -induced cardiotoxicity. The affinity and kinetic parameters of astemizole, dofetilide and ranolazine were derived from our previous investigation.² Astemizole was distributed into quadrant **II**, as it is a specific $K_v11.1$ blocker and has been withdrawn from the market.^{26, 27} On the other hand, ranolazine was assigned to quadrant **IV**, since it inhibits the $K_v11.1$ channel but does not cause proarrhythmic events.²⁸ In addition, dofetilide is restrictedly used in the United States due to its low and finite TdP by blocking the $K_v11.1$ channel,^{27, 47, 48} and consequently, it was scattered into quadrant **III**. Obviously, compounds in quadrant **II** have high affinity ($K_D < 316$ nM), fast association rates ($k_{\text{on}} > 3.2 \times 10^{-4}$ nM⁻¹·min⁻¹) and slow dissociation rates or long RTs (> 10 min) at the $K_v11.1$ channel, indicating that they may cause serious arrhythmias via blockade of the channel. On the other hand, quadrant **IV** comprises compounds with low affinity ($K_D > 316$ nM), slow association rates ($k_{\text{on}} < 3.2 \times 10^{-4}$ nM⁻¹·min⁻¹) and fast dissociation rates or short RTs (< 10 min) at the channel, suggesting their possible cardiac safety in terms of $K_v11.1$ inhibition. Quadrants **I** and **III** encompass moderately active $K_v11.1$ blockers with either relatively low affinity, slow k_{on} ($< 3.2 \times 10^{-4}$ nM⁻¹·min⁻¹) and k_{off} (RT > 10 min, **I**) or comparatively high affinity, fast k_{on} ($> 3.2 \times 10^{-4}$ nM⁻¹·min⁻¹) and k_{off} (RT < 10 min, **III**). Most likely these two different classes of compounds have modest $K_v11.1$ -related cardiac side effects. Taken together, this arbitrary and provisional kinetic map that can be further extended with other suspected $K_v11.1$ blockers sheds light on $K_v11.1$ -induced cardiotoxicity of drugs by bringing together their affinity as the traditional safety parameter with their kinetic parameters of association and dissociation rates (or RTs) at the channel. Therefore, a similar map would provide valuable information on how to accurately and comprehensively evaluate and further circumvent $K_v11.1$ liability of drug candidates in the future.

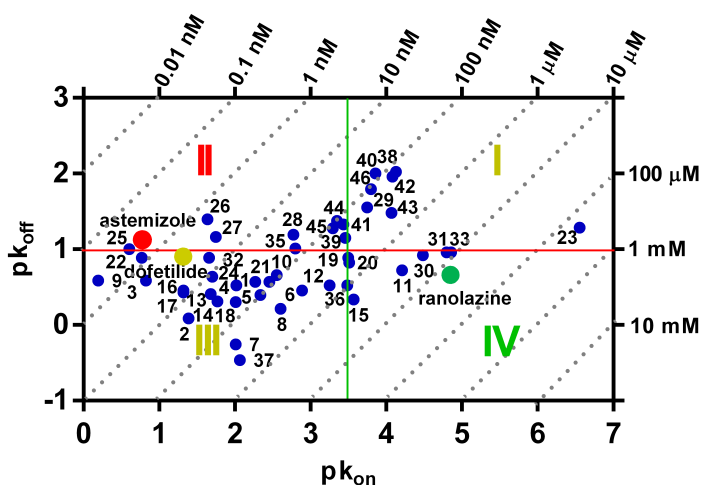


Figure 4. Kinetic map of all tested compounds in which the dissociation rate (pK_{off} , k_{off} ·min⁻¹) is plotted on the y axis, whereas the association rate (pK_{on} , k_{on} ·nM⁻¹·min⁻¹) is plotted on the x axis. Identical K_D values can result from different combinations of k_{on} and k_{off} values ($K_D = k_{\text{off}}/k_{\text{on}}$, diagonal dashed lines). Quadrants (I, II, III, IV) are arbitrarily defined by red horizontal and green vertical lines according to the varied k_{on} , k_{off} and K_D values in combination with three reference compounds astemizole (red dot), dofetilide (yellow dot) and ranolazine (green dot). The intersection of red and green lines are arranged on the diagonal dashed line representing a K_D value of 316 nM, while their intercepts with y and x axis are 1 (RT = 10 min) and 3.5 ($k_{\text{on}} = 3.2 \times 10^{-4}$ nM⁻¹·min⁻¹), respectively. Note that the kinetic parameters of compound **34** could not be determined due to its rather low K_v 11.1 affinity and thus is excluded in this map.

Patch clamp study

A whole-cell voltage patch clamp assay was applied to determine the functional hERG current blockade by **21** and **38**, two compounds with similar affinity but different RTs. As shown in **Figure 5A**, the IC_{50} values for **21** and **38** from their concentration-effect curves in the patch clamp assay were 182 ± 6 and 107 ± 6 nM, respectively. However, **21** and **38** had almost identical affinity in the radioligand binding assay with K_i values of 97 ± 13 and 86 ± 12 nM, respectively. RTs of ligands have been found to be correlated to their efficacies in functional assays rather than affinity at the adenosine A_{2A} receptor.⁴⁹ Thus, we surmised that the difference in IC_{50} values obtained in functional patch clamp assays for these two compounds might be caused by their different RTs, with **38** (long RT of 105 ± 4 min) displaying a higher potency in K_v 11.1 current inhibition than **21** (short RT

of 3.7 ± 0.8 min). The time-dependent inhibition of the $K_v11.1$ current for **21** and **38** was also assessed in the whole-cell patch clamp assay. As shown in **Figure 5B**, compound **21** with a faster association rate ($0.0035 \pm 0.0008 \text{ nM}^{-1} \cdot \text{min}^{-1}$) in the radioligand binding assay almost completely inhibited $K_v11.1$ currents within 10 min, whereas 15 min was required for **38** ($k_{\text{on}} = (7.5 \pm 1.0) \times 10^{-5} \text{ nM}^{-1} \cdot \text{min}^{-1}$) to approach the equilibrated current inhibition. Therefore, association rates measured in the [^3H]dofetilide competition association assay may be linked to the current inhibition rates of compounds in the functional patch clamp experiments. Although different wash-in times for $K_v11.1$ blockers have been observed on an automated patch clamp platform before,²³ this is the first time to interpolate the radioligand binding parameters, especially for the association and dissociation rates, into functional data derived from patch clamp assays.

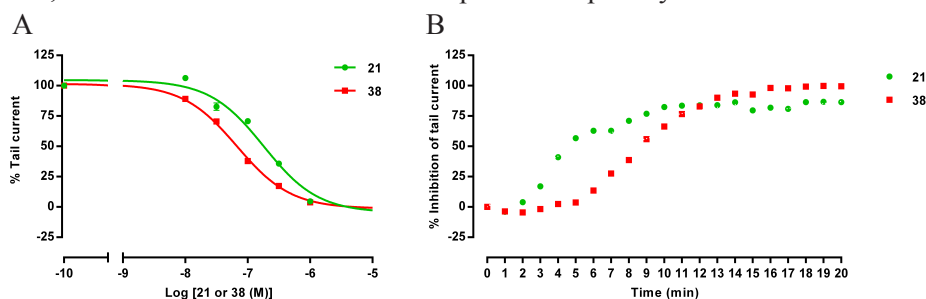


Figure 5. (A) Concentration-dependent inhibition of **21** and **38** for the $K_v11.1$ tail current in electrophysiological experiments. (B) Time-dependent inhibition of the $K_v11.1$ tail current by **21** and **38** ($1 \mu\text{M}$). Experiments were performed at room temperature using HEK293 $K_v11.1$ cells.

Conclusion

Although affinity and association rates of compounds at the $K_v11.1$ channel have been found to differ vastly and are correlated to each other, this study is the first to verify that $K_v11.1$ blockers can possess very different RTs, with up to a more than 300-fold difference (**37** versus **38**) at the channel. Furthermore, this comprehensive investigation on derivatives of dofetilide, E-4031, clofilium and pyridinium over a range of scaffolds is the first to illustrate the impact of several parameters outlined above on association rates and RTs of compounds at the $K_v11.1$ channel in addition to their binding affinity. Notably, unlike the consistency of SARs for all compounds, SKRs are more chemical scaffold-dependent, in particular the structure-RT relationships. According to these findings and helped by the substantial differences in affinity, association and dissociation rate constants or RTs in the current sets of compounds, we delineated a $k_{\text{on}}-k_{\text{off}}-K_D$ kinetic

map, and divided all these compounds into four quadrants (toxic for quadrant **II**, safe for quadrant **IV** and suspicious for quadrant **I** and **III** in **Figure 4**), which might provide valuable information for pharmaceutical researchers to devise better strategies for assessing $K_v11.1$ liability. Additionally, the association rates of two selected compounds were found to correspond well with their current block rates in the patch clamp studies, and their distinct RTs are a possible reason for their differences in functional potency when compared to their binding affinity. Although far from complete this analysis further indicates that kinetic parameters (k_{on} and RTs) should be taken into consideration as well as affinity (K_i) during the investigation of $K_v11.1$ -mediated adverse reactions. To conclude, the new finding of large variations in RTs promotes the extensive analysis of structure-RT relationships, and the combination of SARs and SKRs opens a new avenue for medicinal chemists to more efficiently design new chemical entities with low or negligible $K_v11.1$ -induced cardiotoxicity.

Experimental section

Chemistry

All commercially available chemicals and solvents were used without purification, except for ethyl acetate, which was distilled before usage. Demineralized water will be referred to as H_2O , unless otherwise stated. Reactions were monitored by thin-layer chromatography (TLC) using TLC silica gel 60 F254 aluminum sheets. TLC visualization was performed by a LAMAG UV-light at a wavelength of 254 or 366 nm. Grace Davison Davisil silica column material (LC60A 30-200 micron) was used for purification by column chromatography. 1H and ^{13}C NMR spectra were recorded on a Bruker AV400 or AV600 spectrometer. Deuterated solutions $CDCl_3$, DMSO or MeOD were used for sample preparation. Chemical shifts (δ) are given in ppm and coupling constants (J) in Hertz. Trimethylsilane was used as internal standard for calibrating chemical shift for 1H , ^{13}C NMR spectroscopy. HPLC-analysis was carried out on a Phenomenex Gemini reversed-phase C18 column (50 mm \times 4.6 mm \times 3 μm) coupled to a UV-detector at 254 nm. Final compounds were dissolved in either a mixture of acetonitrile:tert-butanol:water (1:1:1) or in pure acetonitrile and were eluted from the column at a flow rate of 1.3 mL \cdot min $^{-1}$ with 10/90 acetonitrile/water + 10% TFA, decreasing polarity of this mixture in time. LC-MS analysis was performed on an LCQ Advantage Max (Thermo Finnigan) ion-trap spectrometer (ESI $^+$) coupled to a Surveyor HPLC system (Thermo Finnigan) equipped with a C18 column (Phenomenex Gemini, 50 mm \times 4.6 mm, 5 μm). A linear gradient of 10/90 acetonitrile/water + a constant

10% of an 1% TFA in water solution was used as the mobile system. The purity of all final compounds was > 95%. High-resolution mass spectral analysis (HRMS) was performed by Leiden Institute of Chemistry by direct injection (2 μ L of a 2 μ M solution in water/MeCN; 50/50; v/v and 0.1% formic acid) on a LTQ-Orbitrap FTMS operated in a positive ionization mode with an electrospray ionization (ESI) source (source voltage 3.5 kV, sheath gas flow 10%, capillary temperature 275 °C) with resolution $R = 60000$ at m/z 400 (mass range $m/z = 150$ -2000) and calibrated for dioctylphthalate ($m/z = 391.28428$). All microwave reactions were performed in a Biotage initiator 2.5 in a sealed microwave vial.

3-(*P*-tolyl)prop-2-yn-1-ol (S13). To a solution of 4-iodotoluene (5.45 g, 25 mmol) in THF (33 mL) and Et₃N (7.3 mL) were added PdCl₂(PPh₃)₂ (35 mg, 0.5 mmol) and CuI (327 mg, 1.7 mmol). The mixture was stirred for 30 minutes and a solution of propargyl alcohol (1.48 mL, 25 mmol) in THF (10 mL) was added dropwise. The mixture was stirred at r.t. for 12 hours and filtered on Celite. The solvents were evaporated and the crude residue was purified by flash chromatography on silica gel (33% EtOAc-Petroleum ether) to afford pure **S13** (2.54 g, 70%) as an oil. Spectral data were in agreement with literature.⁵⁰

3-(*P*-tolyl)prop-2-yn-1-yl 4-methylbenzenesulfonate (S14). To a stirred solution of **S13** (1 g, 6.8 mmol) in diethylether (45 mL) at 0 °C was added tosyl chloride (1.6 g, 8.2 mmol) followed, portionwise, by freshly powdered KOH (3.8 g, 68 mmol). After the addition was complete, the reaction mixture was stirred at room temperature for 3.5 h and then poured into water (90 mL). The layers were separated and the aqueous phase was extracted with EtOAc (3 \times 40 mL). The combined organic extract was dried, filtered, concentrated *in vacuo* and chromatographed (25% EtOAc - Petroleum ether) to obtain the title compound **S14** (1.9 g, 91%). ¹H NMR (400 MHz, CDCl₃) δ 7.87 (d, $J = 8.2$ Hz, 2H), 7.34 (d, $J = 8.2$ Hz, 2H), 7.17 (d, $J = 8.1$ Hz, 2H), 7.11 (d, $J = 8.1$ Hz, 2H), 4.97 (s, 2H), 2.42 (s, 3H), 2.36 (s, 3H) ppm.

General Sonogashira coupling procedure (S23a-e).

PdCl₂(PPh₃)₂ (148 mg, 0.21 mmol, 0.05 eq.) and CuI (121 mg, 0.63 mmol, 0.15 eq.) was added to a solution of 2,6-dibromopyridine (1000 mg, 4.22 mmol, 1.0 eq.) in Et₃N (10 mL) and stirred for 30 min under a nitrogen atmosphere. The appropriate alkyne (10.1 mmol, 2.4 eq.) was added drop wise, and the mixture was stirred overnight at room temperature after which full conversion was shown by TLC. The reaction mixture was adsorbed on silica and purification by FCC yielded the desired compound.

2,6-di(hex-1-ynyl)pyridine (S23a). Prepared from hex-1-yne. FCC (petroleum ether: ethyl acetate 60:1 to 20:1) gave the desired product in a yield of (635

mg) 63%; ^1H NMR (400MHz, CDCl_3): δ 7.52 (t, J = 8.0 Hz, 1H), 7.25 (d, J = 8.0 Hz, 2H), 2.42 (t, J = 7.0 Hz, 4H), 1.64-1.56 (m, 4H), 1.52-1.42 (m, 4H), 0.93 (t, J = 7.4 Hz, 6H).

2,6-Di(hept-1-ynyl)pyridine (S23b). Prepared from hept-1-yne. FCC (petroleum ether:dichloromethane 4:1 tot 2:1) gave the desired product in a yield of (241 mg) 21%. ^1H NMR (400MHz, CDCl_3): δ 7.53 (t, J = 7.6 Hz, 1H), 7.25 (d, J = 7.6 Hz, 2H), 2.41 (t, J = 6.8 Hz, 4H), 1.64-1.60 (m, 4H), 1.44-1.31 (m, 8H), 0.91 (t, J = 7.2 Hz, 6H).

2,6-Di(non-1-ynyl)pyridine (S23c). Prepared from non-1-yne. FCC (petroleum ether:dichloromethane 30:1 tot 4:1) gave the desired product in a yield of (247 mg) 18%. ^1H NMR (400MHz, CDCl_3): δ 7.52 (t, J = 7.6 Hz, 1H), 7.25 (d, J = 8.0 Hz, 2H), 2.41 (t, J = 7.2 Hz, 4H), 1.65-1.57 (m, 4H), 1.45-1.39 (m, 4H), 1.35-1.26 (m, 12H), 0.89 (t, J = 6.4 Hz, 6H).

2,6-Di(dec-1-ynyl)pyridine (S23d). Prepared from dec-1-yne. FCC (petroleum ether:dichloromethane 5:1 to 3:1) gave the desired product in a yield of (210 mg) 14%. ^1H NMR (400MHz, CDCl_3): δ 7.53 (t, J = 8.0 Hz, 1H), 7.25 (d, J = 7.6 Hz, 2H), 2.41 (t, J = 7.2, 4H), 1.65-1.57 (m, 4H), 1.45-1.39 (m, 4H), 1.30-1.24 (m, 16H), 0.88 (t, J = 6.8 Hz, 6H).

2,6-Di(dodec-1-ynyl)pyridine (S23e). Prepared from dodec-1-yne. FCC (petroleum ether : dichloromethane 5:1 to 2:1) gave the desired product in a yield of 79% (1131 mg). ^1H NMR (400MHz, CDCl_3): δ 7.53 (t, J = 7.6 Hz, 1H), 7.25 (d, J = 8.0 Hz, 2H), 2.41 (t, J = 7.2 Hz, 4H), 1.64-1.57 (m, 4H), 1.44-1.39 (m, 4H), 1.32-1.26 (m, 24H), 0.88 (t, J = 6.4 Hz, 6H).

General procedure for reduction of pyridine alkynes (S24a-e).

The appropriate alkyne (**S23a**) (600 mg, 2.52 mmol) was dissolved in THF (3 mL) and MeOH (3 mL) under a N_2 atmosphere. 10% Pd/C (120 mg, 1.14 mmol) was added and H_2 was introduced via a balloon. The mixture was stirred overnight at r.t. after which the reaction mixture was filtered over Celite. The filtrate were concentrated under reduced pressure and FCC (petroleum ether:ethyl acetate 20:1) gave the desired compound.

2,6-Dihexylpyridine (S24a). Prepared from **S23a** and purified by FCC (petroleum ether:ethyl acetate 20:1) which gave the desired product in a yield of (469 mg) 75%. ^1H NMR (400MHz, CDCl_3): δ 7.48 (t, J = 7.6 Hz, 1H), 6.94 (d, J = 7.6 Hz, 2H), 2.75 (t, J = 7.6 Hz, 4H), 1.73-1.65 (m, 4H), 1.39-1.26 (m, 12H), 0.88 (t, J = 6.8 Hz, 6H).

2,6-Diheptylpyridine (S24b). Prepared from **S23b** and purified by FCC (petroleum ether:dichloromethane 4:1 to 1:2) which gave the desired product in a yield of (106 mg) 43%. ^1H NMR (400MHz, CDCl_3): δ 7.47 (t, J = 7.6 Hz, 1H),

6.93 (d, $J = 7.6$ Hz, 2H), 2.75 (t, $J = 7.6$ Hz, 4H), 1.71-1.66 (m, 4H), 1.34-1.23 (m, 16H), 0.87 (t, $J = 6.8$ Hz, 6H).

2,6-Dinonylpyridine (S24c). Prepared from **S23c** and purified by FCC (petroleum ether:dichloromethane 4:1 to 1:2) which gave the desired product in a yield of (91 mg) 78%. ^1H NMR (400MHz, CDCl_3): δ 7.47 (t, $J = 7.6$ Hz, 1H), 6.93 (d, $J = 7.6$ Hz, 2H), 2.75 (t, $J = 8.0$ Hz, 4H), 1.73-1.65 (m, 4H), 1.36-1.16 (m, 24H), 0.86 (t, $J = 4.4$ Hz, 6H).

2,6-Didecylpyridine (S24d). Prepared from **S23d** and purified by FCC (petroleum ether:dichloromethane 3:1 to 1:1) which gave the desired product in a yield of (153 mg) 71%. ^1H NMR (400MHz, CDCl_3): δ 7.48 (t, $J = 7.6$ Hz, 1H), 6.94 (d, $J = 7.6$ Hz, 2H), 2.74 (t, $J = 8.0$ Hz, 4H), 1.73-1.65 (m, 4H), 1.32-1.25 (m, 28H), 0.88 (t, $J = 6.8$ Hz, 6H).

2,6-Didodecylpyridine (S24e). Prepared from **S23e** and purified by FCC (petroleum ether:dichloromethane 4:1 to 1:1) which gave the desired product in a yield of (440 mg) 86%. ^1H NMR (400MHz, CDCl_3): δ 7.48 (t, $J = 7.6$ Hz, 1H), 6.94 (d, $J = 7.6$ Hz, 2H), 2.75 (t, $J = 7.6$ Hz, 4H), 1.73-1.65 (m, 4H), 1.35-1.25 (m, 36H), 0.88 (t, $J = 6.8$ Hz, 6H).

2,6-Bis((trimethylsilyl)ethynyl)pyridine (S32). 2,6-dibromopyridine (9.00 g, 38.0 mmol), $\text{Pd}(\text{PPh}_3)_4$ (2.20 g, 1.90 mmol), CuI (361 mg, 1.90 mmol), diisopropylamine (9 mL) and toluene (100 mL) were stirred at r.t. and trimethylsilylacetylene (13.0 mL, 91.2 mmol) was added. The mixture was stirred overnight followed by filtration over Celite using CH_2Cl_2 . The filtrate was concentrated under reduced pressure, dissolved in CH_2Cl_2 , and washed with an 1M aqueous NH_4Cl solution. The organic layer was dried over MgSO_4 , filtered and evaporated to dryness. Yield quantitative and used in the next step without further purification. ^1H NMR (CDCl_3): δ 7.61 (t, $J = 8.0$ Hz, 1H), 7.38 (d, $J = 7.6$ Hz, 2H), 0.25 (s, 18H).

2,6-Bis((4-bromophenyl)ethynyl)pyridine (S33). To a solution of CuCl (346 mg, 3.50 mmol), PPh_3 (918 mg, 3.50 mmol) and potassium benzoate (11.3 g, 70.7 mmol) in 38 mL DMI (1,3-dimethyl-2-imidazolidinone) were added compound **S32** (9.60 g, 35.4 mmol) and 1-bromo-4-iodobenzene (20.0 g, 70.7 mmol) at r.t. The mixture was stirred at 120 °C for 4 h after which full consumption of **S32** was seen. The mixture was cooled down, quenched with a 3M HCl (aq.) solution. The organics were extracted with CH_2Cl_2 , and washed with subsequently NaHCO_3 and brine. The organic layer was dried over MgSO_4 , filtered and the solvents were evaporated under vacuum. FCC (petroleum ether:dichloromethane 10:1 to 2:1) gave the desired product. Yield (4.44 g) 29%; ^1H NMR (CDCl_3): δ 7.70 (t, $J = 8.0$ Hz, 1H), 7.52-7.45 (m, 10H).

General Suzuki reaction procedure yielding compounds S34a-e.

Compound **S33** (0.2 mmol, 1.0 eq.), the respective substituted-phenylboronic acid (0.4 mmol, 2.0 eq.), 2M K₂CO₃ (10 eq.) (aq.) were dissolved in a mixture of 3 mL toluene and 0.4 mL of ethanol. Pd(PPh₃)₄ (0.02 mmol, 0.1 eq.) were added and the mixture was heated in the microwave at 100 °C under a nitrogen atmosphere for 24 h. After cooling down to room temperature, EtOAc was added and a precipitate was formed (**S34b-e**). The precipitate was collected by filtration, resulting in the desired products.

2,6-Bis((2'-methylbiphenyl-4-yl)ethynyl)pyridine (S34a). Prepared from 2-methylphenyl boronic acid according to the general procedure, but a precipitate was not formed after addition of EtOAc. The organic layer was washed with a 2 × 0.5 M NaOH solution, dried over MgSO₄, filtered and the solvents were evaporated *in vacuo*. Used this as a crude mixture in the next reaction. Yield (37 mg) 50%. ESI-MS: 460.2 [M+H]⁺.

2,6-Bis((3'-methylbiphenyl-4-yl)ethynyl)pyridine (S34b). Prepared from 3-methylphenyl boronic acid according to the general procedure. Yield (17 mg) 16%; ¹H NMR (CDCl₃): δ 7.72-7.67 (m, 5H), 7.60 (d, *J* = 8.4 Hz, 4H), 7.50 (d, *J* = 8.0 Hz, 2H), 7.42 (d, *J* = 8.8 Hz, 4H), 7.35 (t, *J* = 7.2 Hz, 2H), 7.19 (d, *J* = 7.2 Hz, 2H), 2.43 (s, 6H).

2,6-Bis((4'-methylbiphenyl-4-yl)ethynyl)pyridine (S34c) was obtained as a white solid. Yield (13 mg) 18%; ¹H NMR (CDCl₃): δ 7.72-7.70 (m, 5H), 7.59 (d, *J* = 8.0 Hz, 4H), 7.52-7.49 (m, 6H), 7.30-7.24 (m, H), 2.41 (s, 6H).

2,6-Bis((4'-methoxybiphenyl-4-yl)ethynyl)pyridine (S34d). Prepared from 4-methoxyphenyl-boronic acid according to the general procedure. Yield (55 mg) 49%; ¹H NMR (CDCl₃): δ 7.72-7.64 (m, 5H), 7.57-7.45 (m, 9H), 7.00 (d, *J* = 8.0 Hz, 4H), 7.30-7.24 (m, H), 2.41 (s, 6H).

2,6-Bis((4'-chlorobiphenyl-4-yl)ethynyl)pyridine (S34e). Prepared from 4-chlorophenyl boronic acid according to the general procedure. Yield (56 mg) 49%; ¹H NMR (CDCl₃): δ 7.74-7.65 (m, 5H), 7.59-7.47 (m, 10H), 7.43 (d, *J* = 8.4 Hz, 4H).

4'-Bromo-3-methoxybiphenyl (S43a). Palladium acetate (40.0 mg, 0.18 mmol) was added to mixture of 1-bromo-4-iodobenzene (500 mg, 1.77 mmol), 3-methoxy-phenylboronic acid (269 mg, 1.77 mmol), triphenylphosphine (139 mg, 0.53 mmol), a 2M K₂CO₃ aqueous solution (5 mL) in toluene (15 mL) and EtOH (2 mL). This mixture was heated at 50 °C for 24 h., after which it was cooled to room temperature and partitioned between ethyl acetate and water. The organic layer was washed with brine, dried over MgSO₄, filtered and evaporated. FCC (petroleum ether:ethyl acetate 1:0 to 4:1) gave the desired product. Yield

(126 mg) 27%; ^1H NMR (CDCl_3): δ 7.55 (d, J = 8.4 Hz, 2H), 7.45 (d, J = 8.8 Hz, 2H), 7.36 (t, J = 8.0 Hz, 1H), 7.15-7.13 (m, 1H), 7.08 (t, J = 2.4 Hz, 1H), 6.93-6.90 (m, 1H), 3.86 (s, 3H).

4'-Bromo-3-chlorobiphenyl (S43b). Prepared from 1-bromo-4-iodobenzene and 3-chloro-phenylboronic following the procedure of 4-bromo-3-methoxybiphenyl (S43a). The reaction was performed at 80° C for 20 h. FCC (petroleum ether) gave the compound 190 mg, 40%. ^1H NMR (CDCl_3): δ 7.56 (d, J = 8.4 Hz, 2H), 7.53 (t, J = 1.6 Hz, 1H), 7.47-7.43 (m, 3H), 7.36 (t, J = 8.0 Hz, 1H), 7.34-7.31 (m, 1H).

General procedure for Sonogashira coupling between 4'-bromo-3-substituted-biphenyl and ethynyltrimethylsilane. Compound S43a (126 mg, 0.48 mmol), $\text{PdCl}_2(\text{PPh}_3)_2$ (7.0 mg, 0.01 mmol), CuI (4.0 mg, 0.02 mmol), PPh_3 (5.0 mg, 0.02 mmol) and trimethylsilylacetylene (123 μL , 0.86 mmol) were dissolved in THF (1 mL) and piperidine (200 μL) was added. This was heated in the microwave at 120 °C for 12 min. The mixture was extracted with diethyl ether and washed with aq. H_2SO_4 (10%), water and brine. The organic layer was dried over MgSO_4 , filtered and evaporated. FCC (petroleum ether:ethyl acetate 1:0 to 10:1) gave the desired ((3'-Methoxybiphenyl-4-yl)ethynyl)trimethylsilane (S44a). Yield (104 mg) 78%. ^1H NMR (CDCl_3): δ 7.53 (s, 4H), 7.35 (t, J = 8.0 Hz, 1H), 7.18-7.15 (m, 1H), 7.12-7.00 (m, 1H), 6.90 (dd, J' = 8.0 Hz, J'' = 2.8 Hz, 1H), 3.86 (s, 3H), 0.27 (s, 9H).

((3'-Chlorobiphenyl-4-yl)ethynyl)trimethylsilane (S44b). Following the procedure of S44a starting from S43b. Yield (49 mg) 64%. ^1H NMR (CDCl_3): δ 7.56 (t, J = 2.0 Hz, 1H), 7.53 (d, J = 8.4 Hz, 2H), 7.50 (d, J = 8.8 Hz, 2H), 7.45 (dt, J' = 7.6 Hz, J'' = 1.6 Hz, 1H), 7.36 (t, J = 7.6 Hz, 1H), 7.32 (dt, J' = 8.0 Hz, J'' = 2.0 Hz, 1H), 0.27 (s, 9H).

4'-Ethynyl-3-methoxybiphenyl (S45). To a solution of S44a (104 mg, 0.37 mmol) in diethyl ether (3 mL) was added methanol (3 mL) and 2M NaOH (1 mL). After 10 min of stirring at room temperature the mixture was neutralized with 2M HCl (aq.). The layers were separated and the organic layer was washed with brine and water, dried, filtered over MgSO_4 and concentrated. The product was used without further purification.

2,6-Bis((2'-methoxybiphenyl-4-yl)ethynyl)pyridine (S46). Reaction conditions according to the general Sonogashira coupling procedure (S23a-e), starting from S45 and S21. Purified by FCC (petroleum ether:ethyl acetate 4:1 to 1:1). Yield (23 mg) 25%. ^1H NMR (CDCl_3): δ 7.72-7.65 (m, 5H), 7.60 (d, J = 8.4 Hz, 4H), 7.51 (d, J = 7.6 Hz, 2H), 7.38 (t, J = 8.4 Hz, 2H), 7.20 (d, J = 8.0 Hz, 2H), 7.14 (s, 2H), 6.93 (dd, J' = 8.2 Hz, J'' = 2.0 Hz, 2H), 3.88 (s, 6H).

2,6-Bis((2'-chlorobiphenyl-4-yl)ethynyl)pyridine (S47). Starting from

compounds **S21** and **S44b**. FCC (petroleum ether:dichloromethane 20:1 to 1:2). Yield (16 mg) 19%. ^1H NMR (CDCl_3): δ 7.70–7.66 (m, 4H), 7.59–7.55 (m, 6H), 7.53 (d, $J = 5.2$ Hz, 1H), 7.50–7.44 (m, 4H), 7.39 (t, $J = 8.0$ Hz, 2H), 7.34 (d, $J = 8.0$ Hz, 2H).

***N*-Ethyl-*N*-(3-(*p*-tolyl)prop-2-yn-1-yl)heptan-1-amine (19).** To a solution of **S14** (300 mg, 1 mmol) in DMF (5 mL) was added K_2CO_3 (415 mg, 3 mmol) followed by *N*-ethylheptylamine (280 μL , 1.5 mmol). The mixture was stirred at r.t. for 1 hour and diluted with water (5 mL), extracted with EtOAc (3×10 mL) and the organic layers were dried on MgSO_4 , filtered and the solvent was removed *in vacuo*. The crude residue was purified by flash chromatography on silica gel (20% EtOAc-Petroleum ether) to afford pure **19** as an oil. Yield (228 mg) 84%; ^1H NMR (400 MHz, CDCl_3) δ 7.32 (d, $J = 8.0$ Hz, 2H), 7.10 (d, $J = 8.0$ Hz, 2H), 3.62 (s, 2H), 2.61 (q, $J = 7.2$ Hz, 2H), 2.53 (t, $J = 7.6$ Hz, 2H), 2.34 (s, 3H), 1.52–1.49 (m, 2H), 1.31–1.26 (m, 8H), 1.11 (t, $J = 7.2$ Hz, 3H), 0.88 (t, $J = 7.2$ Hz, 3H) ppm; ^{13}C NMR (101 MHz, CDCl_3) δ 137.9, 131.6, 129.0, 120.3, 85.0, 83.8, 53.6, 47.7, 42.1, 31.9, 29.3, 27.6, 27.5, 22.7, 21.4, 14.1, 12.7 ppm. HPLC: $t_{\text{R}} = 7.39$ min; HRMS (ESI): m/z [$M + \text{H}$] $^+$ calcd for $\text{C}_{19}\text{H}_{29}\text{N}$: 272.2373, found: 272.2370.

***N*-Ethyl-*N*-propyl-3-(*p*-tolyl)prop-2-yn-1-amine (20).** To a solution of **S14** (300 mg, 1 mmol) in DMF (5 mL) was added K_2CO_3 (415 mg, 3 mmol) followed by *N*-ethylpropylamine (180 μL , 1.5 mmol). The mixture was stirred at r.t. for 1 hour and diluted with water (5 mL), extracted with EtOAc (3×10 mL) and the organic layers were dried on MgSO_4 , filtered and the solvent was removed *in vacuo*. The crude residue was purified by flash chromatography on silica gel (20% EtOAc-Petroleum ether) to afford pure **20** as oil. Yield (170 mg) 79%; ^1H NMR (400 MHz, CDCl_3) δ 7.32 (d, $J = 8.0$ Hz, 2H), 7.10 (d, $J = 8.0$ Hz, 2H), 3.62 (s, 2H), 2.61 (q, $J = 7.2$ Hz, 2H), 2.50 (t, $J = 7.6$ Hz, 2H), 2.34 (s, 3H), 1.53 (sex, $J = 7.6$ Hz, 2H), 1.11 (t, $J = 7.2$ Hz, 3H), 0.93 (t, $J = 7.6$ Hz, 3H) ppm; ^{13}C NMR (101 MHz, CDCl_3) δ 137.9, 131.6, 129.0, 120.3, 85.0, 83.8, 55.6, 47.6, 42.1, 21.4, 20.8, 12.7, 12.0 ppm. HPLC: $t_{\text{R}} = 5.70$ min; HRMS (ESI): m/z [$M + \text{H}$] $^+$ calcd for $\text{C}_{15}\text{H}_{21}$: 216.1747, found: 216.1745.

General methylation procedure to yield pyridines **24**, **25**, **27–30**, **39–44** and **46**.

The respective compound **S23e**, **S24a–e**, **S34a–e**, **S46** and **S47** (1.0 eq.) was dissolved in CH_2Cl_2 (40 mL per mmol) and stirred at 0 °C under a N_2 atmosphere. Methyl trifluoromethanesulfonate (2.8 eq.) was added and the mixture was stirred overnight. After adsorption of the crude on silica, FCC gave the desired compound eluting with a mixture of dichloromethane:methanol.

2,6-Dihexyl-1-methylpyridinium trifluoromethanesulfonate (24). Prepared from **S24a** and purified by FCC (dichloromethane:methanol 60:1 to 20:1) to give the desired product. Yield (660 mg) 85%; ^1H NMR (400MHz, CDCl_3): δ 8.20 (t, $J = 8.0$ Hz, 1H), 7.64 (d, $J = 8.0$ Hz, 2H), 4.21 (s, 3H), 3.12 (t, $J = 7.6$ Hz, 4H), 1.81-1.74 (m, 4H),), 1.52-1.45 (m, 4H), 1.39-1.29 (m, 8H), 0.91 (t, $J = 6.8$ Hz, 6H); ^{13}C NMR (101 MHz, CDCl_3): δ 159.7, 144.2, 126.0, 39.7, 34.5, 31.4, 28.9, 27.6, 22.5, 14.1 ppm. HPLC purity: 99.3% (t_{R} 8.24 min); ESI-MS: 262.27 [M].

2,6-Diheptyl-1-methylpyridinium trifluoromethanesulfonate (25). Prepared from **S24b** and purified by FCC (dichloromethane:methanol 30:1 to 20:1) to give the desired product. Yield (143 mg) 86%; ^1H NMR (400MHz, CDCl_3): δ 8.18 (t, $J = 7.6$ Hz, 1H), 7.63 (d, $J = 8.0$ Hz, d), 4.22 (s, 3H), 3.13 (t, $J = 8.0$ Hz, 4H), 1.82-1.74 (m, 4H), 1.52-1.44 (m, 4H), 1.41-1.36 (m, 12H), 0.90 (t, $J = 6.4$ Hz, 6H); ^{13}C NMR (101 MHz, CDCl_3): δ 159.8, 144.1, 126.0, 122.4, 119.2, 39.7, 34.6, 31.7, 29.3, 29.0, 27.7, 22.7, 14.2 ppm. HPLC purity: 97% (t_{R} 8.96 min); ESI-MS: 290.33 [M].

2,6-Dinonyl-1-methylpyridinium trifluoromethanesulfonate (27). Prepared from **S24c** and purified by FCC (dichloromethane:methanol 30:1 to 15:1) to give the desired product. Yield (87 mg) 65%; ^1H NMR (400MHz, CDCl_3): δ 8.18 (t, $J = 8.0$ Hz, 1H), 7.63 (d, $J = 8.0$ Hz, 2H), 4.22 (s, 3H), 3.12 (t, $J = 7.6$ Hz, 4H), 1.82-1.74 (m, 4H), 1.50-1.46 (m, 4H), 1.44-1.28 (m, 20H), 0.89 (t, $J = 6.4$ Hz, 6H); ^{13}C NMR (101 MHz, CDCl_3): δ 159.9, 144.0, 126.0, 39.8, 34.6, 32.0, 29.5, 29.4, 27.7, 22.8, 14.2 ppm. HPLC purity: 100% (t_{R} 10.21 min); ESI-MS: 346.40 [M].

2,6-Didecyl-1-methylpyridinium trifluoromethanesulfonate (28). Prepared from **S24d** and purified by FCC (dichloromethane:methanol 60:1 to 10:1) to give the desired product. Yield (166 mg) 74%; ^1H NMR (400MHz, CDCl_3): δ 8.18 (t, $J = 8.0$ Hz, 1H), 7.63 (d, $J = 8.0$ Hz, 2H), 4.22 (s, 3H), 3.13 (t, $J = 8.0$ Hz, 4H), 1.82-1.74 (m, 4H), 1.50-1.44 (m, 4H), 1.39-1.28 (m, 24H), 0.89 (t, $J = 6.8$ Hz, 6H); ^{13}C NMR (101 MHz, CDCl_3): δ 159.7, 144.0, 125.9, 39.6, 34.4, 31.9, 29.5, 29.4, 29.3, 29.2, 27.6, 22.7, 14.1 ppm. HPLC purity: 100% (t_{R} 10.77 min); ESI-MS: 374.40 [M].

2,6-Didodecyl-1-methylpyridinium trifluoromethanesulfonate (29). Prepared from **S24e** and purified by FCC (dichloromethane:methanol 30:1 to 20:1) to give the desired product. Yield (536 mg) 87%; ^1H NMR (400MHz, CDCl_3): δ 8.19 (t, $J = 8.0$ Hz, 1H), 7.63 (d, $J = 7.6$ Hz, 2H), 4.21 (s, 3H), 3.12 (t, $J = 8.0$ Hz, 4H), 1.81-1.73 (m, 4H), 1.51-1.44 (m, 4H), 1.38-1.27 (m, 32H), 0.88 (t, $J = 6.8$ Hz, 6H); ^{13}C NMR (101 MHz, CDCl_3): δ 159.8, 144.1, 126.0, 39.7, 34.6, 32.0, 29.8, 29.7, 29.7, 29.6, 29.5, 29.4, 29.3, 27.7, 22.8, 14.2 ppm. HPLC purity: 100%

(t_r 11.84 min); ESI-MS: 430.53 [M].

2,6-Di(dodec-1-ynyl)-1-methylpyridinium trifluoromethanesulfonate (30). Prepared from **S23e** and purified by FCC (dichloromethane:methanol 40:1 to 20:1) to give the desired product. Yield (675 mg) 94%; ^1H NMR (400MHz, CDCl_3): δ 8.38 (t, $J = 8.0$ Hz, 1H), 7.90 (d, $J = 8.0$ Hz, 2H), 4.49 (s, 3H), 2.65 (t, $J = 7.2$ Hz, 4H), 1.74-1.65 (m, 4H), 1.48-1.41 (m, 4H), 1.30-1.27 (m, 24H), 0.88 (t, $J = 6.8$ Hz, 6H); ^{13}C NMR (101 MHz, CDCl_3): δ 144.3, 139.5, 130.7, 112.8, 72.9, 45.1, 32.0, 29.7, 29.5, 29.4, 29.2, 29.1, 27.6, 22.9, 20.3, 14.2 ppm. HPLC purity: 100% (t_r 11.57 min); ESI-MS: 422.40 [M].

2,6-Di([4-(2-methylphenyl)phenyl]ethynyl)-1-methylpyridinium trifluoromethanesulfonate (39). Prepared from **S34a** and purified by FCC (dichloromethane:methanol 30:1 to 20:1) and preparative HPLC to give the desired product. Yield (1 mg) 96%; ^1H NMR (400MHz, CDCl_3): δ 8.47 (t, $J = 8.0$ Hz, 1H), 8.10 (d, $J = 8.0$ Hz, 2H), 7.77 (d, $J = 8.0$ Hz, 4H), 7.46 (d, $J = 8.0$ Hz, 4H), 7.31-7.09 (m, 8H), 4.74 (s, 3H), 2.30 (s, 6H). HPLC purity: 96% (t_r 9.97 min); ESI-MS: 474.33 [M].

2,6-Di([4-(3-methylphenyl)phenyl]ethynyl)-1-methylpyridinium trifluoromethanesulfonate (40). Prepared from **S34b** and purified by FCC (dichloromethane:methanol 30:1 to 20:1) to give the desired product. Yield (18 mg) 78%. ^1H NMR (400MHz, CDCl_3): δ 8.40 (t, $J = 8.0$ Hz, 1H), 8.03 (d, $J = 8.0$ Hz, 2H), 7.73 (d, $J = 8.0$ Hz, 4H), 7.65 (d, $J = 8.0$ Hz, 4H), 7.41-7.37 (m, 4H), 7.35 (t, $J = 7.6$ Hz, 2H), 7.22 (d, $J = 7.2$ Hz, 2H), 4.65 (s, 3H), 2.41 (s, 6H); ^{13}C NMR (101 MHz, CDCl_3): δ 145.0, 143.9, 139.5, 138.9, 133.5, 129.4, 129.1, 128.1, 127.7, 124.4, 117.5, 109.0, 81.2, 45.5, 21.7 ppm. HPLC purity: 98.65% (t_r 10.24 min); ESI-MS: 474.33 [M].

2,6-Di([4-(3-methoxyphenyl)phenyl]ethynyl)-1-methylpyridinium trifluoromethanesulfonate (41). Prepared from **S46** and purified by FCC (dichloromethane:methanol 20:1 to 10:1) to give the desired product. Yield (12 mg) 36%; ^1H NMR (400MHz, CDCl_3): δ 8.39 (t, $J = 8.0$ Hz, 1H), 8.02 (d, $J = 8.0$ Hz, 2H), 7.73 (d, $J = 8.0$ Hz, 4H), 7.65 (d, $J = 8.4$ Hz, 4H), 7.37 (t, $J = 7.6$ Hz, 2H), 7.18 (d, $J = 8.0$ Hz, 2H), 7.11 (s, 2H), 6.94 (dd, $J' = 8.2$ Hz, $J'' = 2.0$ Hz, 2H), 4.63 (s, 3H), 3.86 (s, 6H); ^{13}C NMR (101 MHz, CDCl_3): δ 160.3, 144.6, 143.9, 140.9, 139.3, 133.5, 130.8, 130.3, 127.7, 119.7, 117.7, 114.0, 113.0, 108.8, 81.3, 77.4, 55.5, 45.5, 29.9 ppm. HPLC purity: 99% (t_r 9.56 min); ESI-MS: 506.33 [M].

2,6-Di([4-(3-chlorophenyl)phenyl]ethynyl)-1-methylpyridinium trifluoromethanesulfonate (42). Prepared from **S47** and purified by FCC (dichloromethane:methanol 20:1 to 10:1) to give the desired product. Yield (9 mg) 45%; ^1H NMR (400MHz, CDCl_3): δ 8.43 (t, $J = 8.0$ Hz, 1H), 8.08 (d, $J = 8.0$ Hz, 2H), 7.78 (d, $J = 8.0$ Hz, 4H), 7.65 (d, $J = 8.0$ Hz, 4H),

7.57 (s, 2H), 7.48 (d, $J = 7.2$ Hz, 2H), 7.42-7.37 (m, 4H), 4.70 (s, 3H); ^{13}C NMR (101 MHz, $\text{CDCl}_3/\text{MeOD}$): δ 143.8, 143.4, 141.0, 139.3, 134.9, 133.3, 130.7, 130.3, 128.5, 127.6, 127.1, 125.3, 117.9, 108.5, 80.8, 45.0, 29.5 ppm. HPLC purity: 99% (t_{R} 10.20 min); ESI-MS: 514.33 [M].

2,6-Di(4-(4-methylphenyl)phenylethynyl)-1-methylpyridinium trifluoromethanesulfonate (43). Prepared from **S34c** and purified by FCC (dichloromethane:methanol 30:1 to 5:1) to give the desired product. Yield (27 mg) 48%; ^1H NMR (400MHz, CDCl_3): δ 8.43 (t, $J = 8.0$ Hz, 1H), 8.06 (d, $J = 8.0$ Hz, 2H), 7.75 (d, $J = 8.4$ Hz, 4H), 7.67 (d, $J = 8.4$ Hz, 4H), 7.52 (d, $J = 8.0$ Hz, 4H), 7.29-7.26 (m, 4H), 4.68 (s, 3H), 2.41 (s, 6H); ^{13}C NMR (101 MHz, $\text{CDCl}_3/\text{MeOD}$): δ 144.9, 143.9, 139.4, 138.8, 136.3, 133.4, 133.3, 130.6, 129.8, 127.4, 127.0, 117.0, 109.1, 80.9, 77.3, 21.1 ppm. HPLC purity: 99% (t_{R} 10.28 min); ESI-MS: 474.40 [M].

2,6-Di([4-(4-methoxyphenyl)phenyl]ethynyl)-1-methylpyridinium trifluoromethanesulfonate (44). Prepared from **S34d** and purified by FCC (dichloromethane:methanol 30:1 to 10:1) to give the desired product. Yield (42 mg) 58%; ^1H NMR (400MHz, CDCl_3): δ 8.42 (t, $J = 8.0$ Hz, 1H), 8.04 (d, $J = 8.0$ Hz, 2H), 7.73 (d, $J = 8.4$ Hz, 4H), 7.65 (d, $J = 8.4$ Hz, 4H), 7.57 (d, $J = 8.8$ Hz, 4H), 7.00 (d, $J = 8.8$ Hz, 4H), 4.67 (s, 3H), 3.86 (s, 6H); ^{13}C NMR (101 MHz, $\text{CDCl}_3/\text{MeOD}$): δ 160.1, 144.5, 143.7, 139.3, 133.3, 131.6, 130.4, 128.3, 127.0, 116.5, 114.5, 109.3, 80.7, 55.4, 44.9 ppm. HPLC purity: 100% (t_{R} 9.78 min); ESI-MS: 506.33 [M].

2,6-Di([4-(4-hydroxyphenyl)phenyl]ethynyl)-1-methylpyridinium trifluoromethanesulfonate (45). **44** (27 mg, 0.04 mmol) was dissolved in 2 mL CH_2Cl_2 and cooled to -78°C under a nitrogen atmosphere. An 1M solution of BBr_3 in CH_2Cl_2 (0.4 mL) was added and the reaction mixture was allowed to warm up to room temperature and stirring was continued for 2 h at room temperature, after which as shown by TLC (dichloromethane:methanol 30:1) full conversion was reached. The reaction mixture was re cooled to -78°C and quenched with H_2O . After an hour the precipitate was filtered off and washed with H_2O and CH_2Cl_2 respectively and dried *in vacuo*. Yield (12 mg) 48%. ^1H NMR (400MHz, DMSO): δ 9.81 (s, 2H), 8.56 (t, $J = 8.4$ Hz, 1H), 8.36 (d, $J = 7.6$ Hz, 2H), 7.89 (d, $J = 8.0$ Hz, 4H), 7.83 (d, $J = 8.4$ Hz, 4H), 7.64 (d, $J = 8.4$ Hz, 4H), 6.90 (d, $J = 8.8$ Hz, 4H), 4.58 (s, 3H); ^{13}C NMR (151 MHz, DMSO): δ 158.2, 143.6, 143.2, 133.3, 130.6, 129.1, 128.2, 126.3, 116.4, 115.9, 106.0, 81.7, 45.2 ppm. HPLC purity 99% (t_{R} 8.38 min); ESI-MS: 478.33 [M].

2,6-Di([4-(4-chlorophenyl)phenyl]ethynyl)-1-methylpyridinium trifluoromethanesulfonate (46). Prepared from **S34e** and purified by FCC (dichloromethane:methanol 30:1 to 10:1) to give the desired product. Yield (42 mg) 58%; ^1H NMR (400MHz, CDCl_3): δ 8.43 (t, $J = 8.0$ Hz, 1H), 8.08 (d, $J = 8.4$ Hz, 2H),

7.79 (d, $J = 8.4$ Hz, 4H), 7.67 (d, $J = 8.4$ Hz, 4H), 7.56 (d, $J = 8.4$ Hz, 4H), 7.46 (d, $J = 8.4$ Hz, 4H), 4.74 (s, 3H); ^{13}C NMR (101 MHz, $\text{CDCl}_3/\text{MeOD}$): δ 143.8, 143.6, 139.3, 137.7, 134.8, 133.4, 130.6, 129.2, 128.4, 127.4, 117.6, 108.6, 80.9, 45.0 ppm. HPLC purity: 99% (t_{r} 10.39 min); ESI-MS: 514.27 [M].

Biology

Chemical and reagents

[^3H]Dofetilide (specific activity 82.3 Ci·mmol $^{-1}$) was purchased from Perkin-Elmer (Groningen, The Netherlands). Astemizole was purchased from Sigma Aldrich (Zwijndrecht, The Netherlands). Bovine serum albumin (BSA, fraction V) was purchased from Sigma (St. Louis, MO, USA). G418 was obtained from Stratagene (Cedar Creek, USA). All the other chemicals were of analytical grade and purchased from standard commercial sources. Human embryonic kidney cells stably expressing the $\text{K}_{\text{v}}11.1$ channel (HEK293 $\text{K}_{\text{v}}11.1$) were kindly provided by Dr Eckhard Ficker (University of Cleveland, USA).

Cell culture and membrane preparation

HEK293 $\text{K}_{\text{v}}11.1$ cells were cultured and membranes were prepared and stored as described previously.⁵¹

Radioligand displacement assay

The binding affinity of all tested compounds was evaluated at 25 °C in a [^3H]dofetilide competitive displacement assay as reported earlier.²

Radioligand competition association assay

The binding kinetics of unlabeled compounds were determined at 25 °C using a [^3H]dofetilide competition association assay as described before,² and the concentrations of unlabeled compounds used in this assay were equivalent to their IC_{50} values.

Patch clamp assay

HEK293 $\text{K}_{\text{v}}11.1$ cells were cultured on 10 mm glass coverslips and placed in a perfusion chamber (Cell Microcontrols, Norfolk, USA) at room temperature and perfused with control or test solutions. Whole cell patch clamp measurements and data acquisition were performed using an Axopatch-200B amplifier controlled by

the pClamp software package version 10 (Axon Instruments, Foster City, CA). Patch pipettes were made with a Sutter P-2000 micropipette puller (Sutter Instrument Company, Novato, USA) and had resistances of 1.5–2.5 M Ω after having been fire polished and filled with pipette solution. Control bath perfusion solution contained (mM): 140 NaCl, 4 KCl, 10 HEPES, 2 CaCl₂, 1 MgCl₂ (pH 7.2, NaOH), and the pipette filling solution consisted of (mM): 10 KCl, 125 K-Gluconate, 0.6 CaCl₂, 2 MgCl₂, 5 HEPES, 4 Na₂ATP, 5 EGTA (pH 7.2, KOH). After establishing the whole cell configuration, capacitive transients and pipette access resistance were compensated for by 80%.

The pulse protocol for whole cell voltage clamp measurements of K_v11.1-mediated ion currents was as following. Cells were depolarized to 20 mV from a holding potential -80 mV for 4000 ms, allowing a step current due to activation and inactivation of the K_v11.1 channels. This was followed by repolarization to a test potential of -50 mV for 5000 ms, during which a tail current was induced by the fast recovery from inactivation and slow deactivation of the channels. The peak tail currents were used for data analysis, and current inhibition was derived from dividing the mean tail current in the presence of selected compounds by the mean tail current under control conditions. Concentration-dependent effects of compounds **21** and **38** on K_v11.1 currents were tested at five different concentrations with an equilibrium time of 6.5 min for each concentration in a perfusion system. To determine time-dependent effects, wash-in experiments were performed with a perfusion of bath solution containing 1 μ M **21** or **38**. Clampfit 10.4 (Axon Instruments, Foster City, CA) and Prism v. 5.1 (GraphPad, San Diego, CA, USA) were used in analyzing, processing and plotting the data.

Data analysis

All experimental data were analyzed using the non-linear regression curve fitting program Prism v. 5.1 (GraphPad, San Diego, CA, USA). Apparent inhibitory binding constants (K_i values) were derived from the IC₅₀ values according to the Cheng-Prusoff equation with the K_D value obtained from saturation assay.^{2,35} Association and dissociation rates for unlabeled compounds were calculated by fitting the data into the competition association model using “kinetics of competitive binding”:³⁴

$$K_A = k_1[L] + k_2$$

$$K_B = k_3[I] + k_4$$

$$S = \sqrt{(K_A - K_B)^2 + 4k_1k_3LI10^{-18}}$$

$$K_F = 0.5 (K_A + K_B + S)$$

$$K_S = 0.5 (K_A + K_B - S)$$

$$Q = \frac{B_{\max} k_1 L 10^{-9}}{K_F - K_S}$$

$$Y = Q \left(\frac{k_4 (K_F - K_S)}{K_F K_S} + \frac{k_4 - K_F}{K_F} e^{(-K_F X)} - \frac{k_4 - K_S}{K_S} e^{(-K_S X)} \right)$$

Where X is the time (min), Y the specific binding of [³H]dofetilide, k_1 and k_2 are the k_{on} ($\text{M}^{-1} \cdot \text{min}^{-1}$) and k_{off} (min^{-1}) of [³H]dofetilide, L the concentration of [³H]dofetilide (nM), B_{\max} the maximum specific binding (dpm) and I the concentration of the unlabelled compound (nM). Fixing these parameters allowed the following parameters to be calculated: k_3 , which is the k_{on} value ($\text{M}^{-1} \cdot \text{min}^{-1}$) of the unlabelled compound and k_4 , which is the k_{off} value (min^{-1}) of the unlabelled compound. The association and dissociation rates were used to calculate the kinetic K_D values from the following equation: $K_D = k_{\text{off}}/k_{\text{on}}$. The residence time (RT) was calculated according to the formula: $\text{RT} = 1/k_{\text{off}}$. All values in this study are means of at least three independent experiments with SEM.

References

1. Heijman, J.; Voigt, N.; Carlsson, L. G.; Dobrev, D. Cardiac safety assays. *Curr. Opin. Pharmacol.* **2014**, *15*, 16-21.
2. Yu, Z.; IJzerman, A. P.; Heitman, L. H. $K_v11.1$ (hERG)-induced cardiotoxicity: A molecular insight from a binding kinetics study of prototypic $K_v11.1$ (hERG) inhibitors. *Br. J. Pharmacol.* **2015**, *172*, 940-945.
3. Sanguinetti, M. C.; Tristani-Firouzi, M. hERG potassium channels and cardiac arrhythmia. *Nature* **2006**, *440*, 463-469.
4. Vandenberg, J. I.; Perry, M. D.; Perrin, M. J.; Mann, S. A.; Ke, Y.; Hill, A. P. hERG K^+ channels: Structure, function, and clinical significance. *Physiol. Rev.* **2012**, *92*, 1393-1478.
5. Townsend, C. Is there a need to add another dimension (time) to the evaluation of the arrhythmogenic potential of new drug candidates *in vitro*? *Circulation* **2014**, *130*, 219-220.
6. Hill, A. P.; Perrin, M. J.; Heide, J.; Campbell, T. J.; Mann, S. A.; Vandenberg, J. I. Kinetics of drug interaction with the $K_v11.1$ potassium channel. *Mol. Pharmacol.* **2014**, *85*, 769-776.
7. Redfern, W. S.; Carlsson, L.; Davis, A. S.; Lynch, W. G.; MacKenzie, I.; Palethorpe, S.; Siegl, P. K. S.; Strang, I.; Sullivan, A. T.; Wallis, R.; Camm, A. J.; Hammond, T. G. Relationships between preclinical cardiac electrophysiology, clinical QT interval prolongation and torsade de pointes for a broad range of drugs: Evidence for a provisional safety

margin in drug development. *Cardiovasc. Res.* **2003**, *58*, 32-45.

8. Di Veroli, G. Y.; Davies, M. R.; Zhang, H.; Abi-Gerges, N.; Boyett, M. R. High-throughput screening of drug-binding dynamics to hERG improves early drug safety assessment. *Am. J. Physiol. Heart Circ. Physiol.* **2013**, *304*, H104-H117.
9. Di Veroli, G. Y.; Davies, M. R.; Zhang, H.; Abi-Gerges, N.; Boyett, M. R. hERG inhibitors with similar potency but different binding kinetics do not pose the same proarrhythmic risk: Implications for drug safety assessment. *J. Cardiovasc. Electrophysiol.* **2014**, *25*, 197-207.
10. Ridley, J. M.; Milnes, J. T.; Duncan, R. S.; McPate, M. J.; James, A. F.; Witchel, H. J.; Hancox, J. C. Inhibition of the hERG K⁺ channel by the antifungal drug ketoconazole depends on channel gating and involves the S6 residue F656. *FEBS Lett.* **2006**, *580*, 1999-2005.
11. Schneider, E. V.; Bottcher, J.; Huber, R.; Maskos, K.; Neumann, L. Structure-kinetic relationship study of CDK8/CycC specific compounds. *Proc. Natl. Acad. Sci. U.S.A.* **2013**, *110*, 8081-8086.
12. Markgren, P.-O.; Schaal, W.; Hämläinen, M.; Karlén, A.; Hallberg, A.; Samuelsson, B.; Danielson, U. H. Relationships between structure and interaction kinetics for HIV-1 protease inhibitors. *J. Med. Chem.* **2002**, *45*, 5430-5439.
13. Tummino, P. J.; Copeland, R. A. Residence time of receptor-ligand complexes and its effect on biological function. *Biochemistry* **2008**, *47*, 5481-5492.
14. Goyal, M.; Rizzo, M.; Schumacher, F.; Wong, C. F. Beyond thermodynamics: Drug binding kinetics could influence epidermal growth factor signaling. *J. Med. Chem.* **2009**, *52*, 5582-5585.
15. Vilums, M.; Zweemer, A. J. M.; Yu, Z.; de Vries, H.; Hillger, J. M.; Wapenaar, H.; Bollen, I. A. E.; Barmare, F.; Gross, R.; Clemens, J.; Krenitsky, P.; Brussee, J.; Stamos, D.; Saunders, J.; Heitman, L. H.; IJzerman, A. P. Structure-kinetic relationships-an overlooked parameter in hit-to-lead optimization: A case of cyclopentylamines as chemokine receptor 2 antagonists. *J. Med. Chem.* **2013**, *56*, 7706-7714.
16. Guo, D.; Xia, L.; van Veldhoven, J. P.; Hazeu, M.; Mocking, T.; Brussee, J.; IJzerman, A. P.; Heitman, L. H. Binding kinetics of ZM241385 derivatives at the human adenosine A_{2A} receptor. *ChemMedChem* **2014**, *9*, 752-761.
17. Winquist, J.; Geschwindner, S.; Xue, Y.; Gustavsson, L.; Musil, D.; Deinum, J.; Danielson, U. H. Identification of structural-kinetic and structural-thermodynamic relationships for thrombin inhibitors. *Biochemistry* **2013**, *52*, 613-626.
18. Sager, P. T.; Gintant, G.; Turner, J. R.; Pettit, S.; Stockbridge, N. Rechanneling the cardiac proarrhythmia safety paradigm: A meeting report from the cardiac safety research consortium. *Am. Heart J.* **2014**, *167*, 292-300.
19. Cavero, I.; Holzgrefe, H. Comprehensive *in vitro* proarrhythmia assay, a novel *in vitro/in silico* paradigm to detect ventricular proarrhythmic liability: A visionary 21st cen-

ture initiative. *Expert Opin. Drug Saf.* **2014**, *13*, 745-758.

20. Windisch, A.; Timin, E.; Schwarz, T.; Stork-Riedler, D.; Erker, T.; Ecker, G.; Hering, S. Trapping and dissociation of propafenone derivatives in hERG channels. *Br. J. Pharmacol.* **2011**, *162*, 1542-1552.

21. Linder, T.; Saxena, P.; Timin, E. N.; Hering, S.; Stary-Weinzinger, A. Structural insights into trapping and dissociation of small molecules in K⁺ channels. *J. Chem. Inf. Model.* **2014**, *54*, 3218-3228.

22. Shagufta; Guo, D.; Klaasse, E.; de Vries, H.; Brussee, J.; Nalos, L.; Rook, M. B.; Vos, M. A.; van der Heyden, M. A.; IJzerman, A. P. Exploring chemical substructures essential for hERG K⁺ channel blockade by synthesis and biological evaluation of dofetilide analogues. *ChemMedChem* **2009**, *4*, 1722-1732.

23. Vilums, M.; Overman, J.; Klaasse, E.; Scheel, O.; Brussee, J.; IJzerman, A. P. Understanding of molecular substructures that contribute to hERG K⁺ channel blockade: Synthesis and biological evaluation of E-4031 analogues. *ChemMedChem* **2012**, *7*, 107-113.

24. Louvel, J.; Carvalho, J. F.; Yu, Z.; Soethoudt, M.; Lenselink, E. B.; Klaasse, E.; Brussee, J.; IJzerman, A. P. Removal of human ether-à-go-go related gene (hERG) K⁺ channel affinity through rigidity: A case of clofilium analogues. *J. Med. Chem.* **2013**, *56*, 9427-9440.

25. Carvalho, J. o. F.; Louvel, J.; Doornbos, M. L.; Klaasse, E.; Yu, Z.; Brussee, J.; IJzerman, A. P. Strategies to reduce hERG K⁺ channel blockade. Exploring heteroaromaticity and rigidity in novel pyridine analogues of dofetilide. *J. Med. Chem.* **2013**, *56*, 2828-2840.

26. Suessbrich, H.; Waldegger, S.; Lang, F.; Busch, A. E. Blockade of hERG channels expressed in xenopus oocytes by the histamine receptor antagonists terfenadine and astemizole. *FEBS Lett.* **1996**, *385*, 77-80.

27. Fitzgerald, P. T.; Ackerman, M. J. Drug-induced Torsades de Pointes: The evolving role of pharmacogenetics. *Heart Rhythm* **2005**, *2*, S30-S37.

28. Rajamani, S.; Shryock, J. C.; Belardinelli, L. Rapid kinetic interactions of ranolazine with hERG K⁺ current. *J. Cardiovasc. Pharmacol.* **2008**, *51*, 581-589.

29. Orita, A.; Nakano, T.; An, D. L.; Tanikawa, K.; Wakamatsu, K.; Otera, J. Metal-assisted assembly of pyridine-containing arylene ethynylene strands to enantiopure double helicates. *J. Am. Chem. Soc.* **2004**, *126*, 10389-10396.

30. Nishihara, Y.; Noyori, S.; Okamoto, T.; Suetsugu, M.; Iwasaki, M. Copper-catalyzed Sila-Sonogashira-Hagihara cross-coupling reactions of alkynylsilanes with aryl iodides under palladium-free conditions. *Chem. Lett.* **2011**, *40*, 972-974.

31. Siemsen, P.; Livingston, R. C.; Diederich, F. Acetylenic coupling: A powerful tool in molecular construction. *Angew. Chem. Int. Ed. Engl.* **2000**, *39*, 2632-2657.

32. Shen, X.; Ho, D. M.; Pascal, R. A. Synthesis of polyphenylene dendrimers related to "cubic graphite". *J. Am. Chem. Soc.* **2004**, *126*, 5798-5805.

33. Aggarwal, A. V.; Jester, S. S.; Taheri, S. M.; Foerster, S.; Hoeger, S. Molecular spoked wheels: Synthesis and self-assembly studies on rigid nanoscale 2D objects. *Chem. Eur. J.* **2013**, *19*, 4480-4495.
34. Motulsky, H. J.; Mahan, L. The kinetics of competitive radioligand binding predicted by the law of mass action. *Mol. Pharmacol.* **1984**, *25*, 1-9.
35. Cheng, Y.; Prusoff, W. H. Relationship between the inhibition constant (K_i) and the concentration of inhibitor which causes 50 percent inhibition (I_{50}) of an enzymatic reaction. *Biochem. Pharmacol.* **1973**, *22*, 3099-3108.
36. Jamieson, C.; Moir, E. M.; Rankovic, Z.; Wishart, G. Medicinal chemistry of hERG optimizations: Highlights and hang-ups. *J. Med. Chem.* **2006**, *49*, 5029-5046.
37. Fernandez, D.; Ghanta, A.; Kauffman, G. W.; Sanguinetti, M. C. Physicochemical features of the hERG channel drug binding site. *J. Biol. Chem.* **2004**, *279*, 10120-10127.
38. Zhu, B.; Jia, Z. J.; Zhang, P.; Su, T.; Huang, W.; Goldman, E.; Tumas, D.; Kadambi, V.; Eddy, P.; Sinha, U.; Scarborough, R. M.; Song, Y. Inhibitory effect of carboxylic acid group on hERG binding. *Bioorg. Med. Chem. Lett.* **2006**, *16*, 5507-5512.
39. CCavalli, A.; Buonfiglio, R.; Ianni, C.; Masetti, M.; Ceccarini, L.; Caves, R.; Chang, M. W. Y.; Mitcheson, J. S.; Roberti, M.; Recanatini, M. Computational design and discovery of "minimally structured" hERG blockers. *J. Med. Chem.* **2012**, *55*, 4010-4014.
40. Mitcheson, J. S.; Chen, J.; Lin, M.; Culberson, C.; Sanguinetti, M. C. A structural basis for drug-induced long QT syndrome. *Proc. Natl. Acad. Sci. U.S.A.* **2000**, *97*, 12329-12333.
41. Czodrowski, P. hERG me out. *J. Chem. Inf. Model.* **2013**, *53*, 2240-2251.
42. Pearlstein, R. A.; Vaz, R. J.; Kang, J.; Chen, X.; Preobrazhenskaya, M.; Shchekotikhin, A. E.; Korolev, A. M.; Lysenkova, L. N.; Miroshnikova, O. V.; Hendrix, J.; Rampe, D. Characterization of hERG potassium channel inhibition using CoMSiA 3D QSAR and homology modeling approaches. *Bioorg. Med. Chem. Lett.* **2003**, *13*, 1829-1835.
43. Kramer, C.; Beck, B.; Kriegl, J. M.; Clark, T. A composite model for hERG blockade. *ChemMedChem* **2008**, *3*, 254-265.
44. Farid, R.; Day, T.; Friesner, R. A.; Pearlstein, R. A. New insights about hERG blockade obtained from protein modeling, potential energy mapping, and docking studies. *Bioorg. Med. Chem.* **2006**, *14*, 3160-3173.
45. Aronov, A. M. Predictive in silico modeling for hERG channel blockers. *Drug Discov. Today* **2005**, *10*, 149-155.
46. Jiang, Y.; Lee, A.; Chen, J.; Ruta, V.; Cadene, M.; Chait, B. T.; MacKinnon, R. X-ray structure of a voltage-dependent K^+ channel. *Nature* **2003**, *423*, 33-41.
47. Abraham, J. M.; Saliba, W. I.; Vekstein, C.; Lawrence, D.; Bhargava, M.; Bassiouny, M.; Janiszewski, D.; Lindsay, B.; Militello, M.; Nissen, S. E.; Poe, S.; Tanaka-Espósito, C.; Wolski, K.; Wilkoff, B. L. Safety of oral dofetilide loading for rhythm control of atrial arrhythmias. *J. Am. Coll. Cardiol.* **2014**, *63*, A435.

48. Ficker, E.; Jarolimek, W.; Kiehn, J.; Baumann, A.; Brown, A. M. Molecular determinants of dofetilide block of hERG K⁺ channels. *Circ. Res.* **1998**, *82*, 386-395.
49. Guo, D.; Mulder-Krieger, T.; IJzerman, A. P.; Heitman, L. H. Functional efficacy of adenosine A_{2A} receptor agonists is positively correlated to their receptor residence time. *Br. J. Pharmacol.* **2012**, *166*, 1846-1859.
50. Xie, Y.; Yu, M.; Zhang, Y. Iron (II) chloride catalyzed alkylation of propargyl ethers: Direct functionalization of an sp³ CH bond adjacent to oxygen. *Synthesis* **2011**, *2011*, 2803-2809.
51. Yu, Z.; Klaasse, E.; Heitman, L. H.; IJzerman, A. P. Allosteric modulators of the hERG K⁺ channel: Radioligand binding assays reveal allosteric characteristics of dofetilide analogs. *Toxicol. Appl. Pharmacol.* **2014**, *274*, 78-86.



Chapter 8

Conclusions and perspectives



About this chapter

In this thesis I have explored the allosteric modulation and the kinetics of ligands at the $K_v11.1$ channel. The research in this thesis may provide valuable information and potential approaches for relieving the $K_v11.1$ -induced cardiotoxicity of drug candidates in the future. This chapter will summarize the major findings from these studies, and propose the future directions of this research field.

Conclusions of this thesis

Allosteric modulations of the $K_v11.1$ channel

Nowadays, $K_v11.1$ blockade by potential drug candidates has received much attention since it potentially causes proarrhythmic side effects. However, at the start of this research allosteric modulation of the $K_v11.1$ channel as an alternative way of drug interaction had not been studied in any significant detail. The unique structural features of the $K_v11.1$ channel, which were thoroughly reviewed in **Chapters 1 and 2**, imply the presence of multiple ligand binding sites at the channel with possible allosteric interactions between them. In **Chapter 3**, the allosteric effects of a plethora of compounds as well as potassium ions on the $K_v11.1$ channel were evaluated in both [3H]astemizole and [3H]dofetilide binding assays. LUF6200 was identified as a negative allosteric modulator, whereas potassium ions behaved as positive allosteric modulators. Moreover, LUF6200 and potassium ions acted on distinct allosteric sites at the $K_v11.1$ channel, and these binding sites showed positive cooperativity. This investigation is the first to provide direct evidence for allosteric modulation of the $K_v11.1$ channel using radioligand binding assays.

Subsequently, a novel negative allosteric modulator LUF7244 was characterized with several different [3H]dofetilide binding assays (**Chapter 4**). LUF7244 was found to decrease the affinity of the prototypical $K_v11.1$ blockers dofetilide, astemizole, sertindole and cisapride. Moreover, the antiarrhythmic propensity of this compound was revealed in a newly validated neonatal rat ventricular myocyte (NRVM) model. Pretreatment of the NRVM monolayers with LUF7244 relieved the arrhythmic events induced by astemizole, sertindole and cisapride. Importantly, LUF7244 *per se* did not significantly affect the action potential durations of NRVMs. Concomittantly, LUF7244 displayed no obvious cytotoxicity upon a long exposure to NRVMs, and exerted negligible effects on astemizole at its intentional target (the human histamine H_1 receptor). Taken together, this study has introduced allosteric modulation of the $K_v11.1$ channel as a new and effective strategy to reduce the unintended binding of drugs to the channel's central cavity and to further prevent the proarrhythmic changes associated with this binding. This opens a promising avenue for abolishment of $K_v11.1$ -induced cardiotoxicity of drug candidates via pharmacological combination therapy. Following this chapter, a series of compounds with the same scaffold as LUF7244 were synthesized and further assessed for their allosteric effects on [3H]dofetilide binding to the $K_v11.1$ channel in **Chapter 5**. Structure-activity relationships were derived for these compounds, which offers important information for future op-

timization of allosteric modulators of the $K_v11.1$ channel. Specifically, compared to LUF7244 several more potent negative allosteric modulators like **7f** and **7p** were obtained, implicating improved potency in subsequent *ex vivo* and *in vivo* antiarrhythmic studies.

Kinetics studies of ligands at the $K_v11.1$ channel

Previous studies on $K_v11.1$ blockers have primarily focused on their equilibrium parameters such as affinity or potency at the channel. The kinetics of the interaction between a drug and the $K_v11.1$ channel has rarely been investigated though, albeit that its importance has been reported with respect to other targets, like enzymes and G protein-coupled receptors. In **Chapter 6**, a novel [3H]dofetilide competition association assay was successfully developed and validated to characterize the kinetic binding parameters of unlabeled compounds at the $K_v11.1$ channel. The association rates of fifteen prototypical, structurally diverse $K_v11.1$ blockers obtained in this assay were extremely divergent, with e.g., a 50,000-fold difference between moxifloxacin and clofilium, and correlated excellently to their affinity values at the channel. Meanwhile, membrane affinity determined in an immobilized artificial membrane column and other calculated physiochemical properties (molecular weight, pK_a , and logD) did not correlate with the binding affinity and kinetics of these blockers at the channel. Collectively, these results lead to the conclusion that a compound's affinity at the $K_v11.1$ channel is mainly regulated by its association rate instead of its dissociation rate. This finding is against the general dogma that affinity values of ligands for their targets are mainly dominated by their dissociation rates with diffusion limited association rates. In this case, association rates can therefore be used to evaluate the $K_v11.1$ liability of drug candidates, apart from the affinity. Since the dissociation rates of the selected $K_v11.1$ blockers in **Chapter 6** only exhibited a 10-fold difference between the fastest and slowest dissociating compounds, we therefore aimed to search for and design compounds with a wide range of RTs, i.e. reciprocal of dissociation rates at the channel, in **Chapter 7** in order to explore the role of the dissociation process in $K_v11.1$ blockade.

In **Chapter 7**, the association rates and RTs as well as affinity values of four compound series (dofetilide, E-4031, clofilium and pyridinium derivatives) at the $K_v11.1$ channel were determined and evaluated. Based on the results, the structure-kinetics relationships of these $K_v11.1$ blockers were explored next to their structure-affinity relationships. Interestingly, the RTs of these compounds, in particular the newly synthesized series of pyridinium derivatives, were up to 300-fold different, in addition to dramatic differences in affinity and association

rates. For instance, compound **38** had a RT of 105 ± 4 min at the $K_v11.1$ channel, while **37** displayed a short RT that was only 0.34 ± 0.04 min. Subsequently, a “ k_{on} - k_{off} - K_D ” kinetic map was constructed to putatively categorize all compounds based on their potential $K_v11.1$ liability, together with three reference drugs (positive control astemizole, negative control ranolazine, and dofetilide). Lastly, two representative compounds were tested in patch clamp assays, and their patch clamp IC_{50} values and current inhibition rates were in agreement with the RTs and association rates derived from radioligand binding experiments, respectively. Altogether, the importance of incorporating kinetic binding parameters (association and dissociation rates or RTs) into the current affinity-dominated paradigm is strongly suggested by our studies in order to more comprehensively and accurately evaluate the $K_v11.1$ liability of drug candidates. Overall, this work offers a new avenue for drug researchers to efficiently design ligands with less $K_v11.1$ -induced cardiac side effects by considering ligand binding kinetics in the drug development trajectory.

Future perspectives

Allosteric modulator as a therapeutic agent

Although the antiarrhythmic property of a negative allosteric modulator (LUF7244) was evidenced in a NRVM model (**Chapter 4**), the capability of this modulator to counteract the proarrhythmic effects of unintentional $K_v11.1$ blockers should be further investigated in human subjects due to a species difference in $K_v11.1$ characteristics between humans and rats.¹⁻³ Recent access to human-induced pluripotent stem cell (hiPSC) derived cardiomyocytes (hiPSC-CMs) has offered a window of opportunity to overcome this bottleneck induced by species-to-species differences. hiPSC-CMs have been demonstrated to exhibit the expected genomic, biochemical, mechanical and electrophysiological behavior of human cardiomyocytes as evidenced by RT-PCR, patch clamp, and/or immunofluorescence techniques.^{2, 4-6} Most importantly, the I_{Kr} current mediated by the $K_v11.1$ channel has been observed in these hiPSC-CMs.^{2, 5, 6} To date, different techniques have been explored to assess the drug-induced electrophysiological alterations of hiPSC-CMs, including whole-cell patch clamp, impedance-based cellular and multi-electrode array (MEA) assays.^{7, 8} For example, the cardiotoxic effects of selective $K_v11.1$ blockers E-4031 and dofetilide were successfully detected with the label-free xCELLigence RTCA Cardio system,⁹ and the MEA assays have been widely utilized to screen the $K_v11.1$ liability of compounds as well.^{8, 10} In this context, the impedance-based xCELLigence system or MEA

technique can be introduced to further investigate the antiarrhythmic effects of LUF7244 in a hiPSC-MC model. In addition, a simple and low-cost integrated platform has been recently reported to mimic the functional properties of native heart by creating large areas of aligned hiPSC-CMs.¹¹ Thus, the latter platform may produce more clinically and physiologically relevant data for drug screening, which can be applied to the follow-up studies on allosteric modulation of the $K_v11.1$ channel. Interestingly, $K_v7.1$ and $K_v11.1$ activators have shown compensatory effects on long QT syndromes (LQTSs) caused by dysfunctions of either channel type.¹³⁻¹⁵ Recently, Zhang *et al.* established a patient- and disease-specific model with hiPSC-CMs from family members affected by the $K_v7.1$ -mediated LQTS type 1, and found that modulation of the $K_v11.1$ channel by ML-T531 restored the action potential prolongation caused by this inherited dysfunction of the $K_v7.1$ channel.¹⁶ As ML-T531 was identified as a negative allosteric modulator in **Chapter 4** of this thesis, $K_v11.1$ modulators are supposed to possess antiarrhythmic roles in congenital cardiac diseases.¹⁶ Therefore, hiPSC-CM models with different patient-specific LQTSs can be used to evaluate the proarrhythmic propensities of LUF7244 and other more potent modulators like **7f** and **7p**. Taken together, negative allosteric modulators of the $K_v11.1$ channel can enable the rescue of inherited LQTSs alone as well as prevent drug-induced arrhythmias via combination therapy, making them an attractive and promising therapy in the future.

The hiPSC-CM differentiation system mentioned above has brought unique *in vitro* cellular- or tissue-based assays for the future development of $K_v11.1$ modulators as a novel alternative to current antiarrhythmic treatments. However, a myriad of *ex vivo* and *in vivo* preclinical studies like Langendorff and animal experiments as well as clinical evaluations are still required to eventually translate our negative allosteric modulators into a new class of therapeutic agents for both acquired and inherited arrhythmias. Currently, a zebrafish model of $K_v11.1$ -mediated LQTS type 2 has been used as a high-throughput screening approach for compounds that are able to reverse the lengthened myocardial repolarization.¹² This high-throughput *in vivo* functional whole-organism model provides an efficient opportunity for the future preclinical investigations of $K_v11.1$ modulators.

Of note, the current generation of negative allosteric modulators of the $K_v11.1$ channel are not very potent (active in the micromolar range), which may raise concerns about their specificity and potential for cardiac and non-cardiac side effects. Thus, the characterization of the binding site of these modulators at the channel will be of particular interest in follow-up studies to facilitate the development of more potent and specific modulators. Here, computational methods, mutational studies and crystallization of the $K_v11.1$ channel will bring useful in-

formation for such research in the future.^{17, 18} Furthermore, more potent allosteric modulators can be synthesized according to the structure-activity relationships concluded in **Chapter 5**.

Binding kinetics of K_v11.1 blockers

Ligand binding kinetics in patch clamp assays

Radioligand binding assays are high-throughput and useful in the early assessment of ligand binding to the K_v11.1 channel, yet they do not provide a functional endpoint.^{19, 20} Conversely, voltage patch clamp assays have capabilities to produce the highest quality and most physiologically relevant data of precise and detailed activity of the channel function among all available methods, albeit with relatively low throughput.^{19, 21} Historically, potency of K_v11.1 blockers has been measured using patch clamp techniques due to the mandatory requirements of the ICH S7B guideline, while the binding kinetics of drugs at the channel were not.^{19, 22-24} Thus, it appears attractive and meaningful to establish patch clamp assays that can be used to directly determine the binding and unbinding kinetics of ligands at the K_v11.1 channel. In **Chapter 7**, two compounds with distinguished kinetic parameters, in particular RTs, were selected to evaluate their binding kinetics in the whole-cell patch clamp assay. Although the K_v11.1 current inhibition rates of tested compounds were in the same rank order as their association rates derived from the radioligand binding assay, the I_{Kr} currents displayed insignificant recovery from the inhibition by both ligands during the washout experiments (data not shown). Subsequently, whole-cell radioligand binding assays, which are different from membrane radioligand binding assays used in the whole thesis, were performed in cells with or without expression of the K_v11.1 channel. In this case, [³H]dofetilide exhibited comparable binding at empty HEK293 cells to that at HEK293 cells expressing the K_v11.1 channel (data not shown). Collectively, we speculated that these K_v11.1 blockers with an intracellular binding site at the channel could be trapped within the cell after diffusing through the cell membrane, which made the direct measurement of ligand's unbinding kinetics impossible. Therefore, a so-called inside-out patch clamp recording without drug trapping phenomena will be particularly useful to verify our speculation, as this technique will allow for accurately determining the “true” binding kinetics of ligands with an intracellular binding pocket at the K_v11.1 channel.²⁵

Ex vivo and *in vivo* investigations

The categorization of all K_v11.1 blockers in **Chapter 7** is relatively arbitrary due

to the lack of arrhythmogenic data for the screened compounds. Monophasic action potentials of isolated Langendorff-perfused heart preparations can be recorded to assess *ex vivo* proarrhythmic liability of $K_v11.1$ blockers,²⁶⁻²⁸ and various animal models such as AV dogs and rabbits are widely applied to evaluate the *in vivo* arrhythmic propensities of drug candidates.^{29, 30} Accordingly, the $K_v11.1$ blockers from **Chapter 7** should be further assessed in these different *ex vivo* and *in vivo* experiments in order to define a more educated and reliable “ k_{on} - k_{off} - K_D ” map that allows for a better indication of torsadogenic risks of compounds. Notably, *ex vivo* and *in vivo* preclinical studies are commonly carried out on animal hearts or whole animals that are unlikely to mimic diseased human subjects and therefore might not be predictive of the clinical situation.^{3, 27, 31, 32} Hence, this kinetic map could be even further improved by incorporating affinity and kinetic parameters of more reference drugs like astemizole, ranolazine and dofetilide, which are selective $K_v11.1$ blockers and have already been assessed for their proarrhythmic profiles in clinical trials. Ultimately, a more complete translational model based on all *in vitro*, *ex vivo* and *in vivo* data can hopefully be elucidated to improve the predictive index of $K_v11.1$ liability of drug candidates in the future.

Rechanneling the $K_v11.1$ liability paradigm

The current assessment of proarrhythmic risks of $K_v11.1$ blockers is predominantly dependent on their IC_{50} values.^{3, 33} However, this approach does not take into account drug binding kinetics, which can have a major impact on cardiac arrhythmias of drug candidates.^{24, 34, 35} In 2013 a Comprehensive *in vitro* Proarrhythmia Assay (CiPA) was proposed as a new paradigm to replace the current regulatory strategy by the Cardiac Safety Research Consortium, and the CiPA was expected to be operational worldwide by July 2015.^{34, 36, 37} In this new CiPA paradigm *in silico* modeling is one of the most important components. In this regard, the best simulation model is suggested to be selected before the release of the CiPA assay, and more sophisticated models that include both simple channel blockade affinity and additional drug binding kinetics are inferred to significantly improve the proarrhythmic assessment for drug candidates.³⁶ Thus, incorporating association and dissociation rates of e.g., the compounds from **Chapter 6** and **7** with their binding affinity may lead to a more efficient, readily applicable computational model for the forthcoming CiPA implementation. As a branch of this extended research, a large library of $K_v11.1$ blockers with varied affinity and kinetic parameters should also be synthesized and evaluated to provide enough data for the representative *in silico* model in the near future. Hopefully, the ultimate, optimized CiPA paradigm will demonstrate much better predictive value for proarrhythmic risks of pharmaceutical products, compared to the traditional

strategy recommended by ICH S7A and S7B guidelines.^{38, 39}

Final note

K_v11.1-induced cardiotoxicity has emerged as an unanticipated adverse effect of many pharmacological agents and has become a major obstacle in drug development over the past decades. In this thesis, allosteric modulation of the K_v11.1 channel has been extensively explored, and negative allosteric modulators were shown to relieve the proarrhythmic effects of structurally and therapeutically diverse K_v11.1 blockers. The most potent modulators can be further assessed in *in vitro* assays based on hiPSC-CM models, *ex vivo* and *in vivo* studies, and may be developed as a new class of antiarrhythmic medications in the future. On the other hand, kinetic binding parameters of a wide range of K_v11.1 blockers at the channel have been thoroughly investigated in this thesis. Association and dissociation rates or residence times are strongly suggested to be integrated with equilibrium affinity values in the future strategies for a better and more comprehensive evaluation of K_v11.1 liability of drug candidates. The “ k_{on} - k_{off} -K_D” kinetic map provides a first and promising classification of K_v11.1 blockers, which could be beneficial and indicative for drug researchers to design compounds with less K_v11.1-mediated cardiac side effects in the early stage of drug development. Functionally determining the kinetic parameters of K_v11.1 blockers at the channel, e.g., by using inside-out patch clamp assays, will facilitate the incorporation of ligand-channel binding kinetics into the novel CiPA paradigm. Hopefully, all findings in this thesis have brought new insights into K_v11.1-induced cardiac arrhythmias, and will offer opportunities for restoring or preventing this kind of arrhythmias in the near future.

References

1. Pond, A. L.; Nerbonne, J. M. ERG proteins and functional cardiac I_{Kr} channels in rat, mouse, and human heart. *Trends Cardiovasc. Med.* **2001**, *11*, 286-294.
2. Honda, M.; Kiyokawa, J.; Tabo, M.; Inoue, T. Electrophysiological characterization of cardiomyocytes derived from human induced pluripotent stem cells. *J. Pharmacol. Sci.* **2011**, *117*, 149-159.
3. Heijman, J.; Voigt, N.; Carlsson, L. G.; Dobrev, D. Cardiac safety assays. *Curr. Opin. Pharmacol.* **2014**, *15*, 16-21.
4. Sirenko, O.; Crittenden, C.; Callamaras, N.; Hesley, J.; Chen, Y.; Funes, C.; Rusyn, I.; Anson, B.; Cromwell, E. F. Multiparameter in vitro assessment of compound effects on cardiomyocyte physiology using iPSC cells. *J. Biomol. Screen.* **2012**, *18*, 39-53.

5. Zwi, L.; Caspi, O.; Arbel, G.; Huber, I.; Gepstein, A.; Park, I.-H.; Gepstein, L. Cardiomyocyte differentiation of human induced pluripotent stem cells. *Circulation* **2009**, *120*, 1513-1523.
6. Ma, J.; Guo, L.; Fiene, S. J.; Anson, B. D.; Thomson, J. A.; Kamp, T. J.; Kolaja, K. L.; Swanson, B. J.; January, C. T. High purity human-induced pluripotent stem cell-derived cardiomyocytes: Electrophysiological properties of action potentials and ionic currents. *Am. J. Physiol. Heart Circ. Physiol.* **2011**, *301*, H2006-H2017.
7. Scott, C. W.; Zhang, X.; Abi-Gerges, N.; Lamore, S. D.; Abassi, Y. A.; Peters, M. F. An impedance-based cellular assay using human iPSC-derived cardiomyocytes to quantify modulators of cardiac contractility. *Fundam. Appl. Toxicol.* **2014**, *142*, 331-338.
8. Harris, K.; Aylott, M.; Cui, Y.; Louttit, J. B.; McMahon, N. C.; Sridhar, A. Comparison of electrophysiological data from human-induced pluripotent stem cell-derived cardiomyocytes to functional preclinical safety assays. *Fundam. Appl. Toxicol.* **2013**, *134*, 412-426.
9. Himmel, H. M. Drug-induced functional cardiotoxicity screening in stem cell-derived human and mouse cardiomyocytes: Effects of reference compounds. *J. Pharmacol. Toxicol. Methods* **2013**, *68*, 97-111.
10. Tanaka, T.; Tohyama, S.; Murata, M.; Nomura, F.; Kaneko, T.; Chen, H.; Hattori, F.; Egashira, T.; Seki, T.; Ohno, Y.; Koshimizu, U.; Yuasa, S.; Ogawa, S.; Yamanaka, S.; Yasuda, K.; Fukuda, K. *In vitro* pharmacologic testing using human induced pluripotent stem cell-derived cardiomyocytes. *Biochem. Biophys. Res. Commun.* **2009**, *385*, 497-502.
11. Chen, A.; Lee, E.; Tu, R.; Santiago, K.; Grosberg, A.; Fowlkes, C.; Khine, M. Integrated platform for functional monitoring of biomimetic heart sheets derived from human pluripotent stem cells. *Biomaterials* **2014**, *35*, 675-683.
12. Peal, D. S.; Mills, R. W.; Lynch, S. N.; Mosley, J. M.; Lim, E.; Ellinor, P. T.; January, C. T.; Peterson, R. T.; Milan, D. J. Novel chemical suppressors of long QT syndrome identified by an *in vivo* functional screen clinical perspective. *Circulation* **2011**, *123*, 23-30.
13. Diness, T. G.; Yeh, Y.-H.; Qi, X. Y.; Chartier, D.; Tsuji, Y.; Hansen, R. S.; Olesen, S.-P.; Grunnet, M.; Nattel, S. Antiarrhythmic properties of a rapid delayed-rectifier current activator in rabbit models of acquired long QT syndrome. *Cardiovasc. Res.* **2008**, *79*, 61-69.
14. Seeböhm, G. Activators of cation channels: Potential in treatment of channelopathies. *Mol. Pharmacol.* **2005**, *67*, 585-588.
15. Xu, X.; Salata, J. J.; Wang, J.; Wu, Y.; Yan, G.; Liu, T.; Marinchak, R. A.; Kowey, P. R. Increasing I_{Ks} corrects abnormal repolarization in rabbit models of acquired LQT2 and ventricular hypertrophy. *Am. J. Physiol. Heart Circ. Physiol.* **2002**, *283*, H664-H670.
16. Zhang, H.; Zou, B.; Yu, H.; Moretti, A.; Wang, X.; Yan, W.; Babcock, J. J.; Bellin, M.; McManus, O. B.; Tomaselli, G.; Nan, F.; Laugwitz, K. L.; Li, M. Modulation of

hERG potassium channel gating normalizes action potential duration prolonged by dysfunctional KCNQ1 potassium channel. *Proc. Natl. Acad. Sci. U.S.A.* **2012**, *109*, 11866-11871.

17. Ghersi, D.; Sanchez, R. Beyond structural genomics: Computational approaches for the identification of ligand binding sites in protein structures. *J. Struct. Funct. Genomics* **2011**, *12*, 109-117.

18. Swale, D. R.; Sheehan, J. H.; Banerjee, S.; Husni, A. S.; Nguyen, T. T.; Meiler, J.; Denton, J. S. Computational and functional analyses of a small-molecule binding site in ROMK. *Biophys. J.* **2015**, *108*, 1094-1103.

19. Fermini, B.; Fossa, A. A. The impact of drug-induced QT interval prolongation on drug discovery and development. *Nat. Rev. Drug Discov.* **2003**, *2*, 439-447.

20. Diaz, G. J.; Daniell, K.; Leitz, S. T.; Martin, R. L.; Su, Z.; McDermott, J. S.; Cox, B. F.; Gintant, G. A. The [³H]dofetilide binding assay is a predictive screening tool for hERG blockade and proarrhythmia: comparison of intact cell and membrane preparations and effects of altering [K⁺]_o. *J. Pharmacol. Toxicol. Methods* **2004**, *50*, 187-199.

21. Danker, T.; Moller, C. Early identification of hERG liability in drug discovery programs by automated patch clamp. *Front. Pharmacol.* **2014**, *5*, 203.

22. Hancox, J. C.; McPate, M. J.; El Harchi, A.; Zhang, Y. The hERG potassium channel and hERG screening for drug-induced Torsades de Pointes. *Pharmacol. Ther.* **2008**, *119*, 118-132.

23. Cavero, I.; Crumb, W. ICH S7B draft guideline on the non-clinical strategy for testing delayed cardiac repolarisation risk of drugs: A critical analysis. **2005**.

24. Hill, A. P.; Perrin, M. J.; Heide, J.; Campbell, T. J.; Mann, S. A.; Vandenberg, J. I. Kinetics of drug interaction with the K_v11.1 potassium channel. *Mol. Pharmacol.* **2014**, *85*, 769-776.

25. Zou, A.; Curran, M.; Keating, M.; Sanguinetti, M. Single hERG delayed rectifier K⁺ channels expressed in *Xenopus* oocytes. *Am. J. Physiol. Heart Circ. Physiol.* **1997**, *272*, H1309-H1314.

26. Jamieson, C.; Moir, E. M.; Rankovic, Z.; Wishart, G. Medicinal chemistry of hERG optimizations: Highlights and hang-ups. *J. Med. Chem.* **2006**, *49*, 5029-5046.

27. Valentin, J.-P.; Hoffmann, P.; De Clerck, F.; Hammond, T. G.; Hondeghem, L. Review of the predictive value of the Langendorff heart model (Screenit system) in assessing the proarrhythmic potential of drugs. *J. Pharmacol. Toxicol. Methods* **2004**, *49*, 171-181.

28. Lawrence, C.; Bridgland-Taylor, M.; Pollard, C.; Hammond, T.; Valentin, J.-P. A rabbit Langendorff heart proarrhythmia model: Predictive value for clinical identification of Torsades de Pointes. *Br. J. Pharmacol.* **2006**, *149*, 845-860.

29. Carlsson, L. *In vitro* and *in vivo* models for testing arrhythmogenesis in drugs. *J. Intern. Med.* **2006**, *259*, 70-80.

30. Potet, F.; Lorinc, A. N.; Chaigne, S.; Hopkins, C. R.; Venkataraman, R.; Stepanovic, S. Z.; Lewis, L. M.; Days, E.; Sidorov, V. Y.; Engers, D. W. Identification and characterization of a compound that protects cardiac tissue from human ether-à-go-go-related gene (hERG)-related drug-induced arrhythmias. *J. Biol. Chem.* **2012**, *287*, 39613-39625.
31. Sanguinetti, M. C.; Mitcheson, J. S. Predicting drug-hERG channel interactions that cause acquired long QT syndrome. *Trends Pharmacol. Sci.* **2005**, *26*, 119-124.
32. Wallis, R. M. Integrated risk assessment and predictive value to humans of non-clinical repolarization assays. *Br. J. Pharmacol.* **2010**, *159*, 115-121.
33. Di Veroli, G. Y.; Davies, M. R.; Zhang, H.; Abi-Gerges, N.; Boyett, M. R. High-throughput screening of drug-binding dynamics to hERG improves early drug safety assessment. *Am. J. Physiol. Heart Circ. Physiol.* **2013**, *304*, H104-H117.
34. Cavero, I.; Holzgrefe, H. Comprehensive *in vitro* proarrhythmia assay, a novel *in vitro/in silico* paradigm to detect ventricular proarrhythmic liability: A visionary 21st century initiative. *Expert Opin. Drug Saf.* **2014**, *13*, 745-758.
35. Di Veroli, G. Y.; Davies, M. R.; Zhang, H.; Abi-Gerges, N.; Boyett, M. R. hERG inhibitors with similar potency but different binding kinetics do not pose the same proarrhythmic risk: Implications for drug safety assessment. *J. Cardiovasc. Electrophysiol.* **2014**, *25*, 197-207.
36. Sager, P. T.; Gintant, G.; Turner, J. R.; Pettit, S.; Stockbridge, N. Rechanneling the cardiac proarrhythmia safety paradigm: A meeting report from the cardiac safety research consortium. *Am. Heart J.* **2014**, *167*, 292-300.
37. Cavero, I. 13th annual meeting of the safety pharmacology society: Focus on novel technologies and safety pharmacology frontiers. *Expert Opin. Drug Saf.* **2014**, *13*, 1271-1281.
38. Guideline, I. H. T. Safety pharmacology studies for human pharmaceuticals S7A. 2000. In.
39. Guideline, I. H. T. The non-clinical evaluation of the potential for delayed ventricular repolarization (QT interval prolongation) by human pharmaceuticals. S7B (<http://www.ich.org/products/guidelines/safety/article/safety-guidelines.html>) **2005**.

Summary

The superfamily of ion channels is a major focus of drug discovery and development programs in the pharmaceutical industry due to their involvement in a number of physiologic functions. However, the binding of several drugs to ion channels is also responsible for a huge number of side effects, and pharmaceutical safety is routinely required by regulatory agencies for certain ion channels, in particular cardiotoxicity mediated by the $K_v11.1$ channel. All these subjects have been generally discussed in **Chapter 1** of this thesis.

Chapter 2 is a literature-based review describing research progress on the $K_v11.1$ channel. In this chapter, we focused on kinetic studies of the channel, including the unique gating kinetics and ligand binding kinetics. In addition, biological production and degradation, structural features, physiological functions, and on- and off-target applications of the $K_v11.1$ channel were briefly introduced. A thorough analysis of the $K_v11.1$ channel is beneficial for the improvement of drug design and reduction of unwanted arrhythmic side effects caused by the blockade of this channel.

In **Chapter 3**, a previously disclosed series of compounds together with three reference compounds, were selected and evaluated for the allosteric modulation of the $K_v11.1$ channel in [^3H]astemizole and [^3H]dofetilide binding assays. One potent negative allosteric modulator (LUF6200) was identified in radioligand dissociation assays, while potassium ions were found to be positive allosteric modulators. These two modulators interacted with the $K_v11.1$ channel via separate allosteric sites with positive cooperativity towards each other. Taken together, this investigation provides direct evidence for allosteric modulation of the $K_v11.1$ channel.

As an extension of the research described in chapter 3, three compounds (ML-T531, VU0405601 and LUF7244) were extensively evaluated for their negative allosteric effects on the $K_v11.1$ channel using different [^3H]dofetilide binding assays in **Chapter 4**. The novel modulator LUF7244 was further assessed for its possible antiarrhythmic propensity in radioligand binding experiments and voltage sensitive optical mapping in a newly validated neonatal rat ventricular myocyte (NRVM) model. The channel affinity of three blockbuster drugs (astemizole, sertindole and cisapride) that have all been withdrawn from market due to their $K_v11.1$ blockade, was diminished in the presence of LUF7244. Furthermore, the heterogeneous prolongation of the action potential duration (APD) and/or a

high incidence of early afterdepolarizations (by astemizole and sertindole only) induced by these $K_v11.1$ drugs were normalized by pretreatment with 10 μ M LUF7244 in the NRVM cultures. Intriguingly, LUF7244 *per se* did not affect the APD and the viability, excitability and contractility of the cardiomyocytes, and exerted no obvious influence on the intentional blockade of the human histamine H_1 receptor by astemizole. Accordingly, these results indicate that further development of LUF7244 raises an opportunity for antiarrhythmic drugs via combination therapy.

Subsequently, in **Chapter 5** the synthesis and allosteric evaluation of 29 compounds, which share the same chemical scaffold as LUF7244, were described. Most compounds emerged as negative allosteric modulators at the $K_v11.1$ channel, and the structure-activity relationships of all these ligands were established. Importantly, compounds **7f** and **7p** were more potent than LUF7244 in negatively modulating the channel, implying promising antiarrhythmic propensities superior to LUF7244.

A new [3H]dofetilide competition association assay was successfully validated in **Chapter 6**, and was further utilized to determine the kinetic parameters of fifteen prototypical $K_v11.1$ blockers. In contrast to a classical ligand-receptor interaction mechanism, the affinity of these blockers was predominantly regulated by their association rates instead of dissociation rates, implicating the role of association rates in $K_v11.1$ blockade. Thereafter, membrane affinity of all these ligands was measured in an immobilized artificial membrane column using HPLC. Similar to general calculated physiochemical properties, it is shown in chapter 6 that membrane interactions of $K_v11.1$ blockers did not significantly impact their affinity and ligand binding kinetics.

Since dissociation rates or residence times (RTs) of all $K_v11.1$ blockers in chapter 6 only exhibited a 10-fold difference, a library of 46 compounds over a wide range of chemical scaffolds were tested for their affinity and kinetic data in **Chapter 7**. $K_v11.1$ blockers were discovered with up to a 300-fold difference in RTs (0.34 min for compound **37** versus 105 min for **38**), which enabled the investigation of the structure-kinetics relationships next to structure-affinity relationships. Afterwards, a “ k_{on} - k_{off} - K_D ” kinetic map was constructed based on the kinetic parameters of these compounds together with those of three reference blockers (astemizole, ranolazine and dofetilide). This kinetic map offers a probable framework for a further and more precise categorization of $K_v11.1$ blockers, inferring distinct proarrhythmic risks. Additionally, two representative compounds, **21** and **38**, were measured in a whole-cell patch clamp assay. It was found that the potency (IC_{50}) of these two ligands was influenced by their RTs, while the I_{Kr} inhibition rates were in line with their association rates. Therefore, association rates and RTs

of $K_v11.1$ blockers are strongly suggested to be incorporated next to their affinity values into the future paradigm for proarrhythmia safety assessment.

Finally, general conclusions of all these chapters were summarized and the corresponding future research directions based on all findings in this thesis were proposed in **Chapter 8**. In conclusion, allosteric modulation and ligand binding kinetics at the $K_v11.1$ channel have been intensively discussed in this thesis. Negative allosteric modulators of the $K_v11.1$ channel open a new avenue for mitigating unintentional, arrhythmic effects of drug candidates via pharmacological combination therapy. Likewise, incorporation of ligand binding kinetics, next to affinity for the $K_v11.1$ channel, into the new Comprehensive *in vitro* Proarrhythmia Assay (CiPA) could improve the traditional screening paradigm for assessment of $K_v11.1$ -induced cardiotoxicity. Hopefully, considering kinetic parameters of $K_v11.1$ blockers at the channel will lead to the design of safer drug candidates as well as to less drug attrition in the near future.

Samenvatting

De familie van ionkanalen is vanwege zijn vele fysiologische functies al vele jaren een belangrijk aandachtsgebied voor onderzoek naar nieuwe geneesmiddelen. Helaas is gebleken dat verscheidene geneesmiddelen bijwerkingen vertonen die veroorzaakt worden door binding aan een ionkanaal, in het bijzonder door $K_v11.1$ kanaal-gemedieerde cardiotoxiciteit. Daarom wordt er tegenwoordig door geneesmiddelautoriteiten onderzoek naar ionkanaal-interacties vereist voordat goedkeuring van een geneesmiddel kan plaatsvinden. Bovengenoemde onderwerpen worden besproken in **hoofdstuk 1** van dit proefschrift.

Hoofdstuk 2 is een literatuurstudie die de voortgang van onderzoek naar het $K_v11.1$ kanaal beschrijft. In dit hoofdstuk hebben we ons gericht op kinetische studies van het ionkanaal, in het bijzonder de unieke kanaalkinetiek en ligand-bindingskinetiek. Daarnaast worden biosynthese, degradatie, structurele eigenschappen, fysiologische functies en on- en off-target toepassingen van het $K_v11.1$ kanaal geïntroduceerd. Het grondig bestuderen van het $K_v11.1$ kanaal draagt bij aan het verbeteren van geneesmiddelenonderzoek en het verminderen van aritmische bijwerkingen die veroorzaakt worden door blokkering van dit ionkanaal.

In **hoofdstuk 3** is een selectie van eerder beschreven liganden, kalium ionen en drie referentie liganden onderzocht. Voor de geselecteerde stoffen is gekeken naar allosterische modulatie van het $K_v11.1$ kanaal in [3H]astemizol en [3H]dofetilide bindingsstudies. In een radioligand dissociatie studie werd gevonden dat één ligand, LUF6200, een potente negatieve allosterische modulator is en dat kaliumionen zich als positieve allosterische modulatoren gedragen. Deze twee modulatoren induceren hun effect op het $K_v11.1$ kanaal via verschillende allosterische bindingsplaatsen met een positieve coöperativiteit. Samengevat levert dit onderzoek direct bewijs voor allosterische modulatie van het $K_v11.1$ kanaal.

Als toevoeging op het in hoofdstuk 3 beschreven onderzoek zijn in **hoofdstuk 4** met behulp van verschillende [3H]dofetilide experimenten drie liganden, ML-T531, VU0405601 en LUF7244, uitgebreid onderzocht op hun negatieve allosterische eigenschappen ten opzichte van het $K_v11.1$ kanaal. De nieuwe modulator LUF7244 werd daarnaast verder onderzocht op een potentieel antiaritmisch effect met behulp van radioligand bindingsstudies en een nieuw gevalideerd model, het neonatal rat ventricular myocyte (NRVM) model. De affiniteit van drie blockbuster geneesmiddelen (astemizol, sertindol en cisapride) die vanwege $K_v11.1$ kanaal blokkering van de markt gehaald zijn, was verminderd in aanwezigheid

van LUF7244. Daarnaast werden de heterogene verlenging van de duur van de actiepotentiaal en/of een hoge incidentie van vroege napolarisaties (door enkel astemizol en sertindol) - veroorzaakt door deze blockbuster geneesmiddelen - genormaliseerd door voorbehandeling van de NRVM culturen met 10 μM LUF7244. Intrigerend genoeg heeft LUF7244 op zichzelf geen effect op de duur van de actiepotentiaal en op de levensvatbaarheid, prikkelbaarheid en contractiliteit van cardiomyocyten. Daarnaast vertoont het geen effect op de gewenste werking van astemizol, namelijk blokkering van de histamine H_1 receptor. Deze resultaten tonen aan dat verdere ontwikkeling van LUF7244 de mogelijkheid biedt om antiaritmische geneesmiddelen te gebruiken als combinatietherapie.

Vervolgens beschrijft **hoofdstuk 5** de synthese en allosterische evaluatie van 29 liganden met een scaffold gelijk aan LUF7244. De meeste liganden bleken negatieve allosterische modulatoren voor de blokkering van het $K_v11.1$ kanaal en structuur-activiteit relaties van al deze liganden werden beschreven. Liganden **7f** en **7p** bleken potenter dan LUF7244 in het negatief moduleren van de receptor. Dit is veelbelovend omdat het laat zien dat deze stoffen mogelijk betere antiaritmische eigenschappen hebben dan LUF7244.

De ontwikkeling van een nieuw [^3H]dofetilide competitie associatie experiment is beschreven in **hoofdstuk 6**. Dit experiment werd vervolgens verder gebruikt om de kinetische parameters van vijftien prototypische $K_v11.1$ kanaal-blokkers te bepalen. In tegenstelling tot het klassieke mechanisme van ligand-receptor interactie werd de affiniteit van deze blokkers voornamelijk bepaald door hun associatie-snelheidsconstanten in plaats van hun dissociatie-snelheidsconstanten. Dit toont duidelijk de rol en het belang van associatie-snelheidsconstanten voor blokkering van het $K_v11.1$ kanaal. Vervolgens is voor al deze liganden de affiniteit voor het celmembraan bepaald met behulp van een geïmmobiliseerde kunstmatige membraankolom in een HPLC machine. Net zoals voor gebruikelijke fysisch-chemische eigenschappen is in hoofdstuk 6 aangetoond dat de membraaninteractie van $K_v11.1$ kanaal-blokkers geen significant effect heeft op hun affiniteit en kinetiek van ligandbinding.

Vanwege het feit dat de dissociatie-snelheidsconstanten en verblijftijden van alle in hoofdstuk 6 beschreven $K_v11.1$ kanaal-blokkers slechts maximaal een factor 10 verschillen, werd in **hoofdstuk 7** een bibliotheek van 46 liganden getest op affiniteit en kinetiek. Er werden $K_v11.1$ kanaal-blokkers ontdekt met een 300-voudig verschil in verblijftijd op het ionkanaal, 0.34 min voor **37** t.o.v. 105 min voor **38**. Dit maakte het voor ons mogelijk om structuur-kinetiek relaties te bestuderen naast de gebruikelijke structuur-affiniteit relaties. Vervolgens is op basis van de kinetische parameters van deze liganden samen met die van de referentie liganden, astemizol, ranolazine en dofetilide, een kinetische " k_{on} - k_{off} - K_D "-

kaart gemaakt. Deze kaart biedt kader voor een verdere en nauwkeuriger indeling van $K_v11.1$ kanaal-blokkers waarmee de risico's van de verschillende blokkers voorspeld kunnen worden. In aanvulling hierop zijn twee representatieve liganden, **21** en **38**, getest in een whole-cell patch clamp experiment. Het bleek dat de potentie van deze liganden (IC_{50}) werd beïnvloed door hun verblijftijd op het ionkanaal, terwijl de I_{Kr} inhibition rates in lijn waren met de associatie-snelheidsconstanten. Om bovengenoemde redenen raden wij sterk aan om bij het bepalen van de veiligheid van potentieel pro-aritmische liganden de verblijftijd en associatie-snelheidsconstante naast de affiniteit mee te nemen ter evaluatie.

Ten slotte zijn de algemene conclusies van de hoofdstukken en de bijbehorende mogelijkheden voor toekomstig onderzoek beschreven in **hoofdstuk 8**. Concluderend, allosterische modulatie en ligandbindingskinetiek van het $K_v11.1$ kanaal zijn uitvoerig beschreven en bediscussieerd in dit proefschrift. Negatieve allosterische modulators bieden nieuwe mogelijkheden tot het verminderen van onbedoelde, aritmische effecten van kandidaat-geneesmiddelen via farmacologische combinatietherapie. Daarnaast kan het gebruikmaken van ligandbindingskinetiek, parallel aan de affiniteit, van het $K_v11.1$ kanaal in de nieuwe FDA guideline Comprehensive *in vitro* Proarrhythmia Assay (CiPA) leiden tot verbetering van de traditionele bepaling van toxiciteit veroorzaakt door het $K_v11.1$ kanaal. Hopelijk zal het evalueren van kinetische parameters van $K_v11.1$ kanaal-blokkers in de toekomst leiden tot het ontwikkelen van veiliger geneesmiddelen en tot minder geneesmiddelen die van de markt gehaald moeten worden.

Curriculum Vitae

Zhiyi Yu was born on January 5th, 1986 in Hubei, China. After graduating from high school in 2004, he moved to Sichuan to study pharmacy in Western China School of Pharmacy at Sichuan University. In 2008 he received a bachelor degree, and then he continued a master study in the same university, majoring in medicinal chemistry. During this period he performed a series of studies on chemical synthesis and biological evaluation of antimicrobial compounds under the supervision of Prof. Taiping Hou.

After obtaining his master degree in 2011, Zhiyi Yu was supported by the China Scholarship Council to conduct a Ph.D study in Division of Medicinal Chemistry at the Leiden Academic Centre for Drug Research (Leiden University, The Netherlands) under the supervision of Prof. Ad IJzerman and Dr. Laura Heitman. His doctorate dissertation consisted of two main projects, which were allosteric modulation and ligand binding kinetics at the K_v11.1 (hERG) channel. During his Ph.D studies from 2011 to 2015, Zhiyi Yu together with his supervisors developed several valuable collaborations with Leiden University Medical Center and University Medical Center Utrecht, where he acquired different research skills in cellular electrophysiology. From October 2015 on, he will work as a postdoctoral fellow in the laboratory of Prof. Jonathan Cohen in Harvard Medical School at Harvard University. He will be applying protein chemistry as well as electrophysiological techniques to study allosteric modulations of neuronal AChRs and GABA_A receptors.

List of publications

Yu, Z.; Liu, J.; van Veldhoven, J. P.; IJzerman, A. P.; Schali, M. J.; Pijnappels, D. A.; Heitman, L. H.; de Vries, A. A. F. Allosteric Modulation of $K_v11.1$ (hERG) Channels Protects against Drug-Induced Ventricular Arrhythmias. *Circ. Arrhythm. Electrophysiol.* submitted.

Yu, Z.; van Veldhoven, J. P.; Louvel, J. A.; 't Hart, I. M.; Kopf, A. H.; Heitman, L. H.; IJzerman, A. P. Synthesis and biological evaluation of negative allosteric modulators of the $K_v11.1$ (hERG) channel. *Eur. J. Med. Chem.* submitted.

Yu, Z.; van Veldhoven, J. P.; Louvel, J. A.; 't Hart, I. M.; Rook, M. B.; van der Heyden, M. A.; Heitman, L. H.; IJzerman, A. P. Structure-affinity relationships (SARs) and structure-kinetics relationships (SKRs) of $K_v11.1$ blockers. *J. Med. Chem.* **2015**, *58*, 5916-5929.

Yu, Z.; IJzerman, A. P.; Heitman, L. H. $K_v11.1$ (hERG)-induced cardiotoxicity: a molecular insight from a binding kinetics study of prototypical $K_v11.1$ (hERG) inhibitors. *Br. J. Pharmacol.* **2015**, *172*, 940-955.

Yu, Z.; Klaasse, E.; Heitman, L. H.; IJzerman, A. P. Allosteric modulators of the hERG K^+ channel: Radioligand binding assays reveal allosteric characteristics of dofetilide analogs. *Toxicol. Appl. Pharmacol.* **2014**, *274*, 78-86.

Yu, Z.; Shi, G.; Sun, Q.; Jin, H.; Teng, Y.; Tao, K.; Zhou, G.; Liu, W.; Wen, F.; Hou, T. Design, synthesis and *in vitro* antibacterial/antifungal evaluation of novel 1-ethyl-6-fluoro-1,4-dihydro-4-oxo-7(1-piperazinyl) quinoline-3-carboxylic acid derivatives. *Eur. J. Med. Chem.* **2009**, *44*, 4726-4733.

Vilums, M.; Zweemer, A. J.; Barmare, F.; van der Gracht, A. M.; Bleeker, D. C.; **Yu, Z.**; de Vries, H.; Gross, R.; Clemens, J.; Krenitsky, P.; Brussee, J.; Stamos, D.; Saunders, J.; Heitman, L. H.; IJzerman, A. P. When structure-affinity relationships meet structure-kinetics relationships: 3-((Inden-1-yl) amino)-1-isopropyl-cyclopentane-1-carboxamides as CCR2 antagonists. *Eur. J. Med. Chem.* **2015**, *93*, 121-134.

Vilums, M.; Zweemer, A. J.; **Yu, Z.**; de Vries, H.; Hillger, J. M.; Wapenaar, H.; Bollen, I. A.; Barmare, F.; Gross, R.; Clemens, J.; Krenitsky, P.; Brussee, J.; Stamos, D.; Saunders, J.; Heitman, L. H.; IJzerman, A. P. Structure-kinetic relationships-an overlooked parameter in hit-to-lead optimization: A case of cyclopentylamines as chemokine receptor 2 antagonists. *J. Med. Chem.* **2013**, *56*, 7706-7714.

Louvel, J.; Carvalho, J. o. F.; **Yu, Z.**; Soethoudt, M.; Lenselink, E. B.; Klaasse, E.; Brussee, J.; IJzerman, A. P. Removal of human ether-à-go-go related gene (hERG) K⁺ channel affinity through rigidity: A case of clofilium analogues. *J. Med. Chem.* **2013**, *56*, 9427-9440.

Carvalho, J. o. F.; Louvel, J.; Doornbos, M. L.; Klaasse, E.; **Yu, Z.**; Brussee, J.; IJzerman, A. P. Strategies to reduce hERG K⁺ channel blockade. Exploring heteroaromaticity and rigidity in novel pyridine analogues of dofetilide. *J. Med. Chem.* **2013**, *56*, 2828-2840.

Wen, F.; Zhang, H.; **Yu, Z.**; Jin, H.; Yang, Q.; Hou, T. Design, synthesis and antifungal/insecticidal evaluation of novel nicotinamide derivatives. *Pestic. Biochem. Physiol.* **2010**, *98*, 248-253.

Jin, H.; Geng, Y.; **Yu, Z.**; Tao, K.; Hou, T. Lead optimization and anti-plant pathogenic fungi activities of daphneolone analogues from *Stellera chamaejasme* L. *Pestic. Biochem. Physiol.* **2009**, *93*, 133-137.

Acknowledgements

The completion of this dissertation is one of the most significant challenges I have ever encountered. It is almost impossible to describe my acknowledgements to everyone who contributed to the realization of this dissertation. However, a large group of people should be mentioned within limited pages, as I could not have finished my Ph.D studies without their guidance, support and cooperation.

First and foremost, I would like to express my most sincere appreciation to my supervisors, Ad and Laura, for your continuous encouragement, insight and patience. I feel extremely privileged and fortunate to have been your student.

Secondly, I am deeply grateful to my collaborators, Marcel and Martin, Twan, Daniël, and in particular, Jia who is also my good friend.

Thirdly, a great debt of gratitude should be extended to my lovely colleagues and friends for all the wonderful times that we shared inside and outside of the laboratory. I feel very lucky, comfortable and relaxed to work in the Division of Medicinal Chemistry. I appreciated all people from this division for their help, kindness and support. Particularly, Elisabeth and Dong trained me in different radioligand binding assays during my first semester. My officemates, Julien, Jaco, Maarten, Julia and Indira, provided a lot of assistance in both my professional and personal life. Other colleagues like Andrea, Arnault, Bart, Henk, Lance, Miriam, Natalia, Rongfang, Thea and Xue as well as my students (Erina, Renske, Rochelle, Tirsa and Wanisha) are also gratefully acknowledged. Likewise, there are a large group of friends, who I wish to thank for their help, outside of the medicinal chemistry division, such as Bingxiao, Changsheng, Cui, Dan, Debi, Emile, Hui, Jianbing, Kaixuan, Ke, Li, Lin, Qingju, Qihong, Shuo, Suyun, Xianqin, Yang, Yaowang, Yu, Yuejiao, and Zhengshan. In particular, Xianqin, Yang Wan and Zhengshan had given me a lot of help, advice and support since the first time I met them.

Last but not least, I am deeply indebted to my family members for all your unconditional and constant love, understanding, support and sacrifices during my studies. I particularly owe a great debt to my parents on whom I did not spend so much time. I had been far away from my parents since I went to the university in 2004. I should definitely accompany them more in the near future. Thanks very much for supporting and encouraging me spiritually throughout my life.

